LEIBNIZ UNIVERSITÄT HANNOVER
FAKULTÄT FÜR ELEKTROTECHNIK UND INFORMATIK

Radio Shadowing in Vehicle-to-Vehicle Communication at Urban Intersections – A Measurement and Simulation-based Evaluation

Von der Fakultät für Elektrotechnik und Informatik
der Gottfried Wilhelm Leibniz Universität Hannover
zur Erlangung des akademischen Grades

Doktor-Ingenieur

genehmigte

Dissertation

von

Dipl.-Ing. Hugues Narcisse Tchouankem
geboren am 29. März 1977 in Yaoundé/Kamerun

2016

ABSTRACT

One of the key challenges of Vehicle-to-Vehicle (V2V) communication is to ensure a reliable information exchange in such a way that a cooperative awareness between vehicles is permanently established, regardless of the considered environment and traffic conditions. Consequently, V2V applications have to fulfill quality requirements in order to help drivers in critical situations on rural and motorway roads, as well as in urban and inner-city areas. However, due to the presence of radio shadowing, a significant portion of message transmissions will be susceptible to recurrent signal attenuation caused by buildings or vegetation. For this purpose, it is essential to perform a deep analysis of the fundamental wave propagation characteristics in typical vehicular environments. The first part of this thesis covers a measurement-based evaluation of V2V communication by focusing on stationary radio shadowing at urban intersections. Hereby, we examine, based on several measurement campaigns, the impact of building and vegetation obstructions on the communication quality. In urban agglomerations, the communication performance is directly associated to availability of a constant line of sight between vehicles, which may depend on the distribution of buildings. Therefore, we provided an in-depth analysis and characterization of urban intersections based on digital maps from selected European big cities. It has been found that intersections with three up to four corners occupied by buildings are the most frequent. In addition, while the related work did not sufficiently address the scalability problem of Vehicular Ad-hoc Network (VANET) experimentally, we present an abstraction method to overcome logistic issues during real-world measurements. More particularly, we evaluate the impact of buildings on the severity of co-channel interference through experiments carried out at two different intersections.

The second part of this thesis addresses the performance evaluation of V2V communication at urban intersections by analyzing the influence of building shadowing and penetration rates. Since the evaluation is performed by means of simulation, we propose a hybrid simulation platform composed of a network simulator and a road traffic simulator. To ensure applicability of simulation results, an ITS-G5 conform protocol stack from the application layer up to the physical layer is scrupulously modeled under the simulation tool OMNeT++. As propagation models may directly affect the level of accuracy in simulation-based performance evaluations, we introduce a dedicated urban propagation model designed to reflect radio propagation on urban environments in a realistic way. After a careful selection of representative scenarios, we perform a simulation campaign under variation of environment factors and communication parameters. We particularly concentrate on the scalability issue and the influence of intersection type on the communication performance. The obtained results indicate that performance of V2V communication at urban intersection is directly linked to the type of the intersection, and packet collisions are mainly caused by the channel access mechanism due to the broadcast nature of V2V communication.

Keywords: V2V, VANET, Radio Shadowing, Urban Intersections, Intersection type

ZUSAMMENFASSUNG

Ein Ziel der Fahrzeugkommunikation ist es, durch Informationsaustausch den Fahrer frühzeitig vor kritischen Situationen zu warnen. Dies soll unabhängig der betrachteten Umgebung und den gegebenen Verkehrsbedingungen erfolgen. Eine zentrale Herausforderung der Fahrzeugkommunikation ist es somit, einen zuverlässigen, stabilen und robusten Funkkanal bereitzustellen, sodass eine Interaktion zwischen den Fahrzeugen permanent gesichert ist. Durch die Abschattung von an innerstädtischen Kreuzungen besonders häufig vorhandenen Gebäuden und/oder Vegetation wird jedoch ein erheblicher Teil von Nachrichtenübertragungen den Empfänger nicht erreichen. Die vorliegende Dissertation befasst sich mit der Leistungsbewertung der Fahrzeugkommunikation in Bezug auf stationäre Funkabschattungen in urbanen Umgebungen. Dies setzt ein solides Verständnis der Eigenschaften des Funkkanals sowie dessen Auswirkungen auf die Kommunikationsqualität voraus. Besonders in städtischen Ballungsräumen hängt die Zuverlässigkeit des Nachrichtenaustausches von der Qualität und Verfügbarkeit der Kommunikationsverbindungen zwischen den Fahrzeugen ab. Die Art der Sichtverbindung ist zudem stark mit der Straßentopologie und der Verteilung der Gebäude in Kreuzungsbereichen verbunden. Im Verlauf dieser Arbeit wird zunächst eine Evaluation und eine Charakterisierung von Kreuzungstopologien mit Hilfe digitaler Karten von ausgewählten europäischen Großstädten vorgestellt. Als die am häufigen vorkommende Topologie wurden Kreuzungen mit drei bis vier von Gebäuden besetzten Ecken identifiziert. Auf der Grundlage dieser Erkenntnisse steht im ersten Teil der Arbeit eine messungsbasierte Untersuchung von Kreuzungstopologien auf der Fahrzeugkommunikation im Fokus. Hierbei werden die Auswirkungen von Gebäuden und Vegetation auf die Kommunikationsqualität in mehreren Messkampagnen analysiert und anschließend bewertet. Als ergänzender Beitrag zu den schon existierenden Arbeiten, die die Skalierbarkeit von Fahrzeug-Ad-hoc-Netzen behandeln, stellt die vorliegende Arbeit einen Ansatz vor, der den logistischen Aufwand während der Feldtests minimiert. Darüber hinaus wird der Einfluss von Gebäuden auf Gleichkanalinterferenzen durch Messungen an zwei verschiedenen Kreuzungen gründlich untersucht.

Im zweiten Teil der Arbeit wird die Leistungsbewertung der Fahrzeugkommunikation an städtischen Kreuzungen unter Betrachtung des Einflusses von Gebäudeabschattung und Verkehrsdichte mit Hilfe von Simulationen adressiert. Es wird dazu eine aus einem Netzwerk- und Verkehrssimulator gekoppelte Simulationsplattform entwickelt und vorgestellt. Um einen hohen Realitätsgrad zu gewährleisten, wurde ein dem ITS-G5 Standard entsprechender Protokoll-Stack von der Anwendungsschicht bis zur physikalischen Schicht modelliert und im Simulationswerkzeug OMNeT++ integriert. Darüber hinaus wurde ein dediziertes Ausbreitungsmodell für städtische Kreuzungen entwickelt, um die Eigenschaften des Funkkanals realistisch abzubilden. Das Modell berücksichtigt sowohl die Abschattung durch Gebäude als auch den Signalschwund durch Mehrwegeausbreitung und basiert auf realen Messungen. Nach einer Auswahl repräsentativer Szenarien wurde eine Simulationskampagne unter Variation von Umgebungsfaktoren und Kommunikationsparametern durchgeführt. In diesem Teil der Arbeit wird haupt-

sächlich das Problem der Skalierbarkeit von Fahrzeug-Ad-hoc-Netzen und vor allem die Auswirkung verschiedener Kreuzungstopologien auf die erzielbare Kommunikationsqualität quantifiziert. Ein wesentliches Ergebnis dieser Arbeit zeigt, dass die Topologie der Kreuzung einen signifikanten Einfluss auf die Kommunikationszuverlässigkeit hat. Es konnte weiterhin gezeigt werden, dass Paketkollisionen vorwiegend durch den dezentralen Kanalzugriffsmechanismus der Fahrzeugkommunikation entstehen.

Schlagwörter: Fahrzeugkommunikation, Funkabschattung, Städtische Kreuzungen, Kreuzungstopologie

CONTENTS

LIST OF FIGURES

LIST OF TABLES

INTRODUCTION

1.1 MOTIVATION

The mobility of people and goods is a key factor in the economic expansion of a country. Besides facilitating access to a large range of products, the mobility promotes the tourism branch by motivating to achieve long-distance travels. At the individual level, mobility is closely linked to self-determination and personal freedom. It opens up opportunities to participate in job market abroad, and, therefore, a better chance to get high-quality jobs. To increase their standard of living, people usually need to reach other people, places, goods, and services. For the concrete implementation of the mobility, transport is the instrument that is then required. In contrast to the mobility, transport is only a tool to satisfy the need for mobility and includes vehicles, infrastructures and traffic rules. In other words, transport can be defined as a targeted change of location of persons or goods, news using energy and information including support processes. However, it is hard to say how much traffic is generated or even required in the movement of people from one place to another. In general, people have at least in cities the choice of how and where to satisfy their needs and the means of transport they desire.

While the growth of mobility is socially commendable for the political and economic policy makers, the growth of traffic is an undesirable objective for traffic scientists and road operators. The success of the mobility depends on transport systems, which might provide safer traveling conditions protecting human lives, enhance the quality of life and avoid the waste of material resources and energy. However, mobility and transport on the road, rail, aviation and shipping causes significant environment, social and economic damages mainly due to accidents and traffic jams. In 2004, a study carried out by the Intergovernmental Panel on Climate Change (IPCC) reported that the transport sector has a significant impact on the environment accounting for between 26% of total world energy consumption and 23% of carbon dioxide emissions with about three-quarters coming from road vehicles. The tendency is rising projected to be about 80% higher than the current levels by 2030 [1]. It assumed that the transport activity would increase as the economy grows, which is the case in emerging countries.

According to a study reported by the World Health Organization (WHO), a total of 92 492 people died from road traffic injuries in 2010 in the European Union (EU) [2]. That is 253 people killed every day. When considering the number of serious accidents involving persons killed, different modes of transport come into consideration. Forty-three percent of the people dying in road traffic in the EU are vulnerable road users (27% pedestrians, 12% users of motorized two- and three-wheelers and 4% cyclists), 50% are car occupants and the remaining 7% among unspecified road users. This study also shows that road traffic accidents are even the leading cause of deaths and hospital admissions for citizen under the age of 45 in Europe.

Examining the cause of death among young people between 15-24 years old, road accidents are recognized as the leading cause of non-natural death in Europe [3]. However, it should be noted that the increase of injuries in this age group is related to the lifestyles of young adults. Due to their introduction and integration in motor vehicle traffic and work environments, the risk of dying as a result of a road traffic injury is highest between the age of 15 and 24. As can be seen in Figure 1, two principal causes account for over 70% of all fatal injuries: road injuries (46%) and suicides (24%) in this age group. Clearly, motor vehicle injuries are by far the number one killer among young adults.
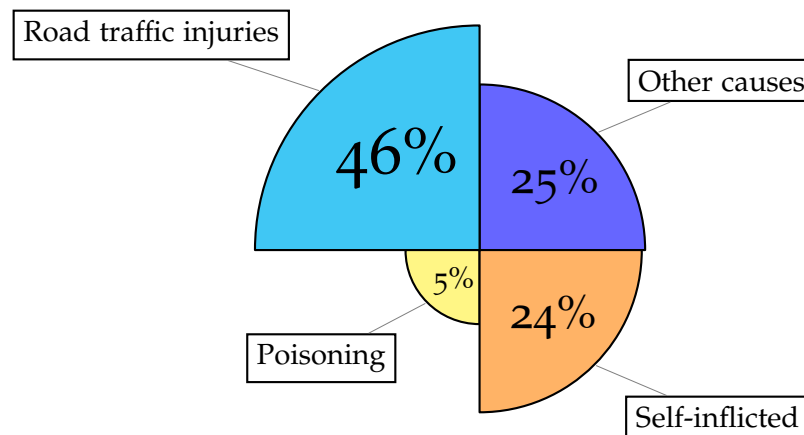
Figure 1: Fatal injuries by causes of death among young people between 15-24 year in the EU-27 [3].

Regarding accident trends by road type, a study of the Royal Automobile Club Foundation reported that urban-related accidents represent 61% of all reported accidents that occurred in the EU in 2007 [4]. Although almost two-thirds of the accidents occur on urban roads, only 56% are serious injuries and 33% are fatal. The same trend is observed on German roads. Figure 2 shows the accident statistic in relation to road types carried out by the German automotive organization ADAC (Allgemeiner Deutscher Automobil-Club) in years 2000 and 2013 [5]. The positive observation is that safety on German roads is increasing steadily. The figure shows that the number of accidents in road traffic fell by almost 25% in 13 years. This effect is even more pronounced when considering the total number of fatalities depicted in Figure 2b, with a fall of 46% for urban roads, 60% for rural roads and 52% for motorways. Nevertheless, the number of accidents remained on a high level. Too many people still have accidents in traffic, especially in urban areas, where the number of the injured road users is by far the greatest (see Figure 2a). In 2013, for example, three-quarters of all recorded traffic accidents occur in urban traffic. These results also show that while the number of collisions is higher in urban areas there is a greater chance of a collision resulting in death on rural roads. Although serious accidents mostly take place on rural roads, we observe in Figure 2b that almost one-third of road traffic facilities occurs in city traffic, which is also not negligible. This deviation is due to the restricted space leading to an automatic reduction of driving speed which consequently results in a low level of crash severity. However, more than two people died every day in road accidents in 2013 in urban agglomerations. This leads us to the conclusion that the speed limit alone does not guarantee absolute safety.

(a) Road accident casualties

(b) Road traffic fatalities
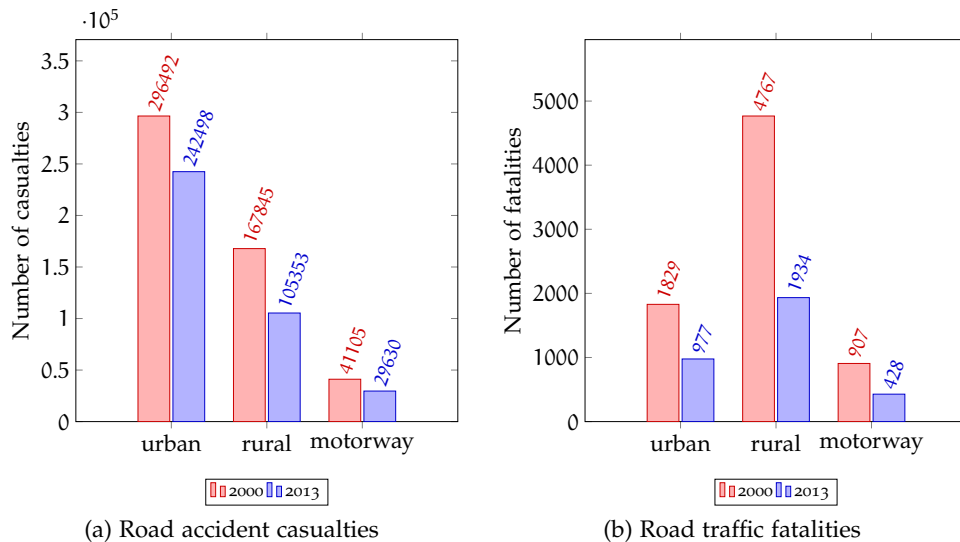
Figure 2: Total number of reported road accidents in Germany from 2000 and 2013 in relation to road types [5].

The big challenge in city traffic is the interaction between different road actors. Cars, buses, trains, motorcycles, bicycles and pedestrians share the same space in the inner-city and rely on mutual respect of each other. A cooperation and communication between the different groups is, therefore, indispensable. For example, a driver who fails to signal his intention by ignoring the indicator could provoke misunderstandings, and at worst a rear-end collision with other traffic participants. Furthermore, information about the actual traffic condition would avoid overloading already saturated intersections by re-routing approaching vehicles.

The growth of the economy and the mobility requirement of European citizen has generated an increase in the volume of road transport. This leads to a rise of congestion of road infrastructures, which is the source of social and environmental problems, such as air and water pollution, noise, and other ecological impacts. Due to space restriction shared by road users, innovation based not only on the expansion of the existing road infrastructure but rather on appropriate and efficient solutions will play a major role in the enhancement of traffic safety and efficiency. This motivates the introduction of Intelligent Transportation System (ITS) which brings advanced applications in order to provide innovative services to all kind of modes of transport and traffic management. Through the use of ITS, traffic participants are better informed, and road infrastructures are optimal utilized to prevent traffic jams and accidents. For instance, ITS through intelligent services would enhance the traffic safety in urban environments by efficiently controlling traffic signal according to the traffic conditions. Additionally, the integration of vehicular communication in advanced vehicle safety systems, so-called Advanced Driver Assistance Systems (ADAS), is identified to be helpful by supporting installed in-car sensors and thus would extend the driver's horizon. Despite the effectiveness of traditional sensors, they are very limited in detection range and are weather-dependent.

Motivated by the rapidly growing advance in the field of communication technologies, ITS integrates information and telecommunication into traffic engineering to control and manage transport systems. More specifically, various forms of wireless communication technologies enable a broad range of services for traffic

safety, efficiency, information and infotainment applications. Applied communication technologies include radio modem communication on UHF and VHF frequencies, short-range communication using IEEE 802.11 protocols and infrastructure-based communication such as WIMAX, GSM, 3G or Long Term Evolution (LTE).

As part of the fight to reduce traffic jams and road fatalities, the European Commission (EC) adopted the decision to provide an EU-wide frequency band to enable immediate and reliable communication between cars and between cars and roadside infrastructures [6]. For this purpose, car manufacturers and research institutions introduced the communication technology called Vehicle-to-Vehicle (V2V) communication operating in the 5.9 GHz frequency band with the aim to open up a wide range of road safety, traffic efficiency and infotainment applications for next-generation vehicular traffic. The term Vehicle-to-X (V2X) communication (in Europe Car-to-X, C2X) is mostly used to encompass the communication between vehicles and infrastructures, where "X" represents other vehicles, traffic infrastructures - Vehicle-to-Infrastructure (V2I) - or home/enterprise equipment. Generally, V2V is the popular term to identify V2X. To ensure robust communication in the context of the highly dynamic vehicular environment, the specific requirements of inter-vehicular wireless communication have been incorporated into the well-known IEEE 802.11 [7] by the standard amendment IEEE 802.11p [8]. For this end, 802.11p introduces several modifications to the Physical (PHY) and Medium Access Control (MAC) layers. The 802.11p PHY is inherited from IEEE 802.11a, but relies on channels of 10 MHz bandwidth instead of the usual 20 MHz. The MAC sublayer of IEEE 802.11p introduces several modifications including the newly defined Outside the Context of a Basic Service Set (OCB) mode, which allows stations to transmit data frames without prior association or authentication with a Basic Service Set (BSS).

Various large-scale field operational tests (FOTs) involving V2V systems were taking place worldwide in the last couple of decades. One can cite the German sim^{TD} project (Safe and Intelligent Mobility - Test Field Germany) and US Department of Transportation (US DOT). On the basis of these FOTs, new insights on the applicability of V2V contributed not only to the harmonization and standardization of V2V communication but also to gain insight into the communication protocol behavior. Moreover, the maturity of Wireless Local Area Network (WLAN) have encouraged governments, partners from automotive industry, and research institutes to join efforts by using V2V as the appropriate technology to ensure a cooperative awareness within nodes through the exchange of message between traffic participants. In this direction, twelve European vehicle manufacturers have signalized their intention to bring cooperative systems based on inter-vehicular communication onto European roads starting this year by signing a corresponding Memorandum of Understanding (MoU). This implies that V2V systems would be mandatory for new cars, and thus are close to market introduction.

However, although V2V has gained a lot of attention, there are several fundamental factors of V2V communication that make its performance challenging and unique compared to traditional WLANs, and include the following:

- Highly dynamic mobility of nodes: Vehicles move at different speeds in varying environments (highway, rural, suburban and urban) resulting in a rapidly and unpredictably network topology.

- Radio shadowing and multipath fading: Radio shadowing describes the random variation of the received signal, which is subject to attenuation caused by surrounding obstacles obstructing the communication link. Fading occurs when multiple times delayed copies of the transmitted signal, each one stemming from a different propagation path, reach the receiver. This results to constructive or destructive interference depending on the amplitude and angle of reflected signals.

- Co-channel interference: Due to the broadcast nature of V2V, its performance will suffer under high traffic densities in urban scenarios since hundreds of vehicles can be present in a relatively small region. However, the traffic pattern at urban intersections is characterized by a heterogeneous concentration of vehicles depending on traffic control and traffic condition. We will observe long queue during red phase due to the flow of moving vehicles toward the intersection.

Through the wireless exchange of information between vehicles and their neighborhood, Vehicular Ad-hoc Network (VANET) based on V2V communication opens up a plethora of road safety, traffic efficiency and infotainment applications. Safety-based applications such as Stationary Vehicle Warning (SVW), which informs approaching vehicles of the risk of collision with vehicles dangerously immobilized on the road and Intersection Collision Warning (ICW), which alerts vehicles entering the intersection of a risk of collision with other vehicles are currently standardized by the Technical Committee for ITS of European Telecommunications Standards Institute (ETSI) [9]. Moreover, also applications aiming to improve road traffic efficiency and driving comfort are conceivable. One can cite among others the Traffic Information and Recommended Itinerary, which informs approaching vehicles of some abnormal traffic conditions and provides circulation advises to circumvent traffic jams.

1.2 PROBLEM STATEMENT

One of the key challenges of V2V is to ensure the communication reliability in such a way that a cooperative awareness between nodes is permanently established, regardless of the considered environment and traffic conditions. This means that V2V applications have to fulfill quality requirements in order to help drivers in dangerous situations on rural and motorway roads, as well as in urban and inner-city areas. Furthermore, a proper and reliable operation of V2V applications requires accurate and timely delivery of vehicle status among nodes, at least in the near surrounding. However, the reliability of these applications depends significantly on the characteristics of the radio channel. Due to the presence of radio shadowing, especially frequent at urban intersections, it is essential to perform a deep analysis of the fundamental wave propagation characteristics in typical vehicular environments. In behalf of communication link obstruction, a significant portion of message transmissions will be susceptible to recurrent signal attenuation caused by buildings and/or vegetation. Consequently, an interesting aspect is a knowledge about the effective distribution of buildings near or around intersections in Europe. We focus the evaluation on urban environments since yet the performance of V2V communication in this area has not been fully quantified. This is primarily attributable to the dynamic and complex topology of vehicular networks at urban

intersections, and most importantly on the inevitable presence of numerous mobile and static obstacles like buildings, vegetation, and other vehicles. Therefore, in order to gain insight into the capability of V2V communication, it is essential to analyze main environment factors influencing the communication performance. We thus state following research questions:

> *How is the distribution of buildings at intersections in some European big cities? How significant is the influence of building shadowing on the performance of the communication? Do intersection characteristics such as building density, street width, and traffic density impact the communication range? How severe is the attenuation caused by vegetation through foliage? How can logistic challenges while measuring with a large number of vehicles be experimentally addressed?*

V2V communication relies on a single-hop broadcast of vehicle status information shared on a single channel. This implies that under harsh traffic conditions and heavy traffic areas, the wireless channel will suffer from severe congestion leading to a rapid degradation of communication performance. Moreover, considering the deployment of V2V systems in a near future, even if in early stage of deployment only a small portion of vehicles will be equipped, traffic densities can be expected to grow considerably during peak hours. Consequently, interference produced by nodes in the network could be a limiting factor of communication performance. Moreover, besides insight into the relationship between radio shadowing and severity of interference, the impact of intersection types on the communication performance is an essential research question. Intuitively, one can argue that, while radio shadowing caused by buildings could significantly affect the signal quality at the receiver, this could on the other hand block co-channel interference from surrounding hidden nodes. For all these reasons, a fundamental task towards market introduction is an assessment about the impact of intersection layout and its relationship to interference under crowded networks. To close this gap, we thus state following research questions:

> *Which type of intersection experiences the best communication performance? Does the intersection type and its influence on networking parameters such as transmission power, message generation rate, vehicle density affect the performance of V2V? Which type of packet collisions mainly occur in urban environments? How severe is the hidden node problem in broadcast-based V2V communication? Are delay requirements of V2V applications fulfilled when considering co-channel interference?*

In general, the evaluation of VANET is mostly achieved through field test measurements and/or simulations. While the former allows a realistic investigation, this expensive approach requires a huge logistic to control the measurement and fails in the reproduction of experiment runs due to the changing nature of traffic participants. However, this method which is generally based on interference-free conditions provides a high accuracy of the path loss estimation. On the other hand, simulation-based evaluations of V2V which include the co-channel interference may directly affect the level of accuracy since scalability effect in the vehicular network is limited by interference. All these reasons together motivate the consideration of field test experiments as well as simulation technique for the evaluation presented in this thesis. However, while the simulation-based evaluation of highway scenarios relies on one-dimensional network topology, the two-dimensional nature of

urban intersections requires a geometry-based representation of results. This introduces a new dimension of complexity during the investigation and representation of results.

1.3 OBJECTIVE AND CONTRIBUTION

This thesis makes contributions in the impact of radio shadowing in V2V communication based on an experimental and a simulative evaluation, especially at urban intersections. The objectives followed within this thesis are briefly described in the following:

ANALYSIS OF URBAN INTERSECTIONS: In contrast to highway scenarios with a frequent availability of Line-of-Sight (LOS) between vehicles, the communication performance at urban intersections is directly linked to the type and intensity of obstruction characterized by the distribution of surrounding buildings. Moreover, from the driver perspective, the presence of buildings around intersection has been identified as factor influencing the accident risk. To gain insight into the building distribution, we provide a detailed analysis of intersection types at some selected Europeans cities. To reinforce the motivation behind the potential of VANET, we provide a survey of accident statistics and critical scenarios specific for city intersections. By taking the influence of traffic on co-channel interference into account, we evaluate the traffic density and behavior at signalized and non-signalized intersections.

EVALUATION OF BUILDING SHADOWING: Based on the characteristics of intersection type implying that a portion of message transmissions will be susceptible to frequent interruptions due to building obstruction, we provide an analysis of main factors influencing the V2V radio propagation and thus the communication performance at urban intersections. For this purpose, we present and discuss results obtained from a measurement campaign performed at four different urban intersections under Non-Line-of-Sight (NLOS) conditions. We further determine reliable communication ranges associated with different intersection characteristics, as insight into these ranges constitutes an important metric for V2V collision avoidance applications.

EVALUATION OF VEGETATION SHADOWING: Similar to building shadowing, obstructions caused by clusters of trees, plants and high bushes may introduce an additional loss component to the overall path loss. One interesting open question in the context of radio shadowing is how severe the signal attenuation due to vegetation affects the performance of V2V. This thesis presents to the best of our knowledge a first contribution to a better understanding of this aspect. We investigate based on measurements the impact of vegetation under varying conditions with respect to intersection layout as well as vegetation type and structure. There, our focus is on understanding the influence of foliage on signal propagation by comparing measurements conducted in summer and winter under a leaf and leafless vegetation type, respectively. In addition, a parametrized vegetation-induced loss model is proposed after a comparison with well-known empirical models found in the literature. This model could be then integrated in further simulation platform in order to consider the non-negligible impact of vegetation on communication performance.

MEASUREMENT-BASED ANALYSIS OF CO-CHANNEL INTERFERENCE: The scalability issue is one of the big challenges that V2V have to deal with. We investigate based on field test experiments the impact of buildings on co-channel interference. To deal with the logistic issue and the post-processing of data during large scale measurements involving a high number of vehicles, we present an abstraction method by which a single vehicle is used to emulate a set of vehicles. To evaluate the impact of buildings on the severity of interference, we conduct a measurement campaign at two different intersections under LOS and NLOS conditions.

COMMUNICATION AND PROPAGATION MODELS FOR VANETS: To ensure applicability of the simulation results for prospective cooperative safety applications, we proposed simulation models for V2V communication following the dedicated ITS-G5 currently developed. On the top, an ITS-G5 conform protocol stack from the application layer up to the physical layer is scrupulously modeled under the simulation tool OMNeT++. Moreover, we proposed a dedicated urban propagation model based on measurements designed to reflect radio propagation on urban environments in a satisfactory manner. This model reflects conditions found in reality sufficiently well to be applicable for VANET simulation studies. Since it is demonstrated in research studies found in the literature that propagation models may directly affect the level of accuracy in simulation-based performance evaluations. To be able to investigate realistic urban scenarios, we linked network model and road traffic model together into a common simulation platform. Doing so, we are not only able to ensure interaction between traffic behavior and communication scalability but are also able to analyze communication performance with a high level of realism.

PERFORMANCE OF VANETS AT URBAN INTERSECTIONS: An assessment of the effectiveness of V2V communication by means of simulation is the second most important contribution made in this thesis. We provide a deeper analysis of environment factors as well as communication parameters on the communication quality by focusing on intersection scenarios. We particularly concentrate on the influence of intersection types on the communication performance. By taking the influence of traffic density and communication parameters into account, we examine if packet latency under varying conditions with respect to intersection types and vehicle positioning would fulfill V2V application requirements.

1.4 OVERVIEW OF THE THESIS

This thesis addresses the above research questions. The structure of this thesis and the main contribution is illustrated graphically in Figure 3.

Chapter 2 presents the scope and background of the thesis in greater detail. The chapter allows to gain a broader understanding of goal and objectives of V2V communication. After an overview of the protocol stack dedicated to vehicular communication, a detailed presentation of each layer is presented. Then road traffic applications based on V2V and their requirements are introduced. Afterwards, methodologies often used to evaluate vehicular networks are demonstrated. The subsequent sections then provide a survey on radio propagation models. An overview of related works on the performance evaluation of V2V communication, highlighting methodologies (experiment and simulation) mostly used for the eval-

uation is also given.

Chapter 3 investigates and classifies the intersection topologies in term of intersection type according to the number of intersection corners occupied by buildings. The classification in the means of distribution of intersection types is performed based on real data sets of some selected Europeans cities. We survey critical intersection scenarios specifically targeted at urban intersections following by a sketch on the intersection stopping distance required for the operation of safety-based applications. An analysis of the traffic density in term of a maximum number of vehicles at a signalized urban intersection concludes this chapter.

After Chapter 3, the thesis is split into two parts. While the first part covers a measurement-based evaluation of V2V communication, the second part deals with a simulation-based approach by evaluating environment factors and communication parameters on the network behavior under consideration of scalability issue introducing interference.

Part I of this thesis is divided into three chapters and begins with the **Chapter** 4. This chapter presents and discusses results from practical field trials at five different urban intersections under NLOS conditions. Hereby, Received Signal Strength Indication (RSSI) levels, Packet Delivery Rates (PDRs), which reflect the ratio between the numbers of successfully received and transmitted frames, and reliable communication ranges associated with different intersection characteristics, such as building density and development, street and intersection width, are quantified.

Chapter 5 assesses and quantifies the impact of vegetation on V2V communication performance in terms of received power levels and packet delivery rates under varying conditions with respect to vehicle positioning, intersection layout and vegetation types. The investigation relies on a profound measurement campaign at three intersections aiming to capture the signal attenuation caused by different type of foliage. Toward these objectives, the measurements for each intersection were conducted both in summer and in winter, which allows comparing the impact of leaved and leafless vegetation. The subsequent sections propose a site-specific vegetation path loss model based on measurements and compare its performance with three well-known empirical models for vegetation-induced path loss.

In **Chapter** 6, the effect of co-channel interference through real-world measurements is presented. Besides the presence of numerous mobile and static obstacles, the natural and non-negligible co-channel interference is of major interest as safety-based applications rely on the single-hop broadcast of status information shared on a single channel. This motivates the following section which presents a detailed investigation of the influence of building shadowing on the severity of interference. For this purpose, an approach aiming to overcome or to facilitate the logistic issue during measurement campaign is proposed. The remainder of the chapter focuses on the discussion of measurement results from field trials, by particularly focusing in gaining insights into the complex inter-dependencies between radio shadowing, interference and communication performance.

Chapter 7 features the main contribution of the second part of this thesis: a simulative evaluation of the performance of V2V communication. To investigate the impact of interference in a realistic environment, we performed in this chapter an evaluation of V2V communication performance based on a detailed simulation study. The chapter introduces the hybrid simulation platform used for the evaluation, which is composed of a network traffic and a microscopic road traffic simulator and presents detailed models used by focusing in particular on the PHY and MAC layer modeling. A dedicated urban intersection propagation model, especially for urban intersections, is proposed in subsequent sections. The remainder of the chapter relies on the assessment of environment factors such as the intersection type and penetration rate as well as the analysis of the influence of communication parameters on the communication performance. Due to the stringent application requirement in term of latency of received messages, we evaluate the end-to-end delay and message age under different intersection layouts and communication parameters. In the next step, we deal with the problem of packet collision by differentiating collisions caused by the Carrier-Sense Multiple Access with Collision Avoidance (CSMA/CA) mechanism from those caused by the hidden node problem.

Finally, **Chapter** 8 concludes the two parts of this thesis, provides a unifying statement about the effective capability of V2V communication at urban intersections and discusses directions for further research.

Chapter 2

Background and Related Work
V2V communication, reference protocol stack,
evaluation methodology

Chapter 3

Analysis of Urban Intersections
Classification of intersection types, critical in-
tersection scenarios, queue length at signalized
intersections

Part 1

Measurement-Based Evaluation

Part 2

Simulation-based Evaluation

Chapter 4

Evaluation of Building Shadowing
Measurement campaign, NLOS condi-
tions, impact of intersection topology,
building density and width

Chapter 7

**Performance Evaluation of Vehicular
Networks**

- Simulation study
- Communication modeling
- Radio propagation modeling
- Combined simulation plattform
- Analysis of environment factors
- Sensitivity analysis of communica-
  tion parameters
- Evaluation of message latencies
- Classification of packet collisions

Chapter 5

Evaluation of Vegetation Shadowing
Measurement campaign, vegetation
obstruction, impact of seasonal effect,
vegetation-induced loss model

Chapter 6

**Evaluation of co-channel Interfer-
ence**
Measurement approach, influence of
co-channel interference, relation between
building shadowing and interference

Figure 3: Detailed overview of the thesis.

BACKGROUND AND RELATED WORK

The benefit and potential of the communication between vehicles (V2V) and between vehicles and infrastructures (V2I) have been well confirmed by the rapid proliferation of consortia involving vehicle manufacturers, research organizations, telecommunications industry, and various government agencies. One can cite the European Car-2-Car Communications Consortium (C2C-CC) or the Vehicle Safety Communications Consortium (VSCC) funded by the United States. To harmonize and facilitate the deployment and advancement of V2V networks, the ETSI has proposed a communication architecture that each ITS station has to implement in order to ensure interoperability between different V2V systems manufacturers. The communication layers architecture standardizes protocols, interfaces and defines the interaction between core components. Besides concepts and background on V2V, this chapter provides a description of functional blocks of the reference architecture by particularly focusing on parts that have been adopted for the deployment of the V2V communication technology. Subsequently, following sections present the reference protocol stack of an ITS station that serves as a basis building block for V2V networks in Europe. Similar to the ISO/OSI reference model, the protocol stack of communication proposed by ETSI follows a layer structure. As we assess the performance of the V2V communication, basics on methodologies mostly used in the evaluation of vehicular networks are provided. The remainder of this chapter provides an overview of related work that investigates vehicular networks in field tests and by means of simulation.

2.1 REFERENCE PROTOCOL STACK

V2V communication enables a wireless communication between mobile ITS stations, and between mobile ITS stations and fixed ITS stations (roadside installations), with single-hops or multiple hops between the source and destination ITS stations. Mobile and fixed ITS stations refer to vehicles and roadside infrastructure, respectively. In the context of safe and efficient transportation of humans and goods supported by communication technologies, ETSI has proposed the architecture of communications supporting a variety of existing and new access technologies and applications. A simplified version of an ITS station reference architecture specified in [10] as depicted in Figure 4 basically follows the ISO/OSI reference model and defines three horizontal protocol layers, two vertical protocol entities and the ITS applications on top [11]. Moreover, the access to public and private networks including the global Internet can be also provided by ITS applications.

Following a top-down approach, the applications and facilities blocks represent the application, presentation and session layers, which corresponds to OSI layers 7 through 5. The networking and transport block represents the transport and network layers together, and therefore, corresponds to OSI layers 4 and 3. The last horizontal access block represents the data link and physical layers, which corresponds to OSI layers 2 and 1, respectively. The left, and right block shows the
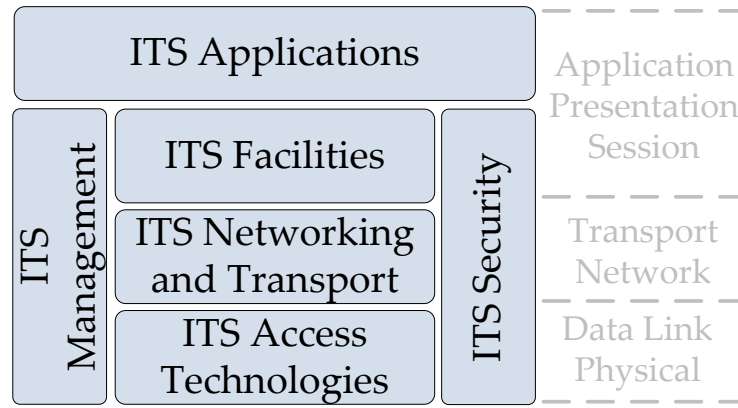
Figure 4: Protocol stack of an ITS station.

management functions and security, respectively, which reside outside the communication protocol suite. The purpose of the management block is to configure an ITS station and also responsible for the cross-layer information exchange among the different layers and other tasks. The security entity is responsible for security and privacy services, including secure messages at different layers of the communication stack, management of identities and security credentials, and aspects for secure platforms.

In the following, we present in detail the purpose of each block of the protocol stack of an ITS station considering a bottom-up approach, that is, by beginning at the physical layer and working its way up to the application layer. As the management and security blocks are out of scope in this thesis, we concentrate on horizontal layers considering that the evaluation presented within this work was performed without any mechanisms used to encrypt or/and authenticate messages.

2.1.1 *ITS Access Technologies*

The ITS access technologies block group the two lowest layers, physical layer, and the data link layer. Besides several communication media, it comprises also related protocols for the physical and data link layers. The access technologies block includes various types of media based on wireless communication for external communication (for example with other ITS stations) such as *ITS-G5*, conventional wireless LAN technologies based on *IEEE 802.11a/b/g/n* and cellular radio technologies such *GPRS, UMTS, LTE* as illustrated in Figure 5. *Bluetooth* could also be used for exchanging data over short distances between ITS stations. For communication among internal components inside of an ITS station, *Ethernet* technology using wired transmission links such as twisted pair and/or fiber optic is an option.

802.11p and ITS-G5

To enable the communication between ITS stations, the specific requirements of inter-vehicular wireless communication have been incorporated into the well-known *IEEE 802.11* [7] by the standard amendment *IEEE 802.11p* [8]. However, since
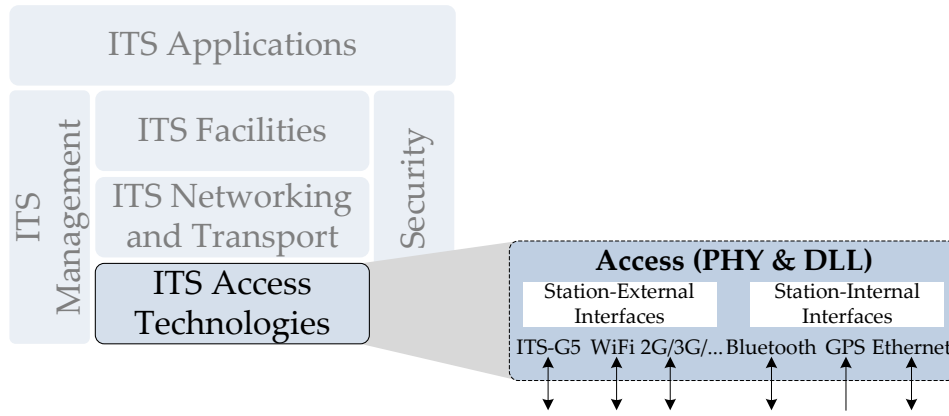
Figure 5: Overview of the access technologies block.

March 2012 a new version of the IEEE 802.11 called *IEEE 802.11-2012* containing all approved amendments produced between 2007 and 2011 including *802.11p* was compiled by the IEEE [12]. Hence, the former *802.11p* amendment is then classified as superseded. In Europe, both standards *IEEE 802.11-2012* and *ANSI/IEEE Std 802.2* [13] lead to the so-called *ITS-G5*, which is being standardized by ETSI group for ITS (ETSI ITS). Within the European Union, 70 MHz of spectrum between 5855 MHz and 5925 MHz has been allocated for data exchange between mobile ITS stations without prior network set-up to form a so-called Cooperative Intelligent Transport Systems (C-ITS) [14]. In order to cover different types of applications, the 70 MHz bandwidth is structured into six *service channels* and one *control channel* with a guard band of 5 MHz between channel as illustrated in Figure 6.
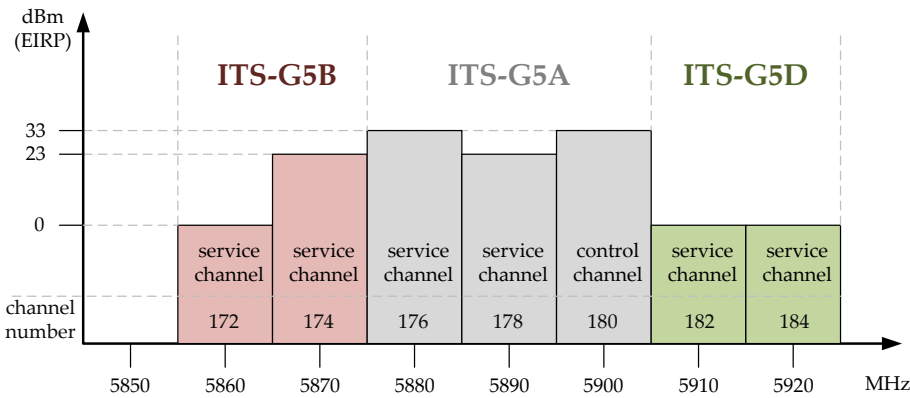
Figure 6: Maximum limit of transmission power for each channel type in ITS-G5A, ITS-G5B, and ITS-G5D [14].

To reduce adjacent-channel interference caused by the non-linear behavior of the transmit stage, a guard band of 5 MHz between channels is introduced. While the exchange safety-based information is restricted on *control channel* over channel number 180, non-safety-related information used the *service channel* for data transmission and reception. According to the type of application, the *ITS-G5* bandwidth is divided into four frequency bands. The *ITS-G5A* and *ITS-G5B* bands are dedicated for safety and non-safety-related applications, respectively. *ITS-G5C* is dedicated for broadband radio access networks (BRAN), radio local area network

(RLAN) and WLAN, and occupies the range 5470-5725 MHz at the bottom end of the spectrum. The *ITS-G5D* frequency band is reserved for future usage of ITS road traffic applications. In order to ensure robust communication in the context of the highly dynamic vehicular environment, which requires short life communication duration, 802.11p introduces several modifications to the physical (PHY) and MAC layers. The 802.11p PHY is inherited essentially from IEEE 802.11a but operates in a 10 MHz bandwidth instead of the usual 20 MHz. Doing so, the capability to be robust against challenges of V2V communication such as the high dynamic of nodes or the multi-path propagation effect, is provided. The change in channel width implies a doubling of all relevant timing parameters as provided in Table 1. This is also known as *half-clocked* operation, which doubles timing parameters associated with the Physical Layer Convergence procedure (PLCP). Particularly, the work in [15] demonstrated that increasing the symbol guard interval enables the possibility to decrease RMS delay spread.

Table 1: Timing parameters comparison between 802.11a and 802.11p.

PARAMETER	802.11a	802.11p
Number of subcarriers	52	52
FFT period [µs]	3.2	6.4
Preamble duration [µs]	16	32
OFDM symbol duration [µs]	4	8
Guard duration [µs]	0.8	1.6
Training sequence duration [µs]	8	16

The 802.11p PHY is based on the Orthogonal Frequency Division Multiplexing (OFDM) modulation scheme where the overall transmission bandwidth is subdivided into 52 sub-carriers of which 48 are reserved to carry data on parallel data streams. These sub-carriers also known as carrier signal are said to be orthogonal to each other, and are modulated using binary or quadrature phase shift keying (BPSK or QPSK) or using 16- or 64-quadrature amplitude modulation (16-QAM or 64-QAM). Although sub-carries overlap in frequency domain, they do not interfere with each other due to the orthogonality of chosen sub-carrier frequencies. Forward error correction coding is used with a coding rate of 1/2, 2/3, or 3/4. This means that depending on the chosen coding rate, a high number of redundant bits is incorporated in the transmitted data stream allowing the correction of corrupted bits during the reception process. One of the advantages of OFDM is that each sub-carrier only experiences flat fading even if the overall spectrum suffers from severe frequency-selective fading due to multipath propagation of the signal. The flat fading nature subjected by sub-carriers allows a simple channel equalization at the receiver side. The OFDM system provides in 802.11a a communication with data payload rate capabilities of 6, 9, 12, 18, 24, 36, 48, and 54 Mbps, whereas the support of transmitting and receiving at data rates of 6, 12, and 24 Mbps is mandatory. Recalling that due to its 10 MHz wide channel, the 802.11p PHY uses a *half-clocked* operation with data rates in half range from 3 Mbps to 27 Mbps. Whereby, 6 Mbps has been identified in [16] to be an optimal data rate when evaluating VANETs under relaxed channel loads.

802.11p MAC

To cope with the rapidly varying environment of vehicular networks, the MAC sub-layer of IEEE 802.11p introduces several modifications compared to the traditional 802.11a MAC protocol. The message exchange within a BSS is administrated by the defined *Outside the Context of a Basic Service Set (OCB)* mode, which allows stations to transmit data frames immediately without prior authentication, association or confidentiality services with a BSS. All nodes are a member of a priori registered BSS. In this way, the management overhead used with the establishment of a network could be easily avoided. Hence, this is especially well-suited for safety-related applications, which cannot tolerate long connection establishment delay prior to the data exchange. In OCB mode, a node transmits and receives on channels known in advance and defined by some regulatory institutions. Another possibility to determine PHY layer parameters or any changes in the operating channel can be achieved through a separate out-of-band communication.

In order to manage the channel access and to reduce the likelihood of packet collision, the 802.11p MAC protocol relies on the Enhanced Distributed Coordination Access (EDCA) and is based on the Distributed Coordination Function (DCF) of IEEE 802.11. It uses the CSMA/CA but with many simplifications in the services and some enhancements in the cross-layer integration and also adds Quality of Service (QoS) attributes. In the context of congestion control, the MAC layer should provide the upper layers with information including the current estimated channel load or received packet statistics.

V2V communication are based primarily on the single-hop broadcast of information within a common channel. However, due to the absence of a central entity capable of regulating the channel access, the CSMA/CA protocol provides a possibility to coordinate access of multiple sending and receiving nodes to a shared broadcast channel. The CSMA/CA is a random access mechanism and follows the principle of *listen before talk* called carrier sensing - a node listens to the channel before transmitting, i.e., the channel is only accessed if it is sensed to be idle - with the goal to minimize the interference in the system, and thus to increase the packet reception probability. When the physical layer observes any activities on it (provided by the Clear Channel Assessment (CCA)), a node then waits a random backoff time chosen from the interval $[0, CW]$ and then schedules the medium access for the duration of the backoff. CW denoted the contention window size and is decremented as the medium is idle. Whenever the countdown reaches zero, the frame is immediately transmitted. It should be noted that the CCA does clearly indicate how exactly a wireless card identifies the channel status, the medium is simply indicated as idle when the measured received power is below a certain threshold. Basically, before transmitting a frame, each node should observe the medium as idle for an amount of time denoted as DCF Interframe Space (DIFS) or Arbitration Interframe Space (AIFS) depending of the mode of operation (DCF or EDCA). Figure 7 illustrates an example for random access mechanism. A node using EDCA shall transmit a frame if the medium is sensed to be idle at the AIFS slot boundary, and the backoff time has expired.

For unicast packets, a binary exponential backoff procedure is applied when no acknowledgement is received. In other words, the Contention Window (CW) is doubled up to at most CW_{max} with every frame collision detected. In this way, the probability of packet collisions would be greatly reduced. However, due to the lack of acknowledgement in broadcast communication, CW in V2V is always set to its
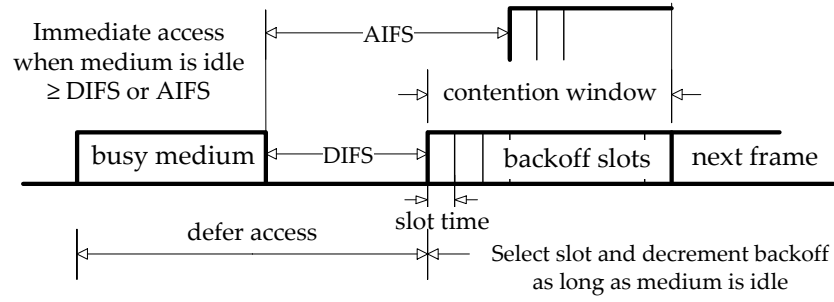
Figure 7: Random access mechanism of IEEE 802.11p MAC adapted from [12].

minimum value CW_{min} and it will never be doubled no matter what the network condition is. This introduced a new challenge that V2V has to deal with. Obviously, an adequate choice of CW will depend on the channel load conditions since if CW is chosen too low, frame collisions might increase under congested network situations. One the other hand, choosing a large value of CW would lead to large delays before frame transmissions even if node densities are considerably low.

Basically, in unicast communications two additional frames Request-To-Send (RTS) and Clear-To-Send (CTS) are used to reserve the medium prior to each data frame transmission. Through this handshake mechanism between transmitter and receiver, packet collisions caused by hidden stations could be partly overcome. A station is declared to be hidden when it is located out of range of the transmitter but close enough to the receiver so that it can disturb any frame transmission between transmitter and receiver. Since the RTS/CTS frame exchange is not used in broadcast environment, the hidden node problem remains a serious challenge in the reliability of V2V-applications. To understand and estimate the impact of hidden stations on V2V communication, a simulation-based analysis is provided in Chapter 7.

Regarding the issue of QoS in VANETs, the MAC layer implements a differentiated queuing scheme according to the priority of the message based on the EDCA mechanism. The EDCA incorporates the IEEE 802.11e amendment by adding QoS to the DCF mechanism with the possibility to set priority to the message according to their urgency. Queues with different AIFS values and CW sizes are maintained by each node for the purpose of giving data traffic with higher priority increased probability to access the channel before data traffic with lower priority. Application messages are therefore mapped to four different access categories (ACs) according to the data traffic types: voice, video, best effort and background. Hereby, voice traffic has the highest priority while background traffic the lowest.

Table 2: Default AIFS values and CW sizes for each access categories in 802.11p.

PRIORITY	TRAFFIC TYPE	AC	CW_{min}	CW_{max}	AIFSN	AIFS
Highest	Voice	AC_VO	3	7	2	58 μs
	Video	AC_VI	7	15	3	71 μs
	Best effort	AC_BE	15	1023	6	110 μs
Lowest	Background	AC_BK	15	1023	9	149 μs

Table 2 gives QoS parameters corresponding to ACs used in EDCA for 802.11p. Different ACs are allocated with different AIFSN. The resulting AIFS is a duration derived from the value AIFSN by the relation

$$AIFS = AIFSN \times T_{slot} + SIFS \tag{1}$$

where AIFSN stands for an integer number and T_{slot} is the duration of a slot time. SIFS and T_{slot} are fixed parameters gathered from the PHY layer. AIFS is calculated according to $T_{slot} = 13\,\mu s$ and Short Interframe Space (SIFS) of $32\,\mu s$. The waiting time also known as channel access time T_{CAT} is the time need for a packet to be served in the queue. It is composed of the time due to AIFS plus the backoff time. Depending on the AC, the time duration due to AIFS is set according to Equation 1. Next, the size of CW is determined, randomly selecting a value between 0 und CW_{min}, hence the contention period equals to $CW \times T_{slot}$. Taking $CW = CW_{min}$ will lead to the upper bound of the channel access time T_{CAT} as depicted in Figure 8. It follows that frames of type voice (AC_VO) have a high chance to access the medium earlier due to the low value of T_{CAT} ($97\,\mu s$) compared to the background traffic type ($344\,\mu s$).
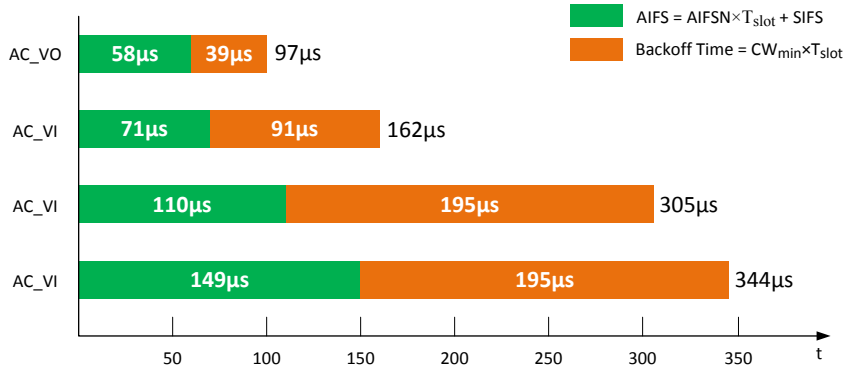
Figure 8: Maximum channel access time T_{CAT} for different access categories caused by contention, considering $T_{slot} = 13\,\mu s$ and SIFS=$32\,\mu s$.

2.1.2 ITS Networking and Transport

The networking and transport layer provides the capability to deliver data among ITS stations as well as from ITS stations to other network nodes. Nodes in the core network could be connected to the Internet and would provide, therefore, the possibility to be connected to servers located in the Internet. ITS network protocols particularly enable a novel addressing scheme that is based on geographical areas. The efficient dissemination of data in geographical regions is assured by intermediate nodes, which use several forwarding algorithms to route data from source to destination. The second role of this layer is to provide the end-to-end delivery of data applied by ITS transport protocols. Depending on requirements of ITS facilities and applications, additional services, such as reliable data transfer, flow control and congestion avoidance, well-suited transport protocols based on connection-less transmission can be implemented. A particular protocol in the ITS network and transport layer is the Internet protocol IP version 6. The usage of IPv6 includes the transmission of IPv6 packets over ITS network protocols, dy-

namic selection of ITS access technologies and handover between them, as well as interoperability issues of IPv6 and IPv4. As illustrated in Figure 9, several different networking modes are identified including GeoNetworking protocol, IPv6 networking with mobility support and other ways of IPv6 networking. Each networking protocol may be connected to a specific dedicated ITS transport protocol or may connect to an already existing transport protocol, e.g. UDP, TCP. As ITS transport protocol, ETSI has proposed the Basic Transport Protocol (BTP) which provides a connection-less transport service similar to UDP. It enables an end-to-end connection in the ad-hoc ITS network without guarantees on the delivery of transmitted packets. It also allows entities running at the ITS facilities layer to directly access the services provided by the GeoNetworking protocol [17].
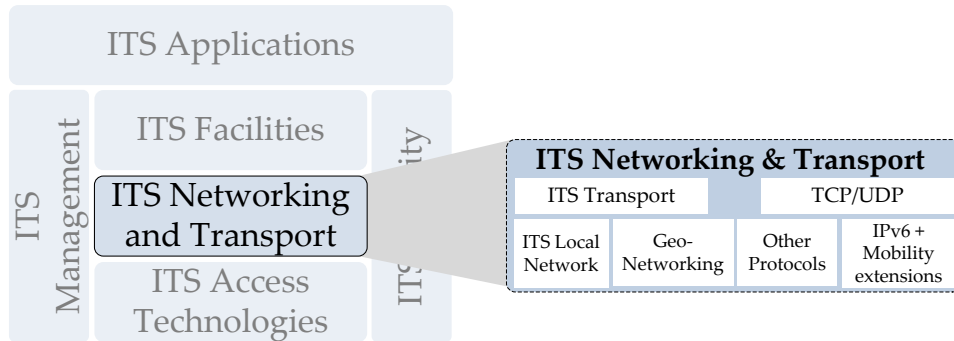
Figure 9: Overview of the ITS networking and transport layer.

Particularly interesting for vehicular networks is the GeoNetworking protocol that sets ad-hoc and multi-hop communication over short-range wireless technologies utilizing geographical positions with the aim to increase the information range. The GeoNetworking protocol enables communication in mobile environments without the need for a central entity or infrastructure for the coordination of the network. Due to the highly dynamic nature of VANET reflected by the varying status of network topology, it provides a well-suited support to heterogeneous application requirements through a rapid multi-hop dissemination of packets in geographical regions. GeoNetworking can send packets to a node by its position or to multiple nodes in a geographical region. This implies that an IP addressing like in conventional networks, where each node is identified by its IP address, is not needed. For the geographical routing aiming to target messages to certain geographical areas, GeoNetworking proposes several forwarding schemes including *GeoUnicast*, *GeoBroadcast*, and *topologically-scoped Broadcast*. For more details on geographical addressing and geographical routing in GeoNetworking, please refer to [18–20]. Furthermore, full details on Internet integration and transmission of IPv6 packets over GeoNetworking protocols can be found in [21].

2.1.3 *ITS Facilities*

The objective of the ITS facilities layer is to provide a collection of functions to support ITS applications while satisfying functional and operational requirements of the defined Basic Set of Applications (BSA) in the application layer. The facilities layer provides data structures to store, aggregate, and maintain data of different type and source (such as from in-vehicle mounted sensors and from data received by means of communication). As for communication, ITS facilities enable various

types of addressing to applications, provide ITS-specific message handling and support establishment and maintenance of communication sessions. An important facility is the management of services, including discovery and download of services as software modules and their management in the ITS station. The general functional architecture of the facilities layer as illustrated in Figure 10 enables facilities, which can be of one of the following types: application, information or communication support.
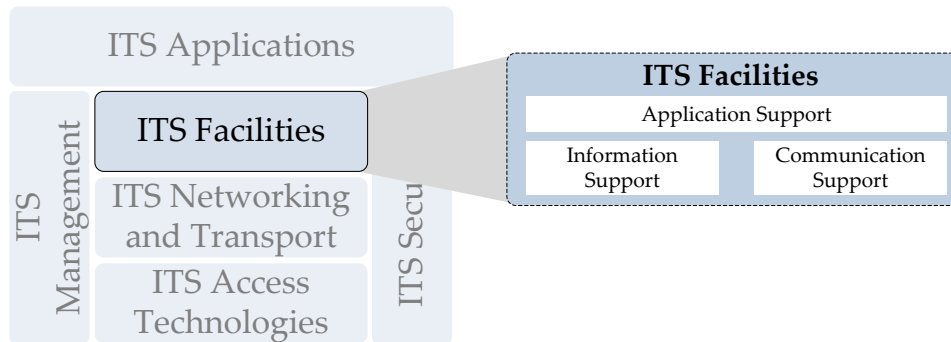
Figure 10: Overview of the ITS facilities layer.

The application support facility supplies the BSA with common services and functionalities for their execution. Particularly interesting for this thesis are the Decentralized Environmental Notification (DEN) and the Cooperative Awareness (CA) basic service, which are responsible for the processing of Decentralized Environmental Notification Messages (DENMs) and Cooperative Awareness Messages (CAMs), respectively. Furthermore, this facility provides support for the data exchange between running applications and Human Machine Interface (HMI) devices. The information support facility assures the maintenance of Local Dynamic Map (LDM) database and management of the database produced by local sensors installed around or/and inside the vehicle. The communication support facility determines the addressing mode for messages according to the dissemination destination as being used by the ITS networking and transport layer protocol.

CA and DEN basic services are mandatory facilities for each kind of ITS station and are responsible for generation, transmission and receiving of messages in the network. As its name suggests, Cooperative Awareness Messages (CAMs) are messages exchanged between vehicles in order to create and maintain a certain awareness of each other enabling a cooperation between road traffic participants. Depending on type of the ITS station (vehicle or Road Side Unit (RSU)), status information such as time, position, motion state, etc. and the attribute information includes data about the dimension, station type and role in the road traffic, can be disseminated. CAMs are generated periodically with a frequency controlled by the CA basic service in the originating station. In the course of message transmission, vehicle's status information is constructed according to a specific format and forwarded to the networking and transport layer. The generation frequency is determined according to the change of vehicle's status, e.g., change of position or speed, and broadcasted within the direct communication range also know as single-hop. The time interval between two consecutive message generations is limited to an upper and lower bound ranging between 1000 ms and 100 ms corresponding to a message generation rate of 1 msg/s and 10 msg/s, respectively. It should be noted that due to the single-hop broadcast, the communication range may be influenced

by the transmission power. Whenever a CAM is received, the CA processes the received CAM information and dispatches its content to ITS applications running at application layer on the receiving station. For more details on the generation trigger conditions, reception management and general structure of CAMs, please refer to [22].

Similar to the processing of the CAM, the DEN constructs, manages and processes a DENM. Its construction is triggered by an ITS application depending on the use case. However in contrast to CAMs, the construction of a DENM is triggered by an application. Upon detection of a dangerous situation (e. g. road hazard or abnormal traffic conditions) by the originating station, a DENM including information such as type, the position, a detection time and eventually the time duration of the event, is generated and forwarded to networking and transport layer to be transmitted. Since the DENM is not periodically generated, its termination is either automatically achieved by the originating station once the event disappears or after a predefined expiry time. In both cases, special messages called *cancellation* and *negation* DENM are used to inform other stations about the abortion of the event. On the receiving side, a station which received a DENM processes the information and may decide to present an appropriate warning or information to the user, as long as the received information is relevant. It should be noted that DENM may be forwarded by intermediate stations in order to extend the information range in order to reach stations which are not located in the direct communication range of the originator. However, the forwarding is accomplished by the networking and transport layer using the GeoNetworking protocol. Full details on trigger, update, repetition, and termination of the DENM as well as on its structure and message content can be found in [23].

2.1.4   *Vehicle-to-Vehicle based Road Traffic Applications*

In order to harmonize the deployment of applications, ETSI has standardized a so-called "Basic Set of Applications" for future C-ITS [9]. These applications considered as *Day one applications* were selected by stakeholder based on a set of criteria including strategic, economical and system capabilities aspects. The deployment of *Day one applications* was expected to be completed within a three-year time frame after the validation of the standardization and following with a market introduction for the period 2012 to 2015. Thereby, three classes of applications have been distinguished: Road traffic safety, traffic efficiency and other applications.

Road Traffic Safety Applications

The principal objective of safety-based applications is the improvement of road safety by supporting the driver in critical situations. Basically, modern vehicles are equipped with safety systems such as Anti-Blocking System (ABS) and Electronic Stability Program (ESP), which are designed to help the driver maintain some steering ability and allow steering while maximizing braking. Since November 2014, both systems are available as standard equipment in all new passenger cars model series in Germany. Nowadays, Adaptive Cruise Control (ACC) is the most prominent driver assistance safety system in term of comfort and safety. It provides the capability to follow a vehicle in front while automatically continually adjusting the speed to maintain a safe longitudinal distance from vehicles ahead. Besides the aforementioned system, there are numerous ADAS developed and be-

ing developed with the objective to adapt and enhance vehicle system by assisting the driver in critical and dangerous situations. In this way, a driver's behavior is passively or actively assisted such that he enjoys a safe and comfortable driving and hence avoids potential collisions and accidents. All these safety systems rely on information gathered from on-board sensors installed in or around the vehicle that measure physical and dynamic values like acceleration, steering wheel angle, distance, and speed. However, an efficient and complete monitoring of vehicle's surrounding requires sensor systems allowing to detect objects or vehicles located far away. Sensors utilized in ADAS such as radar, laser radar or cameras have a limited detection range of around 200 m, which may depend on traffic conditions and the road topology [24]. Although, these sensors provide a high accuracy in term of object detection, their performance is strongly weather-dependent and are additionally limited by high costs. V2V communication technology coupled with ADAS may open up a wide range of road safety applications for next-generation vehicular traffic. In this context, ADAS could exploit V2V to extend the driver's horizon through the exchange of status information and hence ensure a certain cooperative awareness between vehicles and their neighborhood. Vehicles in the surrounding can serve as additional mobile sensor as they can share their own local vehicle dynamics and position to give knowledge about their presence and status. As for instance a vehicle, which detect slippery roadways or pothole, can be shared among vehicles located in a common communication range. When receiving such kind of information, relevant vehicles can predict a potential and imminent collision by continuously monitoring their actions and the position and behavior of all other surrounding vehicles.

To evaluate requirements and performance of safety applications, we divided applications proposed in the BSA catalog into two main groups with regard to the region of a crash on the vehicle: longitudinal and lateral collision warning. Longitudinal collision refers to the collision between vehicles at any part of the front or rear side of the vehicle. From an *ego vehicle* point of view, we distinguish two types of longitudinal collisions: *Forward and rear-end collision* which may occur when the *ego vehicle* detects a risk of a collision with a forward vehicle or an obstacle in its trajectory, whereas *frontal collision* refers to situations where at least two vehicles-inclusive the *ego vehicle* - moving in opposite direction detect the risk of collision between themselves. The lateral collision describes a collision between any vehicle at any part of the *ego vehicle* side. It includes collisions due to lane change or overtaking maneuver but also collisions between vehicles entering an intersection as well as on a crossing roadway belong to this group. Table 3 presents a very short selection of safety related applications according to the type of warning as identified in various European research projects and ITS organizations.

Regarding application reliability of safety applications, the standard has specified for all aforementioned applications a message generation rate of 10 msg/s and a maximum latency of 100 ms. It should be noted that the latency mentioned here is determined as the time difference at which the vehicle data is available at the vehicle electronic systems and the time at which the warning is presented on the receiving vehicle HMI or at which a direct action is performed e.g. brake, change or keep lane. It is also known as end-to-end delay. Moreover, a communication range between 100 meters and 400 meters should be available so that the driver

has enough time to intervene and avoid a crash. In addition to wireless communications, object detection sensors which rely on ADAS might be used to identify vehicles that are not equipped with a communication system. One important challenge in the efficient operation of safety applications is the vehicle positioning performance. Safety applications such as Forward Collision Warning (FCW) or Lane Change Assistance (LCA) require 50 cm to 1 m accuracy of positioning method so that false alarms or missed detection could be eliminated or reduced during the path planning and prediction [25]. Although, Global Positioning System (GPS) is the mostly used technology for vehicle localization, a fusion of methods including MAP matching or RTK system could also be exploited to enhance the vehicle positioning.

Table 3: Some safety applications and theirs collision warning type from [9].

COLLISION TYPE	APPLICATION	DESCRIPTION
LONGITUDINAL	Forward Collision Warning (FCW)	Avoid or mitigate a risk of forward or rear-end collision in the same lane.
	Emergency Electronic Brake Lights (EEBL)	Inform a severe braking to local followers on the same lane.
	Stationary Vehicle Warning (SVW)	Alert approaching vehicles of the risk of collision with vehicles dangerously immobilized on the road.
	Traffic Condition Warning (TCW)	Alert approaching vehicles of the risk of collision with vehicles at the end of traffic jam.
LATERAL	Overtaking Vehicle Warning (OVW)	Inform overtaking maneuver to concerned vehicles to secure the overtaking action.
	Lane Change Assistance (LCA)	Inform a lane change intention to vehicles on neighboring lanes.
	Cooperative Merging Assistance (CMA)	Negotiate the merging process together with involved vehicles to avoid collision.
	Intersection Collision Warning (ICW)	Alert vehicles entering the intersection of the risk of collision with other vehicles.

Traffic Efficiency

The aim of traffic efficiency applications is to improve the traffic flow by exchanging traffic information between traffic management central and drivers on the road network. Traffic conditions based on information collected by the traffic infrastructure provider could be delivered to drivers in the way that they are permanently informed about expected delays or better routes that should be used to circum-

vent the traffic congestion. Consequently, traffic participants benefit from shorter travel times and road operators benefit from reduced expenses to maintain the roadways. A particular interesting traffic efficiency application is Green Light Optimized Speed Advisory (GLOSA), which enables a higher driving comfort to driver approaching an intersection. GLOSA provides a capability to a traffic light equipped with a communication system to periodically broadcast its timing data in order to allow the driver to adapt its speed according to current traffic state and timing. This will result to less stopping on roadways and thus to an increasing traffic flow and a reduction in fuel consumption and CO_2 emission as demonstrated in [26] and [27].

Other Applications

Besides safety and efficiency applications, the last category typically named *other applications* covers all type of applications which do not belong to the safety or efficiency. These applications include services related to Infotainment, comfort and vehicle or service life cycle management. Most of these applications require at least an RSU to access local services provided within the ITS network infrastructure from providers in the wider Internet. As part of *other applications*, one can cite *media downloading* providing the capability to access, purchase, or download multimedia content from a dedicated website over a local RSU connected to the Internet. The *automatic access control/parking access* facilitates vehicle access to controlled areas by supplying its identity to the RSU in order to obtain the right to access the area.

A complete list of traffic efficiency and *other applications* can be found in detail in [9].

2.2 METHODS FOR PERFORMANCE EVALUATION

Despite providing a profound knowledge about the behavior of each component, the performance evaluation is a major step in the design and the development of a system. The evaluation of communication systems requires in addition to an understanding of newly developed protocols, a detailed comprehension of architectures and algorithms and should provide as results a visualization of their component in macro as well as in micro level. Especially for VANETs, the complete environment addressing a mix of road traffic and communication systems introduce a new challenge for protocol designers in the estimation of the effective performance of the network. Basically, the performance evaluation of a communication system is achieved by applying three different methodologies including a mathematical analysis, experiments based on field test measurements and/or simulation techniques. All these methods have their strength and weakness.

2.2.1 *Mathematical Analysis*

The mathematical analysis could be defined as the use of an appropriate process to split a problem into a series of elements easy to understand and thus to solve mathematically. Each element is represented whether with exact phrases or with equations. While a mathematical analysis produces a way to get knowledge about upper and lower bounds of a specific research question on a system, a more fine-

grained analysis requires a lot of equations which are sometimes hard to catch. It is then obvious that complex problems would require not only a dozen of equations but also a wide range of relationships between them.

The goal of the evaluation of VANET is to get a clear statement about the effective performance of the communication through the network. This can be deduced from the nature of information exchanged between traffic participants, thus from the capability of a safety application to inform drivers in dangerous situations. In this context, performance key indicators used to analyze the performance of VANETs need to be defined in advance. One of these indicators is the probability of packet reception, recognized as the most used metric when investigating the communication quality inside the network. The probability of packet reception can be defined as the ratio of the number of received packets and the number of transmitted packets from a specific node during a considered time interval. This quantity is directly related to the communication parameters including transmission power, sending rate as well as the network load or conditions. Furthermore, finding this measure also requires vehicle dynamics and thus a micro-level driver behavior modeling. Bianchi did a pioneer work and was the first to derive a model that incorporate the channel access mechanism in 802.11 as a two dimensional Markov chain to analyze and quantify the throughput in saturated 802.11 WLAN [28, 29]. Works in [30–34] extend the Bianchi's model by considering the accurate specifications of the 802.11p standard including the EDCA mechanism and the effect of hidden nodes under saturated and non-saturated network conditions. However, all of these models rely on many assumptions for the sake of simplification which may lead to inaccurate results in the performance analysis.

(a) 1-D topology
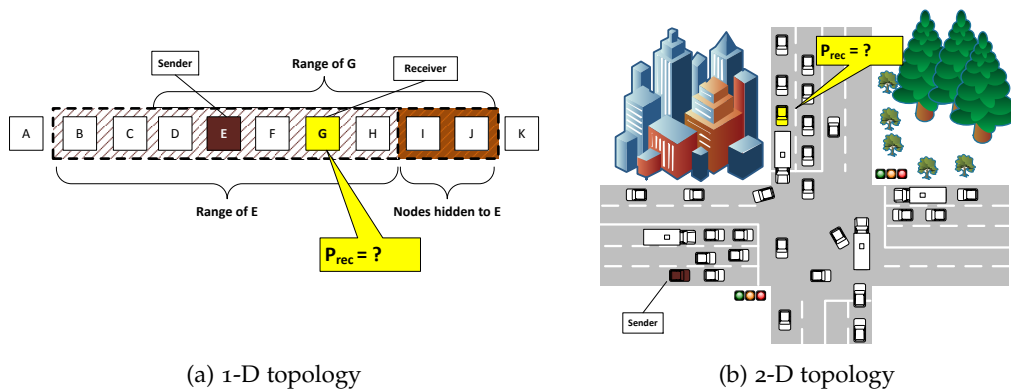
(b) 2-D topology

Figure 11: Modeling the probability of packet reception in 1-D linear topology and a city intersection.

For illustration, let us consider as an example a linear topology and a city intersection scenario as depicted Figure 11. The objective here is to derive the probability of packet reception according to the broadcast mode of VANET. For this purpose and to facilitate the modeling, a network topology could be approximated to a line with nodes uniformly distributed over it. With this abstraction, the probability of reception experienced, for instance, by node G from the sender E considering the location of hidden nodes as well as contending nodes, could be then derived. However, in case of a city scenario characterized by a 2-D topology which reflects a

more realistic use case, additional to aforementioned aspects, the radio shadowing effect should also be considered in the modeling process.

A common measure in modeling packet reception in VANETs is the knowledge about the effective number of contending nodes at any time and location. While the problem statement in a 1-D network topology may lead to an accurate estimation knowing the traffic density, this would be intractable in urban environments reflected by shadowing through buildings, vegetation and other vehicles and heterogeneous node patterns. Moreover, the time factor due to the mobility of nodes and the rapidly changing network topologies, the characteristics of propagation environment, and the requirements of specific applications in VANETs introduce an additional dimension of complexity in the determination of number of contending nodes N, which can be expressed as

$$N(t) = f(R, v(t), \rho(t))$$

where R represents the effective communication range, $v(t)$ the average vehicle speed in the considered region and $\rho(t)$ is the traffic density, which may vary with time of day, and hence depends on the traffic condition.

Taking the unique characteristics of VANETs into account, an adapted performance model would be difficult and very challenging to develop since all major factors affecting the communication performance should be taken into account. This is more desirable but will lead to complexities that will make the mathematical model almost intractable.

However, after a derivation of equations and formulas, mathematical analysis provides a performance bound of a given system based on assumptions which facilitate the examination of a problem statement. Moreover, the variation of model's parameters of a model would allow to evaluate and weigh the scalability of the considered system.

2.2.2 *Field Test Measurements*

An accurate evaluation of communication systems requires real hardware prototypes in field test experiments to measure and experimentally judge their performance. Measurements allow objective statements on the basis of reproducible experiments. An experimental evaluation of VANETs demands not only communication systems but also real vehicles and drivers. Even if communication systems based on hardware prototypes are available, a specific problem statement requiring a dozen of vehicles would be hard to realize. One of the main difficulties in conducting real-world measurements is the logistic issue during experiments. The high mobility of traffic participants and the presence of uncontrolled phenomena such as rain or snow require time and people for a proper planning and implementation of measurements. Additionally, one up to two persons per involving car as well as measurement managers are needed during the evaluation.

However, experiments are often used to develop propagation models which can then be integrated into a simulation environment in order to perform large scale simulation studies involving thousands of vehicles and communication systems.

2.2.3 *Simulation Technique*

Although experimentation plays a principal role in the computer network by allowing the quantification of the performance of a system under realistic conditions, the experimental evaluation of VANETs based on hardware prototypes is very expensive. Moreover, experiments are hard to reproduce in a controlled environment. All aforementioned challenges make, therefore, simulation very attractive by allowing an objective basis of performance evaluation based on the reproducibility of results and the capacity to explore a large range of scenarios in a reasonable amount of time.

However, simulations are based on models developed in advance. The modeling in micro level is very challenging since abstraction errors of the modeling process will lead to inaccurate results during the performance evaluation. Furthermore, as simulating VANET requires the consideration of two parallel research contributions, a detailed modeling procedure of each system component as its implementation is a very complicated task. It requires interdisciplinary knowledge about road traffic engineering and communication technology. However, due to considerable research efforts in the past few years, a set of simulation frameworks based on the coupling of existing simulation tools on road traffic and network are available in the research community.

2.3 RELATED WORK

The past decade has seen a surge of research activities and projects conducted worldwide aiming to estimate the potential benefit of V2V communication. This section will give an overview of related works that evaluate V2V communication based on field test campaigns. Furthermore, we review related work dealing with simulation studies in vehicular networks.

2.3.1 *Measurement Campaigns*

Motivated by the understanding and quantification of channel characteristics of V2V communication, numerous measurement campaigns have been carried out recently. The work in [35] is one of the first real-world V2V measurements in a roadway environment. Although the authors performed RF experiments at 900 MHz, obtained results give an insight into the measurement-based evaluation of V2V communication and its channel characteristic. In [36], the authors studied the fading distribution of the inter-vehicle transmission at 5.2 GHz in four different environments (urban, suburban and highway). To evaluate the impact of environmental factors, experiments with traditional IEEE 802.11b WiFi cards carried out in varying vehicular traffic densities, and scenarios were presented in [37]. As radio standard WiFi chipsets are widely deployed, results from a measurement campaign with off-the-shelf WiFi hardware is presented in [38]. Hereby, the performance of V2V based on three mostly used IEEE802.11a, b, and g standard were investigated and compared. To gain insight into the Doppler problem in V2V, the work in [39] presents measurements of joint Doppler-power profile made at 2.4 GHz in various multipath environments. To understand propagation channel characteristics including path loss, power-delay profiles, and delay-Doppler spectra, a similar measurement campaign using vehicles traveling at high speed on a highway were

performed in [40]. Results of a channel measurement and modeling campaign for the vehicular communication at 5.1 GHz using a wideband (50 MHz) sounding signal are presented in [41]. The authors described nonstationary channel features such as delay spread, multipath component and frequency correlation estimates based on data collected in various cities and on highways. In order to provide a characterization of propagation channels for collision avoidance warning applications, the measurements reported in [42] show that the radio channel in such scenarios is influenced by scatterers such as traffic signs, trucks, and bridges.

Although significant insight into channel characteristics of V2V communication is provided, all measurement studies presented above have been conducted at frequencies outside the 5.9 GHz. Multipath fading and obstruction by mobiles and stationary obstacles might depend on the frequency. This motivated measurement campaigns performed at 5.9 GHz band under realistic driving conditions and presented in [43–45]. Moreover, due to the unavailability of prototypes for V2V radio, the above-mentioned works used measurement equipment such as channel sounders, signal generator or commercial WiFi chipsets.

In the last decade, a wide range of V2V measurement campaigns aiming to investigate the performance of V2V in field tests were conducted using real 802.11p-enabled prototypes [46–50]. The work in [51] presents extensive field trial campaigns carried out in several countries focusing on six safety-based V2V applications. A comparison between off-the-shell WiFi-based radio with an advanced 802.11p compliant radio is also provided. In specific V2V environments, radio signal might be subject to a severe attenuation caused by stationary objects or mobile obstacle such as vehicles.

Regarding the problem of radio shadowing, several research studies were carried out aiming to evaluate the impact of shadowing caused by stationary objects or mobile obstacle such as vehicles, first through simulation and recently in small scale field trials. Field test experiments conducted in various environments (urban, suburban and highway) in [52] reported that vehicular obstructions could significantly attenuate the signal power by analyzing the impact of obstructing vehicles on a communication link. Moreover, the authors point out that the effect of stationary obstacles, such as buildings, is even more pronounced than mobile obstacles. An experimental evaluation found in [53] confirms the significance of the impact of vehicles on the received signal strength. In similar studies, it has been found that a truck and a bus reduce the received signal power by approximately 13 and 20 dB, respectively [54, 55]. To cope with the problem of radio shadowing caused by buildings and other obstacles, few empirical works have proposed different concepts aiming to improve the V2V communication performance under NLOS situations. With regard to message relaying, a study was reported in [56], where the authors performed field test measurements in order to extend the communication range by exploiting the vehicle height in obstructed environments. The obtained results show that even if tall vehicles often obstruct the LOS between communicating vehicles, the height of vehicles could be exploited. Based on experimental measurements, it is demonstrated in [57] that using tall vehicles as relays can significantly increase the effective communication range. The work in [58] used a fixed relay at the center of the intersection assuming LOS between the relay and involving

vehicles. Despite the fact that the communication range could be significantly increased, the complexity of the realization of such multi-hop relaying approaches brings new challenges which include synchronization issues in multi-transceiver architecture and the complexity of the design of relaying strategies.

2.3.2 *Simulative Studies*

A large amount of simulation studies on the performance evaluation of VANET has been made in the two last decades. What distinguishes the evaluation in the research community is the type of models developed and the simulation tool used. A proper and comprehensive simulation-based evaluation of VANETs requires at least a modeling of the communication as well as the mobility of nodes. While simple random-waypoint models are mostly used for Mobile Ad-Hoc Network (MANET), the simulation of vehicle's mobility due to the unique nature of road traffic has to be reproduced in a realistic way. As each node may contribute in the communication, a microscopic simulation of vehicles needs to be considered. Also, car following, lane change, traffic control aspects have to be taken into account to ensure a realistic behavior of models. Starting from random-waypoint mobility models over real-world mobility traces up to microscopic mobility models, the impact of node movement on the network connectivity is yet well investigated. However, the influence of vehicle's behavior during a simulation run is unfeasible. For the simulation of all aspects of VANET scenarios, road traffic simulator, and network simulation have at least to be combined, and interaction among them at simulation runtime has to be enabled. For this purpose, there are a couple of existing bidirectional simulation frameworks for VANET currently used by the research community. V2X Simulation Runtime Infrastructure (VSimRTI) allows the integration of several time-discrete simulators [59]. It provides the integration and exchange of simulators according to the specificity of the research question. Hence, simulators for vehicle traffic, wireless communication, emissions and execution of application can be coupled into a common simulation platform. For immediate use, VSimRTI is per default available with a set of traffic simulators such as VISSIM and SUMO and communication simulators, NS-3, OMNeT++ and JiST/SWANS [60]. An overview of simulation tools and techniques for vehicular communication, in general, can be found in [61, 62]. Beside VSimRTI, the authors present in detail mostly utilized openly available simulation frameworks such as Veins and iTETRIS [63, 64].

Concerning related work on simulation-based evaluation of VANETs, the work in [65] and [66] present an evaluation of IEEE 802.11p standard identifying its performance and limitations using simulations and analytical means. To cope with the abstraction issue by considering frames or packets as indivisible units, thereby ignoring channel effects on individual bits, a physical layer simulator is proposed in [67]. Furthermore, after highlighting the differences in modeling from isolated perspectives, the authors merge a detailed physical layer simulator into the network simulator NS-3. However, the improved accuracy due to bit-level modeling comes at the cost of increased computational effort. Following this trend, the author in [68] investigate based on a simulation study the impact of communication performance on a vehicle collision application. After a modeling of physical layer of V2V in MATLAB, bit error rate and delay spreads are hereby quantified.

To deal with vehicle shadowing on radio propagation, the work in [53] propose a model for integrating vehicles as obstacles in vehicular simulators in order to

increase the credibility of simulation results. In the same trend, the authors in [69] propose a dynamic beaconing algorithm that react to network changes caused by the time-variant signal due to radio signal obstructions created by neighboring vehicles, as well as by buildings. Their results indicate that this algorithm by adapting more quickly to change in network topology could substantially improve the communication performance compared to a traditional static periodic beaconing approach. Motivated by the problem of radio shadowing caused by buildings, a similar simulation study was proposed in [70] with the purpose of using parked vehicles as node relaying which then allow to see around the corner at the intersection areas. A simulation-based analysis of attenuation caused by buildings is provided in [71]. Hereby, the authors make a comparison of three channel modeling techniques aiming to reproduce the effects produced by buildings.

ANALYSIS OF URBAN INTERSECTIONS: TOPOLOGY, CRITICAL ACCIDENT SCENARIOS AND TRAFFIC DENSITY

As mentioned in the introduction in Chapter 1, we focus on the urban environment due to its fast changing nature. In contrast to highway scenarios, the investigation of the communication performance at urban intersections is very challenging. This is primarily due to the two-dimensional nature of intersection topologies - and beyond this - there are a lot of obstacles present around intersections. Especially in this complex environment, drivers have to deal with several parallel tasks involving lane change maneuver, observation of traffic light status and behavior of others traffic participants (pedestrian, and cross traffic). Moreover, the geometry and the intersection layout have been identified as factors influencing the accident risk at urban junctions. From a driver point of view, the complexity of an intersection increases as the number of approach legs to the intersection increases. To cope with this scope and complexity, safety-based V2V applications such as an intersection collision avoidance application coupled with driver assistance systems could help by assisting the driver in critical situations. However, from the evaluation perspectives of the potential of VANET at urban intersection, the understanding of environment factors that may affect the performance of the communication is a crucial task. In contrast to highway scenario with a frequent availability of LOS between vehicles, the communication performance at urban intersections is directly linked to the layout of the intersection as well as the distribution and placement of buildings. This motivates the analysis of urban intersections in this chapter, which is structured as follows: After introducing a classification method to determine the topology of intersections, we will first examine the distribution of intersection types from real data sets of some selected European cities. To reinforce the potential and motivation of VANET, a survey of critical intersection scenarios specifically targeted at urban intersections is then presented. A brief determination of the intersection stopping distance required by safety-based applications to assist drivers in critical situations is provided. Finally, to introduce the scalability issue, we close this chapter with an investigation of the traffic density in term of the number of vehicles at signalized intersections.

3.1 CLASSIFICATION OF URBAN INTERSECTION TOPOLOGIES

In the context of radio shadowing, the analysis of the placement of buildings, especially present at urban intersections is an important task in the investigation of channel characteristics. Depending on the topology of the intersection and on how buildings are distributed around, the performance of V2V will suffer from severe signal shadowing since obstructions caused by stationary obstacles may partially or completely obstruct the communication link between vehicles. Furthermore, an intersection with buildings located at all four corners will indisputably have a strong degree of obstruction compared to one having only one or two corners occupied by buildings. In this section, we investigate the intersection topologies in

term of intersection type following by a discussion of results. We defined the type of intersection according to the number of intersection corners occupied by one or more buildings.

3.1.1 *Data Gathering and Extraction Tools*

To classify intersection types, we require a 2D digital map containing information about the building data as well as road network topology of a given city. Due to the free availability of `OpenStreetMap` data, it is possible to extract a map of a complete city directly from the homepage. For this purpose, there are a lot of tools such as `OSMConvert`, `OSMosis`, and `OSMFilter` that assist in the extraction and processing of specific data-set based on prior given characteristics. In this work, we used the software tool `OSMget`, which enables a capability to download a large area using a prior configured bounding box. It defines the geographical coordinates of the region to retrieve. The extracted map can then be visualized on the graphical user interface of the traffic simulator SUMO. In this way, a verification of the quality of the extracted map. The tool `OSMget` is an open source software written in `Python`.

3.1.2 *Data Post-Processing*

Prior to investigation, we first present the analysis method employed for the evaluation. Figure 12 shows the process flowchart used to analyze the intersection type. Starting in the left corner, the file *city.osm.xml* containing raw data of a given city is downloaded from the `OpenStreetMap` homepage. Next, we used the `netconvert` tool to post-process and extract the road network topology data as well as the building structure from the gathered map. The building's attribute such as identified, type and shape is then selected using the tool `Polyconvert`. In the obtained file *city.poly.xml*, each building is represented as an approximated polygon. Both `netconvert` and `polyconvert` tools are provided by SUMO. The classification algorithm presented in this thesis takes as input the information about the intersection center (from file *city.net.xml*) and building data (file *city.poly.xml*). We used an XML parser to extract useful information and store the content of input files to a list of objects. Each object is defined following the geographical position and the identifier of the intersection center or a list containing the shape of each building for the intersection and the building, respectively.
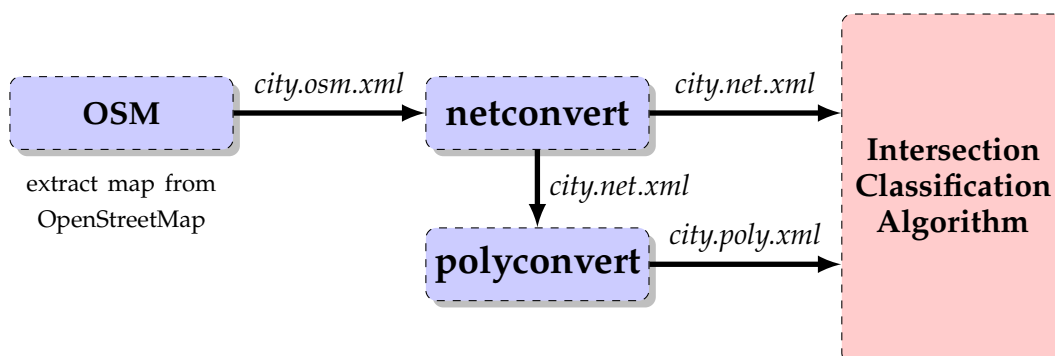
Figure 12: Block diagram of post-processing of the digital map data up through the phase of intersection type classification.

3.1.3 *Intersection Classification Algorithm*

The basic idea it to match a square centered at each intersection to the structure of each building and then judge its existence by evaluating how this square intersects with building polygons around the considered intersection. The below pseudo-code as shown in Algorithm 1 gives a summary about the intersection classification block (red block in Figure 12).

Algorithm 1 Intersection classification algorithm

1: **INPUT**: List of intersections I and list of buildings B
2: **OUTPUT**: List of intersections with type
3: $n \leftarrow \text{size}(I)$
4: $m \leftarrow \text{size}(B)$
5: **for** $i \leftarrow 0$ **to** n **do**
6:     **for** $j \leftarrow 0$ **to** m **do**
7:         InterCenter $\leftarrow$ I[i].*center*
8:         BuildingShape $\leftarrow$ B[j].*shape*
9:         getIntersectionType(InterCenter, BuildingShape)
10:     **end for**
11: **end for**

Based on the intersection center and the considered building's shape, the procedure *getIntersectionType* in line 9 implements a detection algorithm that, in a first step, searches buildings that are around an intersection. Each building's shape is an array of geographical points depending on the structure of the building. Furthermore, a square with sides of length S whose diagonals intersect at the intersection center is defined. Afterward, the existence of building is performed by iteratively checking if each quadrant of this square is overlapped by one or more building polygons. Finally, the type of the intersection is then classified according to the number of quadrants occupied by buildings. We distinguish five types of intersections as depicted in Figure 13: Intersections without buildings at quadrants of the square belong to Type 0, Type 1 corresponds to one or more buildings found at one quadrant, and up to Type 4 with all four quadrants occupied. Type 4 also comprises irregular intersection geometry with more than four legs.

(a) Type 0   (b) Type 1   (c) Type 2   (d) Type 3   (e) Type 4
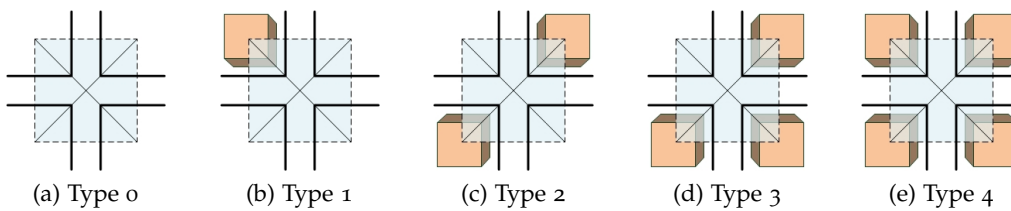
Figure 13: Intersection types assuming that all buildings are regular polygons. The blue area represents the square with sides of length S whose diagonals intersect at intersection center. S is used to check the presence of buildings.

To gain a deeper understanding of the building detection approach, let's consider an example illustrated in Figure 14. It shows an intersection with buildings at its corners. We assume in this example that all polygons are regular meaning that all internal angles have 90°. The blue square is a quadrilateral polygon with four

equal sides and is divided into four quadrants (Q1 to Q4). The intersection between two polygons (Building and Quadrant) is then used for evaluation of the presence of one or more buildings in the corresponding quadrant. In this illustration, three corners (Q1, Q2 and Q3) are occupied with buildings which subsequently leads to an intersection of Type 3. Obviously, the decision behind the presence of a building on a corner depends on the choice of S, since assuming a small value will result in a miss detection of buildings whereas a too large value leads to a misinterpretation.
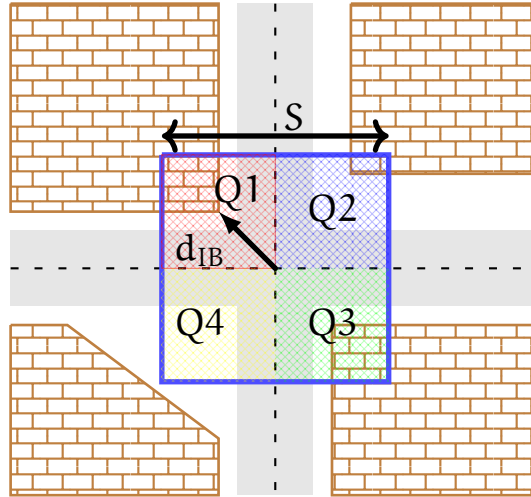
Figure 14: Illustration of the evaluation of the presence of building at intersection corners

Despite the simplicity of the building detection approach, this method may fail when two intersections are close to each other. For this purpose, the total set of intersections was filtered according to their relative distance. However, for handling high computational time and memory constraints caused by the processing of large city maps, we used an efficient search algorithm based on a region clustering method. This technique performed in the same manner as the region-based segmentation algorithm used in the area of digital image processing that consists of partitioning an image into regions.

3.1.4   *Estimation of Square Side S*

To provide reliable detection of buildings required by the classification of intersection type, one of the great challenges is the estimation of the length of the square side S as introduced above. Since the choice of S will influence the accuracy of the building detection algorithm. Moreover, setting high values of S might result to an inaccurate detection because also far away located buildings cannot be detected while lower values will result in a miss detection. To cope with this problem, we have conducted a prior study in order to determine the length of the square side S. Intuitively, the choice of S would be directly linked to the intersection width. But more advantageously is the knowledge about the average intersection-building distance d_{IB} measured at several cities. We denote d_{IB} as the distance from to the intersection's center to the nearest building vertex, which is a meaningful value in the detection of the presence of a building. To estimate optimal and realistic values of d_{IB}, we have performed an experimentation using data sets from five cities in Germany and six cities in Europe. Selected cities differ in the number of population

within the inner city area as well as the amount of intersections. Obtained results in the form of a box plot showing the distribution of d_{IB} are depicted in Figure 15. The plot shows the distributional characteristic of distance d_{IB} and eases its visualization. The bottom of the box represents the 25% quantile while the top of the box 75% quantile. Particularly interesting is the large spread of the box for the city of Charleroi compared for example to Munich. Since half of the distance are between the 25% and 75% quantile, we see that half of the distance for the Munich city are between 10 and 20 meters, whereas half of distance for the city of Charleroi are between 15 and 35 meters. This implies that over 50% of intersections in Charleroi are wider than in Munich resulting in a high availability of LOS at intersection area. In general for all cities, we observe that 75% of the measured intersection-building distance fall below 35 meter. Considering again the example from Figure 14, it has been shown that a building vertex is detected only if the square side $S > \sqrt{2} \cdot d_{IB}$ so that we can argue that choosing the square side S with a length of 50 meters will provide good results.
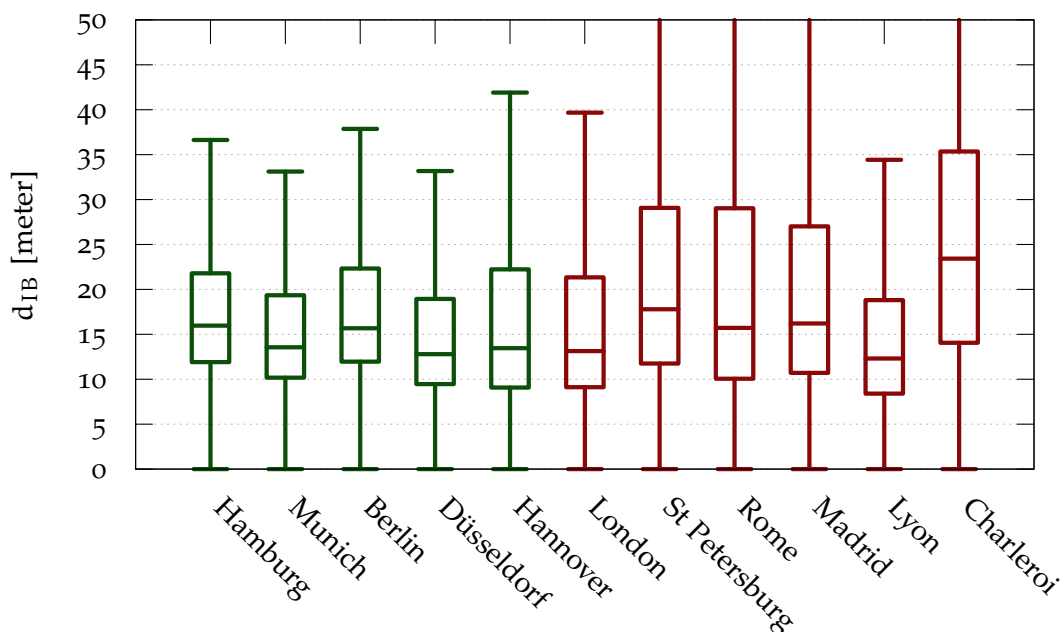
Figure 15: Distribution of the distance from the intersection's center to the nearest building vertex d_{IB} conducted from data of 11 European cities.

3.1.5 *Intersection Type Classification*

After determining the length of the square side S, we have conducted measurement from the data set gathered from `OpenStreetMap` and provided statistics about the intersection type. The data set employed cover 11 big cities in Europe. The obtained results presented in Table 4 show statistics about the distribution of intersection type at different cities. One can conclude that except for the city of Charleroi, 50 to 70% of all intersections from our data set belong to Type 2, 3 or 4 which implies that two up to four corners are occupied by buildings. On the other hand, only 10% to 26% of all intersections provide a perfect availability of LOS (Type 0). These findings emphasize the increasing effect of signal shadowing reflected by

a degradation of the received signal power reflected by a lower communication range when considering performance evaluation at urban intersections. Moreover, the challenging problem of V2V at urban intersections in term of obstacle shadowing is through this presented study validated. For the sake of validity of results, we compared the obtained statistic with those reported in [72] where the authors performed a similar study at the city of Munich. They reported that 70% to 90% of all intersections are of Type 4, whereas we found only 34% in our analysis. The deviation in the results is attributed to the size of the considered map. While we employed data set of the whole city containing 23151 intersections, they concentrated on a data set of the administrative area of the city with only 12307 intersections. Moreover a potential reason of this deviation could be attributed to the inaccuracy of OpenStreetMap data as the map employed in their work was gathered from the city homepage. Nevertheless, both results are in line since the larger the area, the larger the probability to capture rural intersections which are often from Type 0 or 1.

Table 4: Intersection type statistic

CITY	# of Intersections	Type 0	Type 1	Type 2	Type 3	Type 4
HAMBURG	41010	0.13	0.14	0.22	0.21	0.30
BERLIN	30482	0.14	0.16	0.25	0.21	0.24
MUNICH	23151	0.11	0.13	0.22	0.20	0.34
DÜSSELDORF	16082	0.12	0.11	0.19	0.20	0.38
HANNOVER	2116	0.18	0.14	0.21	0.17	0.30
LONDON	60509	0.16	0.12	0.20	0.18	0.34
ST PETERSBURG	20630	0.26	0.19	0.22	0.15	0.18
ROME	13969	0.24	0.17	0.23	0.16	0.20
MADRID	13425	0.23	0.19	0.26	0.15	0.17
LYON	9085	0.10	0.10	0.19	0.22	0.39
CHARLEROI	1234	0.36	0.26	0.22	0.10	0.06

3.2 ROAD TRAFFIC AT INTERSECTIONS

In the previous section, we have presented a classification of intersection types. We are now going a bit more deeply into the analysis of specific intersection accidents independently of the type of intersection. Instead, we focus on the identification of most critical relevant scenarios. Our investigation is based in part on a report of the project Traffic Accident Causation in Europe (TRACE) found in [73, 74]. In the two-year period (2006 - 2008), a descriptive and analytical statistic about accident causation in Europe using existing data sources that includes accident, injury, insurance, medical and exposure data has been provided. For this purpose, in-depth accidents databases were analyzed according to road user situation and accident conditions. The data was obtained from sources available at the 27 member states of the European Union (EU27) and combined in a common database. Moreover, this project has identified the most promising solution - among possible

technology-based safety functions - that can assist the driver or any other traffic participants in a normal road condition or a critical situation. In this section, we concentrate on the statistic of accidents at intersection areas followed by an identification of most critical intersection scenarios.

3.2.1 *Critical Intersection Scenarios*

After a review of intersection situations reported in [73, 74], critical intersection scenarios can be classified according to the cause of accident into four representative groups as illustrated in Figure 16. However, it should be noted that this study considers intersection accidents like those that happen at a junction or close to a junction.

CROSSING SCENARIO: This corresponds to accidents occurring between two or more vehicles coming from crossing directions. Consider, for example, a situation where one driver (red vehicle in Figure 16a) crosses, while the opponent comes, turns left, right or crosses. It represents the most complex scenario regarding the number of object in the surrounding as well as the required driving maneuvers. 70% of all intersection accidents belong to this kind of scenario, and is therefore of particular interest. Obviously, when crossing an intersection, drivers are confronted with a significant amount of information which can lead to misinterpretation of the situation.

REAR-END WITH STRAIGHT PATH: This concerns accidents where involving vehicles drive on the same road and in the same direction so that no turning maneuver except slowing down is required. Here the leading vehicle (see blue vehicle in Figure 16b) is slowing down in order to cross with enough visibility or for another reason. This leads to a misinterpretation of the gap to the following vehicle which has to brake accordingly. Rear-End with straight path accidents occur particularly in queuing traffic and represents 5% of all intersection accidents.

INCOMING SCENARIO: This belongs to accidents where involving vehicles drive on the same road but in different directions, and no turning maneuver except slowing down is required. Accidents caused by an involuntary lane departure due loss of control or sudden conflict situations, among others, belong to this type of scenario. It represents 2% of all intersection accidents.

REAR-END WITH TURN PATH: Similar to the rear-end with straight path scenario except that the leading vehicle performs a left- or right-turning. It represents 2% of all intersection accidents.

By examining critical intersection scenarios presented above, we remark that intersection lateral collision warning applications such as Intersection Collision Warning (ICW) could help to enhance the traffic safety by assisting the driver in case of potential collisions. Through V2V communication, the driver's horizon would be extended so that a better and complete visibility is achieved.

3.2.2 *Intersection Stopping Sight Distance*

The drivers' ability to see the road ahead and other intersection users is critical to the safe and efficient use of all roadway facilities, especially urban intersections. It

(a) Crossing

(b) Rear-End with straight path

(c) Incoming

(d) Rear-End with turn path
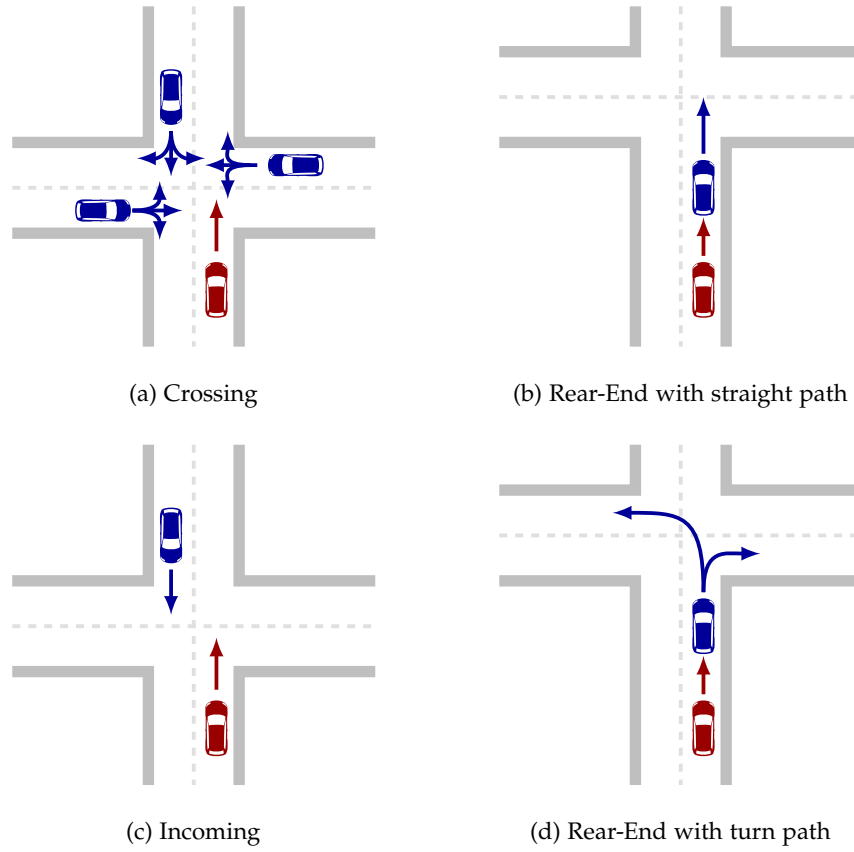
Figure 16: Critical intersection scenarios.

is imperative that intersection collision applications provide drivers sufficient information to the distance to perceive, recognize, and react to the presence of traffic control elements such as traffic signal indications, pavement markings, and signing. In addition, these kinds of applications might enable the possibility to safely maneuver into auxiliary lanes prior to the intersection. Stopping sight distance, decision sight distance, and intersection sight distance are particularly important at signalized intersection [75]. The stopping sight distance is the roadway distance required for a driver to perceive and react to an object in the roadway and to brake to a complete stop before reaching that object. Research documented in the literature often based on a laboratory study performed with a high number of test drivers, expressed the stopping distance as

$$d_{stop} = d_{react} + d_{brake} \tag{2}$$

$$= 0.278 \cdot v \cdot t_{react} + 0.039 \cdot \frac{v^2}{a} \tag{3}$$

where v is the vehicle speed in km/h, t_{react} the driver reaction time in sec and a the deceleration of the vehicle in m/s². Table 5 gives stopping sight distances for varying vehicle speed as computed from the Equation 3 provided by the American Association of State Highway and Transportation Officials (AASHTO) policy and assuming a perception-braking time $t_{react} = 2.5\,s$, and $a = 3.4\,m/s^2$ driver deceleration [76]. By examining these results, it is obvious that the stopping distance

increases with the speed. Moreover, we can conclude that in urban environments considering vehicle speed up to 60 km/h, a minimum communication range of 83 m is required for a proper operation of collision warning applications. From the view of communication designers, the communication quality in term of the probability of packet reception should provide sufficient information to vehicles throughout the intersection and on each entering and exiting this area.

Table 5: Intersection stopping distance.

SPEED [km/h]	REACTION DISTANCE [m]	BREAKING DISTANCE [m]	STOPPING DISTANCE [m]
20	13.9	4.6	18.5
30	20.9	10.3	31.2
40	27.8	18.4	46.2
50	34.8	28.7	63.5
60	41.7	41.3	83.0
70	48.7	56.2	104.9
80	55.6	73.4	129.0
90	62.6	92.9	155.5
100	69.5	114.7	184.2

3.2.3 *Queue Length Analysis: Signalized and non-signalized Intersections*

When judging the communication performance at urban intersections, it is very important to understand the traffic characteristic in term of queue length in this specific traffic environment, and then identify their impact on the communication quality caused by interference from surrounding vehicles, in particular under high congested traffic conditions. Traffic scientists usually expressed queue length as the number of vehicles or in meter depending on the length and type of vehicle present at a given road section or lane. It is a measure used to quantify traffic congestion and associated delays at intersections. Since the longer the queue length, the larger the delay in front of the traffic light.

The estimation of traffic density, as well as queue length, is usually realized using stationary traffic detectors, e.g. magnetic loop detectors but other methods including microwave, radar, photocells, ultrasonics, and video cameras or even manual count could be also employed [77–80]. However, the deployment and maintenance of stationary detectors is associated with significant expense, especially if larger road networks shall be covered instead of single sections.

A real-time optimization of urban intersection capacities can be achieved by continuously adapting traffic signal control systems to current queue length and consequently improve traffic efficiency. More recently, ITSs coupled with the vehicular communication technology was identified as an interesting alternative to provide a real time information about the actual traffic conditions, which is a basic requirement for dynamic traffic management. For this purpose, the capacity of vehicles to exchange information with infrastructure nodes is then exploited to estimate the current traffic condition. As traffic load typically varies strongly

throughout the day, an adaptation of traffic management according to the actual demand is essential and very challenging, especially in urban areas. Due to its two-dimensional nature, traffic distribution at urban intersections is characterized by a heterogeneous concentration of vehicles that directly depends on the actual traffic condition as well as on the time of day.

In a study reported in [81], we presented a travel time estimation approach for urban environments based on V2I communication. Although we focus on the influence of communication parameters on the travel time accuracy, we found that already at a low penetration rate of 10% and a message generation rate of one message per second, the V2I-based travel time estimation approach provides a very good performance compared to conventional approaches. But studying traffic condition methods is out of scope of this work, we concentrate rather in the analysis of queue length which in turn would have an influence of the network load and thus on communication performance. The level of interference will depend considerably on the density and distribution of nodes within the available urban intersection space. By analyzing the characteristics of traffic flow at signalized intersection, it is obvious that we will observe long queues during the red phase created by the flow of vehicles moving toward the intersection as illustrated in Figure 17. Analogically at non-signalized, we may also observe long queues during high congested traffic conditions according to the traffic volume. To date, most researches on traffic control classify urban intersections in two groups: Signalized and non-signalized intersection:

SIGNALIZED INTERSECTION: refers to an intersection controlled by traffic signal indicating which traffic has the right of way at a particular time. The vehicular flow at intersections is traditionally controlled by traffic lights when the density of cars in both perpendicular streets is considerably low [82, 83].

UNSIGNALIZED INTERSECTION: represents an intersection controlled by a give way sign and stop-controlled junctions with one or more STOP signs. This is appropriate when the traffic flow is high.

Basically, while the traffic flow at a signalized intersection is characterized by queue areas induced by the traffic control system, the flow at a non-signalized intersection is dependent on the density of vehicles on the main road. As mentioned above, the performance of the communication will depend on the traffic conditions characterized by the queue length behind the stop line; we will focus on the analysis of length of traffic at signalized intersections. Based on a theoretical study in [84], the authors estimate the number of vehicles that would share a common communication range at intersections under worst-case conditions in rural, suburban and urban environments. They found out that up to 600 vehicles can be sporadically present at city intersections.

Because of the lack of real queue length data from European cities, following investigations with the respect to the approximate number of vehicles at signalized intersections is performed as a theoretical approach. To get an idea about the average queue length Q in some cities, we can estimate the queue length based on the traffic flow and the duration of the red phase by the intuitive expression

$$Q = \frac{f \cdot T_{red}}{3600} \qquad (4)$$
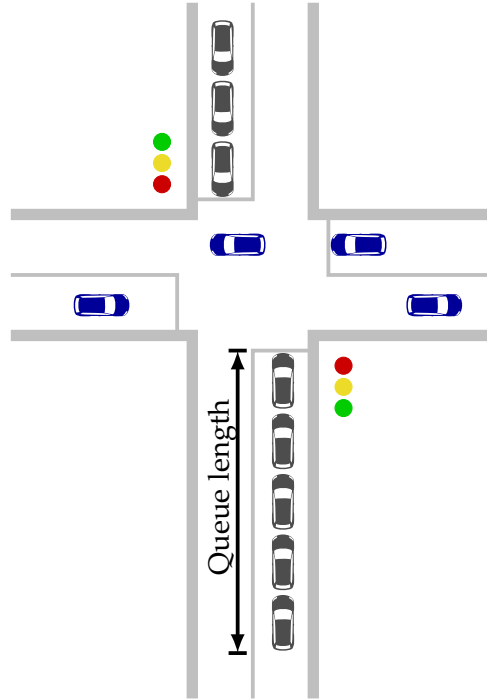
Figure 17: Queue length at a signalized intersection.

where f represents the arrival traffic flow in vehicle/hour and T_{red} the duration of the red phase in second. Note that in Equation 4, a uniform arrival pattern of vehicles is assumed. Furthermore, we assume for the sake of simplicity that vehicles will leave the queue when the light turn to green are not considered. We consider a controlled traffic light at the intersections with fixed timing consisting of green and red phases denoted T_{green} and T_{red}, respectively. Table 6 presents average queue length from selected cities based on traffic flow statistics gathered from respective city homepages [85–87]. The relationship between queue length and number of vehicles N is given by

$$N = 2 \cdot Q \qquad (5)$$

Assuming a typical red phase of $T_{red} = 50$ seconds and a four-leg intersections, the maximal number of expected vehicles within a common communication range for these selected German intersections will vary between 38 and 166 vehicles.

From the communication point of view, considering for example 180 vehicles sending 10 packets per second each of size 500 bytes, the generated channel load will be 7.2 Mbps, which is clearly higher than the recommended data rate of 6 Mbps. This implies an increase of packet losses that would directly influence the accurate operation of safety-based applications in critical situations. As the traffic flows are averaged over 24 hours, the effective traffic flow in peak hours is probably larger than those given by the traffic flow statistic from Table 6. This implies that more vehicles can realistically be expected at intersections, hence, estimated queue length from the table is underestimated during traffic jams. Nevertheless, from the reasoning and investigations presented above, the level of interference could grow significantly in the area around intersections and requires careful investigation to

Table 6: Estimation of queue length in some cities in Germany.

CITY	INTERSECTION	f [veh/24h]	Q [veh]
BRAUNSCHWEIG	Hamburg Str./Rebenring	54600	31
	Hagenmarkt	32400	19
	John F. Kennedy Platz	33912	20
MUNICH	Landshuter/Nymphenb. Str.	142008	83
	Gründwalder/Tegerns.-Allee	123000	72
	Ludwig Str./Von-der-Tann Str.	95040	55
BERLIN	An der Urania/Kleist Str.	65616	38
	Molkenmarkt	69816	41
	Karl-Max-Allee/Lebuser Str.	45312	27

properly assess the performance of V2V in urban environments. This motivates a measurement-based as well as a simulative investigation of the scalability problem at urban intersections presented in the next chapters.

3.3 SUMMARY

In this chapter, we presented an analysis of urban intersections. We focused on the evaluation of building's distribution and classified the type of intersection according to the number of intersection corners occupied by one or more buildings. The backbone of our examination is based on geographical data sets of eleven big Europeans cities provided by OpenStreetMap. First, we explained the architecture and method behind the intersection classification. We particular focused on the choice of the square required to provide a reliable and accurate detection of building's shape. For this purpose, an investigation on the intersection-building distance, which is the separation from the intersection's center to the nearest building vertex, is presented. This is an important quantity required to judge the presence of building obstruction. We found out that 75% of the intersection-building distance in selected European cities are below 35 meter. After the determination of square needed to check building availability, we have then analyzed intersection type. The results revealed that 50 to 70% of all intersections are from Type 2, 3 or 4 implying that two up to four corners contain buildings. In a nutshell, the findings emphasized that only 26% of intersections in European cities provide perfect LOS implying that a significant portion of message transmissions would be susceptible to frequent interruption most of the time.

Part I

EXPERIMENTAL EVALUATION

A determining step during the design and deployment of communication systems is the estimation of their performance in real scenarios. Measurements with real prototypes is therefore the appropriate methodology to investigate and understand the behavior of a given system. As V2V systems are close to market introduction, it is crucial to test and quantify their capability in real traffic conditions. For this purpose, we evaluate in the first part of this thesis the performance of V2V based on several measurement campaigns by focusing on the impact of radio shadowing caused by stationary obstacles, e. g., buildings and vegetation. The most critical challenge that V2V communication has to deal with is the inevitable radio shadowing caused by physical obstruction in the environment such as building, vegetation or traffic infrastructures. These kind of obstacles are unfortunately frequently present at urban intersections. For this purpose, we divide this part into three chapters that are as follows. First, we examine in Chapter 4 the impact of shadowing caused by buildings through measurements. Prior to the evaluation and discussions of results, we first give an overview about hardware and software utilized throughout the whole measurement study. Following the same trend, we performed a second measurement campaign aiming to investigate the impact of vegetation at selected intersections showing different foliage structures. Measurement setup and results are discussed in Chapter 5. Finally, we consider in Chapter 6 the influence of radio shadowing through buildings and its impact on co-channel interference and discuss results obtained from obstructed and non-obstructed environments. For all aforementioned chapters, the investigation is performed at urban environments concentrating on intersections.

EVALUATION OF SHADOWING CAUSED BY BUILDINGS

The analysis of intersection topology in Chapter 3 has demonstrated that only 9% to 23% of intersections at 11 big European cities provide a perfect availability of Line-of-Sight (LOS) between vehicles approaching the intersection, whereas up to 70% have at least 2 corners occupied by buildings. Moreover, this implies that a significant portion of message transmissions will be susceptible to frequent interruption most of the time. Additionally, research in [88] has shown that a significant large proportion of crashes often occurs at intersections. For this purpose, intersection collision avoidance applications, such as intersection collision warning which informs the driver about a risk of collision at an intersection, are currently been developed. Hence, the effort of the research community to improve the traffic efficiency and to reduce road mortality through adequate and intelligent applications based on V2V communication is indisputable. However, from the perspective of communication engineers, the design of such applications is very challenging since obstructions caused by stationary or mobile obstacles, especially frequent at urban intersections, may partially or completely obstruct the communication link between vehicles. This will probably lead to a substantial reduction of the communication range. Moreover, the effectiveness of safety-related applications will strongly depend on the characteristics of the radio channel and the quality of the communication link. Therefore, the analysis of main factors influencing V2V radio propagation is an important task not only for the specification and dimensioning of systems, but also for the investigation of key performance indicators of traffic safety applications. Furthermore, a credible simulation-based evaluation of V2V requires a profound understanding of the wireless channel. In consideration of the quality of communication link depending on the characteristics of the radio channel, reliable and efficient operation of any V2V application requires accurate and timely delivery of vehicle status. Therefore, for enabling these applications, it is essential to perform a deep analysis of the fundamental wave propagation characteristics in typical vehicular urban environments.

This motivates the measurement campaign conducted at five different urban intersections under Non-Line-of-Sight (NLOS) conditions and presented in this chapter. To discuss and evaluate the obtained results, we quantify (i) Received Signal Strength Indication (RSSI) levels defined as the energy measured during the reception of the packet's preamble, (ii) Packet Delivery Rate (PDR) which reflect the ratio between the numbers of successfully received and transmitted frames, and (iii) Reliable Communication Range (RCR) associated with different intersection characteristics, such as building density and development, street and intersection width. Insights into these metrics are necessary to meet the requirements of reliable communication ranges for collision avoidance applications. The results are obtained by means of measurements in realistic V2V application scenarios using a measurement system that meets current standards for vehicular communication. Parts of the contributions of this chapter have been previously published in [89].

4.1   RELATED WORK

Since 2005, there are numerous measurement campaigns which cope with the problem of radio shadowing caused by buildings. The work in [90] presented a profound field test performed at several intersections showing NLOS conditions and found out that urban intersections provide better performance than suburban intersections. This behavior is explained by constructive interferences at the receiver due to the multipath propagation, especially present at urban intersections having all corners occupied by buildings. The impact of street width on the radio signal propagation is empirically investigated in [91]. It is found that the narrower the street, the more dominant the influence of reflected waves by buildings. In [92], results on typical channel properties such as power delay profiles, pathloss and delay spreads derived from a channel measurement are presented. The authors focus on different intersection types which differ in the availability of a LOS component and the location and density of scatterers such as buildings and vehicles. A stochastic model used to estimate communication distances for different data rates and traffic densities, in particular, in NLOS scenarios is provided in [93]. Hereby, a propagation model suitable for typical urban intersection scenarios is derived from narrow-band V2V measurements. A similar model associated with an additional derived empirical fading model is presented in [94]. Following the same trend, the work in [95] presents a computationally inexpensive empirical model for urban environments after a profound investigation of building shadowing on radio communication between vehicles based on real world measurements. In [96], a survey of comprehensive V2V propagation channel measurement campaigns in different relevant environments is given. It is found that propagation aspect of vehicular environment might vary with respect to speed difference, vehicle density, and road and intersection topology. Furthermore, the authors found that the type of equipment mostly used for V2V channel measurement is mostly the same as that for infrastructure-based network which range from signal generators, vector signal analyzers up to wideband sounders.

The majority of works presented above cannot be directly applied to assess the performance of the communication as for a realistic evaluation of V2V, real V2V-based transceivers are needed. For this reason, our work contributes to the general analysis of urban intersections utilizing wireless radio modules that conform with the IEEE 802.11p [8] or ITS-G5 [97] standard. Moreover, we cover additional issues like transmitter location, the impact of street width and traffic density.

4.2   MEASUREMENT EQUIPMENT

The choice of measurement equipment as well as the software set used for measuring V2V communication have an impact on the interpretation of results, hence, influence the quality of performance evaluation. To ensure applicability of the measurement results for prospective cooperative safety applications, the utilized wireless radio have to be compliant with the IEEE 802.11p or ITS-G5 specifications. In this section, we presented self-developed hardware and software used for measurements following by a validation of the proposed measurement set.

4.2.1 *Hardware Components*

The on-board V2V communication module installed in each vehicle is composed of an embedded PC, a wireless radio unit, a GPS receiver, an antenna, an external hard disk and a notebook which allows the configuration, monitoring and control of experiments during the measurement campaign. Due to the limited memory capacity on the compact flash, we use the external hard disk to backup measurement results after each measurement run. The embedded PC is an ALIX3D3 board running an Ubuntu Linux distribution with kernel version 2.6.32. The Linux system was configured to boot directly from a flash memory card mounted on the ALIX3D3 board. As shown in Figure 18, the embedded PC can be equipped with two wireless radio cards. We used commercial off-the-shelf Compex Mini PCI 802.11abg wireless cards based on the Atheros AR5006X (AR5414) chipset. Since no commercial ITS-G5 receiver was available, we adapt the protocol stack for the Atheros by modifying a driver based on ath5k and the Linux wireless subsystem in order to be standard compliant. This allows us to be able to communicate on a 10 MHz channel centered at 5.9 GHz. Furthermore, the MAC part of the driver was extended in order to employ the newly defined OCB in 802.11p and adopted by ITS-G5 mode, which allows stations to transmit data frames without prior association or authentication with a BSS as described in Chapter 2. The communication module was linked to a Navilock NL-402U GPS receiver using the u-blox5 chipset in order to log the vehicle positions and the distance between vehicles.

Figure 18: A detailed view of the embedded PC and the wireless radio board.

Furthermore, each vehicle was equipped with a vertically polarized magnetic mount antenna (Mobile Mark ECOM6-5500) mounted on its roof. The antennas have kindly been measured by Delphi Deutschland GmbH and show an omni-directional radiation pattern and a nominal antenna gain (including antenna cable attenuation) of 3.2 dBi at zero degrees elevation on a metal ground plane. According to the provider's data-sheet, the antenna operates at 5.0-6.0 GHz and is 254 mm long. The transmit power was configured to be 23 dBm. Together with the antenna gain and a system loss of approximately 3 dB caused by the connectors between interface card and external antenna, this resulted in an Equivalent Isotropically Radiated Power (EIRP) of 23.2 dBm.

4.2.2   *Measurement Software*

The measurement software set running on the embedded PC is composed of two self-developed software tools, a CAM generator (*CAM-APP*), a receiver program (*C2XdBm*), as well as several scripts used to control the experiments during the measurements and to adapt the parameter settings based on predefined configuration files.

CAM-APP is a software tool based on a packet generator that generates and sends CAMs of one or several streams with different rates over a User Datagram Protocol (UDP) connection to the network. Its capability to create and configure multiple streams allows a further operation of parallel V2V applications on a single platform. Furthermore, *CAM-APP* supports radiotap header generation to append user defined payload to existing packet header. This allows an integration of information such as sequence number, GPS data and sending time on packet headers giving a possibility to recover even packets of which payloads are corrupted. While a TCP connection establishment requires a handshaking procedure before a data transmission, we chose a UDP protocol because it provides a connection-less transmission without any formal preliminaries. In this way, no additional delay is introduced due to the missing connection establishment procedure as prescribed by the ITS-G5 standard. However, a UDP transmission cannot take care of incrementing sequence or acknowledgement number. For this reason, we implement a packet numbering with a 32-bit sequence number easing a further computation of packet delivery rate at the receiver. During the experiments, the *CAM-APP* was configured based on a configuration file to periodically broadcast CAMs with a constant generation rate and a net message size of 500 bytes on a given network. Including UDP, IP, LLC and MAC header (8/20/8/28 bytes), this resulted in a MAC frame size of 564 bytes.

C2XdBm is a tool running at the receiver that utilizes the *libpcap* library to log the measured RSSI values, sequence number as well as the transmitter and receiver position for each frame reception. Furthermore, the driver supports radiotap header generation to gather measurement data. Based on geographic coordinates gathered at the receiver and those from the sender, a distance separation between sender and transmitter can be computed after a coordinate system conversion from WGS84 datums (latitude and longitude) to two dimensional coordinates UTM on a map projection. In order to compute the PDR, we used a 32-bit sequence number in the message header. The receiving wireless interface remained in monitor mode, passively listening to frames on the configured channel. RSSI values were extracted from the radiotap header and recorded for each successfully received frame together with the separation between involving nodes.

Both *CAM-APP* and *C2XdBm* tools are implemented following a component-based software architecture concept facilitating the reuse of developed modules for further V2V applications. The core program and data post processing algorithms are written in C. The post processing of data is performed using self-developed Matlab and Python scripts. However, one of the challenge during this task is the synchronisation of measured data such as RSSI values, packet sequence number with vehicle position data provided by GPS receivers. Since the type of receivers

used during the experiments have a limited time resolution of data of 200 ms. This is insufficient for a temporal alignment of measured data considering that we performed some experiments with a sending interval up to 1 ms. Therefore, we implemented an interpolation algorithm based on the average driving speed so that an alignment of measured samples to accurate GPS data can be achieved.

4.2.3 *Validation of the ITS-G5-compliant Wireless Interface*

In order to verify and validate the effective operation of the modified driver on the wireless interface, we performed prior tests in a controlled lab environment. As illustrated in Figure 19, the lab environment comprises a transmitter (Tx) and receiver (Rx) side, which include wireless radios, HF cables, adjustable attenuators, a splitter and a spectrum analyzer. While the TX side relies on a wireless module, the Rx side has two branches: a wireless module and a spectrum analyzer. The module at Tx side was configured to transmit periodic CAMs with a constant generation rate of 100 Hz at 5.9 GHz. For each received CAM by the RX side, the RSSI level of the received signal was collected.
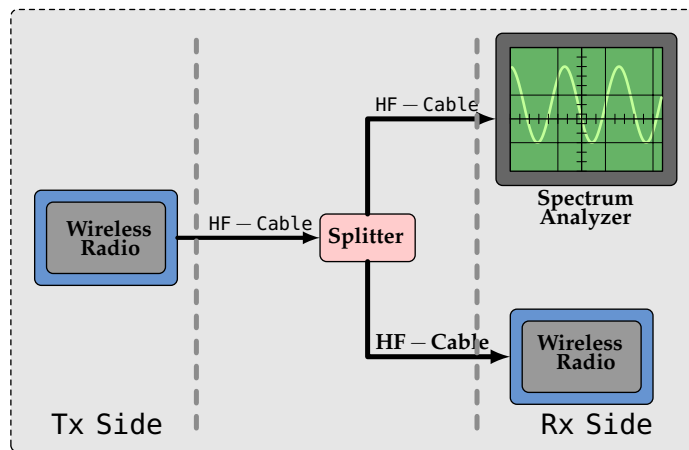
Figure 19: Measurement set-up of the laboratory test environment composed of two wireless radio modules and a spectrum analyzer.

To verify that the signal power at input of the wireless radio corresponds to the transmitted signal power considering losses due to cables and splitters, we evaluated the RSSI levels provided by *libpcap* by comparing with those measured by the spectrum analyzer. As result, we conclude that the RSSI values presented by *libpcap* reflect the real received power (in dBm) almost satisfactorily, but contain a bias of approximately -3 dB for RSSI levels greater than -80 dBm and approximately -6 dB for RSSI levels smaller than -80 dBm. This means that the real received power is generally underestimated by the *libpcap* RSSIs. We therefore corrected the field test RSSI results accordingly to calculate the actual received power P_r.

To ensure an interference-free operation of ITS-G5 devices, the standard has specified transmit spectral masks according to the configured channel bandwidth (5 MHz, 10 MHz or 20 MHz). Therefore, each device shall be associated with a transmit spectral mask limiting the out-of-band energy of the transmitter, which might produce a slightly portion of interference in neighboring bands. In this way, adjacent interference due to imperfect filters in the analog front-end could be re-

duced. For this purpose, we measured the power spectral density (PSD) of the standard-compliant ITS-G5 signal using a spectrum analyzer. The PSD shows the strength of the variation as a function of frequency. The peak of PSD is used as the reference power in the signal, so that spectral masks are measured with respect to the peak. As required by the standard, the measurements were made using a 100 kHz resolution bandwidth and a 30 kHz video bandwidth. As can be seen in Figure 20, the power spectral density has constant transmit spectrum within the range 5895 MHz to 5905 MHz. Moreover, we observe that the transmitted spectral density falls perfectly within the transmit spectral mask according to the spectrum mask defined in [12]. This implies that the wireless card was successfully modified and hence provides the capability to transmit at the center frequency band 5.9 GHz with a channel bandwidth of 10 MHz. In a nutshell, we can argue that utilized wireless radio modules in this thesis were well in line with the IEEE 802.11p or ITS-G5 specifications in term of output power spectrum and occupied bandwidth.
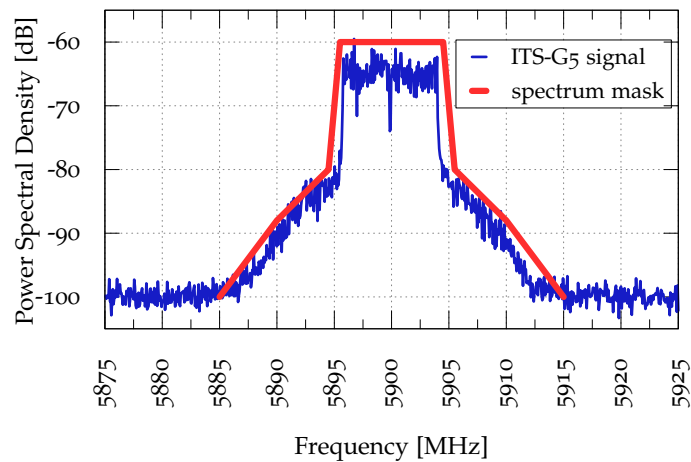
Figure 20: Power spectrum density (PSD) of a transmitted signal using the modified ITS-G5 device. The transmitted spectral density falls within the transmit spectrum mask as specified in [12]. The proper operation of modified wireless interfaces utilized for measurements is therefore validated.

4.3   MEASUREMENT SETUP AND SCENARIO DESCRIPTION

4.3.1   *Measurement Setup*

The test setup included two vehicles of similar height: A Volkswagen Scirocco III with a panorama glass roof was configured as transmitter and a Mercedes-Benz W202 C-Class operated as receiver. While the antenna was mounted at the center of the receiving vehicle's roof, we placed it a little further rearward on the transmitting vehicle due to its panorama glass roof. The transmit and receive antenna heights were approximately 1.5 m. To separate shadowing caused by building and obstructions caused by vehicles, we used video recording during the experiments, which allows an identification of the type of obstruction within the post-processing process. In this way, only runs where the NLOS was caused by building's shadowing were considered for the investigation. A summary of the measurement system parameters is presented in Table 7. We measure with a high message generation

rate of 100 msgs/s to collect as much transmitted frames as possible, which implies a high accuracy in the investigation of channel characteristics.

Table 7: Measurement system parameters.

	PARAMETER	VALUE
PHY	Transmission power (EIRP)	23.2 dBm
	Center carrier frequency	5.9 GHz
	Channel bandwidth	10 MHz
	Data rate	6 Mbps
	Antenna height	1.5 m
CAM	Message generation rate	100 msgs/s
	message payload size	500 Bytes

4.3.2 *Impact of a Panorama Glass Roof*

In [98], the authors analyze the impact of a large panorama glass roof based on 5.9 GHz measurements conducted in an anechoic chamber. Their results indicate that a gain reduction of 15 to 20 dB can be caused by the large glass roof, which the authors attribute to waveguide effects. Motivated by these results, we conducted a preliminary test involving the two test vehicles, one of them also equipped with a panorama glass roof, which, however, was significantly smaller than the one tested in [98]. We performed this test under perfect LOS conditions, moving the receiver around the transmitter while keeping the distance between both unchanged. The obtained results showed no noticeable influence of the glass roof. Additional measurements in an anechoic chamber revealing an omnidirectional antenna pattern confirmed these observations. We attribute this to the fact that the test vehicle's glass roof was significantly smaller and the antenna was in an exposed position.

4.3.3 *Scenario Description*

The measurement campaign was carried out in the city of Braunschweig at selected intersections with different traffic conditions. In order to quantify the effects of buildings, traffic and the layout of the intersections, we selected 9 different scenarios at 6 different intersections in an urban environment. In this thesis, we present the results for 6 of these scenarios at 4 different intersections as shown in Figures 21. All scenarios have in common that the transmitter TX was located at a fixed position on a side street, while the receiving vehicle RX moved towards the intersection with a speed of approximately 20-25 km/h.

Intersection 1

The objective of the first three scenarios is the evaluation of the influence of the transmitter's position. Hence, all of these scenarios were located at intersection 1 (Mittelweg - Nordstrasse), where we varied the transmitter's distance d_{TX} to the

intersection center between 35, 55 and 85 m. As shown in Figure 21a, The intersection is half-open and from Type 2, which means that there are buildings on two intersection quadrants only, although there were several parked vehicles opposite to the buildings. The intersection is of medium width with a distance of approximately 13 m between the intersection center and the corners of the buildings and a width of the side street, where the transmitter was located, of approximately 16 m. The traffic density was very low. The geographic coordinates of the intersection's center are 52°16'36.61"N, 10°31'33.19"E.
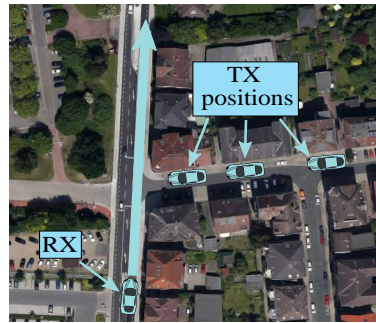
(a) Intersection 1: Varying transmitter positions.

(b) Intersections 2 and 3: Varying street width.
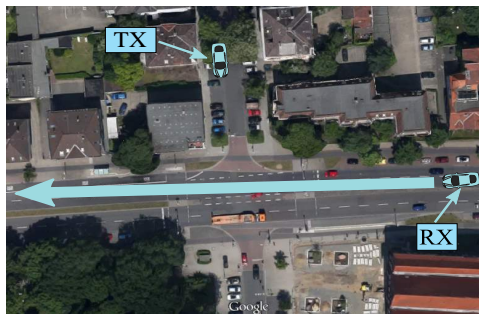
(c) Intersection 4: Large intersection, dense traffic.
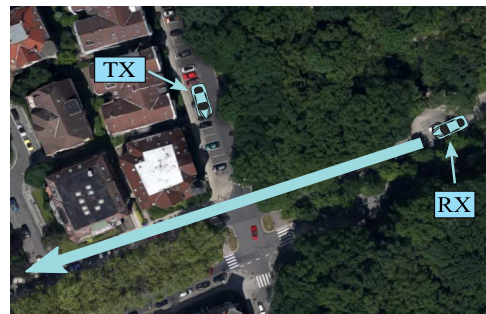
(d) Intersection 5: Mixed environment.

Figure 21: Selected scenarios: Arrows indicate the direction of motion of the receiving vehicle. The transmitting vehicle's position is fixed for each of the 7 scenarios.

Intersections 2 and 3

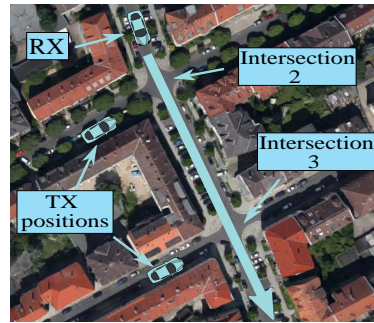The scenarios at intersections 2 (Waterloostrasse - Schunterstrasse) and 3 (Waterloostrasse - Wabestrasse), which are similar to the "narrow urban" intersection type in [92], consider the influence of the intersection and street width. The structure of the surrounding buildings is quite similar in both scenarios. Both intersections are closed and from Type 4, which means that there are multistory buildings on four intersection quadrants. The main difference is related to the width of the streets where the transmitter was located. In the Schunterstrasse (intersection 2), the width of the building canyon is approximately 20 m (which makes this intersection approximately comparable to the "urban main case" in [99]), whereas the Wabestrasse (intersection 3) offers a width of only 10 m. Furthermore, there were thick growing trees on both sides of the Schunterstrasse, while the Wabestrasse showed almost no vegetation. In both cases, the distance between transmitter and

intersection center was $d_{TX} = 25$ m. To reduce the impact of vehicle's obstructions on the communication link, we performed experiments at night time. This implies a very low traffic density during the measurements. The geographic coordinates of the center of intersection 2 and 3 are 52°16′21.60″N, 10°32′25.35″E and 52°16′19.43″N, 10°32′27.01″E, respectively

Intersection 4

The objective of the scenario located at intersection 4 (Rebenring - Geysostrasse) is the impact of traffic density. This intersection of Type 3 is relatively wide with a distance between the intersection center and the corner of the nearest building of approximately 21 m. There are buildings on three intersection quadrants, and the buildings in the side street, where the transmitter was positioned, are located relatively close to the street. On the main street (Rebenring), there are two lanes per direction, in contrast to all other streets being part of the scenarios. The distance between transmitter and intersection center was $d_{TX} = 45$ m. In contrast to the other scenarios, the traffic density was very high, with vehicles often stopping at the traffic lights and occasional appearance of buses. The geographic coordinates of the intersection's center are 52°16′31.76″N, 10°31′42.75″E.

Intersection 5

The last scenario was located at intersection 5 (Jasperallee - Wilhembodestrasse), a intersection of Type 1 with a distance between the intersection center and the corner of the nearest building of approximately 5 m. The objective of this scenario is the investigation of a mixed environment composed of buildings and foliage around the intersection. There are buildings only on one intersection quadrant, and the buildings in the side street, where the transmitter was positioned, are located relatively close to the street. One of the intersection's corner is occupied by foliage. On the main street (Jasperallee), a park area showing a mixed vegetation pattern obstructs the LOS between transmitter and receiver. The distance between transmitter and intersection center was $d_{TX} = 50$ m. The traffic density was very low. The geographic coordinates of the intersection's center are 52°16′10.11″N, 10°32′44.01″E.

4.4 MEASUREMENT RESULTS

In this section, the results from the measurement campaign are presented. In order to ensure statistical validity of the results, we performed at least 5 measurement runs per scenario, driving at low speeds (20-25 km/h) to collect as many samples per run as possible. The time duration of one run of approximately 57 s and message generation rate of 100 msgs/s lead to more than 5700 packet transmissions per run. We evaluated Received Signal Strength Indication (RSSI) and Packet Delivery Rate (PDR) results for the scenarios described above which are plotted against the distance d_{RX} between the receiving vehicle and the center of the intersection. During the approaching phase of the receiver, negative values of d_{RX} are used for presentation purposes. For both performance metrics, we calculate means over 2.5 m distance intervals and include 95 % confidence intervals in the resulting plots. However, it should be noted that RSSI data is only collected for frames that at least

the preamble and message header were correctly received. For this reason, the measured mean received power levels overestimate the real mean levels of all frames significantly for low PDRs, but reflect real mean levels sufficiently well for high PDRs. For the sake of comparison, we determine for every scenario the so-called *Reliable Communication Range (RCR)*, which defined a range from the intersection's center ensuring a PDR of at least 0.9 .

4.4.1 *Transmitter Position*

The resulting mean received power $\bar{P}_r$ for varying transmitter positions at intersection 1 is shown in Figure 22. In this figure, the mean received power $\bar{P}_r$ and mean PDR against the distance d_{RX} for varying distance d_{TX} between transmitter and intersection 1 is shown. Recall that while same traffic condition and the same trajectory was used by receiver during experiments, the transmitter position was the only changing variable. As expected, we observe in Figure 22a differences in the average received power $\bar{P}_r$ according to the transmitter position. This emphasizes the significant influence of the transmitter distance d_{TX} on the received power levels. Furthermore, there is a rapid increase before LOS conditions are available (LOS is only available approximately 10 m ahead of the intersection center), which suggests that, although this is a half-open intersection, lower order reflections significantly contribute to the received power.

Figure 22b depicts the average PDR for varying transmitter positions at intersection 1. It is clearly visible that the edges of the PDR plot are relatively steep, indicating a quick transition from unreliable to reliable communication performance and vice versa. For $d_{TX} = \{35, 55, 85\}$ m, fully reliable communication (PDR $\geqslant$ 0.9) is possible during the approaching phase for $d_{RX} \approx \{65, 30, 20\}$ m, respectively. This leads to reliable communication ranges RCR $= d_{RX} + d_{TX}$ of 100 m, 85 m and 105 m, respectively. Interestingly, we observe a slight increase of the PDR at $d_{RX} \approx 90$ m for $d_{TX} = 35$ m (see Figure 21a). This can be explained by gaps between buildings in the side street, which allow reflected waves to constructively contribute on the achieved Signal-to-Interference-and-Noise Ratio (SINR). The benefit of multipath effect caused by reflected rays on buildings, especially at urban intersections, is therefore, highlighted in this case.

4.4.2 *Intersection Street Width*

Figures 23 show mean PDRs and mean received power levels as well as the raw received power levels indicating the signal fading for the medium-wide side street at intersection 2 and the narrow side street at intersection 3. Although the transmitter's distance to the intersection was the same in both scenarios and the development of the surrounding buildings is very similar, the communication performance is considerably different. For the narrow side street, a PDR higher than 0.9 is achieved approximately 60 m ahead of the intersection center. On the contrary, the same PDR is observed approximately 90 m ahead of the intersection center for the medium-wide side street. Regarding a distance $d_{TX} = 25$ m of the static transmitter to the intersection center in both scenarios, reliable communication ranges RCR $= d_{RX} + d_{TX}$ of 85 m and 115 m, respectively, can be achieved.

Obviously, the opening width of an urban canyon has a significant impact on the maximum communication range. As diffraction is negligible at 5.9 GHz, a rea-

(a) Mean received power $\bar{P}_r$
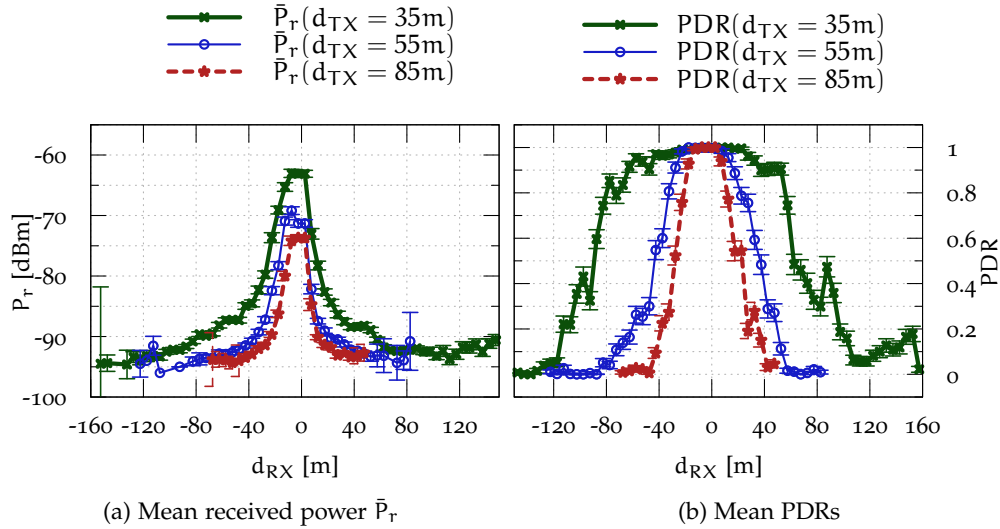
(b) Mean PDRs

Figure 22: Impact of transmitter positions: (a) Mean received power $\bar{P}_r$ and (b) mean PDR against the distance d_{RX} for varying distance d_{TX} between transmitter and Intersection I.

sonable explanation for this effect might be reflections of first and higher orders that reach the receiver earlier in a wider canyon. However, this phenomenon requires a deeper analysis in the future. Likewise, the effects of vegetation, which did not substantially influence the results in these scenarios, will be subject of further studies. Again for both intersections and similar to intersection 1, we observe again PDR peaks at several distances d_{RX}. These peaks result probably from the multipath effect caused by gaps between surrounding buildings.

Despite differences concerning intersection topology and measurement setup, the results for intersection 2 are well in line with those for intersection 10 ("urban main case") in [99], which shows a similar, albeit not fully identical topology.

(a) Intersection 2: Medium-wide side street
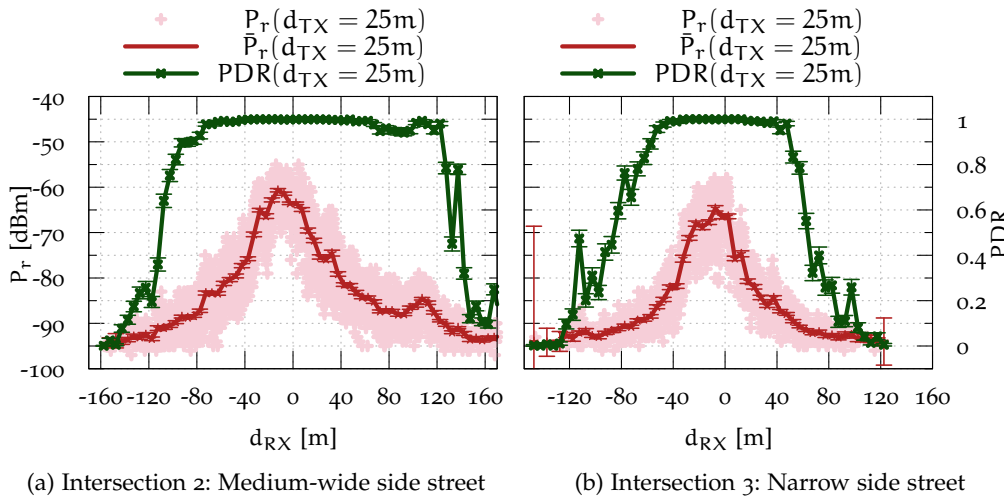
(b) Intersection 3: Narrow side street

Figure 23: Impact of intersection street width: Raw received power P_r, mean received power $\bar{P}_r$ and mean PDR against the distance d_{RX} for Intersections 2 and 3.

4.4.3 Road Traffic Condition

To track the impact of the traffic condition on the communication performance, we performed experiments with the same configuration at intersection 1 at two different day periods: rush hour and late night. While the transmitter was located at a distance $d_{TX} = 35\,\text{m}$ of the intersection's center, we measured at day and night time implying an automatic variation of the traffic density. This allows an investigation of surrounding vehicles, which somewhat partially obstruct the path between the transmitter and receiver [52–55]. Figure 24 shows the significant impact of surrounding vehicles on the obtained PDR. As expected, we observe a difference between both plots. Under high traffic PDR higher than 0.9 is achieved only at $d_{RX} = 40\,\text{m}$ implying approximately $RCR = d_{RX} + d_{TX}$ of 75 m, while this range is almost doubled (RCR=105 m) when considering low traffic density.

Furthermore, we investigate the effect of the traffic condition on the communication performance at wide intersections. For this purpose, we performed measurements at intersection 4 under rush hour traffic and compare the results with those obtained at intersection 2 under low traffic density. The results of both intersections are shown in Figure 25. We observe that although the intersection 4 is relatively wide, the communication performance is significantly worse than at intersection 2. However, it should be noted that the transmitter in intersection 4 is located farer from the intersection's center, which results obviously in a higher path loss due to large a distance between vehicles. Reliable communication is only possible approximately $d_{RX} = 50\,\text{m}$ ahead of the intersection 4, which results, considering $d_{TX} = 45\,\text{m}$, in an increasing of the reliable communication range of $RCR = d_{RX} + d_{TX} = 95\,\text{m}$ compared with $RCR = 145\,\text{m}$ for intersection 2, considering $d_{RX} = 120\,\text{m}$ and $d_{TX} = 25\,\text{m}$. This behavior is clearly caused by the influence of surrounding cars and especially buses on the propagation of the radio signal, which can be regarded as a kind of probabilistic shadowing. This could also cause the relatively gentle slope of the PDR plot. Similar to measurements reported in [53], we observe that vehicles present at urban intersections act as obstacles, and could partially affect the communication performance. However, compared to static radio shadowing, the impact of buildings is found to be pronounced.

4.4.4 Mixed Environment: Building and Vegetation

As vegetation is often present at intersections, especially at suburban environment, we performed a set of experiments at the intersection 5 showing a mixed shadowing medium composed of buildings and foliage around the intersection. Negative d_{RX} distances in Figure 26 correspond to obstruction caused by vegetation while positive distances belong to building shadowing. The asymmetry as well as the difference of PDR between positive and negative d_{RX} distances shows the severity of obstruction caused by buildings. While the reliable communication range is possible already at $d_{RX} = 90\,\text{m}$ (negative part of the figure) ahead of the intersection center for the vegetation obstruction, a range of $d_{RX} = 50\,\text{m}$ (positive part of the figure) can only be achieved under building obstruction. Moreover, we observe a deviation of the mean received power $\bar{P}_r$ of about 9 dBm when considering the same distance between both intersection legs, for example at $d_{RX} = -40\,\text{m}$ and $d_{RX} = 40\,\text{m}$. This brings us to the conclusion that buildings appear to attenuate the transmitted signal more likely than vegetation composed of foliage and tree

Figure 24: Impact of the traffic condition: Raw received power P_r, mean received power $\bar{P}_r$ and mean PDR against the distance d_{RX} for varying day periods and for Intersection 1.
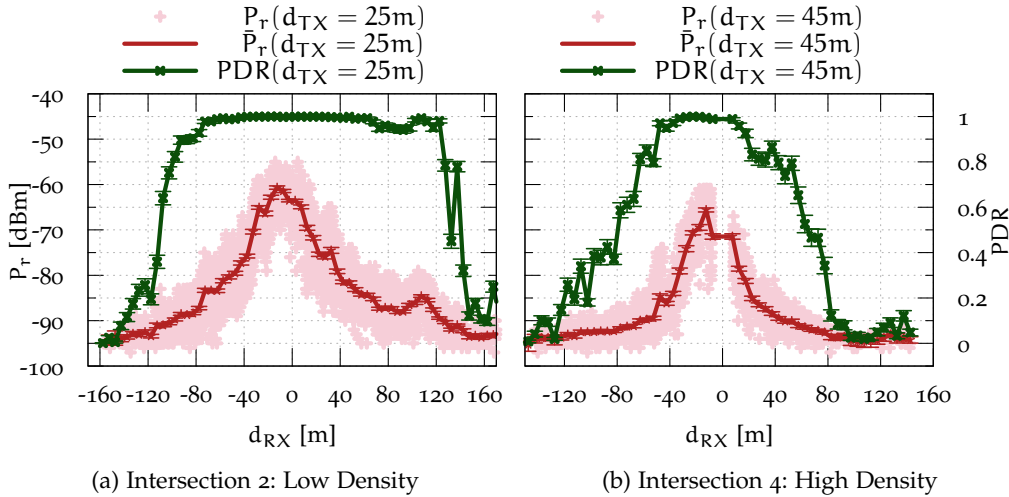
Figure 25: Impact of the traffic condition at wide intersections: Raw received power P_r, mean received power $\bar{P}_r$ and mean PDR against the distance d_{RX} for Intersection 2 and 4.

trunks. An assessment about the influence of the vegetation based solely on one scenario and environment is not representative and the conclusion will be very limited. Since the level of signal attenuation due foliage will probably depend on the texture, the structure as well as the depth of vegetation in the signal path. This motivated the detailed investigation of the impact of foliage in the next chapter, where we performed measurements at several intersections showing different vegetation structures and topologies.
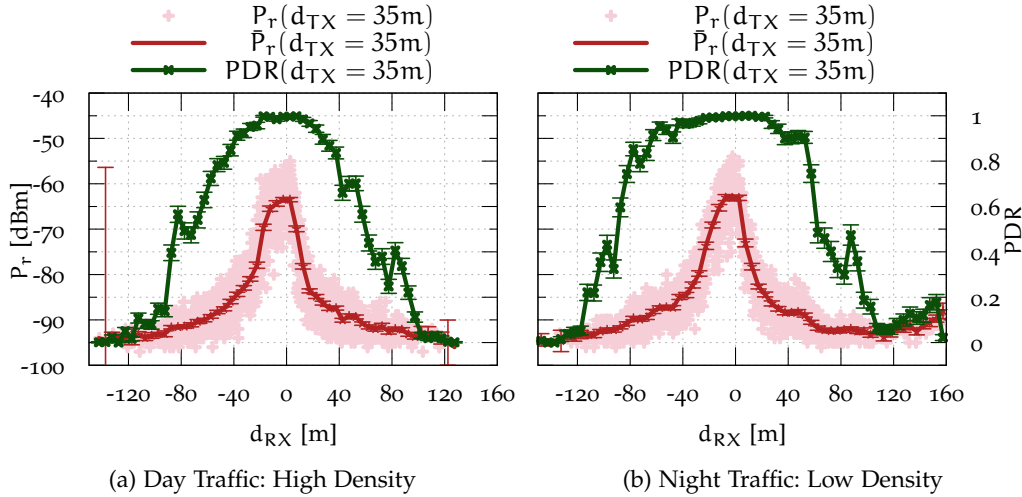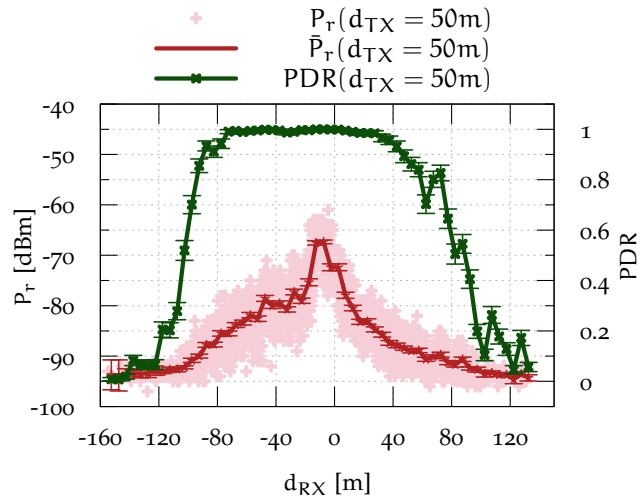
Figure 26: Impact of mixed environment: Raw received power P_r, mean received power $\bar{P}_r$ and mean PDR against the distance d_{RX} for Intersection 5.

4.5 SUMMARY

In this chapter, we presented and discussed results of a performance measurement campaign at five different urban intersections under NLOS condition. Experiments were carried out in realistic vehicular scenarios using a measurement platform that meets current standards for V2V communication. We quantified received signal strength levels, packet delivery ratios, which reflect the ratio between the numbers of successfully received and transmitted frames, and communication ranges associated with different intersection characteristics, such as building density and development, street and intersection width. Over the course of the chapter, we have summarized our findings in the following:

1. The transmitter location relative to the intersection has an influence on the communication reliability. The nearer the transmitter, the better the packet delivery rate.

2. The opening with of an urban intersection has a significant impact on the effective communication range. Medium-wide side streets at intersection have shown to be favorable than narrow side streets.

3. The traffic condition impacts the communication performance. Surrounding vehicles have an influence of the achievable communication range according to day and night traffic.

Furthermore, when comparing the level of signal attenuation caused by different radio shadowing medium, the results have shown that shadowing through building is likely more severe than through vegetation. However, an accurate assessment about the impact of vegetation requires deeper investigations and will be subject of the following chapter. In this chapter, we are going to investigate the impact of vegetation on communication performance based on a profound measurement campaign at different intersections showing an environment, which differ in the type and structure of vegetation.

EVALUATION OF SHADOWING CAUSED BY VEGETATION

After the measurement-based investigation of V2V radio propagation in several urban intersection scenarios presented in the previous chapter, in particular focusing on the impact of buildings, we extend our work in this chapter by an examination of intersections with LOS obstructions caused by clusters of trees and high bushes, since these conditions characterize many rural as well as some urban intersections. In general, radio waves propagating through vegetation experiences different propagation mechanisms such as diffraction, multiple scattering and absorption of radiation. This is mainly caused by the random distribution of leaves, tree trunks and branches, which might result in severe signal fading in the received signal power. Moreover, the foliage density defined as the average number of trees per meter differs with the period of the year. The foliage density of vegetation in summer is higher than in winter resulting in an excess vegetation induced loss produce by foliage. Street trees, in particular at main avenues in big urban cities, play a major role by enabling a certain comfortable and safe feeling, and thus, psychologically and physically protect pedestrians from moving vehicle traffic. On the other hand, trees around intersections would reduce the driver's ability to see potential conflicts immediately in the intersection or before entering an intersection [100]. In such situations, intersection collision applications based on V2V communication could help by giving the capability to see around the corners even in the presence of vegetation. In this context, an important task before the design and deployment of such safety-based applications is a concrete assessment about the impact of vegetation on the communication performance.

Despite an extensive investigation of radio shadowing by the research community, the vegetation effect is largely ignored during the development and design of realistic radio propagation models. This motivates the following measurement campaign, where we investigate radio shadowing by examining the impact of vegetation on V2V communication performance under varying conditions with respect to vehicle positioning, intersection layout and vegetation types. To capture the additional signal attenuation caused by foliage, the measurements for each intersection were conducted both in summer and in winter, which allows comparing the impact of leaved and leafless vegetation. Moreover, we derive the additional attenuation caused by vegetation and compare the measurement results with three well-known empirical models for vegetation-induced path loss. Based on the acquired sets of measurement data, we present a simple parametrized model for estimation of path loss caused by vegetation in V2V scenarios. Parts of the contributions of this chapter have been previously published in [101].

5.1 RELATED WORK

Over the past years, several measurement campaigns investigating radio propagation in forest environments have already been carried out. A critical summary of models for predicting the attenuation of radio waves by trees in the frequency

range of 200 MHz to 9000 MHz is available in Weissberger's final report [102] from 1982. Moreover, the results of a measurement campaign at 11.2 GHz that was conducted at a planted apple orchard with considerable foliage depth in the signal path are presented in [103]. The authors use a theoretical model based on the theory of radiative energy transfer for attenuation and scattering predictions to evaluate the measurement results.

The work presented in [104] provides an empirical model that combines edge diffraction, ground reflection and a direct (through vegetation) signal. The model is based on an elaborate measurement study conducted at twelve locations in England, including different types of trees, both leaved and leafless, considering propagation through single trees, lines of trees, and dense woodland. A methodology to model near-ground short-range propagation loss in forested areas for the VHF and the UHF frequency bands is presented in [105], where the authors also show that reflections caused by a dense tree canopy are of great importance for VHF short-range near-ground propagation.

All these results, however, are applicable for antenna heights from 5 m to 19 m above the ground level only. In the context of V2V communication, taking into account relatively low antenna heights, already small trees or groups of high bushes can provoke radio signal attenuation. Moreover, an excess signal attenuation can be engendered due to humidity of the foliage, which depends on current weather conditions and additionally varies due to seasonal effects. When waves are traveling through sparse and dry vegetation areas, attenuation can be approximately two times smaller [106, 107].

Moreover, particular findings aimed to investigate vegetation impact on radio wave propagation in operating frequencies from 100 to 20.000 MHz have been made in [108], but for up to 5000 meters effective antenna heights, distances up to 1000 kilometers and vertical polarization. Findings in [109] are applicable for frequencies between 2 and 200 MHz. The vegetation layer is a semi-transparent obstacle for centimeter radio waves. They are partially reflected from the obstacle, diffracted from the side and top of the foliage and partly penetrate the tree itself, being absorbed there in the wood and foliage. Moreover, when a radio wave enters a scattering medium, such as vegetation, depolarization of the incident signal may take place. Longer radio waves are mostly absorbed in the tree trunks and branches, whereas the absorption of radio waves at SHF band occurs primarily in the foliage and needles [110]. Hence, deciduous forest in the winter causes practically no additional attenuation on the centimeter radio waves field strength, whereas in the spring or summer vegetative regions can cause already significant signal strength impairment [106].

Up to now, research studies carried out in order to investigate channel impairments due to vegetation have mostly been conducted under conditions that are not directly applicable to V2V environments. To the best of our knowledge, currently there are no publications available which deal with foliage in V2V scenarios.

We present and discuss in this chapter the results of the performance measurement campaign at three intersections showing different vegetation structure and type. Similar to the previous chapter, we quantify RSSI levels, PDRs, and RCRs associated with different intersection and vegetation characteristics. Results are discussed by analyzing the effects of different vegetation types, investigating seasonal effects under leafed and leafless vegetation. The remainder of the chapter provides a survey of vegetation-induced path loss models found in the literature. After-

wards, a derivation of the additional attenuation caused by vegetation is presented. Finally, we present a simple parametrized model for estimation of path loss caused by vegetation in V2V scenarios based on measurement data followed by a comparison with three well-known empirical models for vegetation-induced path loss.

5.2 SCENARIO DESCRIPTION

To investigate the impact of vegetation on radio propagation, we have conducted a measurement campaign at three selected intersections showing different topographies in the area of Braunschweig, Germany. The intersection topographies were selected based on the structure (height and spacing) and growth form of the predominant vegetation as well as on the types of leaves (shape, size, and texture). At all intersections, the transmitter TX was located at a fixed position on a side street, while the receiving vehicle RX moved on an intersecting street, approaching the intersection with a speed of approximately 20 - 25 km/h (see Figure. 27). The test setup included two vehicles of similar height: A Volkswagen Passat was configured as transmitter and a Audi A9 operated as receiver. The measurement parameter setup is the same as described in detail in Table 7 in Chapter 4.
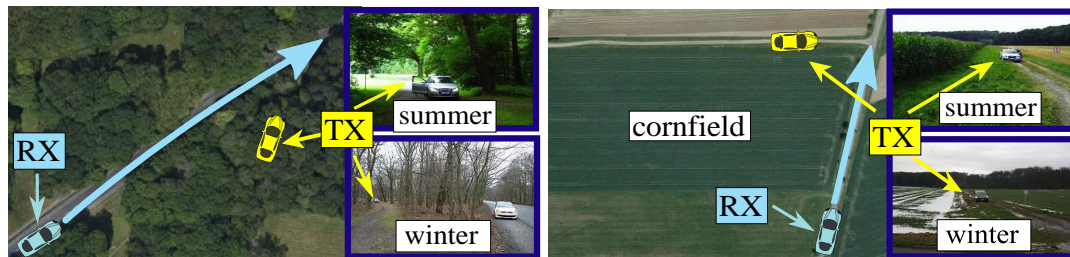
(a) Intersection I: City park area with vegetation of mixed type.

(b) Intersection II: Rural area with a cornfield.
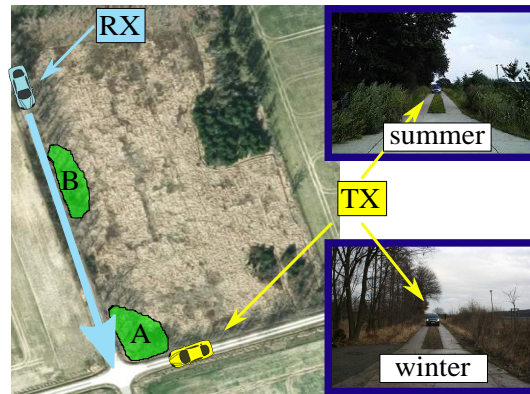
(c) Intersection III: Rural area with thick growing trees and bushes.

Figure 27: Selected intersections (summer and winter): Arrows indicate the direction of motion of the receiving vehicle. The transmitting vehicle's position is fixed.

As reported in related work in Section 5.1, foliage has a significant impact on radio propagation. In order to quantify the impact on V2V communication, we conducted leaved (summer) and leafless (winter) measurements for all three intersections. All measurements were performed under sunny, dry and windless

conditions with almost no other traffic. In the following, we summarize the characteristics of the selected intersections.

Intersection I

The first intersection, which is depicted in Figure 27a, is located within a park area in the outskirts of Braunschweig (Elbertallee) and shows a mixed vegetation pattern. The vegetation is dominated by trees and bushes of unequal height with different foliage densities, types of wood and leaf sizes. As the area is not fully covered with vegetation, the LOS between transmitter and receiver is only partially obstructed. While the receiver moves toward the intersection center, the transmitter is located inside the park. The intersection layout can be considered as a typical on-ramp scenario suitable for V2V merging assistance applications, where one vehicle enters the highway, while another vehicle approaches at high speed. For this purpose, reliable communication at distances sufficient to perform safe merging is necessary even in NLOS situations. The distance between transmitter and intersection center was $d_{TX} = 50\,\text{m}$. Traffic density was very low during the measurements. The geographic coordinates of the center of intersection I are 52°15′59.4″N, 10°33′28.2″E.

Intersection II

At the second intersection, depicted in Figure 27c, a cornfield over a nearly flat terrain completely obstructs LOS between vehicles during summer. This intersection is located on a rural road (K4) in Rieseberg, a city east of Braunschweig. In contrast to the mixed vegetation patterns at intersection I, corn plants have approximately identical height, width, leaf size, chemical composition, etc. Typically, they grow very thick and with approximately equal distances from each other, creating a relatively homogeneous type of vegetation. The height of the plants exceeds 1.5 m and thus creates NLOS conditions between the vehicles' antennas. During summer measurement, the corn plants were dry with slight or no wind. Therefore, in the scope of radio wave propagation through a vegetation layer, a cornfield scenario can be seen as challenging, due to extremely high leaf thickness at the antenna height. There was limited traffic, and the transmitter was placed at a distance $d_{TX} = 30\,\text{m}$ from the intersection center. The geographic coordinates of the center of intersection II are 52°17′10.8″N, 10°47′00.0″E.

Intersection III

Located in a rural area east of Braunschweig, the third intersection shows densely growing trees and bushes, as depicted in Figure 27b. It is characterized by thick-growing trees, dense underbrush, and high grass (at several places up to ca. 1 m). Compared to Intersection I, trees at intersection III have a lower height, and it can be observed that their branches start to grow only several centimeters above the ground. Moreover, the vegetation is very dense (large trees, grass and bushes) along the roads, but considerably sparser (small young trees, a lot of high grass, less bushes) in between. Therefore, the total vegetation density might be lower than at intersection I, but the density of leaves and high grass at antenna height is significantly higher. At a distance of approximately 70 m from the intersection

center as well as directly at the intersection, there are considerable expansions of bushes next to the roads (see areas A and B marked in Fig. 27b). The transmitting vehicle was positioned at a distance $d_{TX} = 50\,\mathrm{m}$ from the intersection center, and there was no other traffic or other human activities. The geographic coordinates of the center of intersection III are 52°15′22.2″N, 10°38′54.6″E.

5.3 MEASUREMENT RESULTS

In this section, we discuss the results from the measurement campaign. First, we analyze the effects of different vegetation types. Second, we investigate seasonal effects by comparing the measurements performed in summer and in winter. For these purposes, we evaluate the received power P_r for each successfully received frame and its arithmetic mean $\bar{P}_r$ for each distance interval of $5\,\mathrm{m}$ length, and we calculate the ratio of the numbers of successfully received and transmitted frames for each distance interval, which we refer to as the PDR. Furthermore, we define the RCR as the vehicle's distance to the intersection center where the PDR decreases below 90 %, which should ensure proper operation of V2V crash avoidance applications. However, the study in [111] recommended to consider the threshold at 95 %, which implies that we use a more relaxed assumption. Nevertheless, applying a threshold at 90 % in the investigation will not influence the interpretation of results. Besides its importance on the evaluation of the reliability of safety-based applications, this metric allows a comfortable comparison of results.

At each intersection, we conduct six measurement runs to ensure statistical validity of the results. Arithmetic means are calculated based on all runs for each intersection and presented with 95 % confidence intervals. In order to be able to assess the impact of the vegetation type, we focus on the received power P_r for each received frame, indicating the signal fading, the mean received power $\bar{P}_r$ and the PDR for each distance interval. As received power samples can only be collected for successfully received frames, the calculated arithmetic mean $\bar{P}_r$ reflects the real mean received power sufficiently well only for distance intervals with high PDRs, while it significantly overestimates the real mean received power for low PDRs.

5.3.1 *Vegetation Structure and Type*

To track the impact of the vegetation structure and type in term of growth form of the predominant vegetation (foliage, tree trunk) as well as the shape, size, and texture of leaves, we performed experiments with the same configurations at three different intersections showing different vegetation structure.

Summer measurements

For measurements performed in summer, Figure 28 presents the aforementioned performance metrics as a function of the distance d_{RX} between the receiving vehicle and the center of intersection I, II and III. First of all, we observe that, in general for all intersections, both $\bar{P}_r$ and PDR decrease with increased distance d_{RX} between the receiving vehicle and the intersection center. We also notice that the maximum values of P_r and $\bar{P}_r$ are achieved at the minimal distance between transmitter and receiver. However, particularly for the intersection I as illustrated in Figure 27,

(a) Intersection I

(b) Intersection II

(c) Intersection III

Figure 28: Measurement results in summer: Raw received power (P_r), mean received power ($\bar{P}_r$) and mean PDR against the distance d_{RX} between the receiving vehicle and the center of the intersection I, II and III.

these values are at maximum when the receiver is at a the distance $d_{RX} = 50\,\text{m}$ from the intersection center.

Moreover, the results significantly differ for different types of vegetation. In particular, P_r as well as PDR indicate stronger signal fading for intersection I (see Figure 28a) than for Intersection II (see Figure 28b). This can be attributed to the heterogeneity of vegetation structure observed at intersection I, where size and density of trees and bushes widely vary, causing stronger fluctuations of the propagating signal. The compact and homogeneous structure of the vegetation around intersection II strongly attenuates the received signal power, which is comparable to the impact of a NLOS obstruction caused by a building as found in Chapter 4. The PDR results at intersection III (see Figure 28c) are particularly interesting, where we observe two significant PDR drops for $d_{RX} \approx 25\,\text{m}$ and for $d_{RX} \approx 65\,\text{m}$, which corresponds according to Figure 27c to areas A and B, respectively. This indicates that these drops are caused by the areas around intersection III where the vegetation structure is extremely dense and impenetrable, as described in Section 5.2. We conclude that with respect to different types and structures, the vegetation has not only a significant influence on received power, but also on the number of successfully received frames.

Winter Measurements

As foliage may considerably affect radio propagation in terms of attenuation and multipath propagation, we investigate its influence on the communication performance in this subsection. For this purpose, we conduct a second measurement campaign in winter, which exactly reproduces the summer measurement campaign's configuration. Tree leaves die and fall off due to the extreme coldness in winter, which leads to a low density of foliage up to no leaves on trees. At the first glance, the results in winter and plotted in Figure 29 appear to be similar to those obtained in summer. However, we observe, in general for all intersections less signal fluctuation of the received signal power. Especially for intersection I in Figure 29a, the PDR presents a smooth course with weak signal fading and remains at maximum up to $d_{RX} = 200$ m, implying that all transmitted packets reached the receiver. By observing the achieved PDR in particular for intersection I and II, we can conclude that the absence of foliage could significantly improve the communication performance. Moreover, drops at areas A and B on the PDR course in Figure 29c at intersection III remain even when there are almost no more foliage obstructing the communication link. This may be attributable to the considerable amount of wide tree trunks, which are still present in winter.

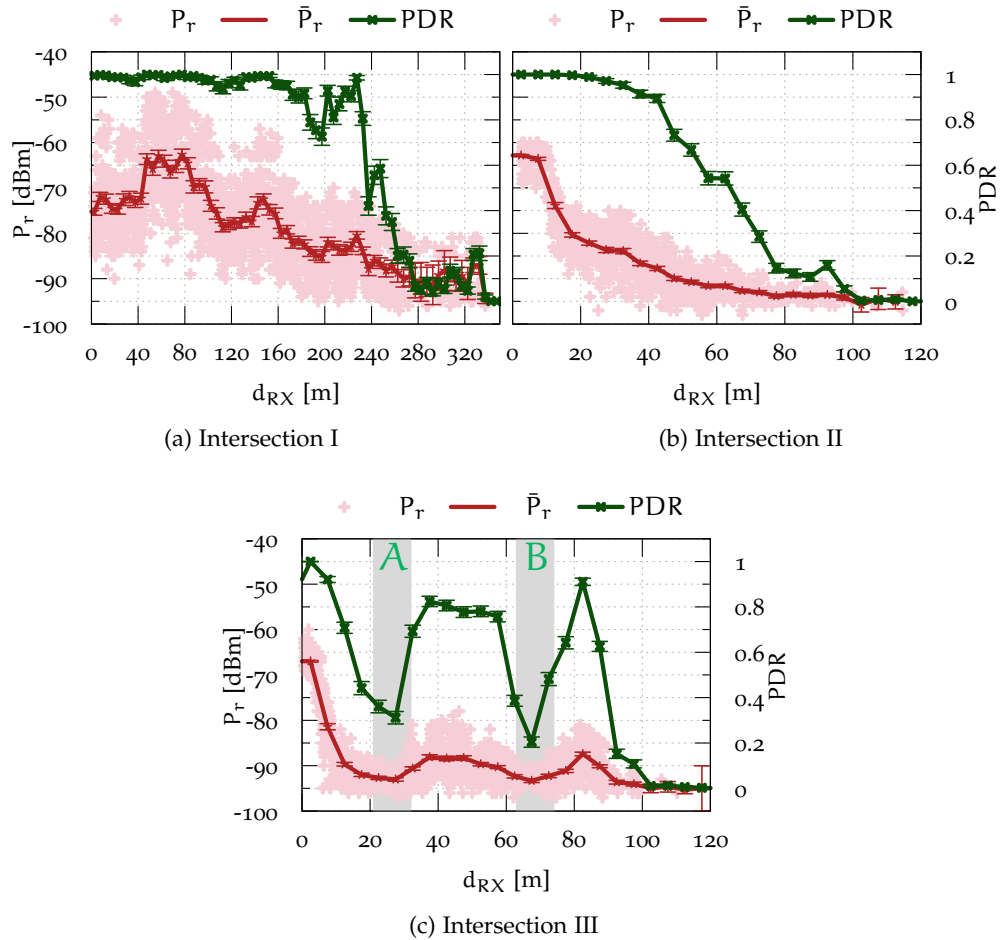(a) Intersection I

(b) Intersection II
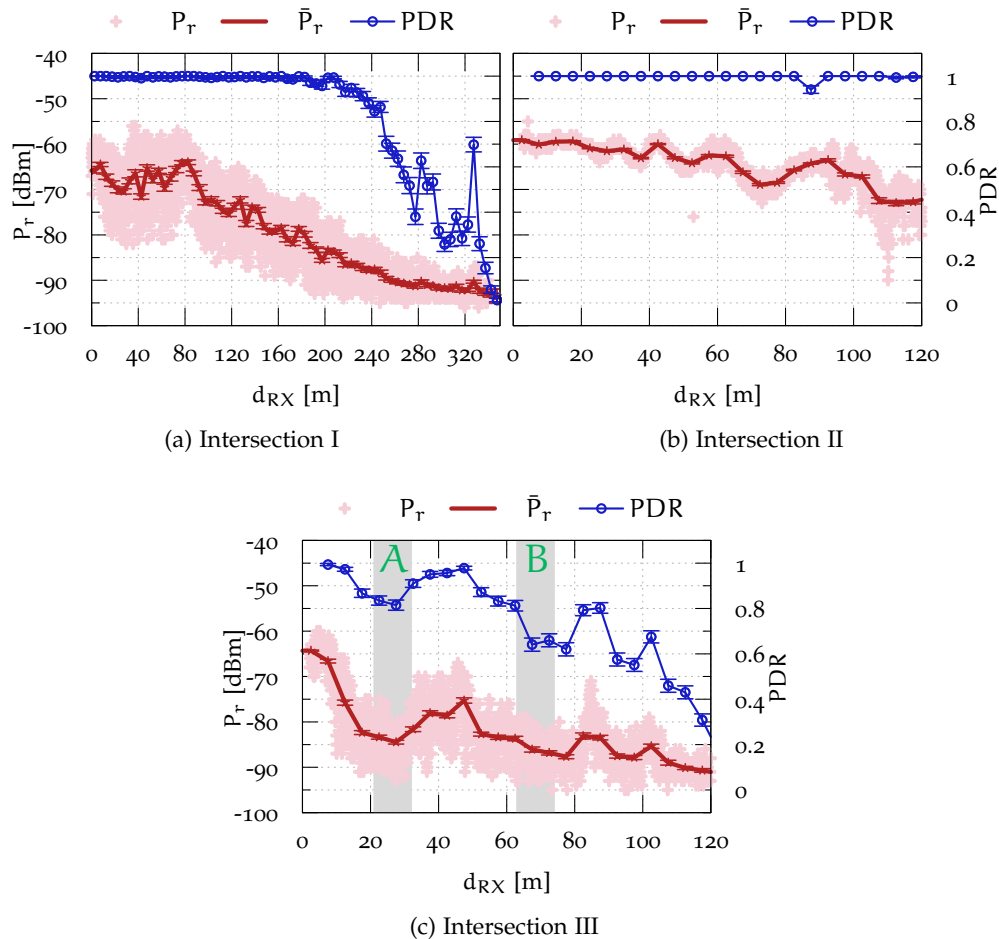
(c) Intersection III

Figure 29: Measurement results in winter: Raw received power (P_r), mean received power ($\bar{P}_r$) and mean PDR against the distance d_{RX} between the receiving vehicle and the center of the intersection I, II and III.

5.3.2 *Seasonal Effects on Communication Reliability*

For a reasonable comparison and discussion of results, we plot results from measurements performed in summer and in winter together in a common Figure 30.

(a) Intersection I

(b) Intersection II
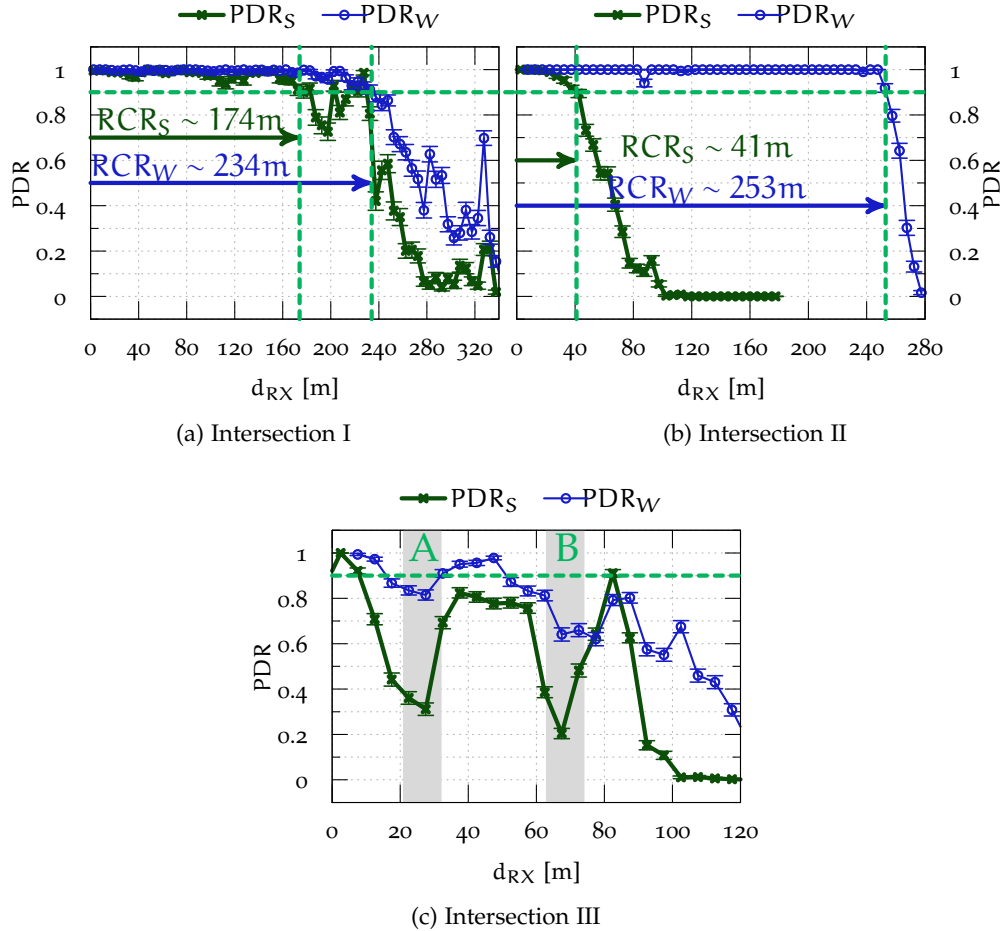
(c) Intersection III

Figure 30: Comparison of the mean PDR for the measurement performed in summer and in winter for intersection I, II and III.

For the sake of clarity, we only present PDR and the aforementioned RCR results here. The horizontal dashed lines on the figures represent a PDR of 90 % needed to estimate the RCR. As expected, results clearly demonstrate that the absence of foliage considerably improves communication reliability. At intersection I, the RCR is approximately doubled from $RCR_s \approx 174$ m to $RCR_w \approx 234$ m (see Figure 30a). The RCR obtained at intersection II increases even more substantially from $RCR_s \approx 41$ m to $RCR_w \approx 253$ m (see Figure 30b), which corresponds to an increase by almost 600 %. In this context, it has to be noted that due to the fact that the cornfield between both vehicles has lain fallow, the winter measurements have been performed under perfect LOS conditions. For intersection III, Figure 30c illustrates that the PDR drops corresponding to areas A and B in Figure 27c are considerably less pronounced in winter, which emphasizes the negative impact of leaves. However, we still observe substantial packet losses, which assert the severity of tree trunks and branches on the communication performance. In summary, these results show very

clearly that there is a fundamental impact of foliage on V2V communication reliability, which cannot be neglected in the context of VANET performance evaluation.

5.4 VEGETATION PROPAGATION MODELING

After a detailed investigation of vegetation effects on the communication performance, we propose in this section a site-specific vegetation path loss model based on the acquired sets of measurement data. This simple parametrized model for estimation of path loss caused by vegetation can be then integrated in a simulation platform for more realistic performance evaluation of VANETs, especially at rural environments.

5.4.1 *Survey of Vegetation-induced Loss Models*

Particularly for rural and suburban environments, propagation models which include the impact of vegetation characteristics and types are essential for safety-based application designers. Because a credible simulation-based evaluation of the capability of V2V applications requires accurate modeling of the radio propagation channel. Based on existing radio propagation models found in the literature, we classify propagation models that quantify path loss under consideration of vegetation effects into three types of models: analytical, empirical and semi-empirical models.

ANALYTICAL MODELS: These models are based on detailed modeling of the vegetation's physical effects on radio wave propagation in order to provide electromagnetic formulas used to determine the path loss between two points. Research results in [104] report that dielectric objects such as branches, twigs and leaves significantly attenuate the received signal level at higher frequency bands. A review of models available in the literature reveals that theoretical models require the use of a large number of equations describing the physical structure of radio wave propagation. Moreover, the models tend to be extremely complex and require excessive computational resources. However, these physics-based models provide a high accuracy of the path loss estimation. Two common approaches can be distinguished: solving electromagnetic equations and using ray tracing, which is the most widespread method.

EMPIRICAL MODELS: While semi-empirical models are created using a combination of measurement data collected in the real world and analytical modeling, empirical models are solely based on characteristic experimental results. In contrast to analytical models, empirical models have the advantage of being easy to apply, due to the simplicity of the resulting mathematical expressions that characterize path loss.

In this section, we investigate the effects of different vegetation types empirically and deduce additional vegetation-induced path loss. For this purpose, we compare our measurement results with selected well-known empirical models for estimation of vegetation-induced path loss, which are shortly summarized in the following.

The *Modified Exponential Decay Model* developed by Weissberger in [112] and given in Equation 6 is based on the results of a profound measurement campaign in

the United States at frequencies from 230 MHz to 96 GHz. It quantifies vegetation-induced path loss in dB as

$$L_{MED} = \begin{cases} 0.45 \cdot f^{0.284} d_v \, , & 0\,m \leqslant d_v \leqslant 14\,m \\ 1.33 \cdot f^{0.284} d_v{}^{0.588} \, , & 14\,m < d_v \leqslant 400\,m \end{cases} \, , \qquad (6)$$

where f denotes the carrier frequency in GHz and d_v the depth of vegetation in meters. It is applicable to situations where the propagation is likely to occur through a cluster of trees rather than by diffraction and hence might also be applicable to scenarios investigated in this work.

The *COST235 Model* [113] in Equation 7 is based on measurements at frequencies from 9.6 MHz to 57.6 GHz through a small (d_v < 200 m) cluster of trees. This model takes into account seasonal effects by distinguishing between winter, when trees are leafless, and summer, when they are in leaf:

$$L_{COST} = \begin{cases} 15.6 \cdot f^{-0.009} d_v{}^{0.26} \, , & \text{with leaves} \\ 26.6 \cdot f^{-0.2} d_v{}^{0.5} \, , & \text{without leaves} \end{cases} \, . \qquad (7)$$

The *ITU-R Model* [114] is based on measurements validated at frequencies from 200 MHz to 95 GHz and for distances d_v through vegetation consisting of trees up to 400 m, and is given as

$$L_{ITU} = 0.2 \cdot f^{0.3} d_v{}^{0.6} \qquad (8)$$

In contrast to *Modified Exponential Decay Model*, for the *COST235* and *ITU-R*, f is expressed in MHz.

5.4.2 *Site-specific Vegetation Loss Model*

Prior to the development of the model, we require knowledge about the signal attenuation caused by vegetation. To derive this additional component from our summer measurements, we employ the *Log-Distance Path Loss Model* to approximate vegetation-free (LOS) propagation conditions. In this model, the received power $P_{r,LOS}$ (in dBm) at a distance d from the transmitter is calculated as

$$P_{r,LOS}(d) = P_t - PL(d_0) - \alpha 10 \log \left(\frac{d}{d_0} \right) \, , \qquad (9)$$

where P_t denotes the transmit power in dBm and $PL(d_0)$ the path loss in dB at a reference distance d_0, which can be calculated, for example, using the free space model. The parameter α is known as the path loss exponent and depends on the propagation environment. Hence, the additional vegetation-induced path loss $L_{add}(d)$ (in dB) compared to perfect LOS conditions between two stations can be computed as

$$L_{add}(d) = P_{r,LOS}(d) - P_{r,meas}(d) \, , \qquad (10)$$

where $P_{r,meas}(d)$ (in dB) is the average measured received power. Based on an investigation of the previously presented models, it is found that in general, the additional loss induced by vegetation can be adequately represented by

$$L_{veg} [dB] = K \cdot d_v{}^\beta \; , \tag{11}$$

where d_v is the vegetation depth in meters. However, all models described above require knowledge about the depth of the vegetation d_v, which is difficult to obtain. In order to overcome this limitation, we propose a simple empirical model for vegetation-induced path loss at 5.9 GHz, which is derived from our measurement results using regression analysis. This deterministic model only requires knowledge about the distance between transmitter and receiver, and hence can easily be integrated into simulation-based performance evaluation. For this purpose, using regression techniques based on our summer measurements, we fit Equation 11 to the measured vegetation-induced signal path loss L_{add} at intersection I in order to obtain a site-specific vegetation model that is based on the distance between the transmitter and the receiver only. Applying linear regression to the measured additional path loss yields $K = 2.6$ and $\beta = 0.42$, which corresponds to the best fit. Using these findings, the vegetation-induced path loss at intersection I can be quantified as

$$L_{veg} [dB] = 2.6 \cdot d^{0.42} \; , \quad 10\,m < d \leqslant 200\,m \tag{12}$$

where d is the distance between transmitter and receiver in meters. This model is valid for distance d up to 200 m.

For intersection I, Figure 31 shows a comparison of the additional vegetation-induced path loss resulting from our measurements, the results of the existing models presented above and the results of our parametrized model according to Equation 12 as a function of the linear distance $d_{TX\text{-}RX}$ between transmitter and receiver. Root-Mean-Square Errors (RMSEs) were calculated for each investigated model based on the measurement results in order to compare the accuracy of the vegetation-induced path loss estimation. The results show that the ITU-R (L_{ITU}) and COST (L_{COST}) models significantly overestimate the attenuation, as RMSEs of 19.7 dB and 14.2 dB, respectively, indicate. Only the Modified Exponential Decay Model (L_{MED}) provides a consistently close fit. Obviously, the proposed model (L_{veg}) yields the smallest RMSE (3.8 dB) due to its site-specific fitting to the measurement results.
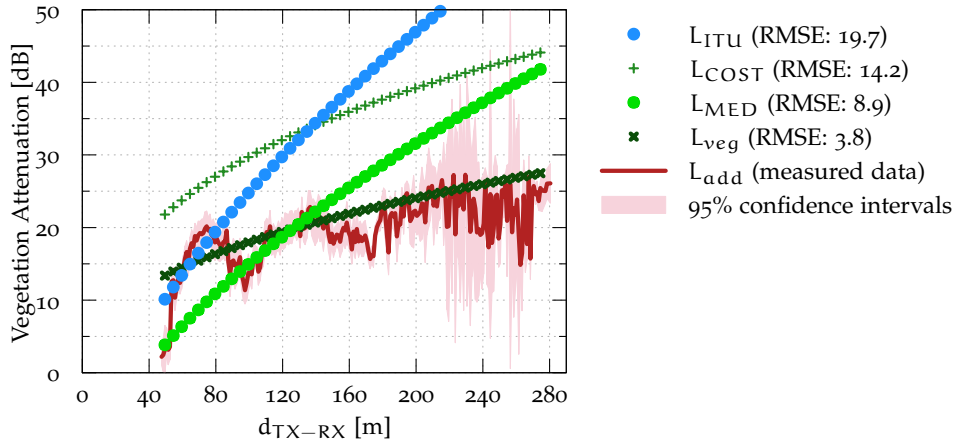
Figure 31: Comparison of vegetation loss models for intersection I.

5.5 SUMMARY

In this chapter, we evaluated based on measurements the impact of vegetation on V2V communication performance. The measurement campaign has been conducted at three different urban and rural intersections with respect to intersection layout and vegetation type. We analyzed received signal power levels, packet delivery ratios, and reliable communication ranges for measurements conducted in summer and in winter. We have clearly shown how different vegetation types and structures impact the communication link. We also demonstrated how seasonal effects characterized by leafed or leafless vegetation, can affect the reliability of the V2V communication in term of achievable communication range. Considering the impact of vegetation structure, a heterogeneous vegetation consisting of a mix of trees and small plants appears to be less aggressive than a homogenous and dense structure of plants such as cornfields.

After surveying well-know empirical models for vegetation-induced loss, we developed a dedicated vegetation-based path loss model, especially for V2V urban intersections. The model was parametrized based on measurement results and can easily be implemented to retrofit path loss models of existing simulation tools. For a proper assessment about the capability of V2V, the additional vegetation-induced attenuation has to be considered in the context of VANET performance evaluation since vegetation is often present in vehicular environments.

Although we covered the problem of radio shadowing caused by vegetation, and by buildings in previous chapters, we should keep in mind that the evaluation was based solely on a pair of communication partners. However, the performance of V2V will depend on the number of nodes sharing a single broadcast channel. This motivates the measurement-based evaluation presented in the next chapter, where we studied the impact of co-channel interference on the communication performance. Moreover, the influence of buildings on the interference is carefully assessed.

RADIO SHADOWING THROUGH BUILDINGS AND ITS IMPACT ON CO-CHANNEL INTERFERENCE

ADAS which are based on on-board environmental sensors could exploit V2V communication to extend the driver's horizon. In this context, safety-based applications in VANETs would support such kind of systems by providing additional information through the wireless exchange of status information and hence ensure a cooperative awareness between vehicles and their neighborhood. Although, the vehicular communication has to deal with a lot of challenges including the highly dynamic topology of vehicular networks and the inevitable presence of numerous mobile and static obstacles, especially frequent at urban intersections, the natural and non negligible co-channel interference is of major interest as safety-based applications rely on the single-hop broadcast of status information shared on a single channel. This implies that under high vehicle densities, the channel will suffer from severe congestion which subsequently leads to a rapid degradation of the communication performance reflected by long delays and packet collisions. Recently, important vehicle manufacturers have signalized their intention to bring cooperative systems based on inter-vehicular communication onto European roads starting this year, which implies that V2V systems are close to market introduction. While in the early stage of deployment only a small portion of vehicles will be equipped with a communication system, traffic density can be expected to grow substantially during peak hours in urban environments. For this reason, a fundamental task before market introduction, is a field test investigation of the scalability effect as safety-based applications should operate in very sparse as well as in highly overloaded networks. Furthermore, it has been shown in several research studies that scalability in vehicular networks is limited by interference [115, 65, 116, 117]. Towards this objective, the analyse of co-channel interference on the performance of V2V communication based on real world measurements is indispensable in order to draw conclusions about the effective contribution of VANET on urban road traffic.

In general, the scalability evaluation of VANETs is mostly achieved through simulation technique. Because it allows an investigation of large scale scenarios involving a high number of vehicles. However, due to the low degree of realism of integrated communication models, this approach fails in the achievement of high levels of accuracy. Furthermore, assumptions about the scenario-specific radio propagation in terms of path loss and signal fading have to be made. This might lead to limited statements through the use of inaccurate communication and propagation models. However, the simulation method includes somehow the co-channel interference and its severity on the communication performance. On the other hand, the measurement-based evaluation which is generally conducted under interference-free conditions, requires a huge logistic to control experiments whenever the co-channel interference shall be considered. Moreover, the synchronization of measurement runs as well as the post-processing of data gathered during measurement campaigns introduce a new dimension of complexity. To provide a meaningful evaluation of interference, an aggregation of measurement data col-

lected at each participating vehicle is indispensable. This motivates the presented work in this chapter which introduces an abstraction method by which a single vehicle is configured as a set of vehicles. Through this assumption, a measurement-based evaluation of co-channel interference can be achieved.

In general, there are two main types of interference in wireless transmission: Adjacent channel interference and co-channel interference. While the former is caused by imperfect filters in the analog front-end, which produce a small portion of interference in neighboring bands, the latter happens due to nodes operating in the same frequency band. As we are interested on co-channel interference, investigating adjacent interference is out of scope in this thesis and is not further taken into consideration. The effect of co-channel interference in VANETs has been scarcely investigated by the research community from the empirical point of view. Measurement studies found in the literature, and presented in the next section, do not address the problem of building shadowing and its relation to interference. Hence, we are particularly interested in gaining insights into the complex inter-dependencies between radio shadowing, co-channel interference and communication performance. Therefore, the purpose of this chapter is to explore the possibility of using a single node to emulate a set of nodes aiming to overcome or to facilitate the logistic issue during measurement campaigns. We are also considering the impact of interference as well as the impact of buildings on the communication performance in real world measurements. In this chapter, after presenting a survey on the experimental evaluation of VANET, we will give a brief overview about the approach behind the emulation of co-channel interference in vehicular networks. The subsequent section describes test scenarios and the measurement setup. After that, we will discuss obtained results by firstly analyzing the position accuracy during the experiments. Following sections deal with the building shadowing and its impact on co-channel interference by examining packet delivery ratios with respect to intersection types. finally, an assessment about packet delays in term of inter-reception time closes this measurement-based study. Parts of the contributions of this chapter have been previously published in [118].

6.1 RELATED WORK

In the last years, several research studies on the performance evaluation of V2V communication were conducted with the aim of characterizing the radio propagation channel in small scale field trials. The main goal is often to gain insights into adequate path loss modeling applicable for V2V communication which can be then integrated in simulation studies. One of the first measurement studies in the 5.9 GHz frequency band using channel sounder was reported in [119]. The authors have developed a channel emulator model for a doubly selective vehicle-to-vehicle wireless channel based on measurements taken in an expressway environment. A similar study using a prototype Dedicated Short Range Communications (DSRC) module was conducted in [43] where the authors have presented narrow-band measurements of a channel by modeling and predicting the channel Doppler spread and coherence time under realistic suburban driving conditions.
Regarding the effect of radio shadowing caused by stationary objects or mobile obstacles such as vehicles, there are several research studies evaluating the impact of shadowing on the communication performance through field test experi-

ments [94, 120]. A measurement campaign conducted at various environments in [56] reported that while vehicular obstructions could significantly attenuate the signal power, the effect of stationary obstacles such as buildings is even more pronounced. A similar study was reported in our previous chapter, where we concentrated on the evaluation of the impact of vegetation on V2V communication through a 5.9 GHz measurement campaign conducted at intersections with different types of vegetation. In [51], results for 35 field trial data sets collected in Australia, Austria, Germany, Italy, and the United States, covering over 1100 km on the road in a wide variety of physical environments were presented. The performance of commercial off-the-shelf radio wireless cards compared with a more advanced 802.11p compliant radio was also presented.

With respect to the complexity in the execution of field test experiments involving more than two vehicles, only few empirical studies on the evaluation of interference in VANETs are available. More recently, Boban et al. [121] have evaluated the capability of cooperative awareness for vehicular networks based on data collected within an extensive measurement campaign at four European test sites showing different type of environments (urban, suburban and highway). To the best of our knowledge, this is one of the few in the context of empirical evaluation approaches that involves up to 7 vehicles during the experiments. Similar to our investigation approach, Schmidt et al. [122] analyzed the degradation of communication range caused by co-channel interference through real world measurements. While the interferer was configured to fully utilize the channel capacity by sending at maximum rate, the authors have focused more on the impact of the distance to the interferer in order to investigate the placement of the nodes on the interference severity. Following the same trend, the work in [123] uses a five vehicles configuration in order to investigate the inter-reception time based on real-world measurements. The goal hereby was to derive the packet inter-reception time and provide a model used to estimate the application reliability in presence of radio channel congestion. Despite the consideration of co-channel interference, the impact of building obstruction was not considered in this work.

These studies present significant differences in their measurement methods as well as in their objectives. Therefore, we believe that additional measurements are needed to thoroughly analyze in a realistic way the influence of interference on the communication performance. Motivated by this fact, we are interested in investigating the impact of interference as well as the impact of buildings through real world measurements, especially at intersections. To achieve this goal, we put attention to a careful selection of representative intersections and to find test scenarios that allow a meticulous evaluation.

6.2 APPROACH FOR THE EMULATION OF CO-CHANNEL INTERFERENCE

The key challenge of V2V is to ensure the reliability of the communication in such a way that a cooperative awareness between nodes in a direct neighborhood can be permanently achieved, even in saturated network conditions. For this purpose, the MAC sublayer of IEEE 802.11p is inherited from IEEE 802.11a and, thus, based on the CSMA/CA protocol, which provides a simple mechanism to manage channel access in a distributed and scalable way. This protocol allows a node to sense the channel before effectively transmitting. Depending on the channel state (e.g.,

idle or busy), the transmission is started or postponed. Considering the single-hop broadcast nature of VANETs, where all nodes share a common channel, packet receptions will be subject to co-channel interference. In addition, the broadcast transmission is more probable to collisions since the RTS/CTS frame exchange and fault recovery mechanisms based on ACKs are missing. For all the aforementioned reasons, packet collisions due to co-channel interference are inevitable since they will occur not only when two nodes start simultaneously to transmit their frames, but also due to the well-know *hidden node problem*. Recall that a node is declared to be hidden when it is located out of range of the transmitter but close enough to the receiver so that it can disturb any frame transmission between transmitter and receiver. However, a measurement-based characterization of packet collisions is, thus, out of scope of this work and will be subject of further studies, we rather focus on the inter-dependency between building shadowing and co-channel interference.

Typically, most wireless interfaces assume that a packet can be successfully decoded if the SINR during packet reception is greater or equal to a given threshold. This ratio can then be used to understand the influence of interference on packet loss, since the stronger the interference level, the lower the probability of packet reception. In other words, only the strongest signal at the receiver can be decoded, treating the other signals as interference. For the sake of simplicity, the SINR can be expressed as

$$\text{SINR} = \frac{P_r}{N + \sum_{i=0}^{I} P_i} = \frac{P_r}{N + P_1 + P_2 + \cdots + P_I} \tag{13}$$

where P_r is the received power of the strongest signal, N the background noise and $\sum_{i=0}^{I} P_i$ the interference generally considered as the sum of all interfering signals P_i. As the probability of packet reception is based on the achieved SINR, investigating the effect of co-channel interference in field tests requires to involve a large number of vehicles represented by the set I. Each interfering vehicle i will then produce an interference signal due to its received signal power P_i at a certain receiver. Basically, most of the field test experiments found in the literature rely on two vehicles involving two up to four people so that their execution appear to be relatively manageable. But for the scalability evaluation, the human factor constitutes the main bottleneck in the measurement execution reflected by the increasing number of helpers.

By studying how VANET scales, the authors in [124] have defined a metric, the so-called *communication density CD*, which is used to quantify the input of the channel. It is expressed as the product of the vehicle density ρ, the message generation rate f_g, and the transmission range R, given by

$$CD = \rho f_g R \tag{14}$$

It is shown in this work that simulations with comparable broadcast transmissions have the same communication performance in different scenarios setup as long as the transmission power is the same. For example, a scenario with vehicle density ρ and sending at rate f_g experiences the same or very similar communication

performance as in a scenario with density $\frac{\rho}{k}$ and rate kf_g, as mathematically given by

$$\rho f_g = \frac{\rho}{k} k f_g \qquad (15)$$

This insight leads to the realization that the channel load produced by a group of vehicles can be simply summed up to form the load generated by only a single vehicle. Figure 32 illustrates this interpretation where a set of interfering vehicles IX in a real traffic situation is substituted by a single vehicle. For this purpose, our approach consists of using a single node as a set of interferers by sending at a higher transmit rate. Through this abstraction, we are then able to investigate the impact of interference by using only three vehicles. This simple assumption reduces the level of complexity not only during the measurement, but also in the post-processing of gathered data.

However, using this abstraction, it should be noted that the level of interference severity is being significantly underestimated since collisions caused by packet overlaps from several interferers would be hard to capture. Furthermore, even if the channel utilization will not be fully comparable with that achieved by a large scale field test involving hundreds of vehicles, using this emulation approach is a good compromise between accuracy and logistic issue during the measurement.

(a) Real Scenario   (b) Abstracted Scenario
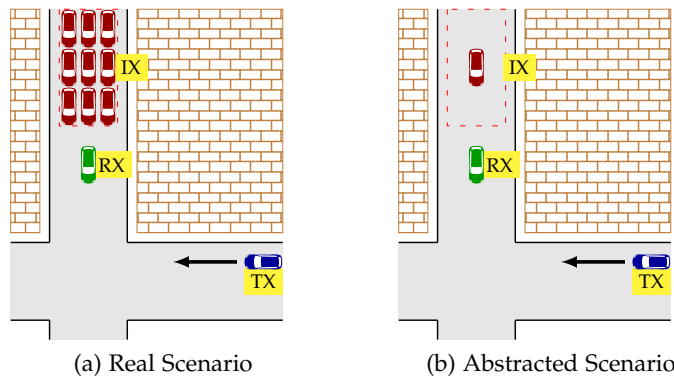
Figure 32: Approach: Set of interferers substituted by a single node.

6.3 MEASUREMENTS SETUP AND SCENARIO DESCRIPTION

6.3.1 *Measurement Setup*

In order to set up, control and monitor the experiments during the measurement, we extend our measurement platform by integrating a real time monitor system in the existing measurement software presented in Chapter 4.2. The monitoring system includes a web-based front-end interface which provides real time information about received signal power, packet delivery ratio, current speed, distance between transmitter and receiver as well as a map for the geographical visualization of the participating vehicles using data from `OpenStreetMap`. Moreover, communication parameters as transmit power, packet generation rate, and data rate could be set through the interface based on `HTML5` and Websockets. In the context of measurement results validity, taking into account the performance of the CPU of the communication module, high CPU loads during measurements can provoke

packet loss. Hence, to evaluate the influence of such a monitoring system on the reliability of the measurement results, we conducted a preliminary lab test involving three communication modules. Two modules were configured as transmitter and the third one as receiver and located close to each other. We performed this test under perfect LOS condition and high network loads by setting the packet generation rates of the interferer close to the network limit. We compared then the measured PDR first performed without the monitoring system and then including it. The obtained results of CPU load show no noticeable influence of the monitoring system.

We conducted the measurement campaign at two different days under sunny and dry conditions. Each scenario was conducted first without IX and then including it with the aim to capture the impact of interference. During the whole experiments, TX and IX were configured to send with 10 msgs/s and 1000 msgs/s, respectively. The technical parameters of the measurement are listed in Table 8.

	PARAMETER	VALUE
PHY	Transmission power (EIRP)	23.2 dBm
	Center carrier frequency	5.9 GHz
	Channel bandwidth	10 MHz
	Data rate	6 Mbps
	Antenna height	1.5 m
CAM	Message generation rate	10 msgs/s for TX
		1000 msgs/s for IX
	Message payload size	500 Bytes

Table 8: Measurement system parameters

6.3.2 Selected Intersections

To evaluate the impact of stationary obstacles on the severity of interference, we conduct a measurement campaign at two different intersections under LOS and NLOS conditions. As depicted in Figure 33a, the intersection *Elisen* is a typical inner-city intersection with low traffic density located in the city of Hannover while the second intersection *Messegelände* is a rural intersection located within an exhibition site in the outskirts of Hannover in Germany (see Figure 33b). The intersection *Elisen* is closed and belongs, therefore, to Type 4 according to the study presented in Chapter 3. This implies that there are buildings at each four corners creating shadowing in the communication link between the transmitting TX and the receiving RX vehicle while approaching the intersection's center. Whereas, the intersection *Messegelände* belongs to Type 0 due to missing buildings around. The distance between the intersection center and the corner of the nearest building was approximately 13 m. Moreover, there were cars parked on both sides of the streets and the traffic density was low during the measurements. Despite the relatively high height of surrounding buildings, GPS positioning data was always available during the experiments. We select a representative open-area environment without buildings and obstacles around the corners for the rural intersection so that the

between vehicles was constantly available. In contrast to intersection *Elisen*, the measurements in intersection *Messegelände* were performed under almost no other traffic.

(a) Intersection Elisen: Closed inner-city intersection with buildings on four legs. 52°22′27.15″N, 9°42′27.15″O

(b) Intersection Messegelände: Rural intersection within an exhibition site under open environment. 52°18′50.53″N, 9°49′19.70″O

Figure 33: Intersection *Elisen* (a) and *Messegelände* (b): Arrows indicate the direction of motion of the transmitting (TX) vehicle. The receiving (RX) and the interfering (IX) vehicle's position are fixed. Geographic coordinates of each intersection's center are given.

6.3.3 Scenario Description

In order to quantify the effect of buildings, vehicle's position and the presence of interference, we selected 3 different scenarios in urban as well as in rural environments. Each scenario was reproduced with the same configuration on both environments and differ in the placement of communicating vehicles. In the following, we summarize the objectives and characteristics of the selected scenarios.

Scenario A

The objective of this scenario is to evaluate the influence of hidden nodes created by the vehicle IX by focusing on the link between the transmitter TX and the receiving vehicle RX. As illustrated in Figure 34a, depending on the location of TX and IX , and also through the building's shadowing, both nodes would be out of range of each other and so cannot detect a collision while transmitting. In such case, these nodes are known as hidden. Moreover, the SINR of the transmitting frame would probably be degraded by the high level of interference due to the closeness between the interferer and the receiving vehicle. This scenario can be considered as a typical use case where one vehicle (RX) in the front of a cluster of vehicles (IX) traverses the traffic light, while another vehicle (TX) is moving toward the intersection at high speed. In such situations, it is expected that intersection collision avoidance applications, such as intersection collision warning which informs the driver about a risk of collision, perform successfully. Regardless of the intersection type, the receiver and interferer in this scenario were parked at a fixed distance $d_{RX} = 75\,\text{m}$ and $d_{IX} = 95\,\text{m}$, respectively, while the transmitter is moving starting at a distance of $d_{IX} = 170\,\text{m}$ from the intersection center.

Scenario B

The key objective in this scenario is the evaluation of the impact of the building shadowing on the packet delivery ratio. Considering the link between TX and RX, buildings may block the interference signal produced by IX. It is interesting to quantify the portion of interference which can be attenuated by comparing the communication performance on both intersection types. In other words, the main question is to investigate how buildings limit the undesirable interference and if in such situations, they will bring a positive effect, as such use cases are typical in urban traffic. Like Scenario A, IX will be hidden to TX, which - depending on the location of the transmitter TX - will lead to packet collisions at the receiver. As illustrated in Figure 34b, receiver and interferer were parked at a fixed distance $d_{RX} = 70$ m and $d_{IX} = 75$ m, respectively, while the transmitter is moving toward the intersection, starting at a distance of $d_{IX} = 170$ m.

Scenario C

In this scenario, we address the problem of sudden appearance of interference. For example, in the inner-city intersection, the ray path between IX and RX is completely obstructed by buildings, depending on the location of RX. It is expected that obstructed buildings block or limit the interference level generated by IX so that the near far effect could be observed. According to the location of RX, it will receive more power from TX, then due to building obstruction, the signal of IX will be considerably attenuated so that it slightly contributes on the achieved SINR. In contrast to the aforementioned scenarios, transmitter and interferer were parked at the intersection center $d_{TX} = 0$ m and $d_{IX} = 75$ m, respectively, while the receiver is moving toward the intersection, starting at a distance of $d_{IX} = 170$ m (see Figure 34c).
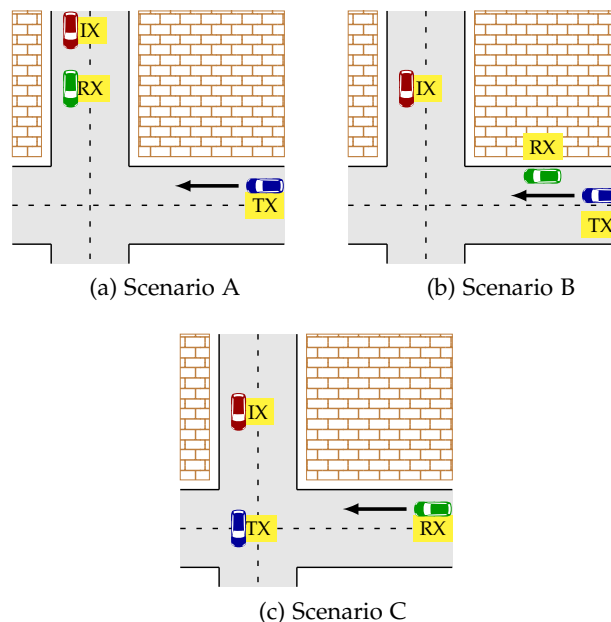

(a) Scenario A

(b) Scenario B

(c) Scenario C

Figure 34: Scenarios conducted on both intersections *Elisen* and *Messegelände* which differ in the placement of participating vehicles.

In this section, we discuss the results obtained from the measurement campaign. Prior to the analysis of the results, we first conduct a validation of the measured data provided by a commercial off-the-shelf GPS receiver used to extract the vehicle positions and the distance between participating vehicles. Second, we investigate the impact of co-channel interference by comparing the measurements performed first without the interferer and then also including it. An evaluation of the impact of buildings by comparing the measurements performed in inner-city and in rural intersection is also presented. For each environment conditions, we determine the raw received power, the mean received power and the mean PDR under different network loads reflected by the presence of the interferer.

6.4.1 *Evaluation of the GPS Position Accuracy*

We use for the measurements low cost GPS receivers as described in section 4.2. To ensure applicability of the measurement results, we evaluate the accuracy of measured vehicle's positions which depends on the environment conditions during the experiments. While the position accuracy is defined as the degree of closeness of an estimate to its true value, the precision is the degree of closeness of observations to their mean value. Therefore, we determine the position accuracy in term of precision due to the lack of a reference GPS receiver. To quantify the position accuracy, we determined the Distance Root Mean Squared (DRMS) as a single number that expresses 2D accuracy and is defined as the square root of the average of the standard deviation of estimated coordinates x and y (in UTM coordinates). The DRMS is given as

$$\text{DRMS[m]} = \sqrt{\sigma_x{}^2 + \sigma_y{}^2} \tag{16}$$

where σ_x and σ_y (in m) are the standard deviation of estimated coordinates (x, y) of each point.

	DRMS [M]	
	INNER-CITY	OPEN AREA
Scenario A	4.01	0.36
Scenario B	4.37	0.58
Scenario C	0.95	0.48

Table 9: GPS position accuracy obtained from measurements for all scenarios at the inner-city intersection and the rural intersection (Open area).

Results of DRMS in Table 9 show a considerable difference in the measuring accuracy of GPS data during experiments at both intersections. Most probably, high values of the DRMS for the inner-city (4.37) compared to the rural intersection (0.58) might be explained by the fact that the open area permits a clear view up to the satellite elevation since the rural intersection was located in an unobstructed environment. To obtain a more detailed investigation of the position accuracy, we show in Figure 35 the values Δ_x and Δ_y which are the deviation of the measured

values of x and y to their mean values. We observe a maximum deviation of about 7 m. For both environments, such results are already quite reasonable. Based on these findings, we can conclude that the obtained position accuracy provided by the low cost GPS receiver is satisfactory, which implies that the positioning error has no noticeable influence on the measurement results.
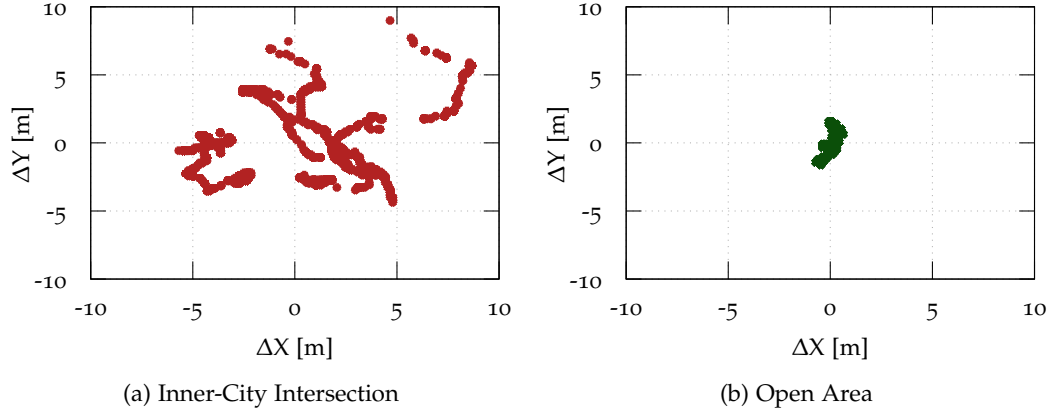

(a) Inner-City Intersection   (b) Open Area

Figure 35: Δ_x and Δ_y: Deviation of the measured values of x and y to their mean values measured at both intersections.

6.4.2 *Inner-City Intersection in Obstructed Environment*

In this section, we present results obtained at the inner-city intersection first without the interferer and then including it. This allows an evaluation of the impact of co-channel interference as well as the effect of building shadowing on the communication performance. For these reasons, we evaluate the received power P_r for each successfully received frame and its arithmetic mean $\bar{P}_r$ for each distance interval of 5 m length, and we calculate the ratio of the numbers of successfully received and transmitted frames for each distance interval, which we refer to as Packet Delivery Rate (PDR). For each test scenario depicted in Figure 34, we conduct six measurement runs to ensure statistical validity of the results. Arithmetic means are calculated based on all runs for each scenario and presented with 95% confidence intervals. Each scenario was examined individually in order to highlight the main impact of co-channel interference.

Scenario A

The impact of the buildings as obstacle on the severity of interference is clearly demonstrated when we compare results shown on Figure 36. In this figure, the aforementioned performance metrics (P_r, $\bar{P}_r$ and PDR) as a function of the distance d_{TX} of the transmitter to the center of intersection, are presented. In interference-free conditions as depicted in Figure 36a, the received power is, as expected, proportional to the distance and depends as well as on environment conditions between transmitter and receiver. The abrupt decrease of the PDR at $d_{TX} \approx 100$ m is due to the presence of the building block indicating a relatively rapid change from LOS to NLOS communication. Similar to results obtained in Chapter 4, we also observe a slight increase of the received power and PDR at $d_{TX} \approx 70$ m. This can

be explained by gaps between buildings in the side street, which allow reflected waves to constructively contribute on the overall received power. Moreover, we remark particularly for the scenario A, that depicted results above are well in line with those presented previously in Chapter 4, where we have investigated V2V radio propagation in several urban intersection scenarios, by an examination of intersections with LOS obstructions in interference free conditions.
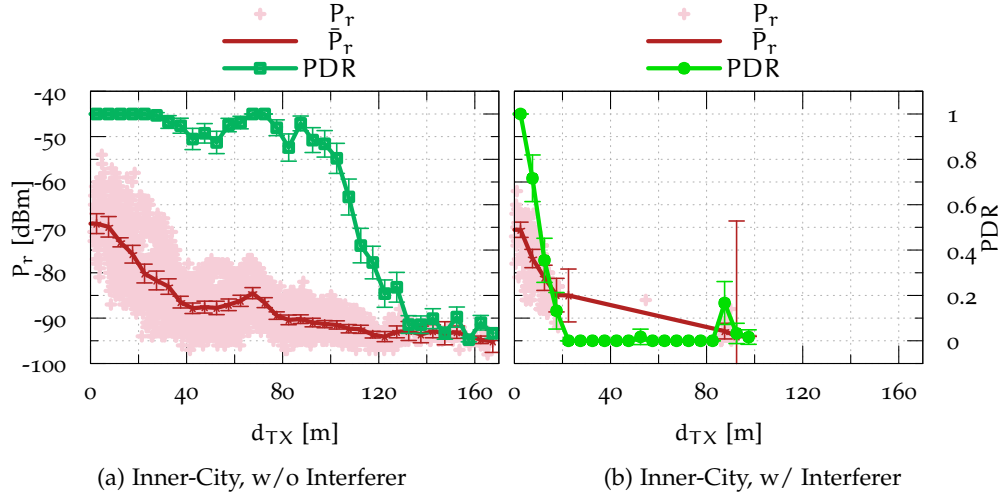

(a) Inner-City, w/o Interferer   (b) Inner-City, w/ Interferer

Figure 36: Measurement results for scenario A at inner-city intersection: Raw received power (P_r), mean received power ($\bar{P}_r$) and mean PDR against the distance d_{RX} between the receiving vehicle and the center of the intersection without (a) and with (b) interferer.

Results obtained in Figure 36b point out the significant severity of interference on the achieved PDR. The hidden node effect is also observed in this scenario because each frame sent by TX will may suffer from a high level of interference, and hence, results to packet collision due to a low SINR value. Moreover, buildings may significantly attenuate the propagating waves so that only a signal with low intensity reaches the RX. This is probably the reason of a heavy abrupt decrease of the PDR indicating a quick transition from reliable to unreliable communication performance even when transmitter and receiver are in perfect LOS conditions. Once transmitter and receiver are in LOS, a stronger signal from TX will then reach RX. This may, thus, result to a high probability of packet reception reflected by the increase of the PDR starting at distance $d_{TX} < 20$ m. It should be noted that the quick transition from reliable to unreliable communication performance could be problematic for an intersection collision warning application when co-channel interference is taken into account. As drivers should be warned in advance of potential side impact when entering an intersection. In this case, a safety-based application supported by V2V communication might not properly operate even if a low PDR of 10% is required.

Scenario B

Results obtained in this scenario, and depicted in Figure 37, are less surprising compared to scenario A. In general, we notice that the maximum values of P_r and $\bar{P}_r$ are achieved at the minimal distance between transmitter and receiver e. g. at $d_{TX} \approx 70$ m. The results also reveal the approximate receiver sensitivity of

$P_{r,th} = -91\,\text{dBm}$ which confirms that reliable frame reception is only possible for $P_r \geqslant P_{r,th}$, reflected by high PDRs in interference-free conditions (see Figure 37a). We observe that the severity of interference is less pronounced on the communication performance. This can be explained by the fact that the interference level is strongly attenuated by the building block obstructing the communication link IX-RX. As a consequence, up to 90% of packets are successfully decoded by the receiver, regardless of the presence of the interferer (see Figure 37b). One might conclude that buildings have a positive effect on the communication performance. However, for a proper discussion of results, a further comparison of results with those gathered at the rural intersection in unobstructed environment should be conducted before.
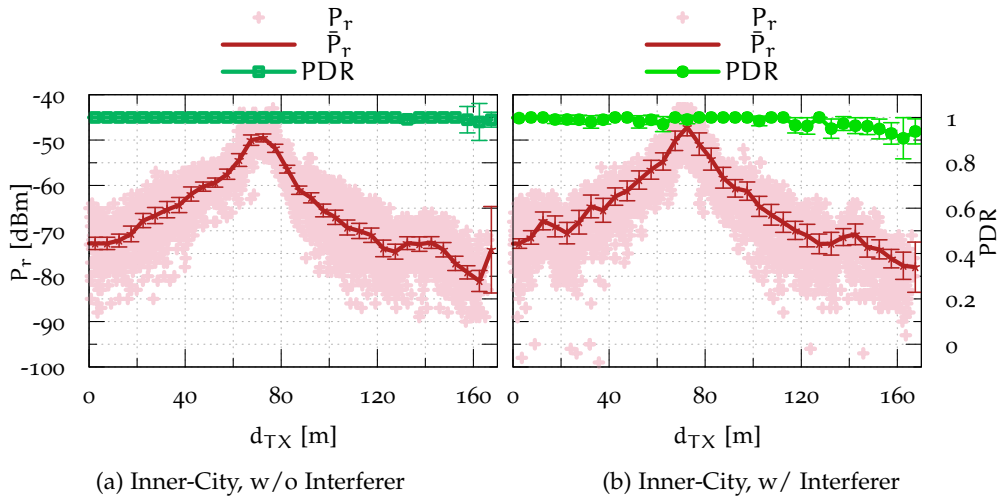

(a) Inner-City, w/o Interferer

(b) Inner-City, w/ Interferer

Figure 37: Measurement results for scenario B at inner-city intersection: Raw received power (P_r), mean received power ($\bar{P}_r$) and mean PDR against the distance d_{RX} between the receiving vehicle and the center of the intersection without (a) and with (b) interferer.

Scenario C

Similar to scenario B, results depicted in Figure 38 emphasize once again the impact of buildings on the co-channel interference. This observation was expected because the building block obstructing the communication link IX-RX appears to significantly attenuate the signal power produced by the interferer IX. An examination of this behavior at the rural intersection without building obstruction would contribute to further substantiate such environmental aspects. Additionally, the receiver sensitivity of $P_{r,th} = -91\,\text{dBm}$ is also confirmed in this scenario since frames with received power P_r above -91 dBm are correctly decoded up to a distance of $d_{RX} \approx 85\,\text{m}$ correspond to maximal PDRs.

Regarding the received power, we observe that, in general for all scenarios, the results depicted in Figures 36, 37, and 38 show severe signal fading, which can be recognized by a large variation of the measured signal power P_r around its average value $\bar{P}_r$. This is probably due to the pronounced multipath propagation effect, which is especially frequent at urban environments.
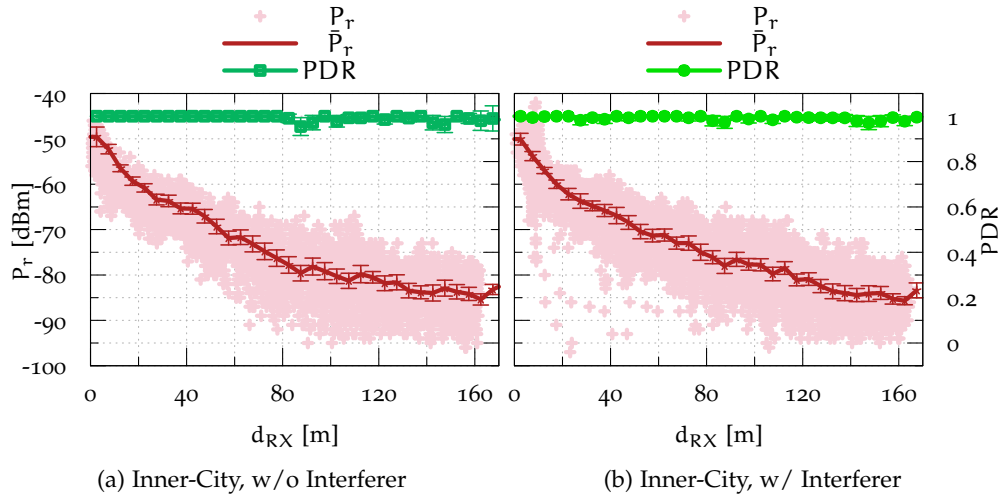
Figure 38: Measurement results for scenario C at inner-city intersection: Raw received power (P_r), mean received power ($\bar{P}_r$) and mean PDR against the distance d_{RX} between the receiving vehicle and the center of the intersection without (a) and with (b) interferer.

6.4.3 *Rural Intersection in Unobstructed Environment*

In contrast to the inner-city intersection, LOS conditions in the rural intersection were permanently maintained during the whole measurement campaign. We present again in this section results obtained first without the interferer and then including it. This allows an evaluation of the influence of building shadowing and its impact on co-channel interference. We evaluate the received power P_r for each successfully received frame and its arithmetic mean $\bar{P}_r$ for each distance interval of 5 m length, and we calculate the PDR, which is the ratio of the numbers of successfully received and transmitted frames for each distance interval. For the sake of completeness, arithmetic means are calculated based on 6 measurement runs for each scenario and presented with 95% confidence intervals. Analogously to results obtained at the inner-city intersection, we examine also each scenario individually.

Scenario A

From results depicted in Figure 39, we observe that, although the impact of interference is confirmed, this leads, however, only to a packet loss of approximately 15%. This could be explained by the fact that, due to the absence of radio shadowing on the communication link TX-RX, the transmission signal power from TX reaches the receiver with enough signal strength. This will consequentially leads to high SINR values and hence to a low probability of packet collision. However, an interesting behavior is observed in Figure 39b, where the PDR appears to be constant regardless of the location of the transmitter to the intersection. In such situations, a safety-based application supported by V2V communication might not properly operate if a PDR of at least 90% is required. Moreover, received power values and PDR drops around $d_{TX} \approx 160$ m emphasize once more the receiver sensitivity as indicated in previous results.
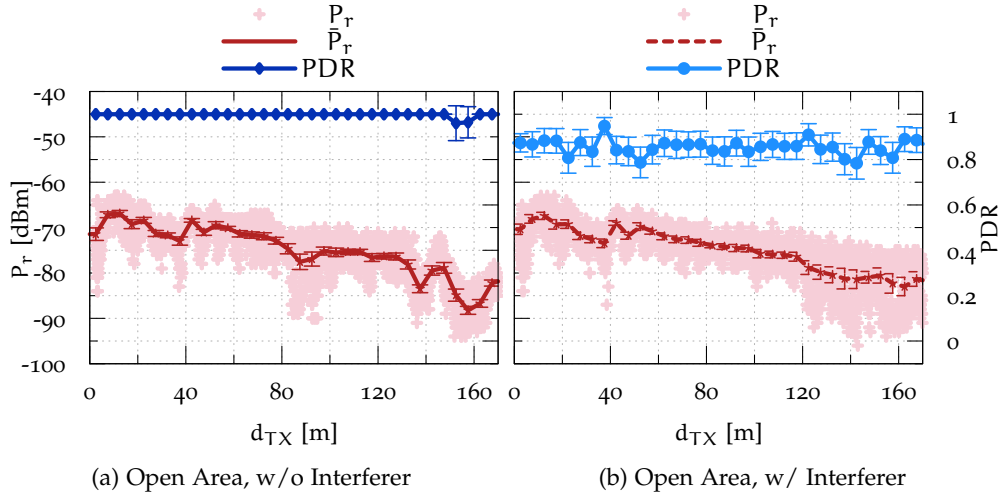
(a) Open Area, w/o Interferer   (b) Open Area, w/ Interferer

Figure 39: Measurement results for scenario A at rural intersection: Raw received power (P_r), mean received power ($\bar{P}_r$) and mean PDR against the distance d_{RX} between the receiving vehicle and the center of the intersection without (a) and with (b) interferer.

Scenario B

From results depicted in Figure 40, we notice in general that maximum values of P_r and $\bar{P}_r$ are achieved at the minimal distance between transmitter and receiver, e. g., at $d_{TX} \approx 70\,$m. However, this is not surprising. Even more interestingly, we observe regions of up-fade and down-fade of the $\bar{P}_r$, which are produced by the constructive and destructive combination of two rays caused by signal reflection. This indicates that the received power in an open environment appears to follow a *Two-Ray Interference* model which applies a superposition of the LOS signal component and the ground reflection component as reported in [125]. Unlike results presented in scenario A, we notice an appearance of a near-far effect on the communication performance. We observe with the presence of the interferer that, the PDR increases as the distance between transmitter and receiver decreases as shown in Figure 40b. This implies that for safety-based applications supported by V2V such as Forward Collision Warning (FCW) and Lane Change Assistance (LCA) requiring precise and accurate information about immediate neighborhood, the communication performance will be a bottleneck for a proper operation of these kind of applications. Hence examining such behaviors is beneficial for an efficient operation of the application even under a highly congested network. However, the impact of the interference appears to be more significant as packet loss of about 20% is achieved at higher distances between transmitter and receiver.

Scenario C

Similar to scenario B, we observe in Figure 41 once more up-fade and down-fade regions of the received signal power. Moreover, we see that the near-far effect is also noticed, because the PDR increases as the receiver approaches the intersection or the transmitter as well. The negative impact of interference on the communication performance is recognized in this scenario since the PDR remains greater than 90%

Figure 40: Measurement results for scenario B at rural intersection: Raw received power (P_r), mean received power ($\bar{P}_r$) and mean PDR against the distance d_{RX} between the receiving vehicle and the center of the intersection without (a) and with (b) Interferer.

for $d_{RX} \leqslant 50\,\text{m}$, but decreases quickly and remains constant, irrespective of the location of the receiver (see Figure 41b).

Regarding the received power, we observe that, in general for all scenarios in the rural intersection, the results depicted in Figures 39, 40, and 41 show temperate signal fading, which can be recognized by a relatively narrow variance of the measured signal power P_r. This is probably due to the almost channel invariant environment, which characterizes radio propagation in rural environments.

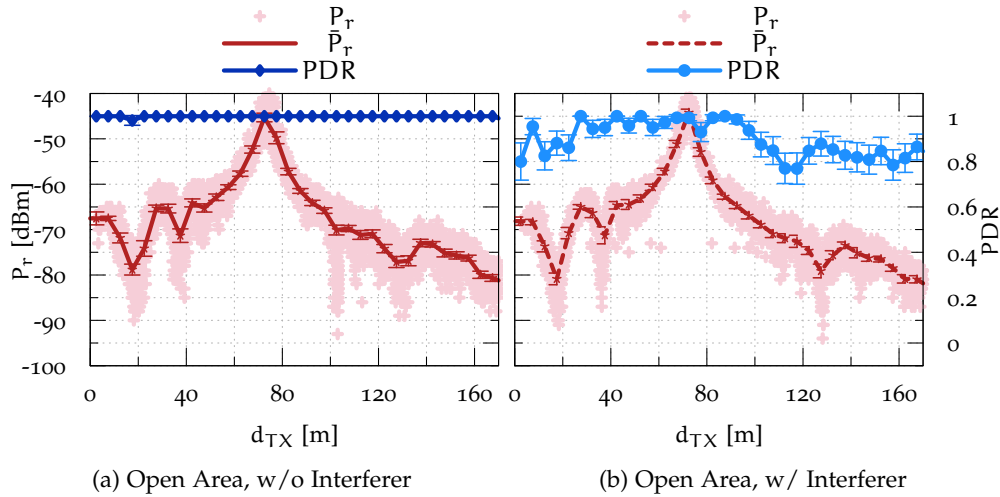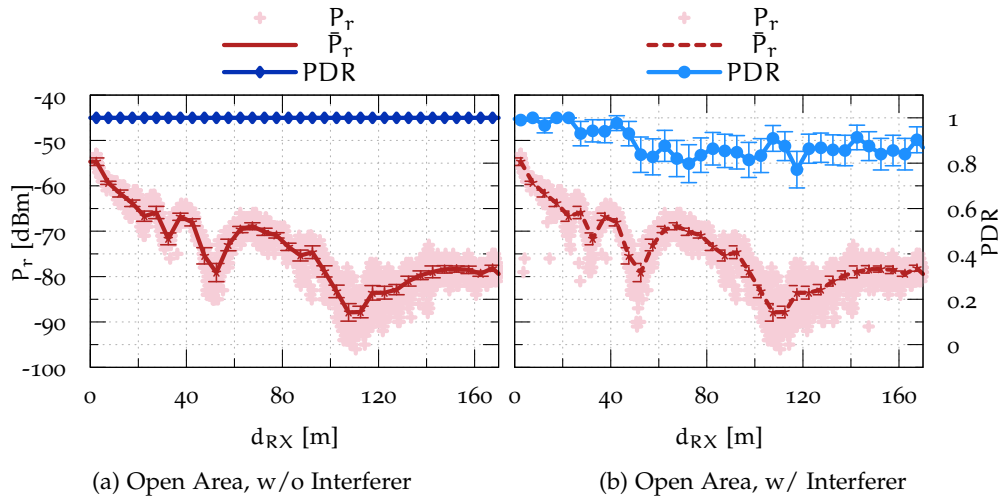

Figure 41: Measurement results for scenario C at rural intersection: Raw received power (P_r), mean received power ($\bar{P}_r$) and mean PDR against the distance d_{RX} between the receiving vehicle and the center of the intersection without (a) and with (b) interferer.

6.5   EVALUATION OF CO-CHANNEL INTERFERENCE

Whereas the previous section examined each environment individually, here we compare the intersection type and highlight the impact of buildings on the co-channel interference for each scenario.

6.5.1   *Building Placement*

To evaluate the impact of buildings, we concentrate on PDRs obtained under the presence of interference by comparing the inner-city with rural intersection and summarize all results in Figure 42, 43 and 44 for the scenario A, B and C, respectively. The negative effect of building shadowing can easily be noticed from Figure 42 for scenario A, where we can see that, while almost every packet is successfully received for a distance $d_{TX} \leqslant 10\,\text{m}$ in the inner-city, the PDR remains constant and relatively high (PDR ≈ 0.80) in the rural intersection independently of the distance d_{RX} between transmitter and intersection center.

Figure 42: Comparison between inner-city and rural intersection: Mean PDR against the distance d_{TX} for scenario A with interferer.

However, for scenario B comparing PDR in Figure 43, we notice a slightly positive impact of buildings. Obviously, the interfering signal from IX is attenuated by building obstruction so that transmitted packets reached the receiver with relatively higher SINR values, which then implies a better PDR for the communication link TX-RX. Moreover, even at close distances between transmitter and receiver ($d_{TX} \approx 70\,\text{m}$), sporadic packet collisions can be seen. This highlights the pronounced effect of interference in open environments. In such situations, the immediate neighborhood of the transmitter cannot be perfectly informed about its presence.

The same behavior is also observed in scenario C, but here, the severity of interference decreases as the receiver approaches the transmitter as shown in Figure 44. While in the rural intersection about 15% of the packets are lost already at distance $d_{TX} = 50\,\text{m}$, the PDR remains high and constant in the inner-city intersection. Here, we clearly see that the presence of buildings improves the performance of the communication by reducing co-channel interference. On the other hand, the
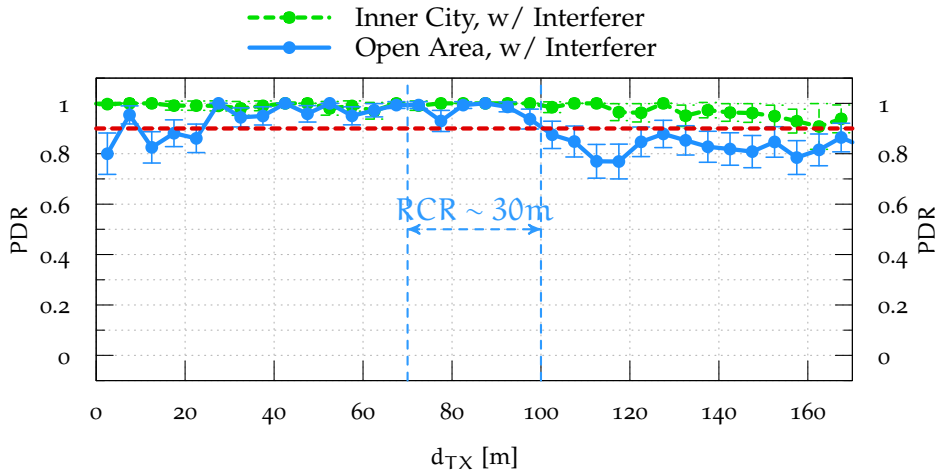
Figure 43: Comparison between inner-city and rural intersection: Mean PDR against the distance d_{TX} for scenario B with the receiver at $d_{RX} \approx 70\,m$ to intersection center and with interferer.

building obstruction will probably limit the transmission range by attenuating the transmission power as already proved in the evaluation presented in Chapter 4.
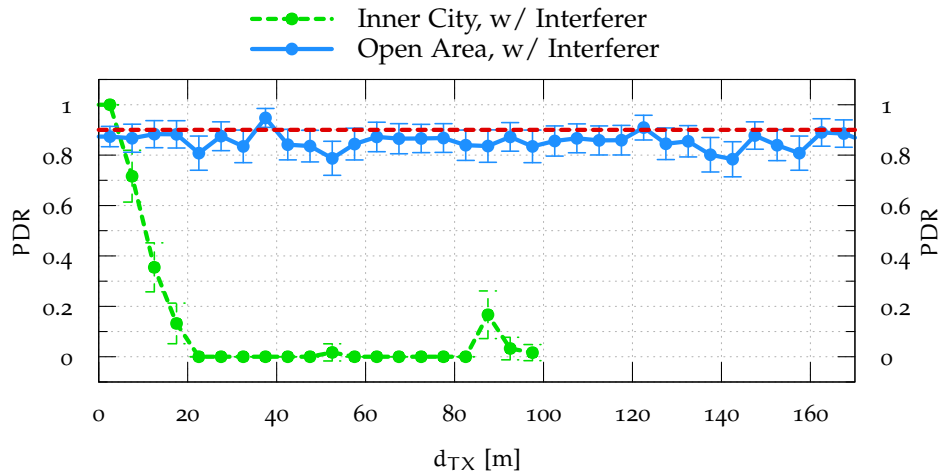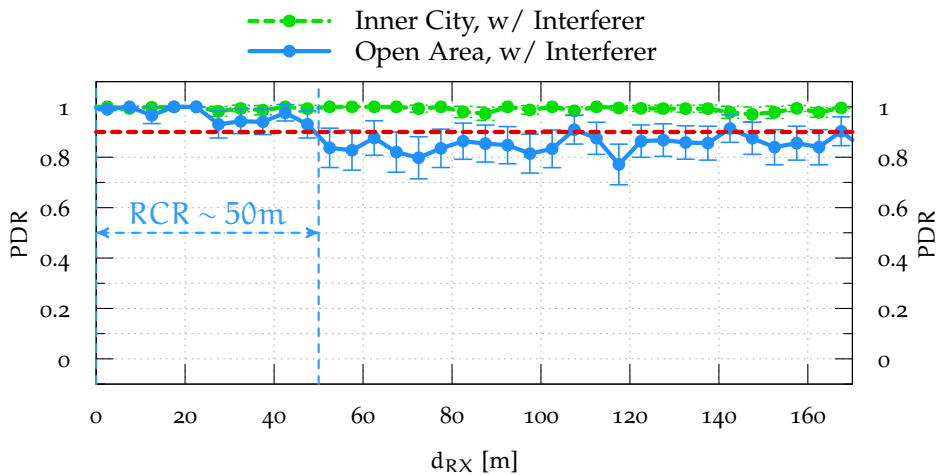

Figure 44: Comparison between inner-city and rural intersection: Mean PDR against the distance d_{RX} for scenario C with interferer and transmitter at intersection center.

In the context of application reliability, but more for a reasonable comparison and discussion of results, we additionally evaluate the aforementioned RCR, which indicates the maximal distance between transmitter and receiver where the PDR decreases below 90 %. This threshold is represented as the horizontal red dotted line in the figures. For the sake of clarity, we only show the communication range for the rural intersection. Whereas in scenario A, it could not be noted any reliable communication range both in inner-city and open area environments, in scenario B and C, however, a reliable communication range can be achieved only up to 30 m and 50 m in the open area, respectively (see Figures 43 and 44). In contrast to the rural intersection, the inner-city shows very high reliable communication ranges.

Considering the stopping distance defined as the minimum distance necessary to perform a safe braking and reach a complete stop, we investigate whether a Forward Collision Warning (FCW) is able to efficiently operate by performing a safe braking. If we assume a vehicle speed of 100 km/h as it corresponds to the speed limit in rural environment, a stopping distance of $d_{stop} = 184.2$ m could be achieved according to the Table 5 in Chapter 3.2. Assuming that an application is declared to be reliable when RCR $\geqslant d_{stop}$, we observe that FCW might obviously fail in an open area environment. These observations consolidate the positive effect of building on performance of safety applications based on V2V communication.

However, we need to admit that this investigation is more aggressive as it was shown in our work in [126] that an application could also be reliable if already at least one packet is received within a certain time window.

6.5.2   *Distribution of Interference Signal Power*

In order to gain more insights into the severity of interference on the communication performance, we plot in Figure 45 the receiver power distribution from interferer for all scenarios collected at both the inner-city as well as the rural intersection. Although the distance between receiver and interferer was the same at both intersections in scenario A, the power distribution does not overlap as expected, as can be seen in Figure 45a. Furthermore, we observe that the receiver experiences on average stronger signal power in the inner-city than in the rural intersection. This is probably due to the multipath effect caused by reflections and refractions on surrounding buildings, which constructively participate on the overall signal power at the receiver. This in turn results to low SINR values during frame receptions and, hence noticeably affects the communication performance.

One of the most interesting results is that the building block obstruction in scenario B considerably attenuates the co-channel interference and thus reduced the interference severity as expected. It should be noted that on both intersections, receiver and interferer were on the same location during the experiments. Figure 45b shows this behavior, where we observe a signal attenuation caused by buildings of almost 23 dB in their mean. In other words, this implies that the interference signal reaches the receiver with on average 23 dB less signal power resulting consequently to higher SINR values during frame receptions.

For the scenario C, the distribution of the interference power appears to be flat and spans over a larger range compared to scenario A and B. This behavior is due to the mobility of the receiver as it moved toward the intersection center during the measurement. Results in Figure 45c include then the distance related path loss since the smaller the distance between receiver and interferer, the larger the signal power strength. Furthermore, as expected, the shadowing effect on the interference intensity is confirmed by the power distribution shifted to the left in the inner-city intersection.

(a) Scenario A

(b) Scenario B
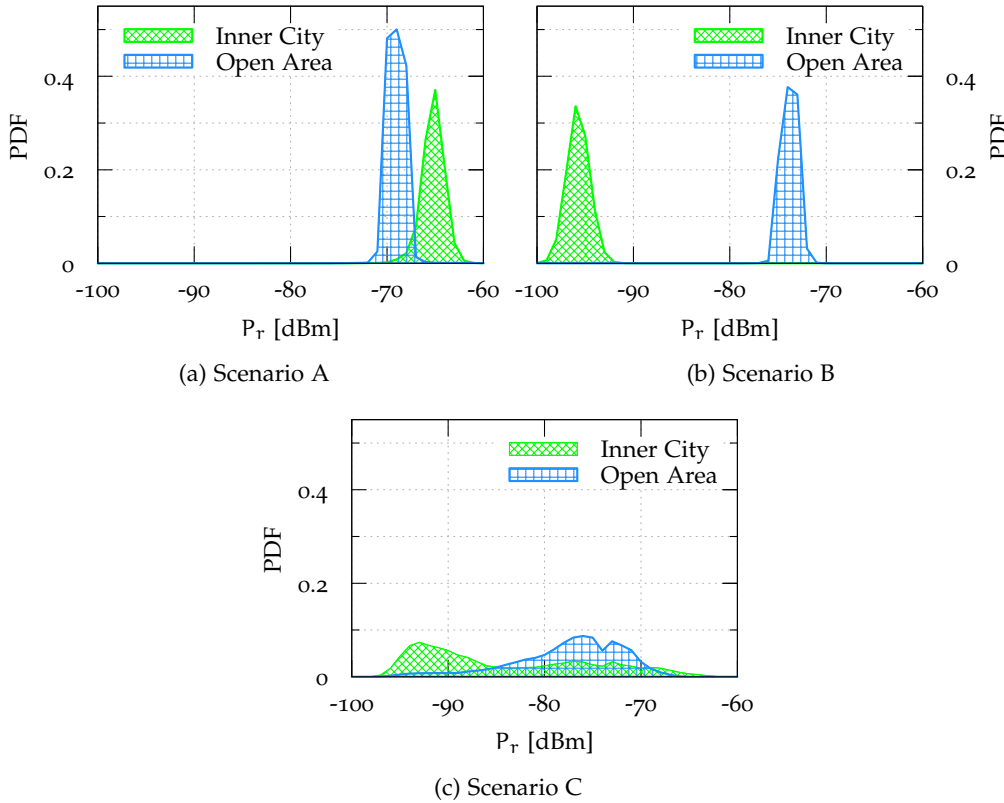
(c) Scenario C

Figure 45: Distribution of the received power (P_r) from the interferer measured at the receiver for all scenarios.

6.5.3 *Packet Delays*

Besides a high reliability of the communication, a proper operation of safety applications such as FCW requires an extremely low-latency of messages exchanged between nodes in their direct neighborhood. To gain an understanding on the impact of co-channel interference on packet delays, we examine the Cumulative Distribution Function (CDF) of the packet inter-reception time collected at the receiving vehicle. We defined the inter-reception time as the elapsed time between two consecutive successfully packet receptions from the same transmitter. As safety-based applications should provide a permanent awareness between nodes, a large burst of packets missed might impair their performance. For this reason, the inter-reception time metric, can be used to evaluate awareness blackout within vehicles in the network. It is also related to the age of the information stored in a given vehicle and represents the freshness of status messages received from neighboring vehicles. To be able to analyze also the influence of buildings, we summarize all results in Figure 46 by comparing the distribution of inter-reception times at the inner-city and the rural intersection.

First of all, we observe a stair behavior of the CDF, which well emphasizes the value of the message generation period of 100 ms set at the transmitter. The influence of interference is clearly highlighted in Figure 46a, especially for scenario A. We can see that about 95% of received packets have an inter-reception time lower than 200 ms compared to approximately 70% considering co-channel interference. This means that a relatively high portion of packets is lost leading to large

Figure 46: CDF of inter-reception time collected at the receiver for scenarios A and B under both intersection types.

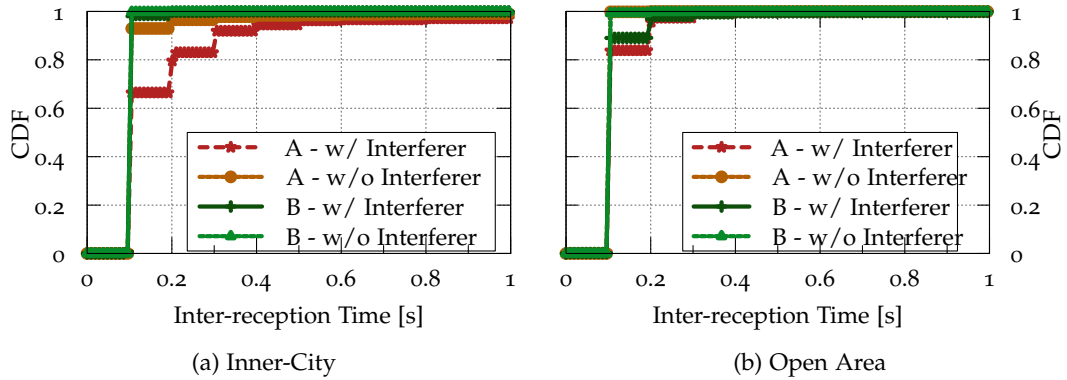inter-reception times. Considering scenario B, obtained results are not really surprising because the obstruction of interference assures a perfect packet reception ratio. Conversely, despite the severity of co-channel interference on the PDR in the rural intersection as demonstrated previously, results plotted in Figure 46b show a slight impact of interference on the inter-reception time in the rural intersection.

In conclusion, we can argue that sporadic communication outage due to large packet delays appears to be impacted more by buildings obstruction than by channel congestion. Furthermore, regardless of the considered environment, the inter-reception time remains relatively low, in particular when transmitter and receiver are located near the intersection center.

6.6 SUMMARY

In this chapter, we evaluated the impact of co-channel interference on the performance of V2V communication based on real world measurements conducted at LOS and NLOS intersections. In particular, we addressed the problem of building shadowing and its impact on interference generated by nodes sharing a common radio channel as specified by the ITS-G5 standard. To facilitate or overcome the logistic constraints, we introduced an approach consisting of the configuration of a single vehicle with the aim to emulate a set of vehicles during vehicular measurements. According to different scenario objectives and intersection types, we quantified packet delivery ratios, received signal strength indication levels, interference power distributions, and packet delays. We showed that while the received power in urban environments experiences severe signal fading, the signal propagation at the rural intersection shows temperate signal fluctuations. However, we further demonstrated that under presence of interference, larger communication ranges can be achieved at inner-city intersections than at rural intersections. The results showed that the presence of buildings could improve the communication performance by limiting or blocking co-channel interference. On the other hand, the building shadowing in interference-free situations may attenuate the wanted signal power leading to a limitation of the achievable communication range. We clearly demonstrated that building shadowing and its impact on interference has a substantial influence on the communication performance in vehicular networks.

However, the co-channel interference has no noticeable influence on the packet delays. Sporadic communication outage due to packet losses are likely to be caused by building shadowing than by channel congestion.

While the idea of configuring a single node as a set of vehicles may led to incomplete due to the omission of packet collisions caused by frame overlaps, we pursue in the next chapter the evaluation of scalability issue involving hundreds of vehicles at urban intersections by means of simulation.

CONCLUSION

In this section, we summarize lessons learned from the first part of this thesis, which deals with the measurement-based evaluation of V2V communication. In particular, we investigated the impact of stationary radio shadowing such as building and vegetation on the communication performance at urban intersections.

We first started by investigating the problem of radio shadowing through buildings in Chapter 4. We found out that vehicle positioning according to the location of transmitter and receiver relative to the intersection center has a substantial impact on the communication performance. Moreover, considering intersection type and width as well as traffic condition, the quality of the communication will be influenced by these environment factors. Examining achievable communication ranges deduced from measurements led to the conclusion that V2V could assist intersection-based applications by allowing to *look* around the corner, in particular at night traffic. It has been show in the literature that traditional vehicle-mounted sensors such as radar, lidar, or camera present system limitations in term of detection range and object monitoring. Consequently, ADASs can be fused with V2V communication to augment the system accuracy and reduce the probability of false alarm even in severe environment conditions. In this way the driver's horizon is extended so that vehicles perceive surrounding potential obstacles sooner even in a highly obstructed environment such as inner-city intersections.

As plants, bushes and trees are often present at rural intersections as well as at some city intersections, we examined in Chapter 5 the impact of radio obstruction through vegetation on the communication performance. We came to the conclusion that intersection type with respect to vegetation type and structure could impact the communication link characterized by a noticeable attenuation of the transmitted signal strength. Also the seasonal effect revealing leafed or leafless vegetation affect the reliability of safety-based applications by reducing communication ranges. For these reasons, due to the non-negligible effect of foliage, it is highly recommended to consider the effect of vegetation when modeling V2V in vehicular environments. However, when comparing both radio shadowing obstacles, our findings reveal that obstruction through buildings is likely more aggressive that through vegetation.

Safety-based applications should ensure their effectiveness in free flow traffic as well as in traffic jams, so that a certain cooperative awareness is always established between vehicles at any day time. Furthermore, due to the ongoing deployment of V2V systems in the automotive industry, which favors an increasing number of communicating nodes, the co-channel interference will remain a big challenge and will therefore impair the performance of safety-based applications. This motivated the measurement study presented in Chapter 6, where we investigated the co-channel interference on V2V communication by focusing on the influence of building shadowing. We found out that shadowing situations in urban intersections not only lead to challenges for safety-critical applications such as intersection collision warning or forward collision warning, but also provide opportunities due

to a naturally reduced channel load generated by co-channel interference.

Due to the specific and rapidly changing nature of vehicular networks, we were confronted with very big challenges during the execution of measurement campaigns. Besides logistic and time constraints when measuring VANET in real world scenarios, the reproducibility of experiments as well as the post-processing of data were the most complicated factors that we have to deal with in the performance evaluation. A couple of measurements needed to be repeated due to the sudden appearance of large obstacles such as heavy trucks or garbage trucks, which not only hinder the traffic flow, but even more obstruct the communication link by introducing an additional loss factor in the total link budget. Moreover, self-developed algorithms to support the post-processing and correction of corrupted GPS data was also challenging because geographical coordinates gathered during experiments were found to be sporadically inaccurate. This was attributed to satellite obstructions caused by relatively high building blocks, which are often present in narrow environments such as inner-city intersections.

Motivated by the aforementioned limitations in the experimental performance evaluation of VANETs, we present in the following chapter a simulation-based assessment of environment factors such as intersection type and penetration rate as well as the analysis of network parameters on the communication performance.

Part II

SIMULATION-BASED EVALUATION

7

SIMULATION-BASED PERFORMANCE EVALUATION

A decisive task towards the design and deployment of V2V systems is the estimation of their performance as a proper and accurate assessment will directly depend on the quality of tools and methodologies used during the evaluation. Basically, the performance evaluation of communication systems is achieved by applying three different methods. One can cite the mathematical analysis, experiments with real hardware prototypes and simulation technique. Due to its capacity to explore a vast range of scenarios in a reasonable amount of time, simulation remains the most attractive method for the evaluation of communication systems. In particular for vehicular environments, simulation allows to emulate large-scale scenarios involving a high number of vehicles. In this way, the level of realism is increased as this reflects real traffic behavior. For this purpose, we developed a hybrid simulation platform composed of road traffic and network simulation tools, specially dedicated for vehicular environments. In the previous chapter, we demonstrated that the efficiency of V2V depends mainly on the inevitable interference generated due to the broadcast nature of the vehicular network. Yet, to investigate the impact of interference in a realistic environment, we performed in this chapter an evaluation of V2V communication based on results gathered during a profound and detailed simulation study. Besides considering the scalability issue in a realistic way, we provide a deeper analysis of environment factors such as intersection type - and far beyond these - the influence of communication parameters such as transmission power and message generation rate on the communication capability is considered.

This chapter is organized as follows. Considering simulation as the principal methodology for performance evaluation, we first describe simulation tools and models developed throughout this study. We present in detail models used by focusing in particular on the Physical (PHY) and Medium Access Control (MAC) layer modeling. A dedicated urban intersection propagation model, especially for urban intersections, is proposed. We then describe a representative scenario followed by an introduction of performance metrics used for the evaluation. Due to the stringent application requirement in terms of the latency of received messages, we evaluate the end-to-end delay and message age under different intersection types and communication parameters. In the next step, we deal with the problem of packet collision by differentiating collisions caused by the CSMA/CA mechanism from those generated by the hidden node problem. We conclude this chapter by investigating the asymmetry phenomena appearing under the city intersection when evaluating packet delivery ratios. A profound presentation of and discussion of results conclude this chapter. Parts of the contributions of this chapter have been previously published in [127].

7.1   RELATED WORK

In the last years, several research studies on the performance evaluation of V2V communication were conducted with the aim of evaluating the impact of shadowing caused by stationary objects or mobile obstacles such as vehicles, first through simulation and recently in small scale field trials. Field test experiments conducted in various environments (urban, suburban and highway) in [52] reported that vehicular obstructions could significantly attenuate the signal power by analyzing the impact of obstructing vehicles on a communication link. Moreover, the authors point out that the effect of stationary obstacles, such as buildings, is even more pronounced than mobile obstacles. The authors in [128] propose a dynamic beaconing algorithm that reacts to network changes caused by the time-variant signal due to radio signal obstructions created by neighboring vehicles, as well as by buildings. Their results indicate that this algorithm by adapting more quickly to change in network topology could substantially improve the communication performance compared to a traditional static periodic beaconing approach. With regard to message relaying, a study was reported in [56], where the authors performed field test measurements with the aim to extend the communication range by exploiting the vehicle height in obstructed environments. The obtained results show that even if tall vehicles often obstruct the LOS between communicating vehicles, the height of vehicles could be exploited. Motivated by the problem of radio shadowing caused by buildings, a similar study was proposed in [128] with the purpose of using parked vehicles as node relaying which then allow to see around the corner at intersection areas. Despite the fact that the effective communication range could be significantly increased, the complexity in the realization of such multi-hop relaying approaches brings new challenges which include synchronization issues in multi-transceiver architecture and the conceptual effort in design of relaying strategies.

Although the studies described above contribute to gain insight into the effects of radio shadowing, investigations are made either solely through measurement or simulation. Furthermore, most of the previous studies do not take into account the impact of intersection types. Motivated by the limitations of the related work, we integrate a validated path loss model obtained through a profound measurement campaign into a V2V dedicated simulation platform with the aim to propose a more realistic evaluation of the impact of buildings. Moreover, besides examining the influence of communication parameters, we investigate the impact of shadowing caused by buildings by focusing on intersection types with respect to the building's placement.

7.2   SIMULATION TOOLS

The simulation-based evaluation of VANETs assumed not only a profound modeling of communication systems but also a mobility model that reflects the real behavior of each individual node in the overall system is needed. Considering, for example, the performance evaluation of forward collision warning applications, the processing and analysis of the received information require knowledge about the considered road network. Because only messages exchanged between vehicles located on the same road lane should be processed to support the driver in critical situations. From a communication point of view, path loss modeling in network simulation requires the exact location of nodes for instance to determine

the received signal power between a communicating pair. Moreover, the mobility pattern of vehicles and environment constraints such building location and intersection type are indispensable. All these kind of information could be delivered by vehicular mobility generators that provide knowledge about the position of each node at every time through realistic mobility traces generated offline or through a real-time provisioning during the simulation process. Compared to MANETs where the mobility behavior of mobile nodes could be randomly generated, nodes can only move along the street and according to each other in VANETs. This prompts the need of road traffic models that bring a high level of realism making the evaluation as close to reality as possible. For this purpose, there are a couple of existing simulators for vehicular networks currently used by the research community like iTetris [64], TraNS [129], and the newly developed Veins [63]. All these open source frameworks provide an interaction between a network and road simulator on a common simulation platform. A large number of network simulations applying a discrete event simulation of network protocols are available. The widely utilized open source frameworks by the scientific community are ns-3 [130] and OMNeT++[131] which perform detailed packet-level simulation of the data transmission, reception, routing and the radio channel propagation. As road simulation tools, we can cite Quadstone Paramics [132], Aimsun [133], and SUMO [134]. While the first two simulators are commercial products, and thus are not publicly available, the latter is an open source software and, therefore, gives users the possibility to modify and extend the program without any restriction making it suitable for research purposes.

With respect to the coupling of simulators aiming to evaluate V2V-based applications, the Traffic Control Interface (TRaCI) proposed by [135] provides a technique for interlinking road traffic and network simulators together. In this way, real-time control of vehicle's behavior during simulation run-time by influencing the movement of each vehicle is feasible. The current version of TraNS which supports SUMO traffic simulator and ns-2 network simulator applied TRaCI as feedback loop. However, TraNS has the problem of being no longer actively supported since 2008. For these reasons, its usage with current versions of the coupled simulator SUMO is not any more supported. Additionally, the fact that the simulation time control has not been considered, network simulation using OMNeT++ is missing.

Motivated by the limitations of the related work, we developed a hybrid simulation platform composed of simulation tools SUMO, which provides road traffic simulation, and OMNeT++, which forms the basis for our network simulation. We extended the *INETMANET framework* for OMNeT by adding a communication model of the ITS protocol stack, particularly focusing on ITS-G5 and its medium access control mechanism. In this section, we give a brief introduction into the road traffic simulation SUMO, followed by a detailed description of the ITS protocol stack developed in OMNeT and a validated path loss model obtained through a profound measurement campaign.

7.2.1   *Road Traffic Simulation with SUMO*

Simulation Urban Mobility (SUMO) is a c++-based microscopic, inter- and multimodal, and time-discrete traffic flow simulation platform designed to handle large road networks. Besides a graphical user interface, it provides several utility tools including a road network importer capable of supporting several source formats,

traffic demand generation, and routing utilities, which use a high variety of input sources such as origin-destination matrices and traffic statistics. To adapt and control the simulation run online, the interface TRaCI is implemented and operated as server. Additional tools and scripts for the post-processing of simulation results are available. The simulation of different types of vehicles is freely configurable with each vehicle following pre-computed routes, dynamically generated routes, or driving according to a configured edge table containing a list of road segments. One of the most popular features of SUMO is its ability to work on multiple operating systems, such as the most commonly used Microsoft Windows, Linux and Mac OS X. To set up a complete simulation run, we used following SUMO utilities within this work:

NETCONVERT: Generates road networks representing real-world networks as graphs, where nodes are intersections, and roads are represented by edges. This can be performed by importing from Open Street Map (OSM) or even manually from an XML file. The generated road network is classified into five types, each for the description of nodes, edges, edge types, connections, and traffic light plans. Nodes represent the intersections, edges the road segments and connections describe which lanes incoming into an intersection are connected to which outgoing lanes.

OD2TRIPS: Generates from the so-called origin-destination (O/D) matrix a list of vehicle trips containing vehicle departure time together with the origination and the destination road section for each single vehicle. The O/D matrix describes the number of trips going from each origin to each destination.

DUAROUTER: Computes vehicle routes through the road network based on resulting trips obtained from OD2TRIPS. The route is defined as a list of connected road sections between a vehicle's start and destination. Such routes are usually computed by performing a dynamic user assignment which is an iterative process employing routing algorithms such as shortest path.

To model the dynamics of each individual vehicle through the network, SUMO implements a couple of longitudinal and lateral models. In general, in most microscopic simulations, the so-called *car-following* model and *lane-change* model are performed separably. Due to its efficiency proved within a set of car-following model comparisons, we use an extension of the stochastic *car-following* model developed by Stefan Krauß proposed by SUMO per default [136]. In fact, this model computes an investigated vehicle velocity by looking at its distance to the leading vehicle and the leader's velocity. It is assumed that a change of the velocity is only performed if the current velocity does not coincide with some desired velocity v_{des} determined by safety considerations and/or legal restrictions and can be expressed as:

$$v_{des} = \min\{v_{safe}, v + a, v_{max}\}$$

Where v corresponds to the current velocity from previous time step, a is the maximum acceleration of the vehicle, v_{max} the maximum velocity allowed on the road section and v_{safe} is the velocity assuring a collision-free driving behavior given as:

$$v_{safe} = -\tau \cdot b + \sqrt{(\tau \cdot b)^2 + v_l{}^2 + 2 \cdot b \cdot g}$$

τ corresponds to the driver's reaction time, b the maximum deceleration of the vehicle, v_l the leader's velocity and g is the gap between the front of the subject vehicle and rear of the leading vehicle at the previous time step.

Currently, among others, the following models are available: the intelligent driver model (IDM), Kerner's three-phase model, and the Wiedemann model. All these models are based on the assumption that the traffic is modeled on a single lane but in reality in some situations, vehicles should be able to perform a lane change allowing vehicles to pass, to exit or merge on highways. A lane change is defined as the ability to transfer a vehicle from one lane to the next adjacent lane. The lane change in SUMO is based on simple assumptions and initiated if:

- The difference between the safe velocities on the neighbor and the current lane is larger than a certain threshold.

- The existing space gap between the subject vehicle and preceding vehicle in the current lane is large enough to prevent a collision.

Concerning the usability of SUMO, simulations can be started either on a real time graphical interface or through a command line without a graphical representation producing output files and statistics by which we could measure and evaluate the performance of a given application on the traffic efficiency within a road network. The graphical interface allows the user to have views on simulated objects within the traffic network at the same time while the simulation is running. By doing so the examination of the pattern of traffic flow is provided.

7.2.2 *Network Simulation with OMNeT++*

OMNeT++ is an extensible, modular, component-based simulation library and framework primarily for building network simulator and is written in C++. In fact, its primary application area was not only the simulation of communication networks but can be also utilized in other areas such as queuing networks, communication systems, and hardware emulation. The modularity of the OMNeT architecture, its component re-usability and open-source concept make it a clear choice for academic research. It allows a composition of a model with any granularity that can be easily embedded in every self developed application. Moreover, OMNeT provides a comfortable graphical user interface that can be used to trace and debug simulations. A simulation library facilitating the acquisition of results statistic, data collection, and graphical representation of simulation results is also available. In the essence, OMNeT was not designed as a network simulator but to be as general as possible, procuring available basic instruments and tools to perform simulations. In other words, it serves as the basis for the development of future model frameworks as independent projects. Nowadays the libraries of OMNeT incorporate - especially for computer networks - a couple of model frameworks including *INETMANET*, *MiXiM*, *OverSim* and *Castalia*. While the last two were developed following their own release cycles, we use *INETMANET* in this work primarily due to its support for mobile ad-hoc networks. It is an extension of the INET framework which contains models for several Internet protocols: TCP, UDP, IPv4, IPv6, Ethernet, IEEE 802.11, routing protocols and many other protocols and components. It also contains several network emulation capabilities.

To be able to simulate vehicular networks and thus to provide a high level of realism, we extended the INETMANET framework for OMNeT by adding a model of the ITS protocol stack, particularly focusing on ITS-G5 and its medium access control presented in Chapter 2. As illustrated in Figure 47, a network node implemented in OMNeT consists of a network device that contains several layered mod-

ules connected by simple interfaces for exchanging packets along the layers. Each protocol layer corresponds to the ITS-station reference architecture introduced in Chapter 2. For the sake of simplicity, we implement both the MAC and the Logical Link Control (LLC) into a single module (mac). A network node represents a vehicle that could be equipped with one or more network devices representing a physical device that connects to the channel. The wireless channel represents the medium used to send information between network nodes. Typically, modules in OMNeT communicate with message passing send via *gates*, but it is also possible to send them directly to destination modules. This section presents the simulation modules and components included in OMNeT with respect to a top-down approach. Starting with the application layer modeling, the construction of CAMs and DENMs are presented [22, 23]. The MAC and PHY layer modules which belong to the ITS-G5 Access layer are introduced.
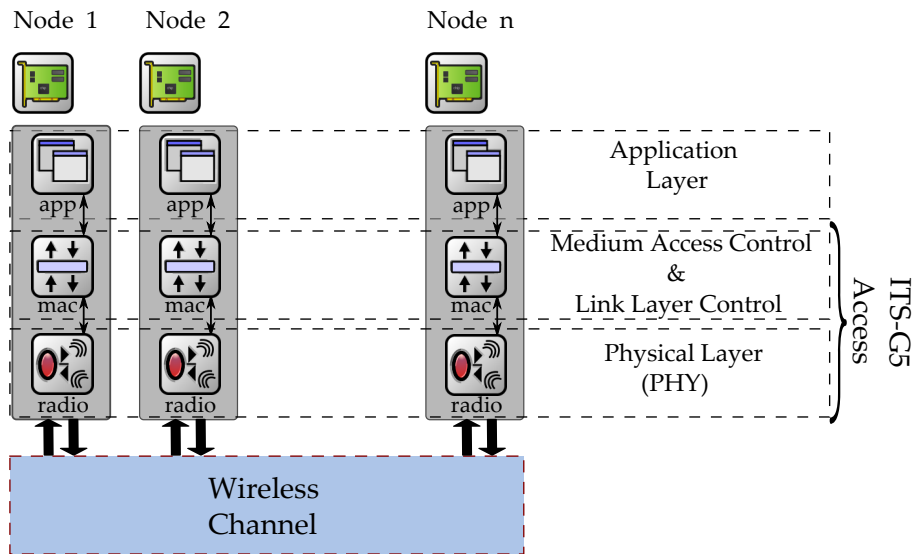

Figure 47: A vehicular network consisting of network nodes and the wireless channel as modeled in OMNeT++.

For this purpose, the implemented simulation model includes a detailed representation of co-channel interference and resulting frame collisions, including Physical Layer Capture (PLC). Furthermore, the OCB mode is used for single-hop broadcast transmission of CAMs, which are periodically generated by each vehicle. In contrast to the IEEE 802.11 standard, we disable the post-backoff mechanism, i. e. stations have to perform the backoff procedure before each frame transmission. The measurement-based Urban Intersection Propagation Model presented in the following Section 7.2.4 as well as geometric properties of buildings are also implemented within the simulation model based on OMNeT.

Modeling of the Application Layer

As mentioned previously in Chapter 2, the facility layer is responsible for functionalities that can be shared by V2X-based applications and their assigned use cases located at the application layer. For the sake of simplicity and to reduce as much as possible message exchanges between the application layer and facility layer, we implement both application's functionalities, the CA basic service, and the DEN basic service module within the application layer of the ITS communi-

cation architecture [137]. The construction, management and processing of CAMs and DENMs are done by the CA and DEN, respectively, which in fact, are part of the facility layer and are therefore mandatory facilities [22, 23]. Periodic messages called CAM are generated by each vehicle to inform surrounding vehicles about its presence by sending status information e. g., speed, position, and direction. But also when an unsafe situation is detected, event-driven messages called DENM are sent to other vehicles. These messages contain apart from their status information also the event type. Periodic messages that are sent because of awareness, whereas those triggered by critical situations, therefore, should have a very high priority to access the channel. Both types of messages are broadcasted within a single hop distance. To avoid the broadcast storm problem leading to packet collisions and large message latencies, the *message generation rules* based on the change in vehicle's dynamic are also implemented. It is a method to limit the channel load by adapting the message generation rate of CAMs accordingly to the change in position, speed and heading of the transmitting vehicle. However, as we are interested in the influence of the message generation rate on the communication performance, we disabled the *message generation rules* mechanism and used rather a fixed generation rate during each parameter configuration.

The modeling of the message exchange within the application layer is as follows: when the safety application needs to send a message, a new object of type "cPacket" is generated containing all relevant sensor information such as the identifier, position and dynamic information of the transmitting vehicle as well as the generation time. Since for the applicability of data, each message generated should be time-stamped ensuring its proper interpretation at the receiving station. To avoid a perfect synchronization between transmitting vehicles, we add a random delay $\varepsilon = \text{uniform}(-\frac{t_g}{10}, \frac{t_g}{10})$ to the generation time t_g. It is applied only for CAMs and will hence limit deterministically repeated packet collisions. The encapsulated packet is then delivered to lower layers. At the receiving side, the CA or the DEN basic service processes the received message and provides the content to an appropriate V2X application.

Modeling of the Medium Access Layer

To be compliant with the newly adapted IEEE 802.11-2012 [12], we extend the MAC protocol of IEEE 802.11a provided by INETMANET by implementing MAC and LLC parts of the ITS-G5 Access layer into the **mac** module depicted in Figure 47. The mode of operation of LLC is set to Type 1 also known as *unacknowledged connectionless mode*. In this mode, data frames are exchanged between LLCs without the need for an establishment of a data link connection. In this mode, there are also no flow control or error recovery. This procedure is similar to the UDP at the transport layer present in the Internet protocol stack. We also introduce the OCB mode used for single-hop broadcast transmission of CAMs, which are periodically generated by each vehicle. In this mode, association, authentication and security between nodes are disabled meaning that each node is responsible for determining network specific features. For this reason, the Basic Service Set ID (BSSID) of the network is set to a wildcard containing only ones. In contrast to the IEEE 802.11 standard, we disable the post-backoff mechanism, i. e. stations have to perform the backoff procedure prior to each frame transmission. However, no backoff is performed after a frame transmission if the transmission queue is empty. Furthermore, we extend and adapt the DCF by adding QoS attributes into the EDCA deployed by

IEEE 802.11p, thus giving the possibility to simulate with different data traffic priorities.

Modeling of PHY Layer

In wireless networks, in general, the PHY layer is responsible for the conversion of bit streams into radio waves and vice versa and also ensuring that the stream sent by the transmitter is the same at the receiver. In some situations, this would be hard to realize since due to inevitable environment factors influencing radio propagation such as shadowing or/and reflection, waves will be distorted during their propagation. Thus, the main challenge of the PHY layer is to ensure an error-free conversion of wave into payload containing useful information. Basically, according to its journey in the PHY layer, data could be represented in five domains: The waveform domain, the sample domain, the symbol domain, the bit domain and the packet domain. Each of these domains performed a given task whether at packet level, bit level or wave level. For more details, the reader is asked to refer to this textbook [138]. Due to the demanding computational complexity introduced by a physical layer simulation at bit level, we concentrate our modeling at the packet domain. This means that a statement can only be derived if a packet is successfully received but not which bits were corrupted in case of erroneous packet reception. However, this assumption is quite reasonable, since for the evaluation of the communication performance, metrics including packet latency, and probability of packet reception are more of interest. Moreover, a statement about the capability of V2X applications is based on the requirements established by application designers which derive from the aforementioned performance metrics.

The *radio* module at the PHY layer is responsible for the sending and receiving of packets or frames. Before the sending procedure, the node shall be in transmission state and no other frames should be currently being received at this time. Packets in OMNeT++are encapsulated into a so-called *air frame* which contains the physical properties of the radio transmission. Moreover when needed, *air frames* could be duplicated for each receiving nodes. There is a separate module that was not shown on Figure 47 monitoring which nodes are within transmission range of others, and more important, at which frequency they actually transmit. This is achieved by calculating the received signal strength for every received transmission based on the considered radio propagation model. When receiving an *air frame*, a detailed representation of co-channel interference and resulting frame collisions, including PLC are applied. We assume that a frame can be successfully decoded if and only if the SINR during the complete frame reception is greater or equal a given threshold $\mathrm{SINR_{th}}$ as:

$$\mathrm{SINR} = \frac{P_r}{N + \sum P_{Ii}} \geqslant \mathrm{SINR_{th}} \tag{17}$$

where P_r is the strongest signal power, $\sum P_{Ii}$ the sum of other ongoing transmissions treated as noise and also known as the interference power and N is the thermal noise constantly present. The decision whether a received frame is successfully decoded and passed to upper layers or treated as noise depends on the cumulative power level of all ongoing transmissions on the medium at this time. The value of threshold $\mathrm{SINR_{th}}$ is defined according to the configured data rate, modulation scheme, and coding rate. In [16], the authors recommended SINR thresholds for
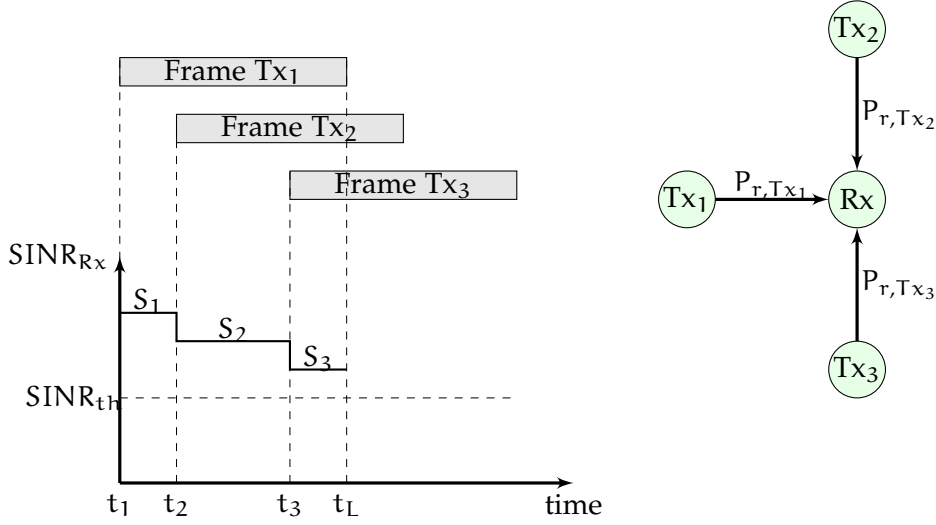
different modulation and coding schemes.

Figure 48: Illustration of the determination of the SINR modeled in the PHY layer.

The illustration in Figure 48 is used to illustrate the basic idea behind the determination and modeling of SINR. Let us consider a simple network consisting of a single receiver (Rx) and three transmitters (Tx_1, Tx_2 and Tx_3). Suppose that all transmitters are hidden to each others and that they start to transmit consecutively. In our case, the *frame Tx_1* is being evaluated. In this scenario, we consider that at time t_1, the receiver RX starts to receive a *frame Tx_1* sent by the transmitter Tx_1 with a power P_{r,Tx_1}. At time t_2, the *frame Tx_2* arrives at the receiver with a power P_{r,Tx_2}. As the receiver was already locked on *frame Tx_1*, the *frame Tx_2* would be treated as noise. This would be the same procedure for *frame Tx_3* arriving at the time t_3 until the *frame Tx_1* is completely received at time t_L. One can conclude that, if a frame is currently received by the PHY layer, all other arriving frames at this time will be treated as noise and added in the interference vector.

Considering the scenario above, the SINR at the receiver RX is calculated as follows:

$$SINR_{RX} = \begin{cases} S_1 = \frac{P_{r,Tx_1}}{N} & \text{for } t_1 \leqslant t < t_2 \\ S_2 = \frac{P_{r,Tx_1}}{N + P_{r,Tx_2}} & \text{for } t_2 \leqslant t < t_3 \ , \\ S_3 = \frac{P_{r,Tx_1}}{N + P_{r,Tx_2} + P_{r,Tx_3}} & \text{for } t_3 \leqslant t < t_L \end{cases} \qquad (18)$$

The PHY layer monitors the SINR of the *frame Tx_1* during the complete frame reception duration t_L, if the $SINR_{RX}$ drops below the $SINR_{th}$ at any time, the frame is marked as collided. Now in this example, the *frame Tx_1* is correctly received because during the whole frame reception time t_L, the following condition is fulfilled:

$$\text{for all } S_i, \quad S_i \geqslant SINR_{th} \qquad (19)$$

The values of denominators in Equation 18 represent the accumulation of all interference signals together with the existing noise floor.

The **radio** module completes the reception process by successfully decapsulating received frames into packets before passing them to the **mac**. The PHY layer

has introduced the so-called *capturing effect* which allows successful reception of packets with stronger signal even in the presence of other interfering signals. In this way, packet collisions caused by two or more nodes transmitting simultaneously by choosing the same backoff, or collisions due to the hidden node problem, would be reduced. Using the *capturing* mechanism, the decision whether a frame is captured at the receiver depends on the difference between its signal power and interfering signals. If this difference is sufficiently large, the considered frame will be successfully decoded and passed to the **mac** module. We implement the *capturing* approach in the PHY layer.

7.2.3   *The Simulation Platform: A combined Network and Road Traffic Simulation*

Our simulation environment is a hybrid simulation platform composed of the simulation tools SUMO, which provides road traffic simulation, and OMNeT, which provides the basis for our network simulation (see Figure 49). The complete ITS protocol stack, particularly focusing on ITS-G5 and its medium access control presented above is implemented within the simulation model. The interaction between both simulators is enabled by the TCP-based client/server TRaCI. It allows to retrieve status information (vehicle's status) of simulated vehicles and to control or manipulate their behavior on-the-fly. Information about traffic infrastructures including traffic light state, induction loops and road network characteristics can also be gathered. There are several commands implemented in both sides permitting to influence the vehicle behavior, for example, by forcing a lane change, adapt the speed of a vehicle or even change a vehicle route accordingly to specific events. A coupled simulation platform creates an opportunity that enables the performance evaluation of V2V-based applications. For any simulation study, a communication configuration file needed by OMNeT++as well as SUMO files containing the complete road network description including traffic flows and building data are prepared in advance. While simulation results are recorded into textual, scalar files and vector files in OMNeT++, those collected in SUMO are based on XML data representation. The post-processing of simulation results are provided by self-developed scripts using *python*, *awk*, and *bash* programming and command languages.

7.2.4   *Urban Intersection Propagation Path-Loss Model*

A proper investigation of the performance of VANET at urban intersections will strongly depend on the accuracy of the radio channel model used. Furthermore, a credible simulation-based evaluation of V2V requires a profound understanding of the wireless channel. The dynamic and complex topology of VANET and the inevitable presence of numerous mobile and static obstacles such as buildings, vegetation and other vehicles, especially frequent at urban intersections, poses a challenging problem. Radio propagation in urban areas is quite complex because it often consists of reflected and diffracted waves produced by multipath propagation. Although the effects that are influencing radio wave propagation have been well investigated [56, 72, 98], a validated and representative 5.9 GHz NLOS path loss model for vehicular networks in urban environments is still missing [93, 63, 139–141]. This is primarily due to the complexity of developing theoretical models which require the use of a large number of equations describing the
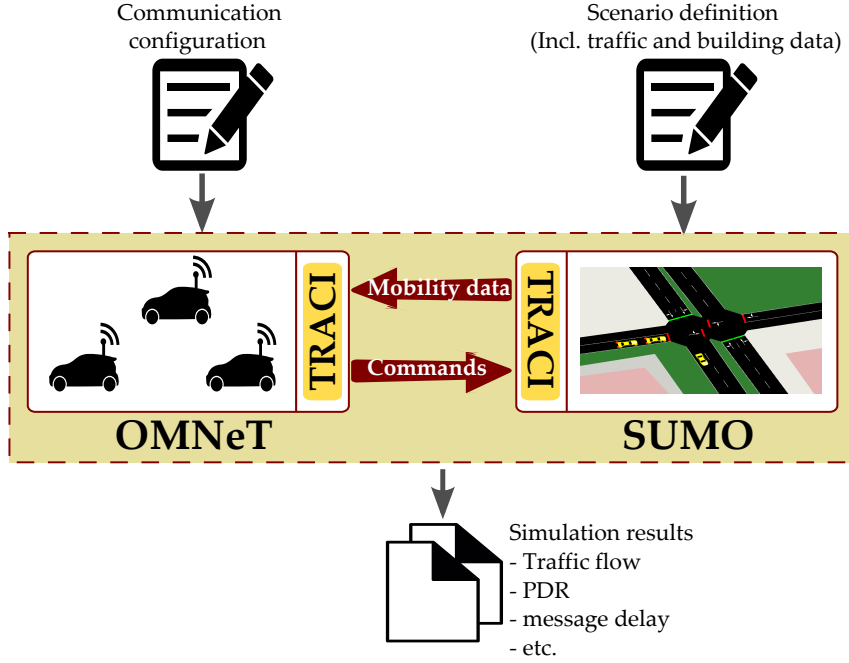
Figure 49: Hybrid simulation platform composed of SUMO and OMNeT++

physical structure of radio wave propagation. Despite the fact that these physics-based models provide a high accuracy of the path loss estimation, these models tend to be extremely complex and require excessive computational resources. The aforementioned reasons motivate the design of a dedicated urban propagation model by means of extensive field measurements conducted at different city intersections and concentrating on effects which influence the received signal power. We consider two separate scenarios and intersections based on shadowing states due to the structure of the intersection and the traffic behavior. We distinguish between LOS and NLOS situations. While the NLOS is caused by buildings and occurs when transmitter and receiver travel on two crossing road segments of the intersection, the LOS implies situations that reflect obstruction-less conditions with no building between the communication link. The measurement performed in the city of Hannover leads to the development of path loss model dedicated for LOS situations while this conducted in Braunschweig in Germany provides a site-specific model for NLOS. As a result, we proposed in this section a measurement-based Urban Intersection Propagation Model for LOS and NLOS situations based on a profound measurement campaign at two different urban intersections located in two Germany cities. The obtained propagation path loss model which distinguishes between obstructed and unobstructed situations constitutes the basis of our simulation study and is given as:

$$
PL(d)\, dB = \begin{cases} PL_{LOS}(d) & \text{LOS situations} \\ PL_{NLOS}(d_{TX}, d_{RX}) & \text{NLOS situations} \end{cases}, \tag{20}
$$

where $PL(d)$ denoted the decibel path loss, $d = \sqrt{d_{TX}^2 + d_{RX}^2}$ is the separation between transmitter and receiver, d_{TX} and d_{RX} the distance of the transmitter, and the receiver relative to the intersection center, respectively.

PATH LOSS FOR LOS SITUATIONS:

In general, the path loss in urban areas can be adequately represented by a *log normal shadowing* path loss model given by:

$$PL_{LOS}(d)\, dB = PL_{LOS}(d_0) + 10 \cdot n \cdot \log_{10}(\frac{d}{d_0}) + X_\sigma(0, \sigma) \qquad (21)$$

where $PL_{LOS}(d_0)$ is the path loss in dB at a distance d_0, n is the path loss exponent dependent on propagation environment, and the additional term $X_\sigma(0, \sigma)$ is the zero-mean Gaussian distributed random variable with standard deviation σ. This variable represents the long term variation of signal power in dB, known as signal fading. It comprises multi-path propagation effects as well as shadowing caused by surrounding vehicles or other objects obstructing the communication path. Typically, all these parameters are empirically determined using regression methods based on measurement results.

To determine the parameters of the model, we performed a set of measurements at a typical city intersection in Hannover. The experiments were performed in rush hour conditions in order to integrate in a simple manner the impact of obstructing vehicles. Also, the effect of multi-path propagation produced by reflected waves on buildings and vehicles parked along the road are taken into account. Typically, reflections from the ground could also occur in unobstructed environments. All these effects contribute constructively or destructively to the received signal power and belong to the nondeterministic component $X_\sigma(0, \sigma)$. The transmitter was located at several positions providing most of the time an almost perfect LOS to the receiver.

Based on the received power samples P_r from the measurements and the transmission power P_t, we can easily deduce the measured path loss as $PL_{LOS}(d) = P_t - P_r$. It should be noted that the transmission power includes already the overall system loss resulting in an EIRP of 23.2 dBm. The system loss comprises cables and connector losses as well as the antenna gain.
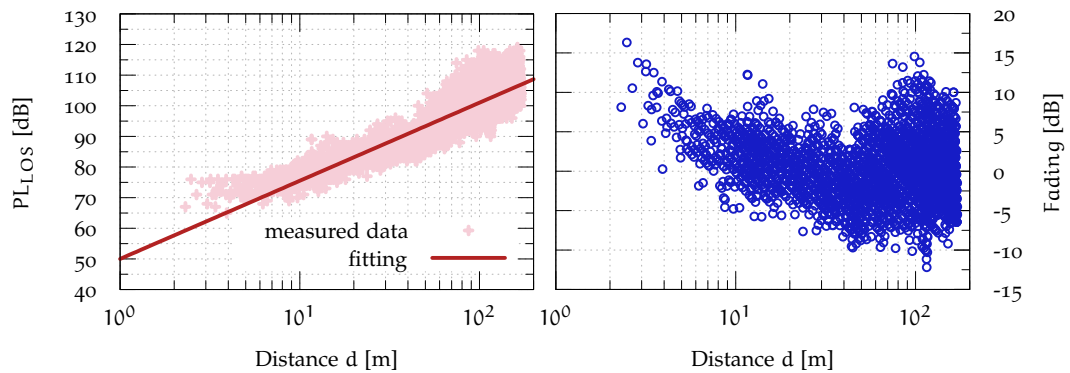
(a) Measured path loss and a line representing the best-fit empirical model

(b) Scatter plot of Fading

Figure 50: Measured path loss and fading under LOS conditions.

Figure 50a shows the path loss over all runs obtained during the experiment. Due to the linearity between the measured path loss and the separation between transmitter and receiver, we carried out the regression using a simple linear regression technique. Applying linear square curve fitting to minimize the root mean

square error, we obtained the red line which yields $d_0 = 1\,m$, $PL_{LOS}(d_0) = 50\,dB$ and $n = 2.55$ corresponding to the best-fit to Equation 21. Furthermore, we determine fading as the deviation between the measured power sample and the fitted curve representing the average signal power over every distance d. Results are depicted in Figure 50b. In order to determine the distribution function approximat-
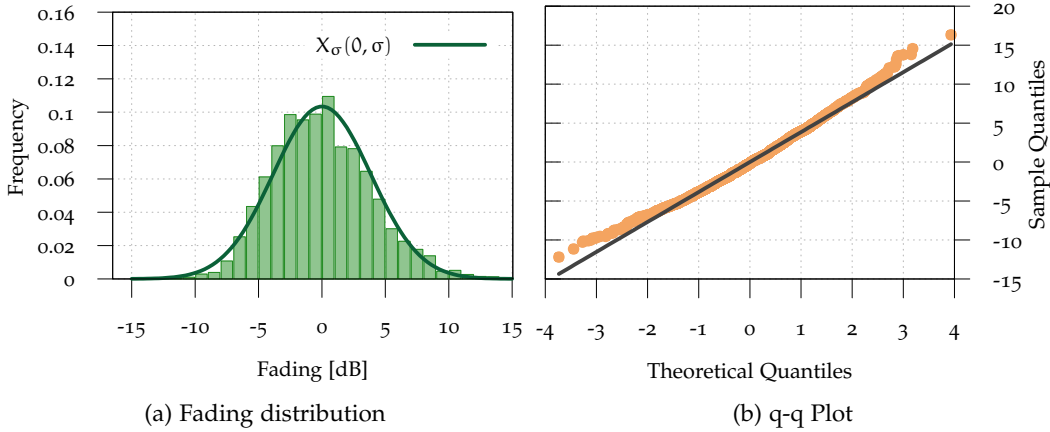

(a) Fading distribution

(b) q-q Plot

Figure 51: Distribution and probability mass function of fading, q-q plot for the validation of the assumed normal distribution.

ing the fading distribution, we determine and show in Figure 51a the Probability Mass Function (PMF) of the measured fading. We observe that the distribution of fading follows a normal distribution with the standard deviation $\sigma = 3.9\,dB$ of the zero-mean Gaussian random variable $X_\sigma(0, \sigma)$.

To check whether the normality of fading is valid, we employ the quantile-quantile plot or q-q plot. It is based in general in the computation of the theoretical expected value for each data point of the measured fading. A normal q-q plot for the fading points is shown in Figure 51b. The x-coordinates are obtained using the unit normal distribution $\mathcal{N}(0, 1)$. In the Figure, a straight line that provides least-squares fit to the points is also shown. We observe that the points of the q-q plot fall approximately on the straight line which implies that the measured fading follow the assumed normal distribution. After determining all parameters, the path loss for LOS for urban areas can be given as

$$PL_{LOS}(d)\,dB = 50.0 + 25.5 \cdot \log_{10}(d) + \mathcal{N}(0, 3.9) \tag{22}$$

PATH LOSS FOR NLOS SITUATIONS:
From a topology point of view, a radio propagation model that takes the distance d_{TX} of the transmitter and the distance d_{RX} of the receiver relative to the intersection center is required, especially at urban intersections. Therefore, we developed a two-dimensional model based on a measurement campaign at the city of Braunschweig for NLOS which can be expressed as follow:

$$PL_{NLOS}(d_{TX}, d_{RX})\,dB = PL(d_{TX}, d_{RX}) + X_\sigma(0, \sigma) \tag{23}$$

The model also incorporates the random variable $X_\sigma(0, \sigma)$ described above reflecting the variation in received signal power due to multipath components.

The experiments were conducted with the transmitter at two fixed positions while the receiver was moving toward the intersection center. Due to the complexity to obtain a complete 2D path loss model, a ray-tracing tool is used to model the wave propagation by reproducing the measurement's scenario while considering a high granularity of communication pairs around the intersection. For each transmitter and receiver pair, a path loss value based on the complex channel impulse is calculated. For this purpose, multipath wave propagation caused by signal reflection or diffraction on surrounding buildings along the intersection are also considered. It requires a 3D building and elevation data which were then integrated into the ray tracer as illustrated in Figure 52.

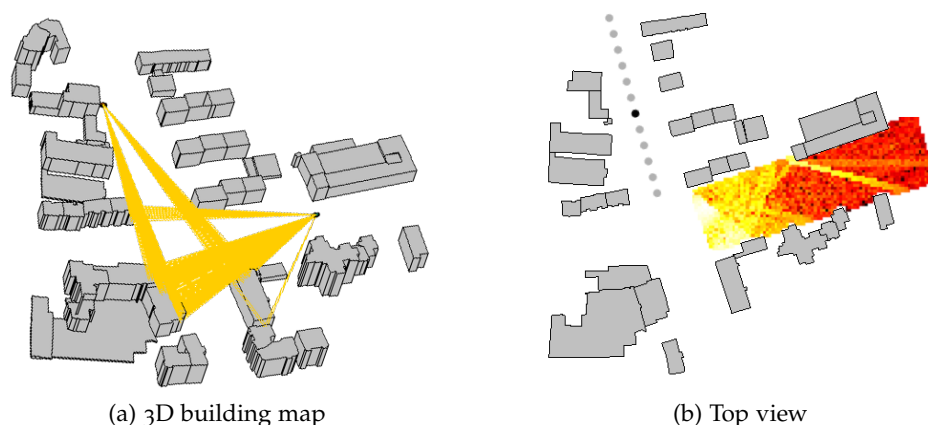(a) 3D building map   (b) Top view

Figure 52: Measurement intersection reproduced in the ray tracing. (a) Reflected and refracted rays between two vehicles. (b) Colored map corresponding to the measured power level. The gray circles represent the varying position of the transmitter.

Based on ray-tracing results, we generate a realistic geometry-based deterministic propagation model that reflects obstruction-less conditions. The obtained term $PL_{meas}(d_{TX}, d_{RX})$ depicted in Figure 53 was then integrated as a lookup table in the simulator platform. This term takes the distance d_{TX} of the transmitter and the distance d_{RX} of the receiver relative to the intersection center into account. To make this empirical model accessible to the research community, we use a regression technique to fit an equation to the measured term $PL_{meas}(d_{TX}, d_{RX})$ in order to obtain a close form which can then be easily imported in network simulators. The fitted term $PL(d_{TX}, d_{RX})$ can then be expressed as

$$PL(d_{TX}, d_{RX}) \, dB = \frac{54 + 0.91(d_{TX} + d_{TY})}{1 + 0.0053(d_{TX} + d_{TY})} \tag{24}$$

For the sake of accuracy, the developed model was compared against with experimental measurements and iteratively fitted. The post processing and integration of the measurement's scenario in the ray tracing tool were performed by the department of mobile systems from the technical university of Braunschweig. Apart the direct and reflected path, the ray tracing tool takes the diffuse scattering of wave into account. More details about the ray tracing tool can be found in [142].
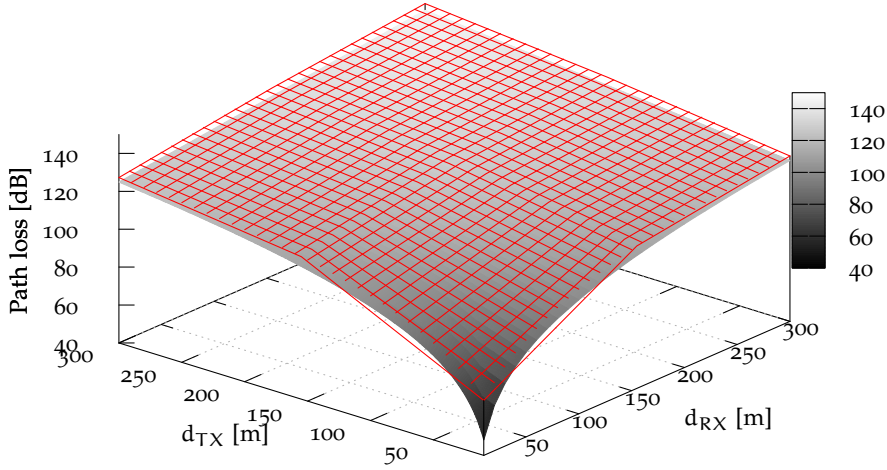
Figure 53: Path loss term $PL_{meas}(d_{TX}, d_{RX})$ for NLOS based on measurements and its fitted curve (in red).

COMMUNICATION RANGE:

In interference-free conditions as well as under high vehicle densities, it is crucial to identify the communication range that ensures a proper operation of V2V applications. The knowledge about the communication range provides a useful information to application designers allowing an efficient investigation and definition of application requirements. Safety critical applications such as collision avoidance may require a high level of information accuracy compared to infotainment-based applications. As a consequence , we adopt a more strict definition of the communication range as the distance between transmitter and receiver where the received signal power is 99% of the time above the receiver sensitivity. As discussed above, due to the stochastic term of the path loss component, the signal strength at the receiver in a given urban area at a fixed position d from the transmitter is log normal distributed with a Probability Density Function (PDF) expressed by

$$p(P_r) = \frac{1}{\sigma\sqrt{2\pi}} \exp^{-\frac{(P_r - \bar{P}_r(d))^2}{2\sigma^2}} \tag{25}$$

The received signal power in dB is expressed by a normal random variable with a mean $\bar{P}_r(d) = P_t - PL_{LOS}(d_0) - 10 \cdot n \cdot \log_{10}(\frac{d}{d_0})$ and a standard deviation σ. To obtain the communication range CR, we first have to determine the probability that the receiver signal power P_r at distance d is above the receiver sensitivity $P_{r,th}$ as

$$P_{P_{r,th}}(d) = P[P_r \geqslant P_{r,th}] = \int_{P_{r,th}}^{\infty} p(P_r)\, dP_r = \int_{P_{r,th}}^{\infty} \frac{1}{\sigma\sqrt{2\pi}} \exp^{-\frac{(P_r - \bar{P}_r(d))^2}{2\sigma^2}}\, dP_r$$

$$= \frac{1}{2} + \frac{1}{2}\mathrm{erf}\left(\frac{\bar{P}_r(d) - P_{r,th}}{\sigma\sqrt{2}}\right) \tag{26}$$

Figure 54 shows the probability $P_{P_{r,th}}(d)$ as function of the distance d between transmitter and receiver. It represents the CDF of the received signal power. In other words, it is the probability that a received packet can be successfully decoded. We observe in this figure that almost 10% of the packets can be successfully decoded at a distance $d \approx 550$ meter. For efficiency-based applications such as the Green Light

Optimized Speed Advisory (GLOSA), a probability of packet reception of at least 10% will already fulfill the application requirement as these kind of applications rely not on a real time information but more on sufficient communication range needed by the driver in order to adjust his speed according to the corresponding traffic light information.
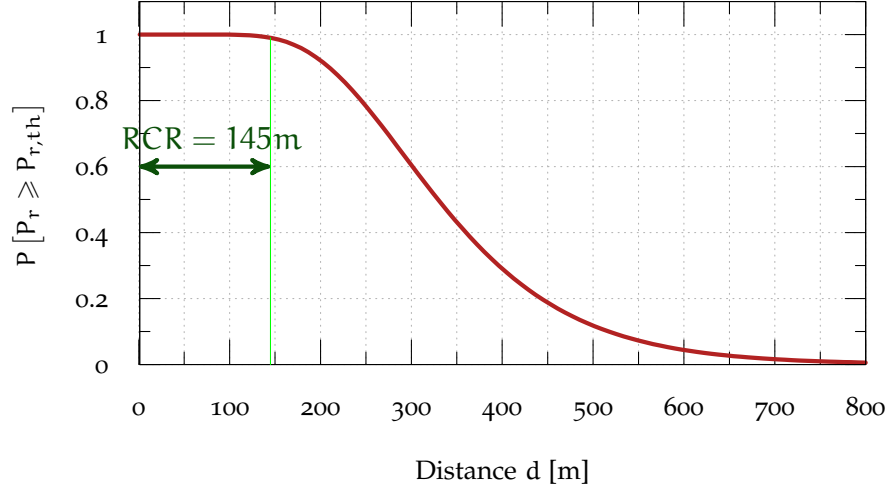
Figure 54: Probability of packet reception $P_{P_{r,th}}(d)$ as function of the distance d between transmitter and receiver.

Since we are interested in the Reliable Communication Range (RCR) assuming a reception probability of at least 99 percent. This could be obtained using Equation 26; we get:

$$P_{P_{r,th}}(RCR) = 0.99 \iff \frac{1}{2} + \frac{1}{2}\mathrm{erf}\left(\frac{\bar{P}_r(RCR) - P_{r,th}}{\sigma\sqrt{2}}\right) = 0.99$$

$$\mathrm{erf}\left(\frac{\bar{P}_r(CR) - P_{r,th}}{\sigma\sqrt{2}}\right) = 0.98$$

Considering that the argument of the error function `erf` that yield 0.98 is about 1.646, it follows

$$\frac{\bar{P}_r(RCR) - P_{r,th}}{\sigma\sqrt{2}} = 1.646 \tag{27}$$

and recalling that $\bar{P}_r(RCR) = P_t - PL_{LOS}(d_0) - 10 \cdot n \cdot \log_{10}(\frac{RCR}{d_0})$, we get

$$\frac{P_t - PL_{LOS}(d_0) - 10 \cdot n \cdot \log_{10}(\frac{RCR}{d_0}) - P_{r,th}}{\sigma\sqrt{2}} = 1.646$$

$$RCR = d_0 \cdot 10^{\frac{P_t - PL_{LOS}(d_0) - P_{r,th} - 1.646 \cdot \sigma\sqrt{2}}{10 \cdot n}}$$

Assuming $P_t = 23.2\,\mathrm{dBm}$, $P_{r,th} = -91\,\mathrm{dBm}$, $PL_{LOS}(d_0) = 50\,\mathrm{dB}$, $\sigma = 3.9\,\mathrm{dB}$, $n = 2.55$, and $d_0 = 1\,\mathrm{m}$, the reliable communication range can be obtained as

$$RCR = 145\,\mathrm{meter} \tag{28}$$

It should be noted that the determined RCR represents the maximum reliable communication range in LOS and under interference-free situations since considering more than one transmitter will result in a reduction of the communication range due to an increasing level of interference. And this is only valid when we assume a reception probability of at least 99%.

7.3 SCENARIO DESCRIPTION AND SIMULATION SETUP

7.3.1 *Scenario Description*

A crucial task envisioning a simulation-based evaluation of vehicular networks is the choice of an adequate simulation scenario that could provide a representative statement about the performance of V2V communication. The selection of the scenario depends on the application as well as the communication protocol under study and has to be carefully chosen and configured. For the sake of comparison with related works in the literature, we select the so-called Manhattan scenario which is the most frequently used scenario and hence provides a good basis for the investigation of vehicular networks in urban areas. Despite its medium level of realism, this kind of scenario provides due to the regularity of buildings and streets, a comfortable environment for the evaluation of vehicular protocols. The Manhattan grid used in this work as illustrated in Figure 55 consists of square grids following a regular structure of similar size with 16 buildings, 9 intersections and 24 road segments with two lanes per direction. Each building has a size of 260x260 m² while roads have a width of 40 m. These dimensions are in accordance with those found in the literature and provide as well a good agreement with the maximal achievable communication range determined above.

As we are interested in the most critical case in terms of the scalability effect, we consider a fixed traffic density of $\rho = 83$ veh/km/lane, which quantifies the aggregated number of vehicles on a roadway segment per km per lane. It corresponds to heavy traffic close to the section's capacity and an average inter-distance between vehicles of 7 m. The traffic load is uniformly distributed over the network topology. The traffic simulator SUMO provides OMNET++ with each vehicle's mobility data through the Traffic Control Interface (TraCI). Each intersection was controlled by traffic lights following a realistic traffic control plan. This implies that on one hand a high density of vehicles is expected around intersections where queuing and clustering phenomena occur. On other hand, there will be a lower density along streets separating intersections. Moreover, vehicles on these streets will drive up to the section's recommended speed. In order to eliminate boundary effects, we chose the intersection in the middle (red square in Figure 55) of the scenario as target intersection. The crossing road sections I, II, III, and IV as well as the area near intersection's center are considered as Region of Interest (RoI). This region is used for statistical evaluation of the communication performance.

In order to consider also the impact of the intersection type, we distinguish based on the study presented in Chapter 3 between three intersection types with respect to the placement of buildings in the region of interest:

URBAN CLOSE INTERSECTION: This intersection as depicted in Figure 55a shows a typical inner city intersection with four corners occupied by buildings and hence may correspond to Type 4. Recall the analysis of the building occupation in the

selected European cities revealing that up to 40% of all 4-leg intersections have a building at each four corners. In this scenario, vehicles located around the intersection center would be likely exposed to interference from crossing road sections, while vehicles approaching might only be influenced by vehicles on their own road sections.

URBAN HALF-OPEN INTERSECTION: In this intersection, two corners were occupied by buildings which provide a mixed environment of obstructed and unobstructed situations as show in Figure 55b. The influence of interference is expected to increase due to the missing of buildings G and K.

URBAN OPEN INTERSECTION: In contrast to the closed and half-open intersection, the absence of building blocks F, G, J, and K leads to a perfect LOS between vehicles in the RoI area as can be seen in Figure 55c. This situation leads to a significant level of interference since all vehicles in the RoI are sharing the same communication range. In other words, all vehicles in road sections I up to IV hear, and hence interfere with each other.
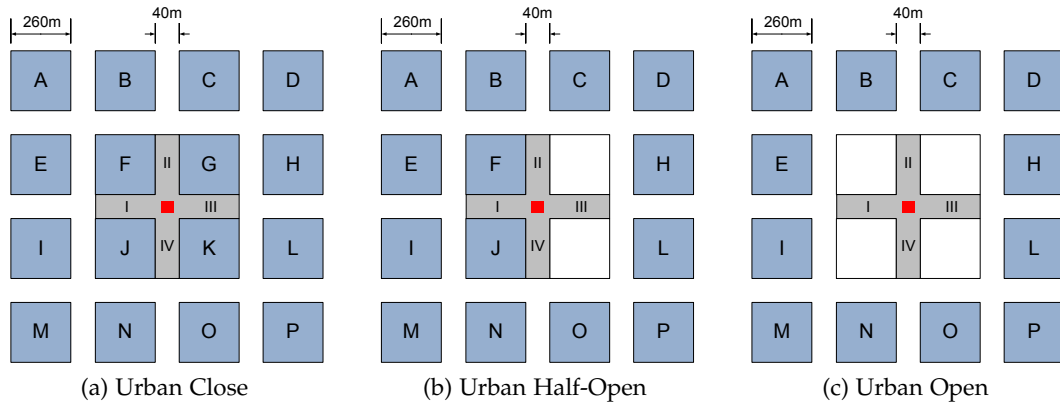
Figure 55: Urban scenarios with different intersection types and the region of interest (gray area). The red square represent the targeted intersection's center.

7.3.2 Simulation Setup

To provide an accurate assessment of the effective potential and limits of V2V communication, a simulation-based evaluation requires a proper simulation setup and configuration using parameters conforming to the established communication standard. In this way, the level of realism is increased. Table 10 summarizes the simulation parameters that all results presented in this section have in common, where f_c denotes the carrier frequency, P_t the transmission power, R_b the data rate used for transmission, and N the noise floor, respectively. The model assumes that a frame can be successfully decoded by the receiver if the SINR during frame reception is greater or equal to $SINR_{th}$. The corresponding received power threshold allowing successful frame reception in absence of interference is referred to as the receiver sensitivity $P_{r,th}$, and $P_{r,cs}$ denotes the carrier sense threshold. The message generation rate f_g represents the frequency of CAM updates. The penetration rate p is defined as the ratio of equipped vehicles with a communication module. All these

parameters were fixed during each simulation run as we only consider single-hop broadcast transmissions in this study and no congestion control was applied. We chose a fixed contention window CW=31 because it was shown in [143] that CW has not noticeable influence on the communication performance. We make use of the proposed simulation platform presented in Section 7.2.3 as well as the developed dedicated urban propagation model to evaluate aforementioned scenarios.

The variation of parameters from the table below leads, considering 10 repetitions per configuration, to a total of 810 simulation runs performed within this thesis. Each simulation run takes an average of 16 hours, depending on the parameter configuration. High penetration rates and message generation rates combinations generate a large number of events that has to be processed by the simulation kernel and thus requires more computational efforts. Summing up all simulation duration, 810 multiplied by 16 hours leads to 540 days of computing time if only a single core is utilized for the whole simulation campaign. To deal with the computational power issue, the Scientific Computing Group at the University of Hannover offers massive parallel computing systems and computers with large memory allowing to run simultaneously several single simulation runs in multiple nodes. In this way, with a maximal jobs of 72 per user, the whole simulation study could be then performed in a couple of days.

Table 10: Communication and simulation parameters used for the evaluation

CATEGORY	PARAMETER	VALUE
PHY	Frequency f_c	5.9 GHz
	Data rate R_b	6 Mbps
	Noise floor N	-100 dBm
	$SINR_{th}$	9 dB
	Receiver sensitivity $P_{r,th}$	-91 dBm
	Carrier sense threshold $P_{r,cs}$	-93 dBm
	Transmission power P_t	{5, 13, 23} dBm
MAC	Slot time	13μs
	SIFS time	32μs
	Contention window CW	31
CAM	Message generation rate f_g	{5, 10, 15} msg/s
	message payload size	1000 Bytes
SCENARIO	Manhattan grid	1200x1200 m²
	# of junctions	9
	Traffic density ρ	83 veh/km/lane
	Intersection type	{Close, Half-Open, Open}
	Penetration rate p	{5, 10, 25} %
	Simulation time	100s
	Repetitions	10

7.4   EVALUATION METRICS

In general, the performance evaluation of a computer systems requires quantities that precisely capture and measure the behavior of a given system. Hence, such systems depend on several factors which directly or indirectly influence its performance. However, unlike typical network-based performance metrics such as throughput, delay and packet loss, vehicular communication requires new metrics that are directly related to the behavior of the vehicular network characterized by the highly dynamic topology of VANETs and its stringent delay requirement. Moreover, QoS requirement of V2X application demands metrics which should deal with the single-broadcast nature of the network. To keep the specificity of single-hop broadcast of vehicular networks from several perspectives and also based on works found in the literature [144], we introduced mostly used QoS metrics in VANETs including packet drop rate, Packet Delivery Rate (PDR), Packet Reception Rate (PRR), Channel Busy Time (CBT) and Message Age (MA):

CHANNEL BUSY TIME (CBT): Fraction of time in which the channel is sensed busy due to own frame transmissions or neighboring frame transmissions during a certain period of time. A channel is considered as busy whenever the measured signal power observed at a node exceeds the carrier sense threshold $P_{r,cs}$ or when a node currently transmits to the wireless channel. The channel busy time is a direct measure of the channel utilization and is also used to estimate the load on the wireless channel allowing the definition of network states e. g. *restrictive*, *active* and *relaxed*, based on predefined assumptions. As the channel load is measured in the Decentralized Congestion Control (DCC) module which introduced a congestion control approach by limiting the channel load according to network states, we integrated this module into our model. Doing so, we were then able to periodically gather CBT samples.

PACKET DROP RATE: The number of packets discarded due to expiry time among the number of packets generated by the application layer. Due to the broadcast nature of VANET, the lifetime of a packet in the MAC queue is bounded by the message generation interval ,e. g., $1/f_g$ so that a newly generated packet would replace the old one. We designed replaced packets due to the expiry time as packet drops. This is also considered as a local loss as it occurs when a node experiences the channel as highly saturated so that new arriving packets from the upper layer are directly dropped. Intuitively, one could argue that a smaller CBT will result in a lower packet drop rate characterized by a relaxed channel status.

PACKET DELIVERY RATE (PDR): The number of packets successfully delivered to the number of packets transmitted by a tagged node. Transmitted packets refer to packets which successfully pass the MAC layer and were therefore not been dropped due to expiry time. Please recall that a packet is assumed to be successfully delivered if the SINR during packet reception is greater or equal to $SINR_{th}$ and the signal power exceeds the receiver sensitivity $P_{r,th}$. In this work, we consider that a packet is not successfully delivered due to two reasons: (i) when backoff counters of two or more nodes located within the same transmission range simultaneously reached zero; or (ii) when nodes which are hidden to each others begin the transmission at the same time. Transmitted packets which are not delivered due to path loss are not considered. This receiver-centric metric is determined at the PHY layer of a specific receiver.

PACKET RECEPTION RATE (PRR): The ratio of the number of packets successfully received to the number of packets generated by the application layer at a tagged node. This metric takes aforementioned metrics such as the packet drop rate and the PDR into account. As the PDR, it a receiver-centric metric determined using the concept of packet numbering which allows to detect lost packets due to collision or drop. In other words, the PDR directly depends on the number of missing sequence numbers in received packets. Regarding the requirement of safety based applications, this metric provides application designers a useful QoS measure which is directly linked to the performance of the communication.

END-TO-END DELAY (D_{E2E}): The time between a packet generation and its reception by a certain node as depicted in Figure 56. Basically, the end-to-end delay in VANETs is the accumulation of channel access time delay, transmission delay, and propagation delay in the channel. The transmission delay is the time needed to push all bits of a packet into the channel. This delay will remain constant since it depends solely on the message size and the data rate. The propagation delay which is the time taken by the signal to travel from the sender to the receiver is negligible since nodes can communicate only in a range of few meters. The delay due to the waiting time in MAC queue is until the packet's transmission, also known as the Channel Access Time (CAT) is a crucial component of the end-to-end delay. The CAT depends on backoff counter chosen as well as on the observed channel load during the frame transmission and can then fluctuate from packet to packet.

MESSAGE AGE (D_{MA}): The time between two successfully received messages inclusive the CAT of the first message from a specific sender. This takes the channel access time in the MAC queue as well as the time due to successive packet losses into account. The illustration in Figure 56 is used to demonstrate how message delays are determined in our evaluation. Let us consider an example showing the timing diagram of two successfully received messages (message 1 and 4) from their generation until their reception point in time. We consider a successful message dissemination as follows: a message i generated at time $t_{g,i}$ passes through the MAC layer and experiences the time in the queue $t_{q,i}$ until reaching the receiver at time $t_{r,1}$. Packet losses due to packet collisions in the channel as well as due to the expiry time in MAC queue are also depicted. This is the case for the message 2 and 3 in the following Figure.

While the end-to-end delay for multi-hop communication might be of interest, for broadcast-based message dissemination, evaluating message latency based solely on this metric will provide limited conclusions about the application's reliability as the message delay does not consider additional time delays due to packet losses. A fraction of lost packets increases when the channel becomes saturated. Motivated by this limitation, we therefore introduced the message age providing a good indicator about the freshness of information received from a specific sender in the node's neighborhood since safety-based applications require low latency for the message exchange in order to provide an acceptable awareness among vehicles in communication range. In the literature, the message age is often simplified to *inter-arrival time* [143], *inter-reception time* [145], *inter-message delay* [146], or simply the *update delay* [147], which are all defined as the time between two consecutive successfully received messages from the same sender.
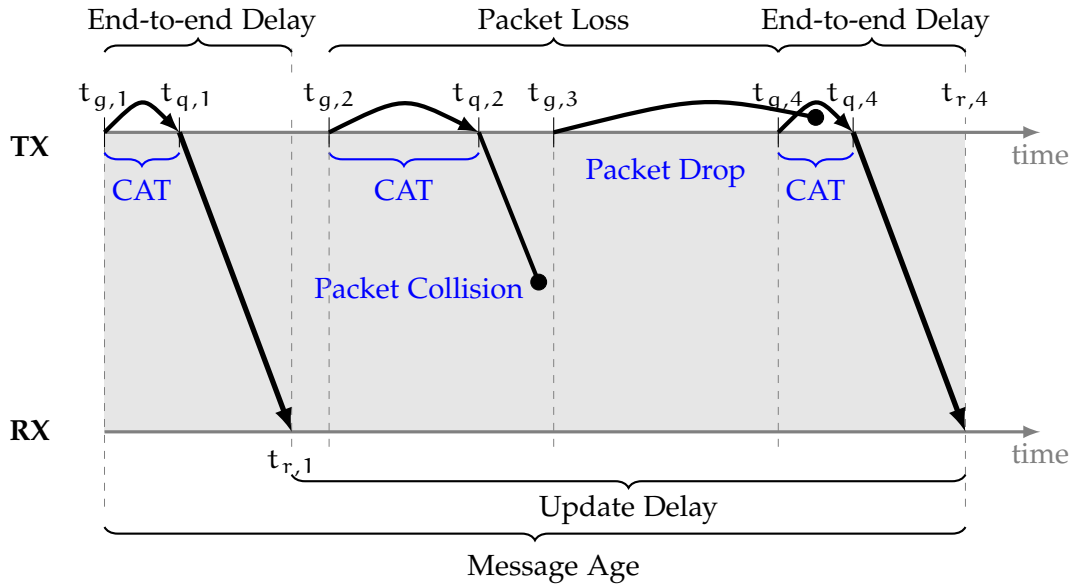
Figure 56: Illustration of delay types and packet loss.

7.5   RESULTS AND ANALYSIS OF FUNDAMENTAL FACTORS

In this section, we discuss results obtained during the simulation campaign. In contrast to a highway scenario characterized by a 1-D road network topology with straight street segments, the investigation of the communication performance at urban intersections requires a 2-D representation of results. This allows a more quantitative transmitter/receiver evaluation as function of the distance d_{TX} of the transmitter and the distance d_{RX} of the receiver relative to the intersection center. In other words, we analyze the performance from a receiver perspective with respect to the distance to a potential transmitter to the intersection implying that we are interested in the level of awareness that a vehicle can achieve from its direct neighborhood. We first investigate environmental factors that affect the communication link. We evaluate in a second part the impact of different communication parameters followed by a profound investigation of packet losses. Hereby, we examine the source of interference followed by a classification of packet collisions, which can occur in VANETs.

7.5.1   *Environmental Factors*

The penetration rate, intersection type, and transmitter/receiver constellation are natural and uncontrollable factors that adversely affect the communication performance. The challenge of V2V is to recognize and eliminate as much of the impact of these factors that participate in the communication process. In fact, in order to obtain a high level of realism during the performance evaluation of VANETs, we deal in our evaluation with all these factors.

Impact of Penetration Rate

Since 2012, twelve important European vehicle manufacturers have signalized their intention to bring cooperative systems based on V2X communication onto roads

starting in 2015 implying that V2V systems are close to market introduction. While in the early stage of deployment only a small portion of vehicles will be equipped with a communication system, traffic density can be expected to grow substantially during peak hours in urban environments. Under high vehicle densities, especially at city intersections, the channel will suffer from severe congestion which subsequently leads to a rapid degradation of the communication performance reflected by long delays and packet collisions. However, a vehicular network should be able to accommodate when a traffic load changes from low to high traffic densities. In order to gain insight into the scalability effect of VANETs, we evaluate the impact of different penetration rates in term of vehicle densities. We defined the penetration rate as the number of communicating vehicles over the total number of vehicles in the considered simulation network. Both factors, penetration rate and vehicle density, are directly dependent. Meaning that the higher the total number of vehicles in the road network, the larger communicating vehicles are involved within a common communication range. To investigate the scalability effect, we explicitly increase the number of communicating vehicles through variation of penetration rates. Following Table 11 underlines the relationship between the penetration rate, traffic density and traffic conditions of the simulated road network.

Table 11: Penetration rates versus traffic conditions

Penetration Rate	Traffic Density ($^{veh}/_{km/lane}$)	Traffic Conditions
5 %	9	Free
10 %	18	Stable
25 %	42	Unstable

Based on the Level of Service (LoS) defined according to traffic conditions defined in [148], a penetration rate of $p = 5\,\%$ represents free flow traffic conditions reflected by a situation where traffic streams are above recommended segment speed and drivers have a complete mobility between lanes. A penetration rate of $p = 10\,\%$ corresponds to stable traffic flows where the ability of drivers to maneuver through lanes is considerably limited, and lane changes require more driver attention. Finally, a penetration rate of $p = 25\,\%$ represents unstable traffic flows that not necessarily lead to traffic congestion but corresponds to situations where the freedom to maneuver within the traffic becomes much more limited and the driver behavior approaches an uncomfortable level. A penetration rate of $p = 100\,\%$ corresponds to a traffic density of 83 $^{veh}/_{km/lane}$.

In Figure 57, the average PDR recorded with different penetration rates and intersection types is depicted as function of d_{RX} and d_{TX} distances. The results presented in this subsection include a fixed message generation rate of $f_g = 10\,\mathrm{msgs/s}$ and a transmission power of $P_t = 23\,\mathrm{dBm}$.

As a first observation, it is apparent that, in general for all intersection types, the PDR decreases with increased distance d_{RX} and d_{TX}, respectively. We can also observe as expected that the PDR is directly linked to the penetration rates as a high number of communicating nodes implies an increasing probability of packet loss
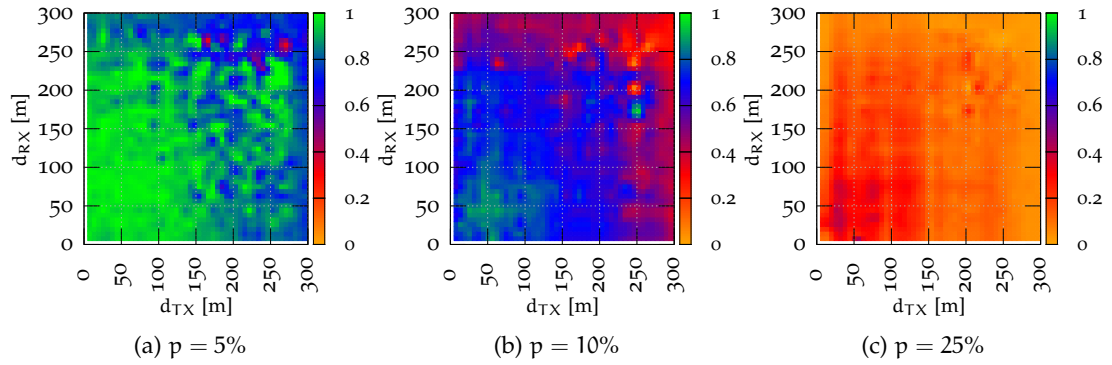
(a) p = 5%   (b) p = 10%   (c) p = 25%

Figure 57: Impact of penetration rate: Average PDR as function of d_{RX} and d_{TX} distances. Comparison of the results by using different penetration rates for the *Open* intersection type with $f_g = 10$ msgs/s and TxPower = 23 dBm.

due to packet collisions in the wireless channel. However for the *Open* intersection type, while simulating with a lower penetration rate of p = 5%, up to 70% of the transmitted packets were successfully received for $d_{TX}, d_{RX} \leqslant 200$ m, respectively. However, the PDR drops considerably to only 10% at a high penetration of p = 25%. As a consequence, safety-based applications which require a packet reception rate of 100% will fail under such channel conditions due to high vehicle densities.

As already noticed, the determination of the PDR does not consider packet losses due to packet drops. Hence, the real communication performance reflected by the aforementioned Packet Reception Rate (PRR) would be considerably worse since this takes packet drops into account. To better examine the effective reception probability also know as PRR, we picked more specifically a pair of vehicles A and B to illustrate the impact of the penetration rate on communication performance. Hereby, we configure the transmitter at a fixed location $d_{TX} = 50$ m on a side street (road section I in Figure 55), while the receiving vehicle B moved on an intersecting street, approaching the intersection with a speed of approximately = 50 km/h (road section II). This could be assimilable to a situation where a vehicle approaching an intersection shall be informed about a risk of collision.

From the results presented in Figure 58, we can conclude that under *free* (p = 5%) as well as *stable* traffic conditions (p = 10%), the communication quality provides acceptable PRR values. However, reaching *unstable* traffic flows (p = 25%), the network will suffer from severe packet losses caused due to packet drops and packet collisions on the communication channel. Clearly, if the number of transmitting nodes located within a common sensing range increases, the probability of packet collision grows accordingly. This is especially true for the *Open* compared to the *Close* intersection type which is part of the following investigation where we concentrate on the impact of intersection topologies. Furthermore, PDR and PRR results reveal that packet losses are not linear to the penetration rates, regardless of the considered intersection type.

As a final note, the subsequent impact of the penetration rate in the VANET at urban environments is confirmed so that this non-negligible environment factor should be taken into account while developing efficient congestion control techniques. The main goal of these network traffic control algorithms should be to

(a) *Open*

(b) *Close*

Figure 58: Average PRR as function of the distance d_{RX} of the receiver relative to the intersection center under varying intersection types and when a transmitter is located at $d_{TX} = 50\,\text{m}$. $f_g = 10\,\text{msgs/s}$ and $P_t = 23\,\text{dBm}$.

regulate channel load according to the current traffic conditions as traffic density cannot be readily influenced.

(a) *Open*, $f_g = 10\,\text{msgs/s}$

(b) *Half-open*, $f_g = 10\,\text{msgs/s}$

(c) *Close*, $f_g = 10\,\text{msgs/s}$

(d) *Open*, $f_g = 15\,\text{msgs/s}$

(e) *Half-open*, $f_g = 15\,\text{msgs/s}$

(f) *Close*, $f_g = 15\,\text{msgs/s}$

Figure 59: Impact of intersection type: Average PDR as function of d_{RX} and d_{TX} distances. Comparison of the results obtained under different intersection types and message generation rates with $p = 10\,\%$ and transmission power $= P_t = 23\,\text{dBm}$.

Impact of Intersection type

In the previous section, we have analyzed the effect of penetration with respect to different traffic densities. However, an interesting research question behind the motivation of this thesis is how a considered intersection type in term of building's placement around the intersection affects the performance of VANETs at urban intersections. Intuitively, one can argue that building's shadowing will attenuate the propagation signal and, therefore, will lead to a reduction of the communication range. But, on the other hand, this negative effect may limit co-channel interference produced by hidden nodes or nodes present in a common communication range as already shown experimentally in the previous chapter. In other words, it is expected that the placement of buildings in intersection areas brings a positive effect through the decrease of the communication cell reflected by a low number of concurrent transmissions to the channel, especially at nodes located near the intersection center. To answer this question, we used, therefore, for the evaluation fixed communication parameters and performed a simulation study by varying intersection types as defined in Section 7.3.1.

As can be seen in Figure 59, the *Open* intersection type provides, in general, the best performance compared to the *Half-open* and *Close* type. This is especially true when the transmitters and receivers are located at a distance lower than 200 m from the intersection center, respectively. The same behavior also appears when we simulate with a higher channel load by considering a set up using a message generation rate of $f_g = 15$ msgs/s (see Figure 59d, 59e, 59f). More interestingly, we observe some areas in the figures where the *Close* type provides best results in term of number of successfully received messages. For example, with a transmitter and a receiver located at $d_{TX} \leqslant 20$ m and 50 m $\leqslant d_{RX} \leqslant 200$ m, respectively, the *Close* , as well as *Half-open* type, perform slightly better than under the *Open* configuration. In order to better investigate this behavior, we concentrate and focus on the examination by fixing the transmitter position at $d_{TX} = 15$ m and present the results in Figure 60. As expected, already at a low channel load e. g. using a message generation rate $f_g = 10$ msgs/s, the performance appears not so significant but increases noticeably when increasing the channel load considering a simulation using $f_g = 15$ msgs/s. Reasons behind these phenomena are subject of detailed investigations in Section 7.5.2 where the influence of the message generation rate is considered.

Impact of Transmitter/Receiver Constellation

Through the 2D representation of the average PDR as a function of the distance d_{TX} of the transmitter and the distance d_{RX} of the receiver relative to the intersection center, we remark that the position of the transmitter and receiver has an influence on the obtained communication performance. In fact, the location of the transmitter has no effect on the achievable PDR; however, the receiver experience is different as packet collisions due to hidden nodes, for instance, is observed at the receiver. Intuitively, a receiver located directly at the intersection's center will suffer from a high level of interference from surrounding nodes located on roads connecting the crossways. To gain insight into the impact of transmitter/constellation, we examine the results by distinguishing between two classes of constellation: When transmitter and receiver are located on the same road segment and when they are

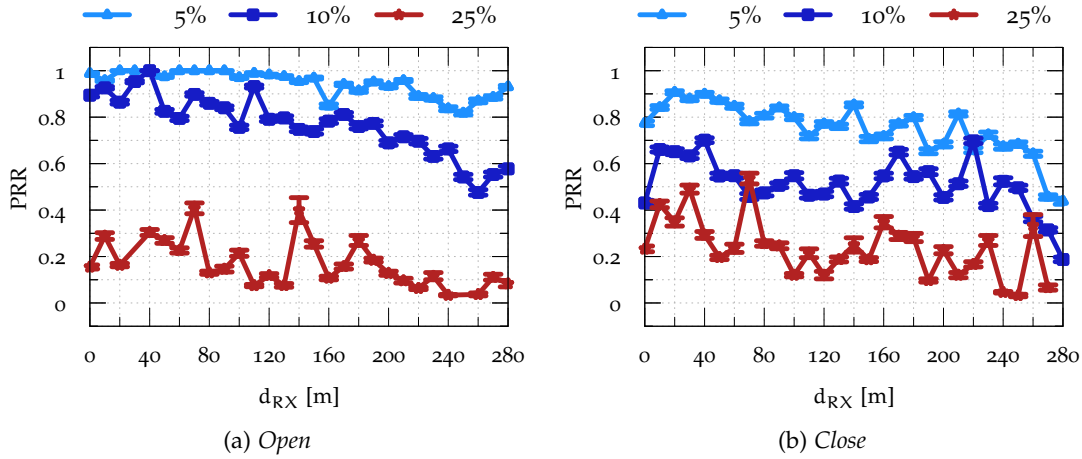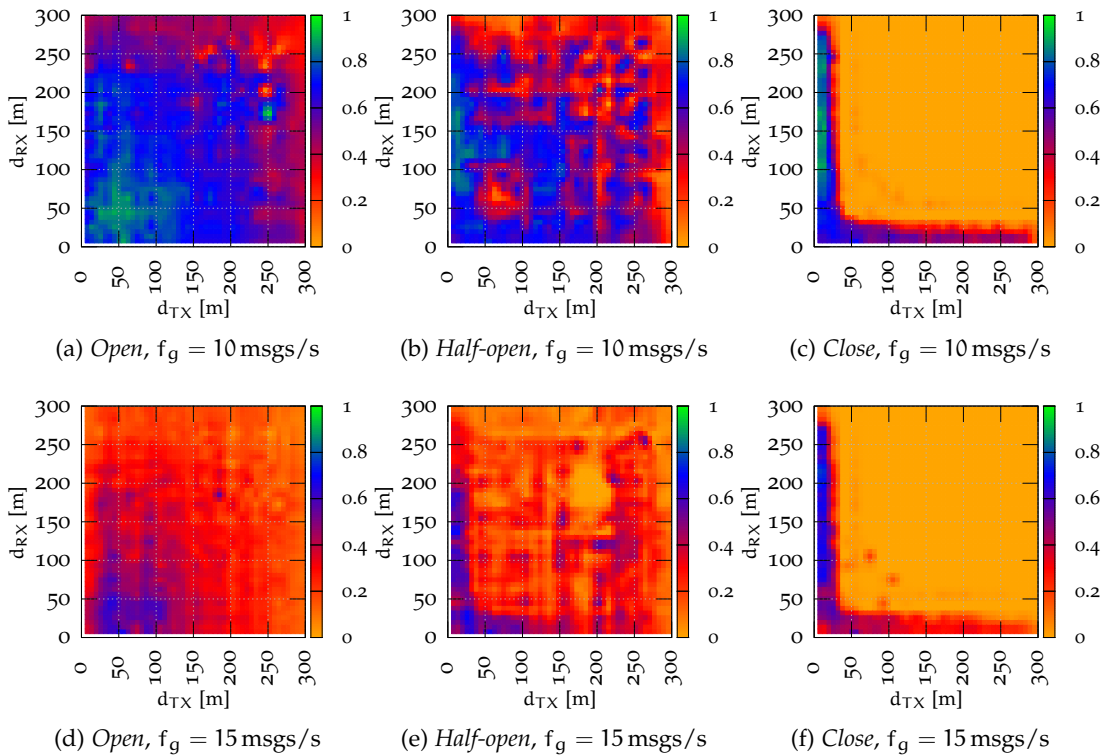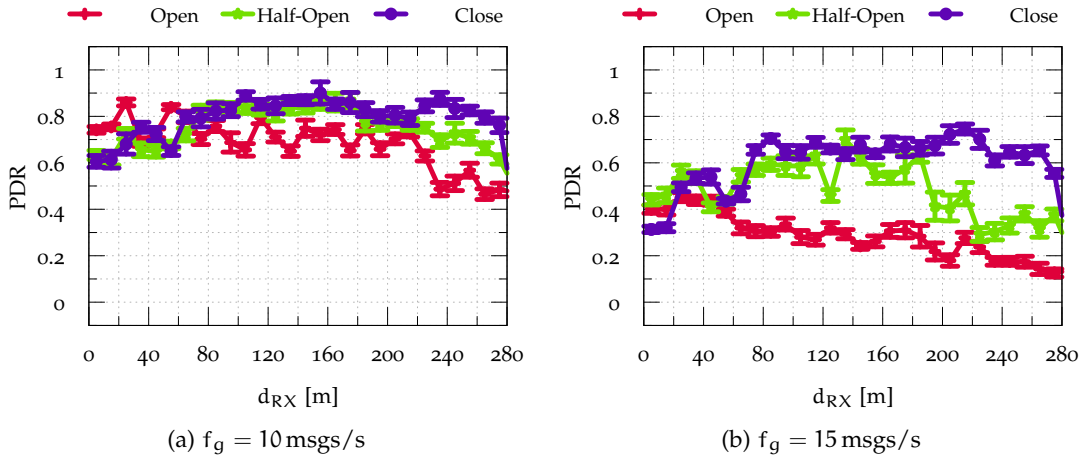(a) $f_g = 10\,\text{msgs/s}$ (b) $f_g = 15\,\text{msgs/s}$

Figure 60: Average PDR as function of the distance d_{RX} of the receiver relative to the intersection center under varying intersection types and when a transmitter is stationed at $d_{TX} = 15\,\text{m}$. Penetration rate $p = 10\,\%$ and transmission power = $P_t = 23\,\text{dBm}$.

on opposite road segments. This implies that both nodes are in perfect LOS situations. As a consequence, we expect that obtained results would be independent of the considered intersection type.

(a) *Open*   (b) *Half-open*   (c) *Close*

Figure 61: Transmitter and receiver on the same road segment: Average PDR as function of d_{RX} and d_{TX} distances. Comparison of the results obtained under different intersection types with $f_g = 10\,\text{msgs/s}$, $p = 10\,\%$ and transmission power = $P_t = 23\,\text{dBm}$.

Same Road Segment

The *same road segment* constellation refers to vehicles which are considered in LOS and traveling on the same street independently of their driving direction. This implies that the maximum distance between these nodes is equal the length of the road segment connected by a crossroad. Furthermore, the diagonal of Figures 61 highlights the proximity between transmitter and receiver, e. g., when $d_{TX} \approx d_{RX}$. We observe in general from this figure that when both transmitter and receiver are near to each other, almost all packets are successfully received. This is particularly valid for the *Open* type represented by the diagonal on the Figure 61a even around

intersection center for d_{TX}, $d_{RX} \leqslant 75\,\text{m}$, respectively. However, under the *Open* as well as the *Close* type, higher PDRs are observed, particularly when the receiver is between $75\,\text{m} \leqslant d_{RX} \leqslant 280\,\text{m}$ independently of the position of the transmitter. This can be explained by the fact that receivers located in this area are protected from interference generated by surrounding nodes. In fact, buildings around the intersection limit interfering signal power and ensure a better SINR at the receiver. However, a deeper investigation will be performed in section 7.5.2. Based on these results, we can conclude that safety-based applications such as lane assistant or lateral collision avoidance which assume an almost perfect communication performance, would perform very well, particularly already at stable traffic conditions.

Opposite Road Segment

The *opposite road segment* constellation refers to vehicles which are considered in LOS and traveling on opposite streets connecting the junction independently of their driving direction. This implies that the maximum distance between these nodes is two times equal the length of the road segment connected by a crossroad. Similar to the *same road segment* constellation, results in Figure 62 show that the *Close* type performs better. Again, we observe a *guard region* due to the reduction of interference level, e. g. at $75\,\text{m} \leqslant d_{RX} \leqslant 280\,\text{m}$. This outlines once more the positive impact of buildings on the communication performance. However, worse results obtained when transmitter and receiver are located on opposite segments compared to the *same road segment*, are not really surprising since nodes are located far away so that the path loss component due to the separation between both considered nodes considerably increase and thus is not more negligible.
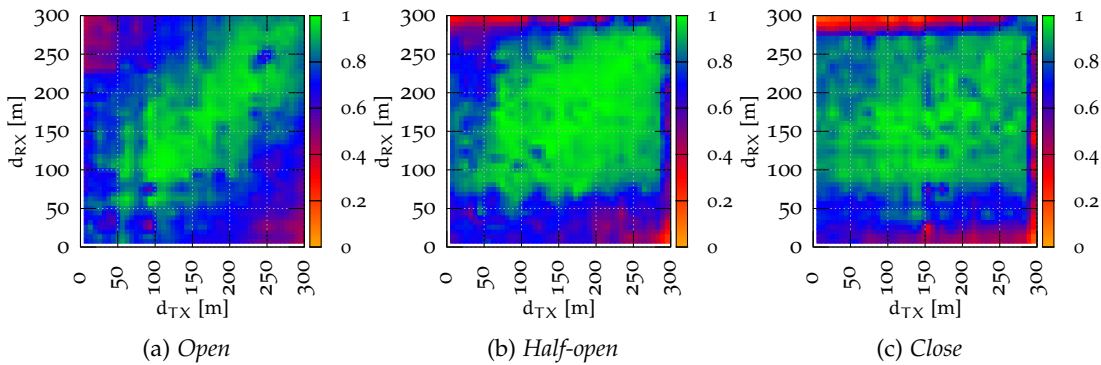

(a) *Open*   (b) *Half-open*   (c) *Close*
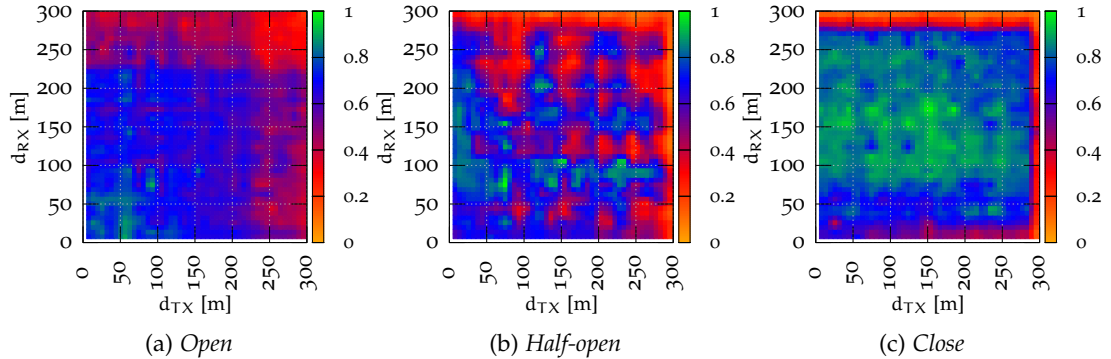
Figure 62: Transmitter and receiver on a opposite road segments: Average PDR as function of d_{RX} and d_{TX} distances. Comparison of the results obtained under different intersection types with $f_g = 10\,\text{msgs/s}$, $p = 10\,\%$ and transmission power = $P_t = 23\,\text{dBm}$.

7.5.2   *Analysis of Communication Parameters*

Communication parameters including transmission power, message generation rate or data rate are controllable that could negatively or positively influence the communication performance. However, the evaluation of the impact of these parameters is of particular importance. For example, while increasing the transmission power in low traffic densities will results in a better reachability of nodes,

in high traffic flow conditions, this will lead to a degradation of the performance due to high channel congestion reflected by packet collisions. In this context, in order to gain insight into their influence, we evaluate and capture in this section the impact of transmission power, message generation rate. Moreover, we consider in the evaluation also the influence of varying intersection topologies as the heterogeneity of network topologies remains one of the main challenges of VANETs, in particular at urban environments.

Impact of Transmission Power

In interference-free situations, the transmission power is of particular importance in order to increase the communication range. But under the presence of interference, increasing the transmission power leads to an augmentation of packet drops and packet collisions due to a larger number of neighbor nodes, which compete for the channel resulting in an increase of the interference level. As can be seen in Figure 63, the PDR decreases as the transmission power increases in particular for the *Open* intersection type. In opposition to the *Open* type, we observe in the *Close* type a slight increase of the PDR in the so-called *guard region* at $75\,\text{m} \leqslant d_{RX} \leqslant 280\,\text{m}$. This is due to the fact that increasing the sensing range will lead to a reduction of the potential hidden nodes. Detailed reasons for the appearance of a *guard region* are provided in Section 7.5.4.

(a) P_t=13 dBm, *Open*, $p = 10\,\%$ (b) P_t=13 dBm, *Close*, $p = 10\,\%$ (c) P_t=13 dBm, *Close*, $p = 25\,\%$

(d) P_t=23 dBm, *Open*, $p = 10\,\%$ (e) P_t=23 dBm, *Close*, $p = 10\,\%$ (f) P_t=23 dBm, *Close*, $p = 25\,\%$

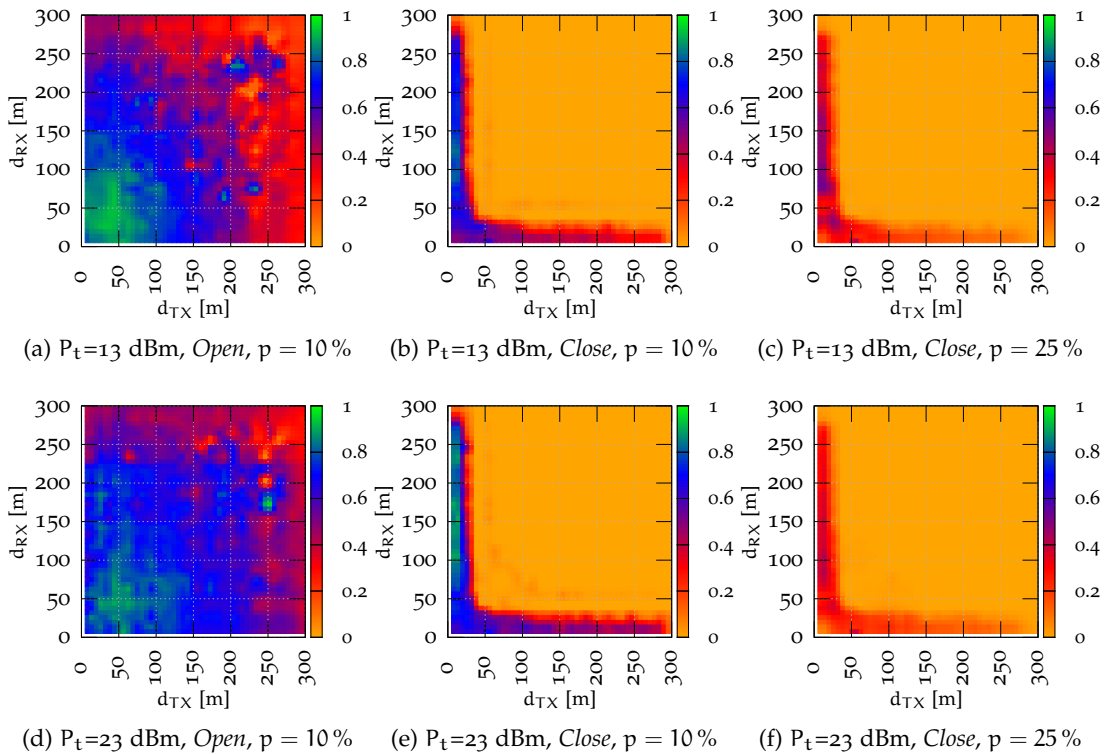Figure 63: Impact of transmission power: Average PDR as function of d_{RX} and d_{TX} distances. Comparison of the results obtained under different transmission power and penetration rates for the *Open* and *Close* intersection type and with $f_g = 10\,\text{msgs/s}$.

Regarding the impact of transmission power on the CBT, we plot in Figure 64 a 2D representation of the average CBT measured at each target vehicle during the

whole simulation duration. There, the aggregated CBT is represented as a function of the absolute position of target nodes distributed over the simulation area (1200 m × 1200 m). Different transmission power values and penetration rates were investigated in order to capture their impact. As already mentioned, the CBT is defined as the fraction of a set period of time that a channel is busy. A channel is reported as busy if the measured signal power is above the carrier sense threshold $P_{r,cs}$ even if no packet is currently received. As a consequence, the transmission power will strongly influence the communication range, and thus impacts the measured CBT. Intuitively, one can argue that the higher the communication range, the higher the signal strength measured at a given node. This leads to an increase of the channel occupancy produced by the exchange of packets between nodes.
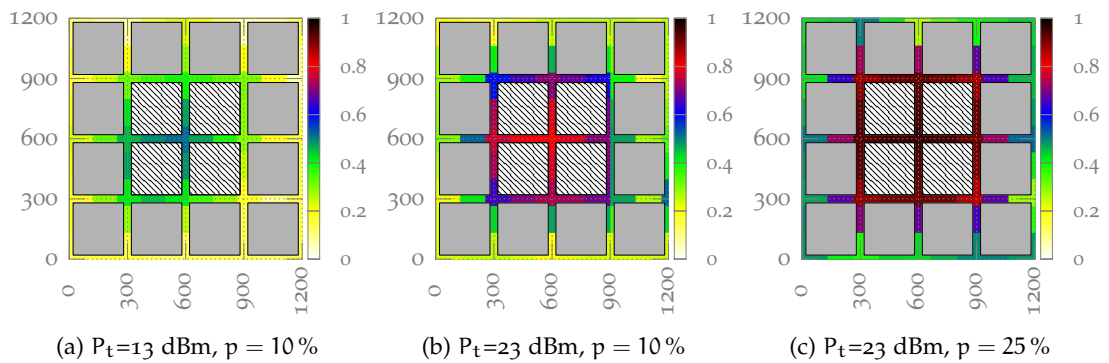

(a) P_t=13 dBm, $p = 10\,\%$ (b) P_t=23 dBm, $p = 10\,\%$ (c) P_t=23 dBm, $p = 25\,\%$

Figure 64: Channel busy time (CBT) for the *Open* intersection type and $P_t = 23\,\text{dBm}$ and with $f_g = 10\,\text{msgs/s}$.

Precisely interesting is the CBT, which already reaches $55 - 62\,\%$ under normal traffic conditions (low penetration rate and transmission power) measured by nodes located in the RoI as shown in Figure 64a. In this case, the DCC algorithm declares the network status to be *restrictive* as the achieved CBT is above $50\,\%$ [149].

By comparing Figures 64b and 64c, we see that once the vehicle density increases, the performance rapidly drops as the CBT increases from almost $80\,\%$ up to $97\,\%$ in the RoI. In other words, more than $80\,\%$ of the time, the channel is observed to be busy leading consequently to a strong increase of packet collisions up to approx. $90\,\%$, and hence, to an unacceptable communication performance (see Figure 63f).

Furthermore, we observe that increasing the transmission power leads to improved packet reception rates in further distances. However, this behavior is verified only under low traffic density, and the situation is completely reversed when the density of vehicles increases. This statement is true for all types of intersections. In a nutshell, increasing transmission power does not necessary lead to a better communication performance.

Impact of Message Generation Rate

Similar to the transmission power, the message generation rate is a crucial parameter that could considerably affect the network condition and thus the performance of V2X applications. The timely delivery of CAMs is a basis requirement for an efficient operation of safety-based applications. To be able to track vehicles in a neighborhood, and therefore to detect potentially dangerous situations for the

driver (e. g., forward collision), received CAMs should be fresh and actual. Under low penetration rate, disseminating at higher message generation rate provides an accurate delivery of vehicle tracking information. However, under high traffic density, this leads to a higher probability of packet collisions, which in turn results in long delays or message age between packets. Ensuring that enough information from each node reached its direct neighbors is the main challenge of VANET. As a consequence, choosing an adequate message generation rate value is of most importance in the design of V2V applications. Motivated by aforementioned reasons, we investigate in following the impact of the message generation rate on the communication performance.

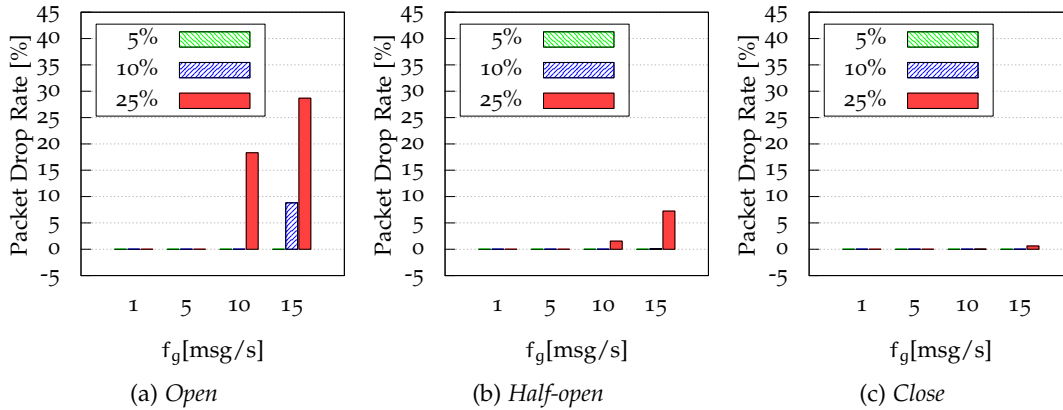(a) *Open*   (b) *Half-open*   (c) *Close*

Figure 65: Packet drop rate for all vehicles against the packet generation rate for the *Close*, *Half-open* and *Open* intersection type and $P_t = 23\,dBm$.

Figure 65 presents the ratio of packet drop obtained with a fixed transmission power of $P_t = 23\,dBm$ while varying the penetration rate, the intersection topology, and the message generation from $1\,msg/s$ to $15\,msgs/s$. Obviously, the fraction of dropped packets increases as the traffic intensity in term of message generation rate increases. However, this behavior is more pronounced when we consider the *Open* intersection type. We observe that the network experiences almost 25 % fewer packet drops in the *Open* type than in the *Close* type (see Figures 65a and 65c). A really interesting finding is the positive effect of surrounding buildings which somewhat limits interference power and thus relaxes the channel load. This aspect is confirmed by the achieved CBT in Figure 66, which results apart from the transmission power also from the message generation rate. However, the influence of message generation rate on the CBT is less pronounced. At higher message generation rate, the channel load remains low below 60 % implying a relatively good communication performance reflected by almost no packet drops.

Regarding the impact of intersection types on the CBT, we observe when comparing Figures 64b and 66b, that the presence of buildings around the intersection provides as expected a positive impact by halving the CBT from 80 % to 40 %.
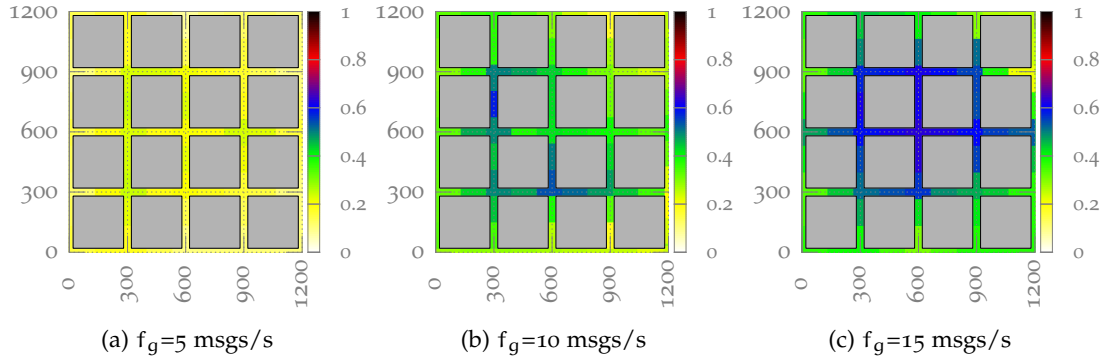
(a) f_g=5 msgs/s   (b) f_g=10 msgs/s   (c) f_g=15 msgs/s

Figure 66: CBT for the *Close* intersection type with $P = 10\%$, $P_t = 23\,\text{dBm}$ and different f_g.

7.5.3 *Packet Delays in VANETs*

In VANET, due to stringent application requirements, knowledge about the latency of received messages is a crucial task in the performance evaluation of V2V communication. It is precisely because VANET has to cope with a lot of challenges including the rapidly changing network topology which is subject to frequent packet losses and lack of connectivity redundancy. Basically, we distinguish many types of delay or latency depending on the scenario and use case. For Georouting applications, each message travels between source and destination through intermediate nodes and communication links. As a message travels from one node to the subsequent node along the path, it will suffer from several type of delays. All these delays together accumulate to give the total end-to-end delay. This metric is sufficient to investigate the efficiency of the routing approach. However, for broadcast-based networks such as VANET, the end-to-end alone would be inadequate according to the single hop message dissemination. Therefore, we evaluate besides the classical end-to-end delay also the message age as defined in section 7.4. Considering that cooperative awareness is achieved through reliable exchange of messages among vehicles, a situation awareness can be impaired when packet losses occur in batch, even when the PDR is relatively high [145]. This aspect is also examined in the following evaluation.

End-to-end Delay D_{E2E}

The end-to-end delay is composed mainly of the channel access time D_{CAT} due to back off process plus the transmission delay also known as *air time* of the packet D_{air}. An illustration is provided in Figure 56. Due to the coordination of channel access mechanism between nodes, a sending node has to wait a random number of idle slots which can be approximated by the duration $D_{CAT} = D_{AIFS} + \frac{CW}{2} \cdot T_{Slot}$. The *air time* depends on the preamble duration D_{pre}, the packet size L and the data rate R_b and is given by $D_{air} = D_{pre} + \frac{L}{R_b}$.

We can then simply deduced the average end-to-end delay of a packet by

$$D_{E2E} = D_{CAT} + D_{air} \tag{29}$$

$$= D_{AIFS} + \frac{CW}{2} \cdot T_{Slot} + D_{pre} + \frac{L}{R_b} \tag{30}$$

$$= SIFS + AIFSN[0] \cdot T_{Slot} + \frac{CW}{2} \cdot T_{Slot} + D_{pre} + \frac{L}{R_b} \tag{31}$$

Considering $SIFS = 32\,\mu s$, $AIFSN[0] = 9$, $T_{Slot} = 13\,\mu s$, $CW = 31$, $D_{pre} = 40\,\mu s$, $L = 1000\,Bytes$, and $R_b = 6\,Mbps$, we get the average end-to-end delay as

$$D_{E2E} = 1.7\,ms \tag{32}$$

This calculated value is valid only under interference-free situations and could represent the lower bound of D_{E2E}. Since a node experiencing a busy channel will freeze his backoff counter and defer the transmission until the channel becomes idle again. In other words, in real traffic situations considering other contending nodes, the end-to-end delay would be longer that the one obtained in Equation 32 by reason of the additional time elapsed during the busy period. However, it is analytically hard to predict the length of such busy periods since it depends on the number of concurrent transmissions heard at a given node. Moreover, the number of hidden nodes shall be also considered which is also difficult to capture mathematically.
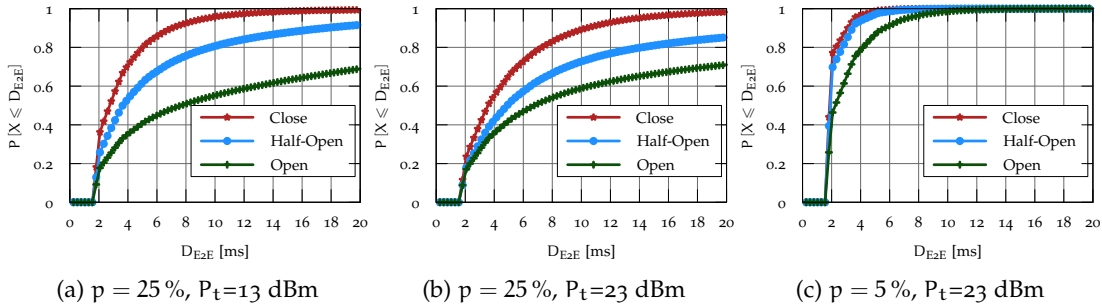

(a) p = 25 %, P_t=13 dBm   (b) p = 25 %, P_t=23 dBm   (c) p = 5 %, P_t=23 dBm

Figure 67: CDF of the end-to-end delay for the *Close*, *Half-open* and *Open* intersection type with $f_g = 10\,msgs/s$.

Figure 67 presents the cumulative distribution of D_{E2E} obtained with a fixed packet generation rate $f_g = 10\,msgs/s$ while varying the penetration rate, the intersection type, and the transmission power. In general, we can observe that D_{E2E} is lower bounded by 1.7 ms irrespective of the configurations. This is - as expected - in line with the value theoretically determined in Equation 32 and also independently found in [150]. Moreover for highly saturated channel (Figure 67a and 67b), the *Open* intersection type experiences significantly larger end-to-end delay values due to longer channel access time and busy periods. For example in Figure 67a, while almost 95% of end-to-end delay values are lower than 8 ms for the *Close*, only 50% are below 8 ms when simulating with *Open* intersection type. On the other hand, under low channel load in Figure 67c, all intersection types experience almost the same end-to-end delay distribution. We remark also that the transmis-

sion power has a slight influence on the obtained end-to-end delay in particular under high channel load. However, we can conclude from the obtained results that the end-to-end delay remains considerably low and is therefore not of greater influence in the performance of V2V. Moreover, these results are in good accordance with those reported in [143] and analytically determined in [151].

It should be said that the end-to-end delay could only be determined when a packet is correctly received. Additional delays caused for example by packet loss would then be hard to capture when investigating message latencies in VANETs. For this reason, we then introduce the message age which includes apart from the end-to-end delay also the additional delay due to packet losses.

Message Age D_{MA}

The message age can be also represented as the lifetime of an information which provides knowledge about the real age of received data. To illustrate how message age is determined, let us consider Figure 68 illustrating a sequence of arriving packets at a receiver. After message dissemination, a receiving node would experience a message age $D_{MA} = (n + 1) \times T_g$, where n represents the number of consecutive lost packets and $T_g = \frac{1}{f_g}$ the message generation period. In ideal conditions characterized by no packet collisions or packet drops implying $n = 0$, the message age could be approximated to T_g. Whereas, in high saturated channel conditions implying several consecutive packets lost, n goes toward infinity resulting in a longer message age.
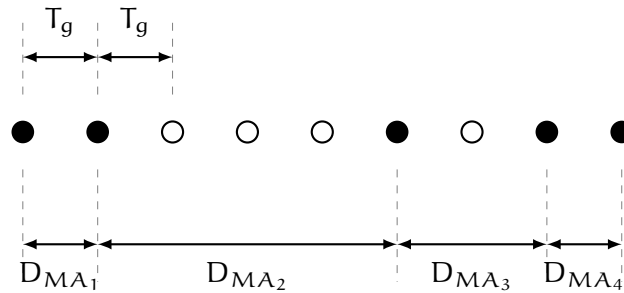

Figure 68: Schematic diagram illustrating the relationship between the message age and the message generation period T_g. Full and empty circles represent received and lost packets, respectively.

Figure 69 presents the cumulative distribution of D_{MA} obtained with a fixed penetration rate $p = 25\%$ while varying the message generation rate, the intersection type, and the distance d_{RX} of the receiver relative to the intersection center. We observe in general that the *Close* type experiences a better message age distribution compared to the *Open* type, irrespective of the location of the receiver and the configured message generation rate. This is mainly due to the large amount of packet drops in high channel load as illustrated in Section 7.4. Apart at a close distance ($d_{RX} = 12\,\text{m}$), 80% of message age samples are lower than 500 ms for the *Close* intersection. More interesting, when considering intersection types, obtained message age values collected at the *Open* intersection are independent of the position of the receiver. All receiver position variations provide almost the same distribution (see Figures 69a, 69b and 69c). However, for the *Close* intersection type in Figures 69d, 69e and 69f, the receiver experiences lower message age values in

further distance than at a close distance. We attribute this behavior to the *guard region* that protect the receiver against interference power and thus diminish the probability of packet collision in this region.

(a) d_{RX}=12 m, *Open*

(b) d_{RX}=35 m, *Open*

(c) d_{RX}=65 m, *Open*

(d) d_{RX}=12 m, *Close*

(e) d_{RX}=35 m, *Close*
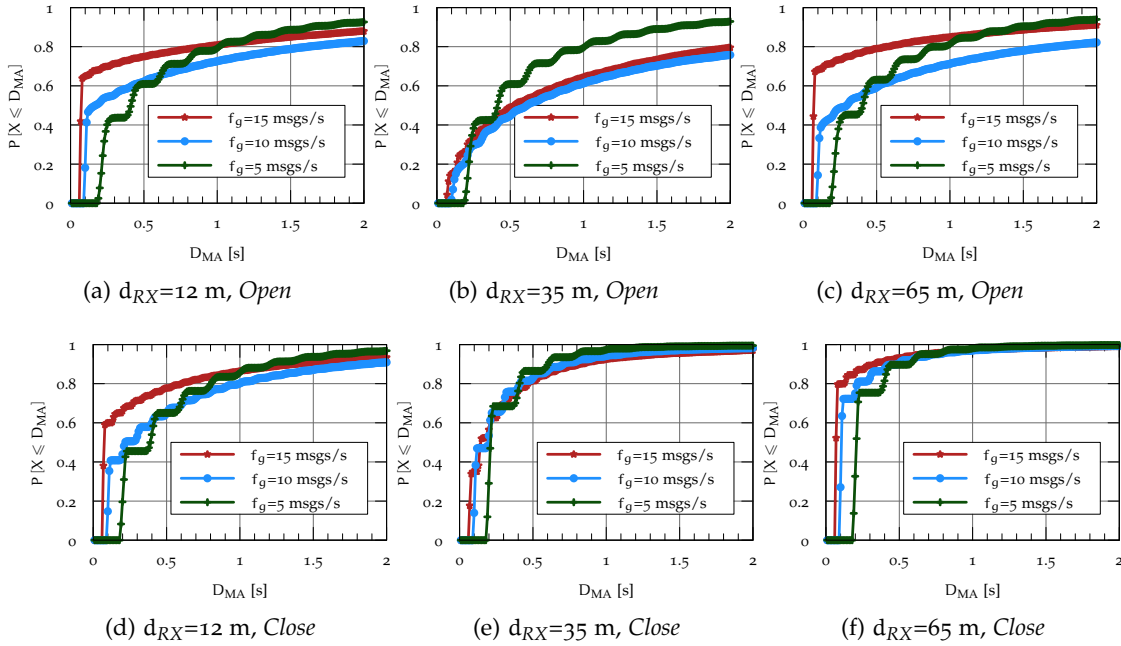
(f) d_{RX}=65 m, *Close*

Figure 69: CDF of the message age D_{MA} for different locations of the receiver to intersection center for the *Close* and *Open* intersection type with $p = 25\,\%$ and $P_t = 23\,\mathrm{dBm}$.

When considering message generation rates, there are not noticeable influence on the message age distribution through sending at higher rates. Consecutive packet losses under higher message generation rate will probably lead to similar message generation periods while transmitting at a lower rate.

To examine the relationship between packet generation rate and the message age, we show in Figure 70 the Probability Density Function (PDF) of the message age while varying message generation rates and intersection types. We observe that the message age is clearly multiple of the message generation period T_g. Considering, for example, $f_g = 5\,\mathrm{msgs/s}$, we observe clusters at every $T_g = 0.2\,\mathrm{s}$ equivalent to $\frac{1}{5}$. This behavior is also the reason of the stair course of the CDF observed in Figure 69, which confirmed the discrete value of the configured message generation period.

A more interesting observation is the distribution of consecutive packet losses. It describes whether packet loss in V2V networks occurs in burst or not. We realize that the majority of packet losses are either single or double-packet loss. This is shown by shorter and thinner peaks of the distribution of message age at 0.13 s and 0.2 s for $f_g = 15\,\mathrm{msgs/s}$, 0.2 s and 0.3 s for $f_g = 10\,\mathrm{msgs/s}$, and 0.4 s and 0.8 s for $f_g = 5\,\mathrm{msgs/s}$. By examining and comparing Figure 70a and 70b, we believe that the aforementioned observations are valid for both intersection types, although the *Close* intersection type experiences a better distribution reflected by lower message age values.

In summary, we find that under *Close* intersection type, packets received by vehicles would experience a lower message age than under an *Open* intersection. Moreover, under high vehicle densities in both intersection types, a vehicle can
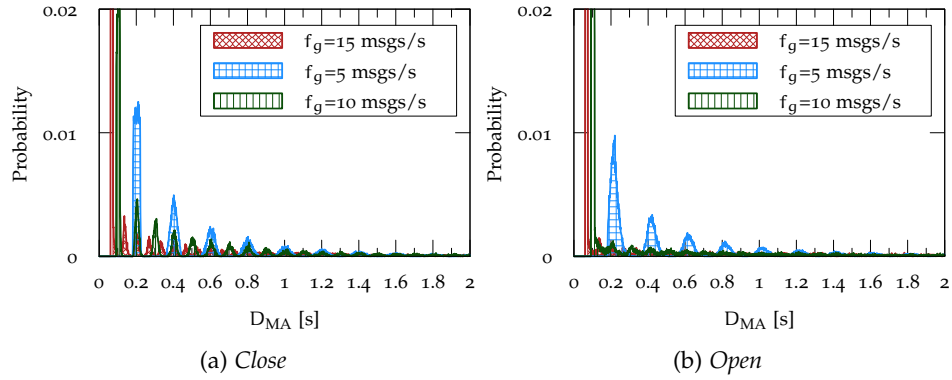
(a) *Close*   (b) *Open*

Figure 70: PDF of the message age D_{MA} with the receiver located at $d_{RX} = 12\,\text{m}$ to intersection center for the *Close* and *Open* intersection type. Simulated with $p = 25\,\%$ and $P_t = 23\,\text{dBm}$.

miss several successive CAMs, especially for which located near the intersection's center. In other words, packet losses seem to be environment-independent.

7.5.4 *Classification of Packet Collisions*

To classify packet collisions, knowledge about the source of interference is indispensable since packets collide mainly when the density of the interference signal is stronger than the wanted signal at the receiver. In this section, we investigate packet collision types according to the source of interference with respect to intersection types and transmission power values.

Source of Interference

To understand the source of interference in VANET, the SINR is an important term which expresses the overall ratio of the wanted signal to any other unwanted power at the receiver side and can be expressed as

$$SINR_i = \frac{P_{ri}}{N + \sum P_{Ii}} \tag{33}$$

P_{ri} is the signal power of the wanted signal at the receiver i. In fact, due to signal fading, P_{ri} may fluctuate and vary over time. For the sake of simplicity, we assume stationary conditions and do not consider therefore the time dependency. N represents the thermal noise and can be calculated as $N = k_B \cdot T \cdot B$, where k_B denotes Boltzmann's constant, T the temperature and B the Bandwidth. It is constantly present at each wireless receiver and does not depend on the existence of other potential transmissions. In the interference-free condition considering only a single transmitter and a single receiver with no other transmission at the same time implying that $\sum P_{Ii} = 0$, the SINR equals the Signal-to-Noise Ratio (SNR) and is expressed as

$$SNR_i = \frac{P_{ri}}{N} \tag{34}$$

This means that the thermal noise is the lower boundary that limits transmission range and should be therefore taken into account for a realistic performance evalu-

ation. A packet can be successfully received if the power level of the wanted signal is several degrees higher than the sum of interfering signals at the same time. Since the medium is shared between nodes in the vicinity, the probability of simultaneous radio transmissions is higher to occur. When this happens, all of the nodes receive multiple frames at the same time. This might result in a collision of the transmitted frame at all of the receivers.

While a measurement-based characterization of packet collisions is hard to realize using an off-the shelf wireless card, a simulative evaluation of VANET allows a comfortable packet collision analysis by separating and classifying the source of interference during each frame reception. Hence the total sum as well as the type of interference collecting at each receiver can be precisely determined.

Cause of Packet collisions

As already mentioned, V2V communication relies on a multiple access protocol such as CSMA/CA in order to coordinate the access of multiple sending and receiving nodes in a common shared channel. Typically, packet collisions in vehicular networks occur when two nodes located in the same carrier sense range transmit at the same time. Moreover, the inevitable and negative effect of hidden nodes - which are out of range of the considered transmitter - could also lead to packet collisions and hence to packet loss at the receiving node. In fact, due to the broadcast nature of V2V communication, the hidden node problem remains unsolved due to the missing of the RTS/CTS mechanism. There is a variety of reasons why a frame may not reach its destination node. Depending on the factor which caused the collision, we classify and distinguish the packet collision occurring in VANET as belonging to one of two main categories: CSMA and hidden node collision. We'll cover these categories of packet collisions in the following two sections.

Packet Collisions through CSMA-CA

Although the CSMA/CA protocol regulates packet transmissions into the shared broadcast channel between nodes, there might be situations where packet collisions will still occur. In fact, there are several reasons inducing this kind of collision but for the sake of clarity, we assume that packet collisions might occur due to CSMA when:

- Two or more stations choose the same random backoff after sensing the channel as idle.

- Two or more stations choose different random backoff but their counter value reached zeros at the same.

It is then obvious that if many nodes want to transmit frequently, many transmissions will result in collisions. Clearly, the probability of packet reception or the PDR depends on the locally generated channel load which is directly linked to the penetration rate (number of nodes) as well as the packet generation rate. Moreover, the number of nodes within a common communication range will in turn depend on the transmission power. At higher transmission power, nodes may have a large number of direct neighbors so that the frequency of accessing the channel will increase as well. This implies a high number of packet collisions. For the sake of simplicity, we denoted packet collisions due to the CSMA channel access protocol simply *CSMA Collision*. We defined the CSMA Collision Rate (CCR) as the ratio of

the number of packets collided due to *CSMA Collision* to the number of packets transmitted by a tagged node.

(a) P_t=13 dBm, *Close*

(b) P_t=23 dBm, *Close*

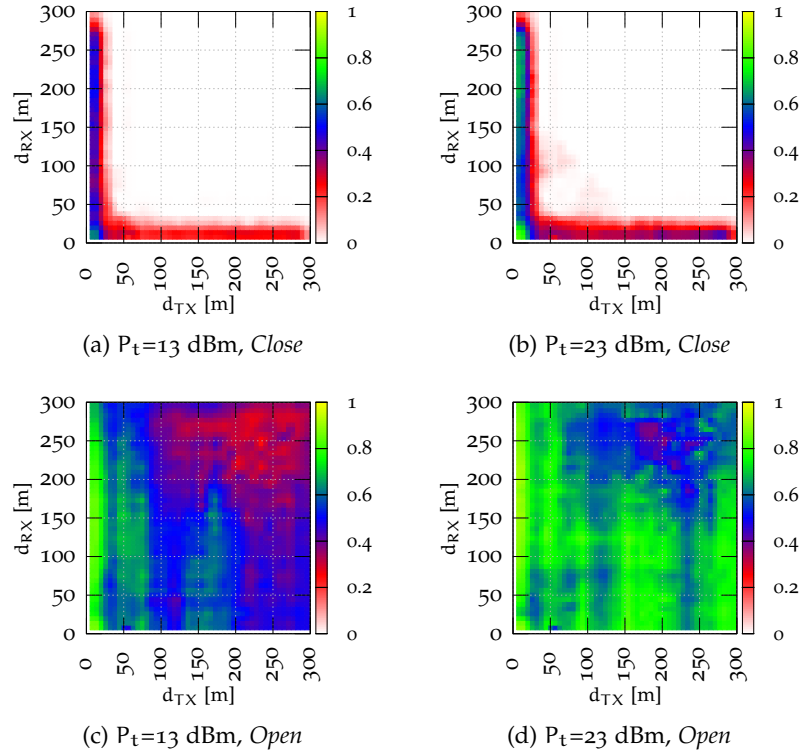(c) P_t=13 dBm, *Open*

(d) P_t=23 dBm, *Open*

Figure 71: Average CSMA Collision Rate (CCR) as function of d_{TX} and d_{RX} distances. Impact of transmission power for the *Open* and *Close* intersection type by using a message generation rate $f_g = 10$ msgs/s and a penetration rate of $p = 25\%$.

To evaluate the impact of transmission power, Figure 71 presents the CCR obtained with a fixed message generation rate $f_g = 10$ msgs/s and a penetration rate of $p = 25\%$ while increasing the transmission power from 13 dBm to 23 dBm. The effect of the intersection topology is also investigated by simulating scenarios with the *Open* and the *Close* intersection type. As expected we observe that increasing the transmission power results to an increase of CCR. This is valid for the *Open* as well as for the *Close* intersection type. However, for the *Open*, this observation is more pronounced due to a large among of contending nodes present within the transmission range. In other words, while increasing the transmission power augment the probability of reaching nodes at a further distance, this will therefore result in a rise of *CSMA Collisions* due to the large number of nodes sharing the channel. The positive effect of intersection topology on the CCR can be also highlighted in Figure 71 due to the presence of buildings which provided a robustness by limiting the amount of additional nodes contending for the channel. One interesting but easily explained behavior is the higher packet collision immediately at the intersection center, this is due to the fact that nodes located in this region *hear* from all other nodes moving along the road segments that join the intersections and, therefore, suffer from high level of interference. Therefore, also as concluded by [152], [153] and [154], to achieve low packet collisions in highly saturated channel load at higher penetration rates, low transmission power values shall be preferred to higher.

Packet Collisions through Hidden Node Effect

Due to the broadcast nature of single-hop communication in VANET, the hidden node problem caused by the missing RTS/CTS strategy poses a challenging issue for the performance of the vehicular communication. This problem occurs when packets disseminated by one or more sending nodes which are located within different communication ranges, collided at a specific common receiving node. To investigate the severity of packet collisions through the hidden node effect, we defined the Hidden Collision Rate (HCR) as the ratio of the number of packets collided due to the hidden node effect to the number of packets transmitted by a tagged node. For reasons of simplicity, *hidden node collision* refers, in this section, to packet collisions through the hidden node effect. We start the analysis by investigating the impact of the transmission power on *hidden node collisions*. Figure 72 presents the HCR obtained with the same parameters as Figure 71, while increasing the transmission power from 13 dBm to 23 dBm. As first finding, we observe that in contrast to the CSMA Collision Rate (CCR), the amount of *hidden node collisions* is likely to decrease by the increase of the transmission power. This relationship can be explained with a reduction of the potential area of hidden nodes. Secondly by looking at intersection types, the *Close* type tends to experience a slightly higher influence of *hidden node collisions* than the *Open* when the receiver is located at $d_{RX} \leqslant 30$ m. Reasons behind this asymmetric behavior are subject to further investigations in the next section.

(a) P_t=13 dBm, *Close*

(b) P_t=23 dBm, *Close*

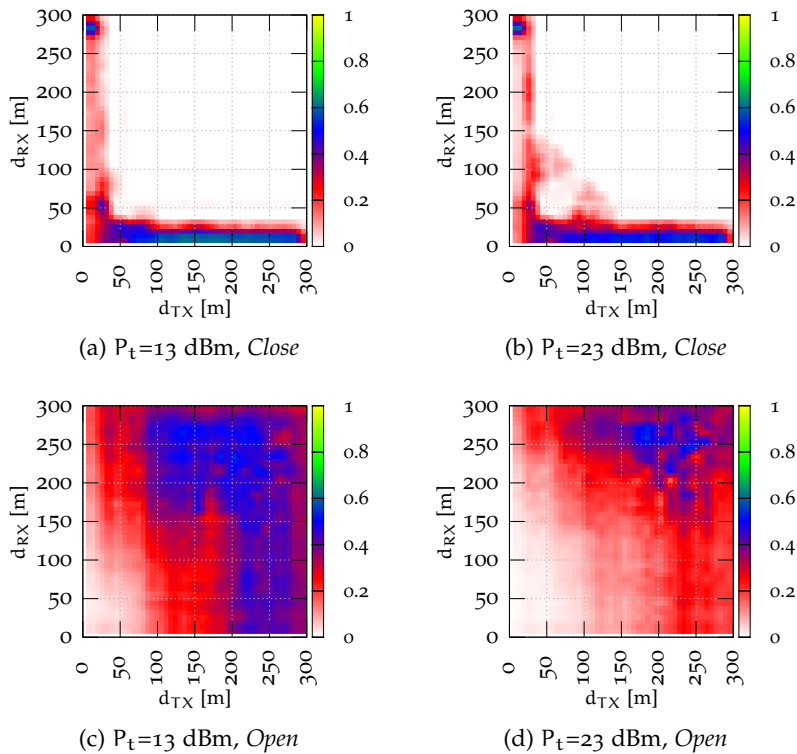(c) P_t=13 dBm, *Open*

(d) P_t=23 dBm, *Open*

Figure 72: Average Hidden Collision Rate (HCR) as function of d_{TX} and d_{RX} distances. Impact of transmission power for the *Open* and *Close* intersection type by using a message generation rate $f_g = 10$ msgs/s and a penetration rate of $p = 25\%$.

As final comment on the classification of packet collisions, it should be said that the transmission power has an influence on both types of collision. However, in particular when considering urban intersections, packet collisions due to CSMA/CA are more severe in comparison to collisions due to the hidden node problem and should, therefore, be an important factor to consider when designing efficient congestion control algorithms. The same trend was also observed in [155], where the authors investigated the impact of hidden nodes in a broadcast scenario and concluded that the hidden node problem is not a major limiting factor in VANETs. However, it should be mentioned that the investigation in this study was performed on a highway scenario which assumes a nearly one-dimensional network topology and thus a less probability of appearance of hidden nodes. To summarize the cause of packet collision, we identify the transmission power and the intersection type as important communication and environmental factors in determining the performance of V2V communication.

7.5.5   *Asymmetry Phenomenon under the* Close *intersection type*

All PDR results obtained under the *Close* intersection type show an interesting asymmetric phenomenon, regardless of the configured simulation and communication parameters. One might expect that the achievable PDR produces almost same results in both communication links e. g. A→B and B→A. This might be valid as we assume in the evaluation that intersection types are homogeneous implying that buildings around the intersection have regular shapes. Moreover, the integrated path loss model for NLOS situations solely depends on the distance d_{TX} of the transmitter and the distance d_{RX} of the receiver to the intersection center and not on the transmitter/constellation. As a consequence, the average received signal power should lead to the same value in both directions. This implies that $PL_{NLOS}(d_{TX}, d_{RX}) = PL_{NLOS}(d_{RX}, d_{TX})$ according to Equation 24. However, the determination of the PDR depends also on the accumulated interference power due mostly to hidden nodes. This motivates the present investigation which provides a comprehensive analysis of the cause and source of asymmetry on obtained PDR results. We, therefore, examine the severity of interference in term of number of potential interferers around the intersection.

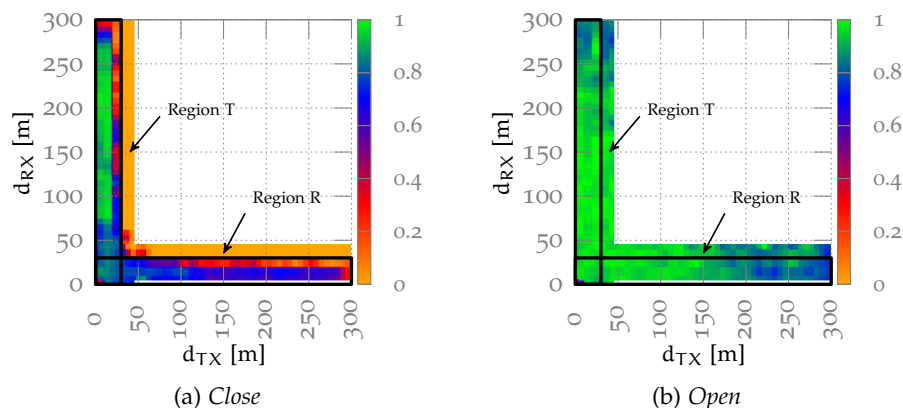(a) *Close*   (b) *Open*

Figure 73: Average PDR as function of d_{RX} and d_{TX} distances illustrating the asymmetry due to transmitter/receiver constellation for the *Close* and *Open* intersection types.

Let us consider the Figure 73 which shows the average PDR as function of d_{RX} and d_{TX} distances for the *Close* and *Open* intersection types. This result is obtained under a penetration rate of $p = 5\%$, a message generation rate of $f_g = 10\,\text{msgs/s}$ and a transmission power $P_t = 23\,\text{dBm}$. We see evidence of two asymmetric regions with respect to receiver and transmitter to the intersection center in the *Close* type. In region T and R, transmitters and receivers are close to the intersection's center, respectively. We remark in particular for the *Close* type that the region T provides better communication performance. To understand this effect, let us consider the scenarios illustrating two use cases or regions as depicted in Figure 74. In this example, HN represents a set of hidden nodes to nodes RX able to interfere with the transmission of TX. Other blue cars are nodes located within a common sensing range than the TX.

To understand the achieved PDR at the region T, let us now take a closer look by considering an illustration in Figure 74a. In this scenario receivers located in region T, fortunately, suffer from interference generated only by a small number of hidden nodes. However, the number of potential hidden nodes will increase while they are moving towards the intersection. This is validated by a decrease of the PDR when $d_{RX} \leqslant 75\,\text{m}$ as depicted in Figure 73a. As a consequence, we can conclude that within the *guard-region*, receivers are protected by buildings from interference power generated by surrounding hidden nodes. In other words, when the transmitter is closer to the intersection, the probability of packet collisions increased as the receiver moves towards the intersection because the number of potential hidden nodes will increases.
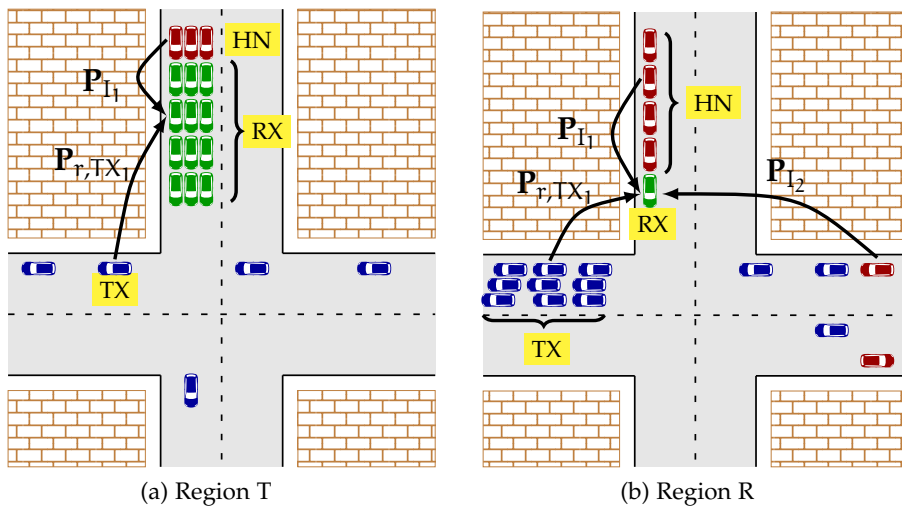

(a) Region T   (b) Region R

Figure 74: Scenario illustrating the asymmetry phenomena of the PDR due to transmitter/receiver constellation in the *Close* intersection type.

As can be seen in Figure 74b for results obtained in region R, hidden nodes appear much closer to a transmitter than typically expected in highway scenarios assuming perfect LOS between nodes. This implies a lower SINR measured at the RX, which is strongly influenced by the interference power P_{I_1} generated by the closest hidden node. This is due to the fact that the received signal from transmitter P_{r,TX_1} is significantly attenuated by the obstructing building. In this case, the obstruction of building may prevent a hidden node HN and TX from hearing each

other transmissions, even though HN and TX transmissions are indeed interfering at RX. This negative effect of the building is clearly observed when comparing results obtained with (Figure 73a) and without (Figure 73b) building's shadowing. Moreover, we observe also a high probability of appearance of hidden nodes (P_{I_2}), in particular when the transmitter is far away from the intersection resulting in a decrease of the PDR. However, it should be said that through the CSMA/CA technique, only a portion of potential hidden nodes, which are in a common sensing range will effectively attend the channel and the rest will be neutralized.

7.6 SUMMARY

In this chapter, we evaluated the performance of V2V communication at urban intersections by analyzing the impact of environment factors such intersection types and penetration rates as well as the influence of communication parameters. Since the evaluation has been performed by means of simulation, we therefore firstly presented a hybrid simulation platform composed of a network simulator and a road traffic simulator. Hereby, to ensure applicability of simulation results, an ITS-G5 conform protocol stack from the application layer up to the physical layer is scrupulously modeled under the simulation tool OMNeT++. Since propagation models may directly affect the level of accuracy in simulation-based performance evaluations, we proposed a dedicated urban propagation model based on measurements designed to reflect radio propagation on urban environments in a realistic way. After a careful selection of representative scenarios, we performed a simulation campaign under variation of environment factors and communication parameters. We particularly concentrated on the scalability issue and the influence of intersection type on the communication performance.

Regarding the penetration rate, results revealed that the traffic density might impact the communication reliability, regardless of the type of intersection. It has been shown that the probability of packet collisions increases as the number of transmitting nodes located in a common transmission range increases. Answering the question of the impact of intersection type, we showed that open intersections from Type 0 provide in general the best performance compared to Type 2 and 4. However, under high traffic densities, Type 4 outperforms Type 0 by providing *guard regions*, where the nodes are protected from interference generated by surrounding nodes. To gain insight into the transmitter/receiver constellation, results showed that depending on the location of the receiver relative to the intersection center, the performance of the communication would be impacted by the type of intersection.

As communication parameters are controllable factors, we investigated the influence of transmission power and message generation rate with respect to intersection type. While in interference-free situations, increasing the transmission power leads to an increase of the communication range, we found out that in high traffic densities, this will result in a degradation of communication performance due to an increase of interference, regardless of the intersection type. We showed, particularly for the open intersection according to observed channel load, that the higher the transmission power, the higher the channel occupancy measured even at far located nodes. Furthermore, it is noted that the Channel Busy Time (CBT) reached a

typical maximum of $54 - 65\%$ in relaxed network conditions, e. g., in normal traffic condition characterized by free flow. We showed that the fraction of dropped packets increases as the message generation rate increases, in particular in the *Open* intersection. This can be explained, as expected, by building blocks in the *Close* intersection, which probably limit co-channel interference through a reduction of the communication range. Achieved CBT measured at both intersection types 0 and 4 further confirmed this finding.

Although the transmission power might slightly influence the end-to-end delay, it remains considerably low even for higher traffic density and should not be a significant problem regarding defined application requirements. As end-to-end delay does not completely assesses the reliability of cooperative awareness applications in an accurate manner, the message age provides information about the real age of received messages by considering additional delays due to consecutive packet losses. Results showed that under high densities and for both intersection types, vehicles located near the intersection center might experience high message ages due to the missing of several successive CAMs. As consequence, the message age seems to be environment-independent.

After an examination of packet collisions, it was shown that packet collisions due to CSMA/CA are more severe in comparison to those generated by the hidden node problem and should, therefore, be an important factor to consider when designing efficient congestion control algorithms. Moreover, with the transmitter at close distances to the intersection center, the intersection type 4 has the most favorable performance compared to intersection type 0 when high traffic density is considered. On the other hand, when considering packet collisions due to hidden nodes, an inverse trend was observable.

CONCLUSION

The growth of the economy and the mobility requirement of European citizen has generated an increase in the volume of road transport. Although the success in this sector is well appreciated by economical players and political policy makers, the transport on road causes not only fatal injuries but is also mainly responsible for social and environmental problems, such as air and water pollution, noise and other ecological impacts. In this context, VANET based on V2V communication opens up a plethora of road safety, traffic efficiency, and infotainment applications with the aim to assure an interaction between different road actors. Through the message exchange between vehicles and between vehicles and infrastructures, drivers are better informed and even more assisted in critical situations. Due to the rapidly growing advance in the field of wireless communication and results gathered from completed and active research projects, V2V has gained a lot of attention and maturity, so that V2V systems would be mandatory for new cars, and hence, are close to market introduction. However, prior to the deployment of V2V systems on the road, an assessment about the effective capability of V2V communication in different vehicular environments such as highway, suburban and urban, is indispensable. This thesis makes contributions to the comprehensive performance of V2V communication based on an experimental and a simulative evaluation in urban environments. More precisely, we focused on radio shadowing caused by buildings and vegetation at urban intersections.

8.1 MAIN FINDINGS

Main contributions from the performance evaluation study presented in this thesis provided following major results.

Statistic of Urban Intersection Types

As radio shadowing caused by buildings and road infrastructures are present at urban intersections, we presented a detailed analysis of intersections from some European cities with respect to the availability of NLOS between vehicles driving toward the intersection. We have particularly investigated the distribution of buildings and classified the type of intersection according to the number of corners occupied by buildings. The results show that only 23% of inner-city intersections in European cities provide a perfect LOS implying that a significant fraction of transmissions will be most of the time susceptible to packet loss due to signal attenuation through buildings.

After evaluating intersection types, we split the thesis into two parts. While the first part covered a measurement-based evaluation of V2V communication, the second part dealt with a simulation-based approach by evaluating environment

factors and communication parameters on the network behavior under consideration of scalability issue in terms of adding interference signals. Results of the first part were carried out from experiments conducted in real-world measurement scenarios utilizing a measurement platform that meets current standard for vehicular communication.

Impact of Radio Shadowing caused by Building and Vegetation

The most critical challenge that V2V communication has to deal with is the inevitable radio shadowing caused by a physical obstruction in the environment such as building, vegetation or traffic infrastructures. As communication performance in urban environments is mainly linked to the distribution of buildings around intersections, we first concentrated on the evaluation of building shadowing based on a campaign measurements performed at five urban intersections under LOS obstructions. We quantified received signal strength levels, packet delivery ratios, which reflect the ratio between the numbers of successfully received and transmitted frames and communication ranges associated with different intersection characteristics, such as building density and development, street and intersection width. We observed that the opening width of intersections has a significant impact of the communication range. Medium-wide intersections appear to be more favorable than narrow intersections. We further identified traffic condition to considerably influence the communication performance implying that reflections on surrounding vehicles destructively participate in the received signal power. Furthermore, when comparing the level of signal attenuation caused by different radio shadowing medium, we observed that shadowing through buildings is likely more severe than through vegetation.

Besides building shadowing, vegetation might also obstruct the communication link as street trees, bushes and plants could grow close to intersection corners, especially in suburban environments. The impact of vegetation on V2V communication performance based on measurements has been quantified. The measurement campaign has been conducted at three urban and rural intersections with respect to intersection layout and vegetation type. We have clearly shown how different vegetation types and structures impact the communication link. We also demonstrated that seasonal effects characterized by leafed or leafless vegetation affect the reliability of the V2V communication in term of achievable communication range. Considering the impact of vegetation structure, a heterogeneous vegetation consisting of a mix of trees and small plants appeared to be less aggressive than a homogenous and dense structure of plants such as cornfields.

Impact of Co-Channel Interference

Due to the broadcast nature of V2V, the vehicular network has to deal with the inevitable co-channel interference generated by nodes exchanging status information on a single radio channel. We evaluated the influence of building shadowing and its impact on co-channel interference. For this purpose, we carried out real-world measurements involving three vehicles at inner-city and rural intersections differing from the presence of surrounding buildings. To cope with the logistic issue,

we proposed an emulation method based on the configuration of a single vehicle as a set of vehicles transmitting at a high rate close to the network limit. Our findings revealed that under co-channel interference, a large communication range can be achieved in the inner-city rather than at rural intersections. Furthermore, it is shown that while building shadowing could improve the communication performance by limiting or blocking co-channel interference, transmitted signal power will strongly be attenuated leading to a degradation of the achievable communication range. This is especially true in relatively interference-free situations characterized by a low traffic density. Regarding packet delays, large inter-reception times due to consecutive packet losses are likely to be caused by building shadowing than by channel congestion. Despite the simplicity of the emulation approach, which does not provide a channel activity fully comparable to a large-scale field involving hundreds of vehicles, a good compromise between accuracy and logistic issue during the measurement is provided. Moreover, this abstraction method gives insight into the measurement-based evaluation of co-channel interference in VANETs.

Sensitivity Analysis of System Parameters

In the second part of this thesis, we evaluated the performance of V2V communication at urban intersections by means of simulation. The goal was to analyze the sensitivity of system parameters such as environment factors and communication attributes on the communication quality. For this purpose, we proposed a hybrid simulation platform including road traffic and network models for the simulation of vehicular scenarios. We showed that the traffic density in term of penetration rate may significantly impact the communication reliability. Furthermore, results revealed that open intersections provided in general better performance than intersections with two up to four corners occupied by buildings. However, under high traffic densities, a close intersection outperformed the others by assuring *guard regions*, where the nodes are protected from interference generated by surrounding nodes. Moreover, a relationship between transmitter/receiver location and intersection type in term of communication reliability was identified. All theses findings lead to the conclusion that the intersection type might impair the communication link, and should be therefore taken into account in the design of congestion control algorithms.

Controllable communication parameters such as message generation rate and transmission power were found to have a considerable influence on the improvement of the overall communication performance as already stated in studies found in the literature. An *open* intersection provides a high probability to reach a large number of nodes. In these conditions, sending with higher message generation rates might lead consequently to an increased number of packets dropped due to already congested network as identified by the measured Channel Busy Time (CBT). Although the transmission power positively influences the communication range, increasing the power might result in an increase of interference level, thus, a degradation of communication performance immediately when the traffic condition becomes dense. This is even problematic as nodes located in direct neighboring would primarily experience a poor probability of packet reception resulting to an inaccurate cooperative awareness between them.

We found in this thesis that the message latency, e.g., end-to-end delay and message age, remains considerable low such that it is not a determinant factor influencing the performance of V2V communication. However, it is necessary to note that, the message age reflected by a burst of packet losses increases as the traffic density increases. It is especially true for nodes located near the intersection center which may experience from time to time awareness blackouts. Answering the question behind the problem and source of packet collisions in VANETs, collisions due to the CSMA/CA mechanism are more severe than those generated by the hidden node problem. Furthermore, the transmission power and the intersection type were identified to significantly influence the probability of packet collisions.

Overall, based on the analysis above, the performance of V2V communication is directly linked to the topology and type of the intersection. While building shadowing might attenuate the propagation signal and, therefore, will lead to a reduction of the communication range, this obstruction effect might limit co-channel interference produced by hidden nodes or surrounding nodes in the communication range. Finally, despite controllable communication parameters such as message generation rate, the transmission power is the most influencing and sensitive factor in the capability evaluation of VANETs and should be carefully handled when designing congestion control algorithms.

8.2   FUTURE WORK

The evaluation of the performance of V2V communication at urban intersections presented in this thesis was solely based on network-centric metrics. Regardless of the applied methodology during the evaluation, one can cite among others the received power strength, packet delivery rate or packet drop rate. However, as V2V communication enables road traffic-related applications aiming to assist the driver in critical situations, a reasonable perceptive would be to investigate rather how safety-based applications perform in urban environments with respect to intersection types. Although, the traffic density, as well as the location of communication pairs, have a noticeable impact on the communication quality, applications such as FCW or ICW may be useless in traffic jams because of limited shared space between vehicles. In other words, a worse communication quality in term of packet reception rate is therefore not always a real issue considering an accurate operation of safety applications. For these reasons, a profound evaluation of these applications after a definition of key performance indicators is thus the next step towards an effective assessment of V2V communication. Moreover, the performance evaluation provided in this thesis could be used to support congestion control algorithms as relevant communication parameters and environment factors influencing the performance were identified and well analyzed, especially under crowded network conditions [156–166]. Considering the impact of intersection type, a further direction could be to integrate the knowledge about the environment as input parameter in order to provide an environment-dependent control algorithm. Technically, this is relatively feasible as information on the type of intersection may be easily inserted in the digital map or iteratively constructed by moving vehicles themselves.

ADAS	Advanced Driver Assistance Systems
AIFS	Arbitration Interframe Space
BSA	Basic Set of Applications
BSS	Basic Service Set
BSSID	Basic Service Set ID
CA	Cooperative Awareness
CAT	Channel Access Time
CAM	Cooperative Awareness Message
CBT	Channel Busy Time
CCA	Clear Channel Assessment
CCR	CSMA Collision Rate
CDF	Cumulative Distribution Function
C-ITS	Cooperative Intelligent Transport Systems
CMA	Cooperative Merging Assistance
CSMA/CA	Carrier-Sense Multiple Access with Collision Avoidance
CTS	Clear-To-Send
CW	Contention Window
DCC	Decentralized Congestion Control
DCF	Distributed Coordination Function
DEN	Decentralized Environmental Notification
DENM	Decentralized Environmental Notification Message
DIFS	DCF Interframe Space
DSRC	Dedicated Short Range Communications
EEBL	Emergency Electronic Brake Lights
EDCA	Enhanced Distributed Coordination Access
EIRP	Equivalent Isotropically Radiated Power
ETSI	European Telecommunications Standards Institute

FCW	Forward Collision Warning
HMI	Human Machine Interface
ICW	Intersection Collision Warning
ITS	Intelligent Transportation System
GLOSA	Green Light Optimized Speed Advisory
GPS	Global Positioning System
GSM	Global System for Mobile Communications
HCR	Hidden Collision Rate
LCA	Lane Change Assistance
LTE	Long Term Evolution
LLC	Logical Link Control
LOS	Line-of-Sight
LoS	Level of Service
MA	Message Age
MAC	Medium Access Control
MANET	Mobile Ad-Hoc Network
NLOS	Non-Line-of-Sight
OCB	Outside the Context of a Basic Service Set
OFDM	Orthogonal Frequency Division Multiplexing
OVW	Overtaking Vehicle Warning
PDF	Probability Density Function
PDR	Packet Delivery Rate
PLC	Physical Layer Capture
PLCP	Physical Layer Convergence procedure
PMF	Probability Mass Function
PHY	Physical
PRR	Packet Reception Rate
QoS	Quality of Service
RCR	Reliable Communication Range
RoI	Region of Interest

RMSE	Root-Mean-Square Error
RSSI	Received Signal Strength Indication
RSU	Road Side Unit
RTS	Request-To-Send
SIFS	Short Interframe Space
SINR	Signal-to-Interference-and-Noise Ratio
SNR	Signal-to-Noise Ratio
SUMO	Simulation Urban Mobility
SVW	Stationary Vehicle Warning
TCW	Traffic Condition Warning
UDP	User Datagram Protocol
V2I	Vehicle-to-Infrastructure
V2V	Vehicle-to-Vehicle
V2X	Vehicle-to-X
WLAN	Wireless Local Area Network
VANET	Vehicular Ad-hoc Network

BIBLIOGRAPHY

[1] R. S. Kahn. Transport and its infrastructure. In Climate Change 2007: Mitigation. Contribution of Working Group III to the Fourth Assessment Report of the Intergovernmental Panel on Climate Change. Technical report, Cambridge University Press, Cambridge, United Kingdom and New York, NY, USA, 2007.

[2] F. Mitis and D. Sethi. European Facts and Global Status Report on Road Safety 2013. Technical report, World Health Organization (WHO), 2013.

[3] EuroSafe. Injuries in the European Union, Report on Injury Statistics 2008-2010. Technical report, European Association for Injury Prevention and Safety Promotion, 2013.

[4] D. Bayliss. Motoring Towards 2050 - Roads and Reality Background Paper No.9. Technical report, Royal Automobile Club Foundation, March 2009.

[5] Unfallgeschehen nach Straßenarten. https://www.adac.de/_mmm/pdf/statistik_4_5_unfallgeschehen_strassenarten_42780.pdf. Accessed: 2015-06-16.

[6] ECC Decision(08)01. *The harmonised use of the 5875-5925 MHz Frequency Band for Intelligent Transport Systems (ITS)*, march 2008.

[7] IEEE 802.11-2007. *IEEE Standard for Information Technology – Telecommunications and Information Exchange between Systems – Local and Metropolitan Area Networks – Specific Requirements; Part 11: Wireless LAN Medium Access Control (MAC) and Physical Layer (PHY) Specifications*, December 2007.

[8] IEEE 802.11p-2010. *Standard for Information Technology – Telecommunications and Information Exchange between Systems – Local and Metropolitan Area Networks – Specific Requirements; Part 11: Wireless LAN Medium Access Control (MAC) and Physical Layer (PHY) Specifications; Amendment 6: Wireless Access in Vehicular Environments*, July 2010.

[9] ETSI TR 102 638 V1.1.1. *Intelligent Transport Systems (ITS); Vehicular Communications; Basic Set of Applications; Definitions*, June 2009.

[10] ETSI EN 302 665 V1.1.1. *Intelligent Transport Systems (ITS); Communications Architecture*, September 2010.

[11] ISO/IEC 7498-1. *Information technology - Open Systems Interconnection - Basic Reference Model: The Basic Model*, November 1994.

[12] IEEE 802.11-2012. *IEEE Standard for Information Technology – Telecommunications and Information Exchange between Systems – Local and Metropolitan Area Networks – Specific Requirements; Part 11: Wireless LAN Medium Access Control (MAC) and Physical Layer (PHY) Specifications*, March 2012.

[13] ANSI/IEEE Std 802.2. *IEEE Standard for Information Technology - Telecommunications and Information Exchange between Systems - Local and Metropolitan Area Networks - Specific Requirements - Part 2: Logical Link Control*, May 1998.

[14] ETSI EN 302 663 V1.2.0. *Intelligent Transport Systems (ITS); Access Layer Specification for Intelligent Transport Systems operating in the 5 GHz Frequency Band* , 2012.

[15] D. Jiang and L. Delgrossi. IEEE 802.11p: Towards an International Standard for Wireless Access in Vehicular Environments. In *Vehicular Technology Conference, 2008. VTC Spring 2008. IEEE*, pages 2036–2040, May 2008.

[16] D. Jiang, Q. Chen, and L. Delgrossi. Optimal Data Rate Selection for Vehicle Safety Communications. In *Proceedings of the Fifth ACM International Workshop on VehiculAr Inter-NETworking*, VANET '08, pages 30–38. ACM, 2008.

[17] ETSI TS 102 636-5-1 V1.1.1. *Intelligent Transport Systems (ITS); Vehicular Communications; GeoNetworking; Part 5: Transport Protocols; Sub-part 1: Basic Transport Protocol*, February 2011.

[18] ETSI TS 102 636-1 V1.1.1. *Intelligent Transport Systems (ITS); Vehicular Communications; GeoNetworking; Part 1: Requirements*, March 2010.

[19] ETSI TS 102 636-4-1 V1.1.1. *Intelligent Transport Systems (ITS); Vehicular Communications; GeoNetworking; Part 4: Geographical Addressing and Forwarding for Point-to-Point and Point-to-Multipoint Communications; Sub-part 1: Media-Independent Functionality*, June 2011.

[20] CAR 2 CAR Communication Consortium. *CAR 2 CAR Communication Consortium Manifesto: Overview of the C2C-CC System V1.1*, august 2007.

[21] ETSI TS 102 636-6-1 V1.1.1. *Intelligent Transport Systems (ITS); Vehicular Communications; GeoNetworking; Part 6: Internet Integration; Sub-part 1: Transmission of IPv6 Packets over GeoNetworking Protocols*, March 2011.

[22] ETSI EN 302 637-2 V1.3.2. *Intelligent Transport Systems (ITS); Vehicular Communications; Basic Set of Applications; Part 2: Specification of Cooperative Awareness Basic Service*, November 2014.

[23] ETSI EN 302 637-3 V1.2.1. *Intelligent Transport Systems (ITS); Vehicular Communications; Basic Set of Applications; Part 3: Specifications of Decentralized Environmental Notification Basic Service*, September 2014.

[24] M. Pijpers. Sensors in ADAS: A Literature Study on the Working Principles and Characteristics of frequently applied Sensors in Advanced Driver Assistance Systems. In *Universiteit Twente*, jan 2007.

[25] S. E. Shladover and T. Swe-Kuang. Analysis of Vehicle Positioning Accuracy Requirements for Communication-Based Cooperative Collision Warning. *Journal of Intelligent Transportation Systems: Technology, Planning, and Operations*, 10(3):131–140, Jan 2007.

[26] K. Gajananan, S. Sontisirikit, J Zhang, M. Miska, E. Chung, S. Guha, and H. Prendinge. A Cooperative ITS Study on Green Light Optimisation using an integrated Traffic, Driving, and Communication Simulator. In *Australasian Transport Research Forum 2013 Proceedings*, Oct 2013.

[27] K. Katsaros, R. Kernchen, M. Dianati, and D. Rieck. Performance Study of a Green Light Optimized Speed Advisory (GLOSA) Application using an integrated Cooperative ITS Simulation Platform. In *7th International on Wireless Communications and Mobile Computing Conference (IWCMC)*, pages 918–923, July 2011.

[28] G. Bianchi. IEEE 802.11-Saturation Throughput Analysis. *IEEE Communications Letters*, 2(12):318–320, Dec 1998.

[29] G. Bianchi. Performance Analysis of the IEEE 802.11 Distributed Coordination Function. *IEEE Journal On Selected Areas In Communications*, 18(3):535–547, March 2000.

[30] X. Ma and X. Chen. Performance Analysis of IEEE 802.11 Broadcast Scheme in Ad Hoc Wireless LANs. *IEEE Transactions on Vehicular Technology*, 57(6):3757–3768, Nov 2008.

[31] Y. Fallah, C. Huang, R. Sengupta, and H. Krishnan. Analysis of Information Dissemination in Vehicular Ad-Hoc Networks With Application to Cooperative Vehicle Safety Systems. *IEEE Transactions on Vehicular Technology*, 60(1):233–247, Jan 2011.

[32] H Chong, M. Dianati, R. Tafazolli, R. Kernchen, and Xuemin Shen. Analytical Study of the IEEE 802.11p MAC Sublayer in Vehicular Networks. *IEEE Transactions on Intelligent Transportation Systems*, 13(2):873–886, June 2012.

[33] J. Zheng and Q. Wu. Performance Modeling and Analysis of the IEEE 802.11p EDCA Mechanism for VANET. *Vehicular Technology, IEEE Transactions on*, PP(99):1–1, April 2015.

[34] Q. Yang, S. Xing, W. Xia, and L. Shen. Modelling and Performance Analysis of Dynamic Contention Window Scheme for Periodic Broadcast in Vehicular Ad Hoc Networks. *IET Communications*, 9(11):1347–1354, 2015.

[35] II. Davis, J.S. and J.P.M.G. Linnartz. Vehicle to Vehicle RF Propagation Measurements. In *Conference on Signals, Systems and Computers, 1994. Conference Record of the Twenty-Eighth Asilomar*, volume 1, pages 470–474, Oct 1994.

[36] J. Maurer, T. Fugen, and W. Wiesbeck. Narrow-band Measurement and Analysis of the Inter-Vehicle Transmission Channel at 5.2 GHz. In *IEEE 55th Vehicular Technology Conference, 2002. VTC Spring 2002*, volume 3, pages 1274–1278, 2002.

[37] J.P. Singh, N. Bambos, B. Srinivasan, and D. Clawin. Wireless LAN Performance under varied Stress Conditions in Vehicular Traffic Scenarios. In *56th IEEE Vehicular Technology Conference. VTC 2002-Fall*, volume 2, pages 743–747 vol.2, 2002.

[38] M. Wellens, B. Westphal, and P. Mahonen. Performance Evaluation of IEEE 802.11-based WLANs in Vehicular Scenarios. In *65th IEEE Vehicular Technology Conference, 2007. VTC2007-Spring*, pages 1167–1171, April 2007.

[39] G. Acosta, K. Tokuda, and M.A. Ingram. Measured Joint Doppler-delay Power Profiles for Vehicle-to-Vehicle Communications at 2.4 GHz. In *Global Telecommunications Conference, 2004. GLOBECOM '04. IEEE*, volume 6, pages 3813–3817, Nov 2004.

[40] A. Paier, J. Karedal, N. Czink, C. Dumard, T. Zemen, F. Tufvesson, A. Molisch, and C. Mecklenbräuker. Characterization of Vehicle-to-Vehicle Radio Channels from Measurements at 5.2 GHz. *Wireless Personal Communications*, 50(1):19–32, 2009.

[41] I. Sen and D.W. Matolak. Vehicle-Vehicle Channel Models for the 5-GHz Band. *IEEE Transactions on Intelligent Transportation Systems*, 9(2):235–245, June 2008.

[42] A. Paier, L. Bernado, J. Karedal, O. Klemp, and A. Kwoczek. Overview of Vehicle-to-Vehicle Radio Channel Measurements for Collision Avoidance Applications. In *71st IEEE Vehicular Technology Conference*, pages 1–5, 2010.

[43] Lin Cheng, B.E. Henty, D.D. Stancil, Fan Bai, and P. Mudalige. Mobile Vehicle-to-Vehicle Narrow-Band Channel Measurement and Characterization of the 5.9 GHz Dedicated Short Range Communication (DSRC) Frequency Band. *IEEE Journal on Selected Areas in Communications*, 25(8):1501–1516, Oct 2007.

[44] Lin Cheng, B.E. Henty, D.D. Stancil, Fan Bai, and P. Mudalige. Properties and Applications of the Suburban Vehicle-to-Vehicle Propagation Channel at 5.9 GHz. In *International Conference on Electromagnetics in Advanced Applications, ICEAA 2007*, pages 121–124, Sept 2007.

[45] Lin Cheng, B. Henty, Fan Bai, and D.D. Stancil. Doppler Spread and Coherence Time of Rural and Highway Vehicle-to-Vehicle Channels at 5.9 GHz. In *Global Telecommunications Conference, 2008. IEEE GLOBECOM 2008*, pages 1–6, Nov 2008.

[46] J. Yin, G. Holland, T. ElBatt, Fan Bai, and H. Krishnan. DSRC Channel Fading Analysis from Empirical Measurement. In *First International Conference on Communications and Networking in China*, pages 1–5, Oct 2006.

[47] G.P. Grau, D. Pusceddu, S. Rea, O. Brickley, M. Koubek, and D. Pesch. Vehicle-2-Vehicle Communication Channel Evaluation using the CVIS Platform. In *7th International Symposium on Communication Systems Networks and Digital Signal Processing (CSNDSP)*, pages 449–453, July 2010.

[48] A. Paier, R. Tresch, A. Alonso, D. Smely, P. Meckel, Y. Zhou, and N. Czink. Average Downstream Performance of Measured IEEE 802.11p Infrastructure-to-Vehicle Links. In *IEEE International Conference on Communications Workshops (ICC)*, pages 1–5, May 2010.

[49] V. Shivaldova, G. Maier, D. Smely, N. Czink, A. Alonso, A. Winkelbauer, A. Paier, and C.F. Mecklenbräuker. Performance Evaluation of IEEE 802.11p Infrastructure-to-Vehicle Tunnel Measurements. In *7th International Wireless Communications and Mobile Computing Conference (IWCMC)*, pages 848–852, July 2011.

[50] J. Gozalvez, M. Sepulcre, and R. Bauza. IEEE 802.11p Vehicle to Infrastructure Communications in Urban Environments. *IEEE Communications Magazine*, 50(5):176–183, May 2012.

[51] P. Alexander, D. Haley, and A. Grant. Cooperative Intelligent Transport Systems: 5.9-GHz Field Trials. *Proceedings of the IEEE*, 99(7):1213–1235, July 2011.

[52] R. Meireles, M. Boban, P. Steenkiste, O. Tonguz, and J. Barros. Experimental Study on the Impact of Vehicular Obstructions in VANETs. In *IEEE Vehicular Networking Conference (VNC)*, pages 338–345, 2010.

[53] M. Boban, T. Vinhoza, M. Ferreira, J. Barros, and O. Tonguz. Impact of Vehicles as Obstacles in Vehicular Ad Hoc Networks. In *IEEE Journal on Selected Areas in Communications*, volume 29, pages 15–28, January 2011.

[54] R. He, A.F. Molisch, F. Tufvesson, Zhangdui Zhong, Bo Ai, and Tingting Zhang. Vehicle-to-Vehicle Propagation Models With Large Vehicle Obstructions. *IEEE Transactions on Intelligent Transportation Systems*, 15(5):2237–2248, Oct 2014.

[55] D. Vlastaras, T. Abbas, M. Nilsson, R. Whiton, M. Olback, and F. Tufvesson. Impact of a Truck as an Obstacle on Vehicle-to-Vehicle Communications in Rural and Highway Scenarios. In *IEEE 6th International Symposium on Wireless Vehicular Communications (WiVeC)*, pages 1–6, Sept 2014.

[56] M. Boban, R. Meireles, J. Barros, P. Steenkiste, and O. Tonguz. Exploiting the Height of Vehicles in Vehicular Communication. In *IEEE Vehicular Networking Conference (VNC)*, pages 163–170, 2011.

[57] M. Boban, R. Meireles, J. Barros, P. Steenkiste, and O.K. Tonguz. TVR-Tall Vehicle Relaying in Vehicular Networks. *IEEE Transactions on Mobile Computing*, 13(5):1118–1131, May 2014.

[58] Zhinan X., L. Bernado, Mingming G., M. Hofer, T. Abbas, V. Shivaldova, K. Mahler, D. Smely, and T. Zemen. Relaying for IEEE 802.11p at Road Intersection using a Vehicular non-stationary Channel Model. In *IEEE 6th International Symposium on Wireless Vehicular Communications (WiVeC)*, pages 1–6, Sept 2014.

[59] T. Queck, B. Schünemann, and I. Radusch. Runtime Infrastructure for Simulating Vehicle-2-x Communication Scenarios. In *Proceedings of the Fifth ACM International Workshop on VehiculAr Inter-NETworking*, VANET '08, pages 78–78. ACM, 2008.

[60] B. Schünemann. *The V2X Simulation Runtime Infrastructure: VSimRTI*. PhD thesis, Universität Potsdam, 2012.

[61] F. Dressler, C. Sommer, D. Eckhoff, and O.K. Tonguz. Toward Realistic Simulation of Intervehicle Communication. *IEEE Vehicular Technology Magazine*, 6(3):43–51, Sept 2011.

[62] C. Sommer, J. Härri, F. Hrizi, B. Schünemann, and F. Dressler. Simulation Tools and Techniques for Vehicular Communications and Applications. In *Vehicular ad hoc Networks - Standards, Solutions, and Research*. Springer, 2014.

[63] C. Sommer, R. German, and F. Dressler. Bidirectionally Coupled Network and Road Traffic Simulation for Improved IVC Analysis. *IEEE Transactions on Mobile Computing*, 10(1):3–15, January 2011.

[64] V. Kumar, Lan Lin, D. Krajzewicz, F. Hrizi, O. Martinez, J. Gozalvez, and R. Bauza. iTETRIS: Adaptation of ITS Technologies for Large Scale Integrated Simulation. In *IEEE 71st Vehicular Technology Conference (VTC 2010-Spring)*, pages 1–5, May 2010.

[65] S. Eichler. Performance Evaluation of the IEEE 802.11p WAVE Communication Standard. In *IEEE 66th Vehicular Technology Conference (VTC-2007 Fall)*, pages 2199–2203, Sept 2007.

[66] Sebastian Grafling, Petri Mahönen, and Janne Riihijarvi. Performance Evaluation of IEEE 1609 WAVE and IEEE 802.11p for Vehicular Communications. In *2010 Second International Conference on Ubiquitous and Future Networks (ICUFN)*, pages 344–348, June 2010.

[67] J. Mittag, S. Papanastasiou, H. Hartenstein, and E.G. Strom. Enabling Accurate Cross-Layer PHY/MAC/NET Simulation Studies of Vehicular Communication Networks. *Proceedings of the IEEE*, 99(7):1311–1326, July 2011.

[68] J. Yin, T. ElBatt, G. Yeung, B. Ryu, S. Habermas, H. Krishnan, and T. Talty. Performance Evaluation of Safety Applications over DSRC Vehicular Ad Hoc Networks. In *Proceedings of the 1st ACM International Workshop on Vehicular Ad Hoc Networks*, VANET '04, pages 1–9. ACM, 2004.

[69] C. Sommer, S. Joerer, M. Segata, O. K. Tonguz, R. Lo Cigno, and F. Dressler. How Shadowing Hurts Vehicular Communications and How Dynamic Beaconing Can Help. *IEEE Transactions on Mobile Computing*, 2014.

[70] C. Sommer, D. Eckhoff, and F. Dressler. IVC in Cities: Signal Attenuation by Buildings and How Parked Cars Can Improve the Situation. *IEEE Transactions on Mobile Computing*, 13(8):1733–1745, August 2014.

[71] L. Urquiza-Aguiar, C. Tripp-Barba, J. Estrada-Jimónez, and M. Igartua. On the Impact of Building Attenuation Models in VANET Simulations of Urban Scenarios. *Electronics*, 4(1):37, 2015.

[72] T. Mangel, F. Schweizer, T. Kosch, and H. Hartenstein. Vehicular Safety Communication at Intersections: Buildings, Non-Line-Of-Sight and Representative Scenarios. In *8th International Conference on Wireless On-Demand Network Systems and Services (WONS)*, pages 35–41, 2011.

[73] A. Molinero Martinez, E. Carter, C. L. Naing, M. C. Simon, and T. Hermitte. Accident Causation and Pre-accidental Driving Situations: Part 1. Overview and General Statistics. Technical report, TRACE, January 2008.

[74] A. Molinero, J. Perandones, T. Hermitte, A Grimaldi, J. Gwehengerber, D. Daschner, J. Barrios, A. Aparicio, S. Schick, P. Van Elslande, and K. Fouquet. Road Users and Accident Causation. Part 2: In-depth Accident Causation Analysis. Technical report, TRACE, June 2008.

[75] K. Knapp, B. Chandler, J. Atkinson, T. Welch, H. Rigdon, R. Retting, S. Meekins, E. Widstrand, and R. Porter. Road Diet Informational Guide. Technical report, Federal Highway Administration (FHWA), 2014.

[76] D. Frambro, K. Fitzpatrick, and R. Koppa. NCHRP Report 400: Determination of Stopping Sight Distances. Technical report, Transportation Research Board, June 1997.

[77] K. Ashok and M. E. Ben-Akiva. Alternative Approaches for Real-Time Estimation and Prediction of Time-Dependent Origin–Destination Flows. *Transportation Science*, 34(1):21–36, February 2000.

[78] U.A. Khan and B. Rinner. A Reinforcement Learning Framework for Dynamic Power Management of a Portable, Multi-camera Traffic Monitoring System. In *IEEE International Conference on Green Computing and Communications (Green-Com)*, pages 557–564, Nov 2012.

[79] W. Deng, H. Lei, and X. Zhou. Traffic State Estimation and Uncertainty Quantification based on Heterogeneous Data Sources: A three Detector Approach. *Transportation Research Part B: Methodological*, 57(0):132 – 157, 2013.

[80] Y. Yuan, H. Van Lint, F. Van Wageningen-Kessels, and S. Hoogendoorn. Network-Wide Traffic State Estimation Using Loop Detector and Floating Car Data. *Journal of Intelligent Transportation Systems*, 18(1):41–50, 2014.

[81] H. Tchouankem, D. Schmidt, and H. Schumacher. Impact of Vehicular Communication Performance on Travel Time Estimation in Urban Areas. In *6th International Symposium "Networks for Mobility 2012"*, 2012.

[82] M. Ebrahim Foulaadvand and S. Belbasi. Vehicular Traffic Flow at a non-signalized Intersection. *Journal of Physics A: Mathematical and Theoretical*, 40(29):8289, 2007.

[83] S. Belbasi and M. Ebrahim Foulaadvand. Simulation of Traffic Flow at a Signalised Intersection. In S. Bandini, S. Manzoni, H. Umeo, and G. Vizzari, editors, *Cellular Automata*, volume 6350 of *Lecture Notes in Computer Science*, pages 138–141. Springer Berlin Heidelberg, 2010.

[84] S. E. Shladover. Effects of Traffic Density on Communication Requirements for Cooperative Intersection Collision Avoidance System. Technical report, UCB-ITS-PWP-2005-1, Institute of Transportation Studies, University of California, Berkeley, 2005.

[85] Stadt Braunschweig. Verkehrsmengenkarte für den inneren Stadtbereich von Braunschweig. https://www.braunschweig.de/leben/stadtplan_verkehr/verkehrsplanung/verkehrsmengen-city.pdf, 2009. Accessed: 2015-10-15.

[86] Stadt München. Verkehrsmengenkarte für München. http://www.ris-muenchen.de/RII/RII/DOK/SITZUNGSVORLAGE/2224884.pdf, 2009. Accessed: 2015-10-15.

[87] Stadt Berlin. Verkehrsmengenkarte für Berlin. http://www.stadtentwicklung.berlin.de/verkehr/lenkung/vlb/download/verkehrsmengen_2009.pdf, 2009. Accessed: 2015-10-15.

[88] NHTSA. *National Center for Statistics and Analysis - Crash Factors in Intersection-Related Crashes: An On-Scene Perspective*. National Highway Traffic Safety Administration, 2010.

[89] H. Schumacher, H. Tchouankem, J. Nuckelt, T. Kürner, T. Zinchenko, A. Leschke, and L. Wolf. Vehicle-to-Vehicle IEEE 802.11p Performance Measurements at Urban Intersections. In *IEEE International Conference on Communications (ICC)*, pages 7131–7135, 2012.

[90] T. Mangel, M. Michl, O. Klemp, and H. Hartenstein. Real-World Measurements of Non-Line-Of-Sight Reception Quality for 5.9GHz IEEE 802.11p at Intersections. In *3rd International Workshop on Communication Technologies for Vehicles (Nets4Cars), Lecture Notes in Computer Science, Vol. 6596*, pages 189–202, 2011.

[91] F. Erlacher, F. Klingler, C. Sommer, and F. Dressler. On the Impact of Street Width on 5.9 GHz Radio Signal Propagation in Vehicular Networks. In *11th IEEE/IFIP Conference on Wireless On demand Network Systems and Services (WONS 2014)*, pages 143–146, Obergurgl, Austria, April 2014.

[92] J. Karedal, F. Tufvesson, T. Abbas, O. Klemp, A. Paier, L. Bernado, and A. F. Molisch. Radio Channel Measurements at Street Intersections for Vehicle-to-Vehicle Safety Applications. In *IEEE 71st Vehicular Technology Conference*, pages 1–5, 2010.

[93] M. Schack, J. Nuckelt, R. Geise, L. Thiele, and T. Kürner. Comparison of Path Loss Measurements and Predictions at Urban Crossroads for C2C Communications. In *5th European Conference on Antennas and Propagation (EUCAP)*, pages 2896–2900, 2011.

[94] T. Mangel, O. Klemp, and H. Hartenstein. A Validated 5.9 GHz Non-Line-Of-Sight Path-Loss and Fading Model for Inter-Vehicle Communication. In *11th International Conference on ITS Telecommunications (ITST)*, pages 75–80, 2011.

[95] C. Sommer, D. Eckhoff, R. German, and F. Dressler. A Computationally Inexpensive Empirical Model of IEEE 802.11p Radio Shadowing in Urban Environments. In *8th IEEE/IFIP Conference on Wireless On demand Network Systems and Services (WONS)*, pages 84–90, 2011.

[96] A. F. Molisch, F. Tufvesson, J. Karedal, and C. Mecklenbräuker. A Survey on Vehicle-to-Vehicle Propagation Channels. *IEEE Wireless Communications*, 16(6):12–22, December 2009.

[97] ETSI ES 202 663 V1.1.0. *Intelligent Transport Systems (ITS); European Profile Standard for the Physical and Medium Access Control Layer of Intelligent Transport Systems operating in the 5 GHz Frequency Band*, 2010.

[98] A Kwoczek, Z. Raida, J. Lacik, M. Pokorny, J. Puskely, and P. Vagner. Influence of Car Panorama Glass Roofs on Car2Car Communication. *IEEE Vehicular Networking Conference (VNC)*, pages 246–251, 2011.

[99] T. Mangel and H. Hartenstein. 5.9 GHz IEEE 802.11p Inter-vehicle Communication: Non-Line-of-Sight Reception Under Competition. In *Vehicular Networking Conference (VNC), 2011 IEEE*, pages 155–162, 2011.

[100] E. Macdonald, A. Harper, J. Williams, and J. Hayter. Street Trees and Intersection Safety. Technical report, University of California, 2006.

[101] H. Tchouankem, T. Zinchenko, H. Schumacher, and L. Wolf. Effects of Vegetation on Vehicle-to-Vehicle Communication Performance at Intersections. In *IEEE 78th Vehicular Technology Conference (VTC Fall)*, pages 1–6, Sept 2013.

[102] M.A. Weissberger. An Initial Critical Summary of Models for Predicting the Attenuation of Radio Waves by Trees. In *Department of defense, Electromagnetic Compatibility Analysis Center, Annapolis, Maryland*, July 1982.

[103] M. O. AL-Nuaimi and A. M. Hammoudeh. Measurements and Predictions of Attenuation and Scatter of Microwave Signals by Trees. In *IEE Proceeding on Antennas and Propagation, Part H*, volume 141, April 1994.

[104] N. Rogers, A. Seville, J. Richter, D. Ndzi, N. Savage, R. Caldeirinha, A. Shukla, M. Al-Nuaimi, K. Craig, E. Vilar, and J. Austin. A Generic Model of 1-60 GHz Radio Propagation through Vegetation - Final Report. Technical report, QinetiQ, May 2002.

[105] Y. S. Meng, Y. H. Lee, and B. C. Ng. Path Loss Modeling for Near-ground VHF Radio-wave Propagation Through Forest with Tree-canopy Reflection Effect. *Progress In Electromagnetics Research*, 12:131–141, 2010.

[106] G.G. Joshi, C.B. Dietrich, C.R. Anderson, W.G. Newhall, W.A. Davis, J. Isaacs, and G. Barnett. Near-ground Channel Measurements over Line-of-Sight and forested Paths. *IEE Proceedings Microwaves, Antennas and Propagation*, pages 589–596, December 2005.

[107] K. Sarabandi and Il-Suek Koh. A Complete Physics-Based Channel Parameter Simulation for Wave Propagation in a Forest Environment. *IEEE Transactions on Antennas and Propagation*, 49(2):260–271, Feb 2001.

[108] William E. Frazier. Handbook of Radio Wave Propagation Loss, Part II (100 - 20,000 MHz). Technical report, National Telecommunications and Information Administration, April 1989.

[109] T. Tamir. Radio Wave Propagation along Mixed Paths in Forest Environments. *IEEE Transactions on Antennas and Propagation*, 25(4):471 – 477, July 1977.

[110] G. P. Grudinskaya. Propagation of Radiowaves at HF and VHF Frequency Bands. In *Radio and Telecommunications, 3 edition, Moscow, Russia*, page 82, 1981.

[111] N. An, T. Gaugel, and H. Hartenstein. VANET: Is 95% Probability of Packet Reception Safe? *ITS Telecommunications (ITST), 2011 11th International Conference*, 141(2):113–119, August 2011.

[112] M. A. Weissberger. An Initial Critical Summary of Models for Predicting the Attenuation of Radio Waves by Foliage. In *Electromagnetic Compatibility Analysis Center*, 1981.

[113] COST 235. Radiowave Propagation Effects on Next Generation Fixed Services Terrestrial Telecommunications Systems, Final Report. In *Commission of the European Union*, 1996.

[114] International Telecommunication Union (ITU). Attenuation in Vegetation. In *ITU-R Recomm. 833-3*, 2001.

[115] T. Kosch, C.J. Adler, S. Eichler, C. Schroth, and M. Strassberger. The Scalability Problem of Vehicular Ad Hoc Networks and How to Solve it. *IEEE Wireless Communications*, 13(5):22–28, October 2006.

[116] R. S. Schwartz, K. Das, H. Scholten, and P. Havinga. Exploiting Beacons for Scalable Broadcast Data Dissemination in VANETs. In *9th ACM International Workshop on Vehicular Inter-Networking, Systems, and Applications, VANET 2012*, pages 53–62, New York, June 2012. ACM.

[117] K. Bilstrup, E. Uhlemann, E. G. Ström, and U. Bilstrup. On the Ability of the 802.11P MAC Method and STDMA to Support Real-time Vehicle-to-vehicle Communication. *EURASIP J. Wirel. Commun. Netw.*, 2009:5:1–5:13, January 2009.

[118] H. Tchouankem and T. Lorenzen. Measurement-based Evaluation of Interference in Vehicular Ad-Hoc Networks at Urban Intersections. In *IEEE International Conference on Communication Workshop (ICCW)*, pages 2381–2386, June 2015.

[119] G. Acosta-marum and M. A. Ingram. Doubly Selective Vehicle-to-Vehicle Channel Measurements and Modeling at 5.9 GHz. In *International Symposium on Wireless Personal Multimedia Communications*, 2006.

[120] C.F. Mecklenbrauker, A.F. Molisch, J. Karedal, F. Tufvesson, A. Paier, L. Bernado, T. Zemen, O. Klemp, and N. Czink. Vehicular Channel Characterization and Its Implications for Wireless System Design and Performance. *Proceedings of the IEEE*, 99(7):1189–1212, July 2011.

[121] M. Boban and P.M. d'Orey. Measurement-based Evaluation of Cooperative Awareness for V2V and V2I Communication. In *IEEE Vehicular Networking Conference (VNC)*, pages 1–8, Dec 2014.

[122] R. K. Schmidt, B. Kloiber, F. Schüttler, and T. Strang. Degradation of Communication Range in VANETs Caused by Interference 2.0 - Real-world Experiment. In *Proceedings of the Third International Conference on Communication Technologies for Vehicles*, Nets4Cars/Nets4Trains'11, pages 176–188, 2011.

[123] F. Librino, M.E. Renda, and P. Santi. Measurement-based Modeling of Packet Inter-Reception Time in Presence of Radio Channel Congestion. In *Eleventh Annual IEEE International Conference on Sensing, Communication, and Networking (SECON)*, pages 432–440, June 2014.

[124] D. Jiang, Qi Chen, and L. Delgrossi. Communication Density: A Channel Load Metric for Vehicular Communications Research. In *IEEE International Conference on Mobile Adhoc and Sensor Systems, 2007 (MASS 2007)*, pages 1–8, Oct 2007.

[125] C. Sommer, S. Joerer, and F. Dressler. On the Applicability of Two-Ray Path Loss Models for Vehicular Network Simulation. In *4th IEEE Vehicular Networking Conference (VNC)*, pages 64–69, Seoul, Korea, November 2012. IEEE.

[126] T. Zinchenko, H. Tchouankem, L. Wolf, and A. Leschke. Reliability Analysis of Vehicle-to-Vehicle Applications based on Real World Measurements. In *Proceeding of the tenth ACM international workshop on Vehicular inter-networking, systems, and applications*, pages 11–20. ACM, 2013.

[127] H. Tchouankem, T. Zinchenko, and H. Schumacher. Impact of Buildings on Vehicle-to-Vehicle Communication at Urban Intersections. In *12th Annual IEEE Consumer Communications and Networking Conference (CCNC)*, pages 206–212, Jan 2015.

[128] C. Sommer, S. Joerer, M. Segata, O. K. Tonguz, R. L. Cigno, and F. Dressler. How Shadowing Hurts Vehicular Communications and How Dynamic Beaconing Can Help. In *INFOCOM*, pages 110–114, 2013.

[129] M. Piórkowski, M. Raya, A. Lezama Lugo, P. Papadimitratos, M. Grossglauser, and J.-P. Hubaux. TraNS: Realistic Joint Traffic and Network Simulator for VANETs. *SIGMOBILE Mob. Comput. Commun. Rev.*, 12(1):31–33, January 2008.

[130] The Network Simulator - ns-2. http://www.isi.edu/nsnam/ns/. Accessed: 2015-04-01.

[131] A. Varga. The OMNeT++ Discrete Event Simulation System. In *European Simulation Multiconference (ESM'2001)*, June 2001.

[132] Quadstone Paramics: Microscopic Traffic and Pedestrian Simulation Software. http://www.paramics-online.com. Accessed: 2015-04-01.

[133] J. Barceló and J. Casas. Dynamic Network Simulation with AIMSUN. In Ryuichi Kitamura and Maso Kuwahara, editors, *Simulation Approaches in Transportation Analysis*, volume 31 of *Operations Research/Computer Science Interfaces Series*, pages 57–98. Springer US, 2005.

[134] D. Krajzewicz, J. Erdmann, M. Behrisch, and L. Bieker. Recent Development and Applications of SUMO - Simulation of Urban MObility. *International Journal On Advances in Systems and Measurements*, 5(3&4):128–138, December 2012.

[135] A. Wegener, M. Piórkowski, M. Raya, H. Hellbrück, S. Fischer, and J. Hubaux. TraCI: An Interface for Coupling Road Traffic and Network Simulators. In *11th Communications and Networking Simulation Symposium*, pages 155–163. ACM, 2008.

[136] D. Krajzewicz. Traffic Simulation with SUMO - Simulation of Urban Mobility. In Jaume Barceló, editor, *Fundamentals of Traffic Simulation*, volume 145 of *International Series in Operations Research & Management Science*, pages 269–293. Springer New York, 2010.

[137] ETSI EN 302 665 V1.1.1. *Intelligent Transport Systems (ITS); Communications Architecture*, September 2010.

[138] K. Wehrle, M. Günes, and J. Gross. *Modeling and Tools for Network Simulation*. Springer-Verlag Berlin Heidelberg, 1 edition, 2010.

[139] J. Nuckelt, M. Schack, and T. Kürner. Deterministic and Stochastic Channel Models Implemented in a Physical Layer Simulator for Car-to-X Communications. *Advances in Radio Science*, 9:165–171, September 2011.

[140] E. Giordano, R. Frank, G. Pau, and M. Gerla. CORNER: a Realistic Urban Propagation Model for VANET. In *7th International Conference on Wireless On-demand Network Systems and Services (WONS)*, pages 57–60, 2010.

[141] J. Muramatsu, N. Suzuki, Y. Ito, and T. Taga. Measurement of Radio Propagation Characteristics for Inter-Vehicle Communication in Urban Areas. In *Proceedings of the 2007 International Symposium on Antennas and Propagation (ISAP 2007)*, pages 161–164, 2007.

[142] T. Kurner and M. Schack. 3D Ray-Tracing embedded into an Integrated Simulator for Car-to-X Communications. In *2010 URSI International Symposium on Electromagnetic Theory (EMTS)*, pages 880–882, Aug 2010.

[143] R. Reinders, E. M. van Eenennaam, G. Karagiannis, and G. J. Heijenk. Contention Window Analysis for Beaconing in VANETs. In *Seventh IEEE International Wireless Communications and Mobile Computing conference, IWCMC 2011, Istanbul, Turkey*, pages 1481–1487, July 2011.

[144] C. Campolo, A. Vinel, A. Molinaro, and Y. Koucheryavy. Modeling Broadcasting in IEEE 802.11p/WAVE Vehicular Networks. *Communications Letters, IEEE*, 15(2):199–201, February 2011.

[145] F. Martelli, M. Elena Renda, G. Resta, and P. Santi. A Measurement-based Study of Beaconing Performance in IEEE 802.11p Vehicular Networks. In *INFOCOM, 2012 Proceedings IEEE*, pages 1503–1511, March 2012.

[146] Q. Chen, D. Jiang, and L. Delgrossi. IEEE 1609.4 DSRC Multi-Channel Operations and its Implications on Vehicle Safety Communications. In *Vehicular Networking Conference (VNC), 2009 IEEE*, pages 1–8, Oct 2009.

[147] B. Kloiber, C. Rico Garcia, J. Härri, and T. Strang. Update delay: A New Information-Centric Metric for a combined Communication and Application Level Reliability Evaluation of CAM based Safety Applications. In *19th ITS World Congress*, October 2012.

[148] Transportation Research Board. *Highway Capacity Manual (HCM2000)*. National Academy of Sciences, NW, Washington, DC 20418, 2000.

[149] ETSI TS 102 687 V1.1.1. *Intelligent Transport Systems (ITS); Decentralized Congestion Control Mechanism for Intelligent Transport Systems operating in the 5 GHz range; Access layer part*, July 2011.

[150] A. Baiocchi, C. Colombaroni, F. Cuomo, M. De Felice, and G. Fusco. Vehicular Traffic Monitoring through VANETs: Simulation and Analysis in a Real Case Study. In *University of Roma "La Sapienza"*, pages 1–11, September 2013.

[151] A. Vinel, Y. Koucheryavy, S. Andreev, and D. Staehle. Estimation of a Successful Beacon Reception Probability in Vehicular Ad-hoc Networks. In *2009 International Conference on Wireless Communications and Mobile Computing: Connecting the World Wirelessly*, pages 416–420. ACM, 2009.

[152] M. Torrent-Moreno, D. Jiang, and H. Hartenstein. Broadcast Reception Rates and Effects of Priority Access in 802.11-based Vehicular Ad-hoc Networks. In *Proceedings of the 1st ACM International Workshop on Vehicular Ad Hoc Networks*, VANET '04, pages 10–18, New York, NY, USA, 2004. ACM.

[153] Xu G., R. Sengupta, H. Krishnan, and B. Fan. A Feedback-Based Power Control Algorithm Design for VANET. In *2007 Mobile Networking for Vehicular Environments*, pages 67–72, May 2007.

[154] D.B. Rawat, D.C. Popescu, Gongjun Y., and S. Olariu. Enhancing VANET Performance by Joint Adaptation of Transmission Power and Contention Window Size. *Parallel and Distributed Systems, IEEE Transactions on*, 22(9):1528–1535, Sept 2011.

[155] K. Sjoberg, E. Uhlemann, and E.G. Strom. How Severe Is the Hidden Terminal Problem in VANETs When Using CSMA and STDMA? In *IEEE Vehicular Technology Conference (VTC Fall)*, pages 1–5, Sept 2011.

[156] M. Sepulcre, J. Mittag, P. Santi, H. Hartenstein, and J. Gozalvez. Congestion and Awareness Control in Cooperative Vehicular Systems. *Proceedings of the IEEE*, 99(7):1260–1279, July 2011.

[157] M. Torrent-Moreno, J. Mittag, P. Santi, and H. Hartenstein. Vehicle-to-Vehicle Communication: Fair Transmit Power Control for Safety-Critical Information. *IEEE Transactions on Vehicular Technology*, 58(7):3684–3703, Sept 2009.

[158] C. Huang, Y.P. Fallah, R. Sengupta, and H. Krishnan. Adaptive Intervehicle Communication Control for Cooperative Safety Systems. *Network, IEEE*, 24(1):6–13, Jan 2010.

[159] T. Tielert, D. Jiang, Qi Chen, L. Delgrossi, and H. Hartenstein. Design Methodology and Evaluation of Rate Adaptation based Congestion Control for Vehicle Safety Communications. In *IEEE Vehicular Networking Conference (VNC)*, pages 116–123, Nov 2011.

[160] T. Tielert, D. Jiang, H. Hartenstein, and L. Delgrossi. Joint Power/Rate Congestion Control Optimizing Packet Reception in Vehicle Safety Communications. In *Tenth ACM International Workshop on Vehicular Inter-networking, Systems, and Applications*, VANET '13, pages 51–60. ACM, 2013.

[161] Q. Chen, D. Jiang, T. Tielert, and L. Delgrossi. Mathematical Modeling of Channel Load in Vehicle Safety Communications. In *Vehicular Technology Conference (VTC Fall), 2011 IEEE*, pages 1–5, Sept 2011.

[162] J. B. Kenney, G. Bansal, and C. E. Rohrs. LIMERIC: A Linear Message Rate Control Algorithm for Vehicular DSRC Systems. In *Eighth ACM International Workshop on Vehicular Inter-networking*, VANET '11, pages 21–30. ACM, 2011.

[163] S. Subramanian, M. Werner, S. Liu, J. Jose, R. Lupoaie, and X. Wu. Congestion Control for Vehicular Safety: Synchronous and Asynchronous MAC Algorithms. In *Ninth ACM International Workshop on Vehicular Inter-networking, Systems, and Applications*, VANET '12, pages 63–72, 2012.

[164] W. Zhang, A. Festag, R. Baldessari, and L. Le. Congestion Control for Safety Messages in VANETs: Concepts and Framework. In *8th International Conference on ITS Telecommunications, 2008*, pages 199–203, Oct 2008.

[165] M. Sepulcre, J. Gozalvez, J. Harri, and H. Hartenstein. Application-Based Congestion Control Policy for the Communication Channel in VANETs. *IEEE Communications Letters*, 14(10):951–953, October 2010.

[166] S. Kaul, M. Gruteser, V. Rai, and J. Kenney. Minimizing Age of Information in Vehicular Networks. In *8th Annual IEEE Communications Society Conference on*

Sensor, Mesh and Ad Hoc Communications and Networks (SECON), pages 350–358, June 2011.

OWN PUBLICATIONS

[1] Hugues Tchouankem and Torsten Lorenzen. Measurement-based Evaluation of Interference in Vehicular Ad-Hoc Networks at Urban Intersections. In *IEEE International Conference on Communication Workshop (ICCW)*, pages 2381–2386, June 2015.

[2] Torsten Lorenzen and Hugues Tchouankem. Evaluation of an awareness control algorithm for VANETs based on ETSI EN 302 637-2 V1.3.2. In *IEEE International Conference on Communication Workshop (ICCW)*, pages 2458–2464, June 2015.

[3] Hugues Tchouankem, Tetiana Zinchenko, and Henrik Schumacher. Impact of Buildings on Vehicle-to-Vehicle Communication at Urban Intersections. In *12th Annual IEEE Consumer Communications and Networking Conference (CCNC)*, pages 206–212, Jan 2015.

[4] Tetiana Zinchenko, Hugues Tchouankem, and Lars Wolf. Reliability of vehicle-to-vehicle communication at urban intersections. In *7th International Workshop on Communication Technologies for Vehicles (Nets4Cars-Fall)*, pages 7–11, Oct 2014.

[5] Maksims Fiosins, Bernhard Friedrich, Jana Görmer, Dirk Mattfeld, Jorg P. Müller, and Hugues Tchouankem. Autonomic Routing and Grouping with Vehicular Communication for (De-)centralized Urban Traffic Management. In *Autonomic Road Transport Support Systems, Springer*, July 2014.

[6] Hugues Tchouankem, Tetiana Zinchenko, Henrik Schumacher, and Lars Wolf. Effects of Vegetation on Vehicle-to-Vehicle Communication Performance at Intersections. In *IEEE 78th Vehicular Technology Conference (VTC Fall)*, pages 1–6, Sept 2013.

[7] Tetiana Zinchenko, Hugues Tchouankem, Lars Wolf, and André Leschke. Reliability Analysis of Vehicle-to-Vehicle Applications based on Real World Measurements. In *Tenth ACM International Workshop on VehiculAr InterNETworking, Systems, and Applications (ACM VANET)*, pages 11–20, June 2013.

[8] Jerome Härri, Hugues Tchouankem, Oliver Klemp, and Oleksandr Demchenko. Impact of Vehicular Integration Effects on the Performance of DSRC Communications. In *Wireless Communications and Networking Conference (WCNC), 2013 IEEE*, pages 1645–1650, April 2013.

[9] Henrik Schumacher and Hugues Tchouankem. Highway Propagation Modeling in VANETS and its Impact on Performance Evaluation. In *10th Annual Conference on Wireless On-demand Network Systems and Services (WONS)*, pages 178–185, March 2013.

[10] Hugues Tchouankem, Daniel Schmidt, and Henrik Schumacher. Impact of Vehicular Communication Performance on Travel Time Estimation in Urban Areas. *VIth International Symposium on Networks for Mobility*, September 2012.

[11] Henrik Schumacher, Hugues Tchouankem, Jörg Nuckelt, Thomas Kurner, Tetiana Zinchenko, André Leschke, and Lars Wolf. Vehicle-to-Vehicle IEEE 802.11p Performance Measurements at Urban Intersections. In *IEEE International Conference on Communications (ICC)*, pages 7131–7135, June 2012.

[12] Jana Görmer, Jan Fabian Ehmke, Maksims Fiosins, Daniel Schmidt, Henrik Schumacher, and Hugues Tchouankem. Decision Support for Dynamic City Traffic Management using Vehicular Communication. In *1st International Conference on Simulation and Modeling Methodologies, Technologies and Applications (SIMULTECH), Noordwijkerhout, The Netherlands*, pages 327–332, July 2011.

[13] J. Paulo Miranda, Hugues Tchouankem, Jacek Kibilda, and Luiz A. DaSilva. Return path for interactive TV using white spaces: A novel application for 802.22 WRAN. In *Wireless Advanced (WiAd), 2011*, pages 95–100, June 2011.

Name	Hugues Narcisse Tchouankem
Day of birth	March 29, 1977 in Yaoundé/Kamerun

Education

since 11/2009	Research Assistant and Ph.D. student – Institute of Communications Technology, Leibniz Universität Hannover
	Research in the field of Vehicle-to-X Communication. Associated Doctoral Candidate of the Research Training Group "SocialCars" – a DFG funded research project
10/2003 – 10/2009	Studies of Electrical Engineering and Information Technology – RWTH Aachen University
	Diploma thesis at Embedded Software Laboratory, RWTH Aachen and Volkswagen AG, *"Untersuchung und Implementierung einer Fahrzeug-zu-Infrastruktur-Kommunikation am Beispiel einer Ampel-zu-Fahrzeug Kommunikation"*

Work Experience

06/2009 – 10/2009	Student assistant – Institute for Automatic Control, RWTH Aachen University
05/2008 – 10/2008	Internship – Volkswagen Group Research, Wolfsburg
09/2004 – 04/2008	Student trainee (Hardware Development) P3 Communication GmbH, Aachen

Teaching Experience

since 04/2011	Lab exercises on network and protocols
since 07/2010	Supervising several B.Sc. and Diploma/M.Sc. theses
since 04/2010	Hand-on exercises on computer networks

INDEX